The Significance of Specimen End Restraint in High Pressure Triaxial Testing of Cohesive Soil

by

Brendan Casey

B. Eng. in Civil and Environmental Engineering
University College Cork, Ireland, 2009

Submitted to the Department of Civil and Environmental Engineering
in partial fulfillment of the requirements for the degree of

Master of Science in Civil and Environmental Engineering

at the

Massachusetts Institute of Technology

June 2011

Signature of Author.....
Department of Civil and Environmental Engineering
May 9th, 2011

Certified by.....
John T. Germaine
Senior Research Associate of Civil and Environmental Engineering
Thesis Supervisor

Accepted by.....
Heidi M. Nepf
Chair, Departmental Committee for Graduate Students

The Significance of Specimen End Restraint in High Pressure Triaxial Testing of Cohesive Soil

by

Brendan Casey

Submitted to the Department of Civil and Environmental Engineering on May 9th, 2011 in partial fulfillment of the requirements for the degree of Master of Science in Civil and Environmental Engineering

Abstract

This thesis investigates the mechanical behaviour of cohesive soil at relatively high stresses with a particular emphasis on the significance of specimen end restraint on the interpretation of triaxial test results. Undrained triaxial shear tests have been performed on specimens K_O consolidated to stresses ranging from 0.6 to 10 MPa. Behaviour is examined at three well-defined OCRs of 1, 2 and 4 in compression mode of shear. The tests were performed on Resedimented Boston Blue Clay (RBBC), a low plasticity illitic clay resedimented in the laboratory from natural Boston Blue Clay.

The triaxial test results demonstrate a significant and consistent decrease in normalized undrained strength, initial stiffness and friction angle with increasing stress level at each OCR. These trends are observed regardless of specimen end condition and are consistent with the results of previous studies performed on RBBC as well as on other resedimented clays.

Previous investigations which have examined behaviour at high stresses through a program of laboratory triaxial testing have all involved the use of fixed ends in the triaxial device, i.e. the ends of the specimen are restrained from radial deformation by rough porous stones. Problems associated with specimen end restraint can be minimized by using smooth end platens in the triaxial device. The impact of end restraint has been examined by comparing the results of triaxial tests performed using smooth ends with corresponding results obtained using conventional fixed ends. When shearing is carried out at a relatively slow rate, the use of fixed ends has been shown to result in a small but consistent underestimation of undrained strength at each OCR tested. In addition, the use of fixed ends results in the measurement of misleadingly high pore pressures during undrained shearing, even when shearing is performed at a slow rate and pore pressure equalization is allowed to occur throughout a specimen. Slip surfaces were not found to develop during shearing for tests performed with smooth ends, although they do occur if fixed ends are used. The occurrence of a slip surface in resedimented clay is believed to be caused by the boundary conditions of the test.

Thesis Supervisor: John T. Germaine
Title: Senior Research Associate of Civil and Environmental Engineering

Acknowledgements

Without question my greatest thanks must go to my research supervisor, teacher and friend Dr. Jack Germaine. The utmost respect and admiration is given to his knowledge of laboratory testing, and indeed engineering as a whole. Almost as important for a person committing to life as an MIT graduate student, Dr. Germaine's personality and sense of humour makes working with him a pleasure.

I would like to gratefully acknowledge my other teachers of geotechnical engineering; Prof. Andrew Whittle, Dr. Lucy Jen and Prof. Herbert Einstein. I recognize that I have been taught by some of the best in the world.

Much of the research in this thesis is based on a comparison with previous work carried out at MIT by Dr. Naeem O. Abdulhadi. While I only had the opportunity to work with Naeem for my first semester here, in that time I developed a great admiration and respect for his laboratory skills. The exceptional quality of Naeem's work has helped enormously for my own research.

I extend sincere thanks to those friends with whom I began my career at MIT and share almost every day with, in particular Amer, Steve, Aiden, Jana and Rory. The daily banter has made demanding times of assignments and exams less daunting, and indeed often a lot of fun. A special thanks in particular goes to Amy Adams, whose friendship and help in the lab (and healthy competition!) is sincerely appreciated.

Table of Contents

Abstract.....3

Acknowledgements.....5

Table of Contents.....7

List of Tables.....11

List of Figures.....12

List of Symbols.....18

1 INTRODUCTION **22**

1.1 PROBLEM STATEMENT 22

1.2 THESIS SCOPE AND OBJECTIVES 22

1.3 ORGANIZATION OF THE THESIS 23

2 BACKGROUND **25**

2.1 INTRODUCTION 25

2.2 PREVIOUS STUDIES OF HARD CLAYS IN TRIAXIAL COMPRESSION 25

2.3 EFFECTS OF DIAGENETIC CEMENATATION ON BEHAVIOUR 31

2.3.1 Introduction 31

2.3.2 Classification of Cohesive Materials 32

2.3.3 Apparent Preconsolidation 33

2.3.4 Stress-Strain Response during Shear 34

2.3.5 Failure Envelopes 35

2.4 NORMALIZED BEHAVIOUR 37

2.4.1 Introduction 37

2.4.2 Effect of Stress Level on Normalized Strength 37

2.4.3 SHANSEP versus Recompression 40
2.4.4 Normalized Behaviour of Clay Shales 41
2.5 SPECIMEN NON-UNIFORMITY IN TRIAXIAL COMPRESSION 42
2.5.1 Introduction 42
2.5.2 Implications of Specimen Non-Uniformity in Undrained Triaxial Compression 43
2.5.3 Smooth End Platens 46

3 RESEDIMENTED BOSTON BLUE CLAY 65
3.1 INTRODUCTION 65
3.2 THE PROCESS OF RESEDIMENTATION 67
3.2.1 Introduction 67
3.2.2 Resedimentation Procedure 68
3.2.3 Equipment 70
3.2.4 Consolidation Behaviour during Resedimentation 71
3.2.5 Evaluation of Specimen Uniformity 72
3.3 INDEX PROPERTIES 73
3.3.1 Introduction 73
3.3.2 Index Properties of Series IV RBBC 74
3.3.3 Index Properties of Natural Boston Blue Clay 75
3.3.4 Effects of Salt Concentration 76
3.4 ONE-DIMENSIONAL CONSOLIDATION BEHAVIOUR 77
3.4.1 Introduction 77
3.4.2 Compression Curves and Compressibility Parameters 77
3.4.3 Lateral Stress Ratio 78
3.4.4 Secondary Compression 79
3.4.5 Coefficient of Consolidation and Hydraulic Conductivity 79
3.4.6 Consolidation Behaviour of Natural Boston Blue Clay 81
3.5 UNDRAINED SHEAR BEHAVIOUR IN TRIAXIAL COMPRESSION 84

3.5.1 Introduction 84
3.5.2 Stiffness 84
3.5.3 Impact of Lateral Stress Ratio 85
3.5.4 Strain Rate Sensitivity 85
3.5.5 Effect of Salt Concentration 87
3.5.6 Natural Boston Blue Clay 88

4 EQUIPMENT AND PROCEDURES 114
4.1 INTRODUCTION 114
4.2 TRIAXIAL TESTING SYSTEM 114
4.3 SMOOTH END PLATENS 116
4.4 TEST SETUP AND PROCEDURES 117
4.5 STRAIN RATE DURING VIRGIN CONSOLIDATION 120

5 TRIAXIAL TEST RESULTS 129
5.1 INTRODUCTION 129
5.2 ONE-DIMENSIONAL CONSOLIDATION BEHAVIOUR 129
5.2.1 Introduction 129
5.2.2 Compression Behaviour during Triaxial Consolidation 130
5.2.3 K_O during Triaxial Consolidation 131
5.3 UNDRAINED SHEAR BEHAVIOUR 132
5.3.1 Introduction 132
5.3.2 Behaviour at OCR = 1 133
5.3.3 Behaviour at OCR = 2 135
5.3.4 Behaviour at OCR = 4 136
5.3.5 Behaviour at OCRs 1, 2 and 4 138
5.3.6 Evaluation of the Smooth End Platens 141

6 CONCLUSIONS AND RECOMMENDATIONS 163

6.1 INTRODUCTION 163

6.2 CONSOLIDATION BEHAVIOUR 163

6.3 UNDRAINED SHEAR BEHAVIOUR 164

6.4 RECOMMENDATIONS FOR FUTURE RESEARCH 167

References 170

List of Tables

Table 2-1: Summary of the main findings of Abdulhadi (2009) for CK_OUC test program 49
Table 2-2: Summary of reasons for and against fixed ends and smooth ends (Germaine and Ladd, 1988)..... 49
Table 3-1: Overview of previous studies performed using RBBC (extended from Santagata, 1998) 90
Table 3-2: Dimensions and area ratios of consolidometer specimens at the end of resedimentation91
Table 3-3: Index properties of RBBC Series I, II and III (Cauble, 1996) 92
Table 3-4: Index properties of RBBC Series IV (extended from Santagata, 1998)..... 93
Table 3-5: Index Properties of RBBC Series Ia (batch no. MIT 1139) at low and high salt concentrations (Bailey, 1961)..... 94
Table 3-6: Atterberg limits of BBC as a function of salt concentration (Green, 1956)..... 94
Table 3-7: Values of stress sensitivity and strength sensitivity as defined by Cotecchia and Chandler (2000) for various clays in an intact state 95
Table 3-8: Calculation of sensitivity for natural BBC based on the method of Cotecchia and Chandler (2000) 95
Table 4-1: Properties of transducers used with the triaxial cell. 122
Table 5-1: Summary of triaxial consolidation results 144
Table 5-2: Summary of triaxial shear results 144
Table 5-3: AUR values computed for the end of shearing..... 145

List of Figures

Figure 2-1: Effective stress paths (Cambridge stress space) in undrained triaxial compression for Vallericca Clay. The onset and development of slip surfaces in specimens is also shown (Amorosi and Rampello, 2007) 50
Figure 2-2: Virgin compression and critical state conditions for intact and resedimented specimens of Vallericca Clay (Amorosi and Rampello, 2007) 50
Figure 2-3: Normalized effective stress paths (MIT stress space) for RBBC at OCRs 1, 2 and 4 from CK_OUC triaxial tests with σ'_p = 10 MPa (Abdulhadi, 2009) 51
Figure 2-4: Normalized shear stress-strain responses for RBBC at OCRs 1, 2 and 4 from CK_OUC triaxial tests with σ'_p = 0.2 and 10 MPa (Abdulhadi, 2009) 51
Figure 2-5: Variation in normalized undrained strength with stress level for RBBC at OCRs = 1, 2 and 4 from CK_OUC triaxial tests (Abdulhadi, 2009) 52
Figure 2-6: Lateral stress ratio at the end of virgin consolidation (K_{ONC}) versus stress level for RBBC from CK_OUC triaxial tests (Abdulhadi, 2009) 52
Figure 2-7: Normalized undrained secant Young's modulus versus axial strain for RBBC at OCRs 1, 2 and 4 from CK_OUC triaxial tests with σ'_p = 0.2 and 10 MPa (Abdulhadi, 2009) 53
Figure 2-8: Normalized shear induced pore pressure versus axial strain for RBBC at OCRs 1, 2 and 4 from CK_OUC triaxial tests with σ'_p = 0.2 & 10 MPa (Abdulhadi, 2009) 53
Figure 2-9: Deviatoric stress-strain response during undrained triaxial compression for a NC mud volcano clay (Yassir, 1989) 54
Figure 2-10: Effective stress paths (Cambridge stress space) in undrained triaxial compression for a NC mud volcano clay (Yassir, 1989) 54
Figure 2-11: Normalized excess pore pressure (u_e/p'_o) versus axial strain during undrained triaxial compression for a NC mud volcano clay (Yassir, 1989) 55
Figure 2-12: Normalized shear stress versus axial strain for CIUC tests on Kimmeridge Shale and Barents Sea Shale (Gutierrez et al., 2008) 55
Figure 2-13: General forms of stress-strain response for clay shales (Petley, 1999) 56
Figure 2-14: Conceptual form of failure envelopes for clays by Burland (1990) 56
Figure 2-15: Conceptual form of failure envelopes for hard clays and clay shales (Petley, 1999) 57
Figure 2-16: Normalized undrained shear strength versus OCR for a SHANSEP test program on AGS Plastic Marine Clay (Koutsoftas & Ladd, 1985) 57
Figure 2-17: Normalized undrained strengths in TC, TE and DSS as a function of plasticity from CK_OU tests on NC clays and silts (Ladd, 1991) 58

Figure 2-18: Effect of stress level on the SHANSEP S and m parameters for RBBC in triaxial compression (Abdulhadi, 2009) 58
Figure 2-19: Relationship between undrained strength and consolidation stress for CIUC tests performed on resedimented London Clay (Bishop et al., 1975) 59
Figure 2-20: Variation in normalized undrained strength with stress level for Resedimented Ugnu Clay at OCR = 1 from CK_OUC triaxial tests (Jones, 2010) 59
Figure 2-21: Reconsolidation procedures for laboratory CK_oU testing (Ladd, 1991) 60
Figure 2-22: Effect of laboratory reconsolidation procedure on measured stiffness for Boston Blue Clay (Ladd et al., 1999) 60
Figure 2-23: Normalized undrained shear strength versus OCR for four clay shales (Gutierrez et al., 2008) 61
Figure 2-24: Location of conical 'dead' zones in a fixed end triaxial specimen (Rowe and Barden, 1964) 61
Figure 2-25: Effect of end restraint caused by fixed ends on the stress state in a triaxial specimen. 62
Figure 2-26: Post-shear water content distribution (%) in CIUC test specimens of resedimented Mississippi Valley Alluvial Clay at OCR = 16 (Richardson and Whitman, 1963) 62
Figure 2-27: Hypothetical stress paths for slow and fast undrained triaxial compression tests on rate-independent cohesive soil where fixed ends are used (Germaine and Ladd, 1988) 63
Figure 2-28: A picture of NC RBBC specimens after CK_OUC tests showing a bulging mode of failure for the low pressure test and a slip surface for the high pressure test (Abdulhadi, 2009) 63
Figure 2-29: End platen designs (Rowe and Barden, 1964) 64
Figure 3-1: Vacuum setup used to de-air RBBC slurry 96
Figure 3-2: Setup of consolidometer Type I (almost identical to that of Type II) 97
Figure 3-3: Typical settlement-(log)time curves for load increments applied to RBBC samples prepared in each type of consolidometer 98
Figure 3-4: Typical normalized settlement-(log)time curves for load increments applied to RBBC samples prepared in each type of consolidometer compared with what is predicted by Terzaghi's theory 98
Figure 3-5: One-dimensional compression behaviour measured during the resedimentation of RBBC samples as well as during a typical CRS test on RBBC 99
Figure 3-6: Comparison of compression behaviours measured during the K_o consolidation phase of triaxial tests for RBBC samples prepared in a Type II consolidometer ('Plexi.') and in a larger diameter consolidometer ('Stnd.') (Abdulhadi, 2009) 99
Figure 3-7: Comparison of shear stress-strain responses measured during the undrained shear phase of triaxial tests for RBBC samples prepared in a Type II consolidometer ('Plexi.') and in a larger diameter consolidometer ('Stnd.') (Abdulhadi, 2009) 100

Figure 3-8: Grain size distribution for Series IV BBC powder as obtained from hydrometer tests (Abdulhadi, 2009) 100
Figure 3-9: Casagrande plasticity chart showing results from Atterberg limit tests on RBBC Series IV (Abdulhadi, 2009) 101
Figure 3-10: Stratigraphy at the Building 68 site (Berman, 1993) 101
Figure 3-11: Grain size distribution profile for the layer of BBC at the Building 68 site (Berman, 1993) 102
Figure 3-12: One-dimensional compression behaviour of RBBC as obtained from triaxial tests and a typical CRS test (Abdulhadi, 2009) 103
Figure 3-13: The variation in K_O with stress level for RBBC Series IV as measured during the consolidation stage of triaxial tests (Abdulhadi, 2009) 104
Figure 3-14: K_o versus stress level for RBBC Series III as measured during the consolidation stage of triaxial tests (Santagata, 1994) 104
Figure 3-15: Coefficient of consolidation versus stress level for NC RBBC as obtained from CRS tests as well as from the consolidation stage of batching (Abdulhadi, 2009) 105
Figure 3-16: Void ratio versus hydraulic conductivity for RBBC as obtained from CRS tests as well as from the consolidation stage of batching (Abdulhadi, 2009) 105
Figure 3-17: Ratio of C_c/C_k versus stress level for RBBC as obtained from CRS tests (Abdulhadi, 2009) 106
Figure 3-18: One-dimensional compression behaviour of natural BBC (Samples S1 and S2) compared to that of RBBC as obtained from CRS tests 106
Figure 3-19: Variation in virgin compression ratio and swelling ratio with stress for natural BBC (Samples S1 and S2) and RBBC as obtained from CRS tests 107
Figure 3-20: Variation in swelling ratio for natural BBC (Samples S1 and S2) as obtained from CRS tests 107
Figure 3-21: Values of compression ratio and swelling ratio for BBC at the Building 68 site as well as at various other locations around the MIT campus (Berman, 1993) 108
Figure 3-22: Variation in the coefficient of consolidation for natural BBC (Samples S1 and S2) compared to that for NC RBBC as obtained from CRS tests 108
Figure 3-23: Ratio of C_c/C_k versus stress level for natural BBC (Samples S1 and S2) as obtained from CRS tests 109
Figure 3-24: Relationship between initial stiffness of RBBC and mean consolidation stress in undrained triaxial compression (Santagata, 1998) 109
Figure 3-25: Strain to failure for RBBC as a function of OCR and stress level as obtained from CK_OUC tests (Abdulhadi, 2009) 110

Figure 3-26: Normalized undrained strength versus pre-shear lateral stress ratio as obtained from CKUC tests on NC RBBC (Santagata, 1994) 110
Figure 3-27: Effect of strain rate on the normalized shear stress-strain response of NC RBBC as obtained from CK_OUC tests (Sheahan, 1991) 111
Figure 3-28: Effect of strain rate on the normalized effective stress paths of NC RBBC as obtained from CK_OUC tests (Sheahan, 1991) 111
Figure 3-29: Effect of strain rate on the normalized shear induced pore pressures generated in NC RBBC as obtained from CK_OUC tests (Sheahan, 1991) 112
Figure 3-30: Effect of strain rate on the normalized undrained strength of RBBC as obtained from CK_OUC tests (Sheahan, 1991) 112
Figure 3-31: Effect of strain rate on the SHANSEP parameters as obtained from CK_OUC tests (Sheahan, 1991) 113
Figure 4-1: Schematic of the standard automated triaxial testing system used in the MIT Geotechnical Engineering Laboratory (from Santagata, 1998) 123
Figure 4-2: Schematic of triaxial cell (Da Re, 2000) 124
Figure 4-3: Triaxial cell and PVA's in the environmental enclosure 125
Figure 4-4: Design of smooth end platens used by Sheahan (1991) 126
Figure 4-5: Cross-section of specimen setup 127
Figure 4-6: Test setup at the point at which filter paper strips have been positioned around the specimen but before the membranes are placed. The alignment device can be seen to keep the specimen and top cap in place 128
Figure 4-7: The variation in K_O with stress level as measured during the consolidation stage of a triaxial test in which the axial strain rate is varied 128
Figure 5-1: One dimensional compression behaviour as measured during the K_O consolidation stage of triaxial tests (in e-σ'_v space) 146
Figure 5-2: One dimensional compression behaviour as measured during the K_O consolidation stage of triaxial tests (in e-logσ'_v space) 146
Figure 5-3: The variation in K_O with stress level as measured during the consolidation stage of triaxial tests 147
Figure 5-4: Stress-strain responses measured during undrained shearing for tests performed with smooth ends at OCR = 1 147
Figure 5-5: Normalized stress-strain responses measured during undrained shearing for tests performed with smooth and fixed ends at OCR = 1 148
Figure 5-6: Normalized stress-strain responses (at small strains) measured during undrained shearing for tests performed with smooth and fixed ends at OCR = 1 148

Figure 5-7: The variation in normalized secant Young's modulus with axial strain measured during undrained shearing for tests performed with smooth and fixed ends at OCR = 1 149
Figure 5-8: Normalized shear induced pore pressures measured during undrained shearing for tests performed with smooth and fixed ends at OCR = 1 149
Figure 5-9: Normalized shear induced pore pressures (at small strains) measured during undrained shearing for tests performed with smooth and fixed ends at OCR = 1 150
Figure 5-10: Normalized effective stress paths measured during undrained shearing for tests performed with smooth ends at OCR = 1 150
Figure 5-11: Relationship between normalized undrained strength and pre-shear K_O for NC RBBC as found in the experimental programs of the author, Abdulhadi (2009) and Santagata (1994) 151
Figure 5-12: Normalized stress-strain responses measured during undrained shearing for tests performed with smooth and fixed ends at OCR = 2 151
Figure 5-13: The variation in normalized secant Young's modulus with axial strain measured during undrained shearing for tests performed with smooth and fixed ends at OCR = 2 152
Figure 5-14: Normalized shear induced pore pressures measured during undrained shearing for tests performed with smooth and fixed ends at OCR = 2 152
Figure 5-15: Normalized effective stress paths measured during undrained shearing for tests performed with smooth and fixed ends at OCR = 2 153
Figure 5-16: Normalized stress-strain responses measured during undrained shearing for tests performed with smooth and fixed ends at OCR = 4 153
Figure 5-17: The variation in normalized secant Young's modulus with axial strain measured during undrained shearing for tests performed with smooth and fixed ends at OCR = 4 154
Figure 5-18: Normalized shear induced pore pressures measured during undrained shearing for tests performed with smooth and fixed ends at OCR = 4 154
Figure 5-19: Normalized effective stress paths measured during undrained shearing for tests performed with smooth and fixed ends at OCR = 4 155
Figure 5-20: Comparison of normalized effective stress paths measured during undrained shearing for tests TX1034 and TX1057 at OCR = 4 155
Figure 5-21: Comparison of normalized effective stress paths measured during undrained shearing for tests TX1042 and TX1046 at OCR = 4 156
Figure 5-22: Normalized stress-strain responses measured during undrained shearing for tests performed with smooth and fixed ends at OCRs 1, 2 and 4 156
Figure 5-23: Normalized shear induced pore pressures measured during undrained shearing for tests performed with smooth and fixed ends at OCRs 1, 2 and 4 157
Figure 5-24: Normalized effective stress paths measured during undrained shearing for tests performed with smooth and fixed ends at OCRs 1,2 and 4 157

Figure 5-25: The variation in normalized secant Young's modulus with axial strain measured during undrained shearing for tests performed with smooth and fixed ends at OCRs 1, 2 and 4 158
Figure 5-26: Initial undrained secant Young's modulus normalized with respect to void ratio versus stress level 158
Figure 5-27: The variation in secant friction angle with stress level as obtained from tests performed with smooth and fixed ends at OCRs 1, 2 and 4 159
Figure 5-28: The variation in normalized undrained strength with stress level as obtained from tests performed with smooth and fixed ends at OCRs 1, 2 and 4 159
Figure 5-29: Normalized peak undrained strength versus normalized shear induced pore pressures at peak strength for OCR = 1 160
Figure 5-30: Normalized peak undrained strength versus normalized shear induced pore pressures at peak strength for OCR = 4 160
Figure 5-31: The influence of stress level and specimen end condition on the SHANSEP parameters 161
Figure 5-32: Effective stresses at critical state for RBBC as obtained from tests with smooth and fixed ends compared to the K_O virgin consolidation line 161
Figure 5-33: Effective stresses and shear stresses at critical state for RBBC as obtained from tests with smooth and fixed ends compared to the K_O virgin consolidation line 162
Figure 5-34: Possible cause for insufficient radial spreading of the ends of specimens when using smooth ends (Sheahan, 1991) 162
Figure 6-1: Impact of specimen end restraint caused by the use of fixed ends on the form of the effective stress path in slow tests 169

List of Symbols

QBASIC	Quick Beginner's All-purpose Symbolic Instruction Code
BBC	Boston Blue Clay
CIUC	Isotropically Consolidated Undrained Triaxial Compression Test
CK_OU	K_O Consolidated Undrained Triaxial Test
CK_OUC	K_O Consolidated Undrained Triaxial Compression Test
CK_OUDSS	K_O Consolidated Undrained Direct Simple Shear Test
CK_OUE	K_O Consolidated Undrained Triaxial Extension Test
CL	Low Plasticity Clay
CR	Virgin Compression Ratio
CRS	Constant Rate of Strain
CSL	Critical State Line
DSS	Direct Simple Shear
LVDT	Linear Variable Differential Transformer
MIT	Massachusetts Institute of Technology
NC	Normally Consolidated
OC	Overconsolidated
OCR	Overconsolidation Ratio
PSC	Plane Strain Compression
PSE	Plane Strain Extension
PVA	Pressure-Volume Actuator
RBBC	Resedimented Boston Blue Clay
SHANSEP	Stress History and Normalized Soil Engineering Properties
SR	Swelling Ratio
TC	Triaxial Compression
TE	Triaxial Extension

USCS	Unified Soil Classification System
YSR	Yield Stress Ratio

A_f	Skempton's pore pressure parameter A at failure
B	Skempton's pore pressure parameter B
C_c	Compression index
C_k	Permeability change index
C_α, $C_{\alpha e}$, $C_{\alpha \varepsilon}$	Rate of secondary compression, in terms of void ratio, in terms of strain
c_v	Vertical coefficient of consolidation
c'	Apparent cohesion intercept
D_i	Initial specimen diameter
E	Young's modulus
E_u, E_{uMAX}	Undrained secant Young's modulus, initial maximum undrained secant Young's modulus
e	Void ratio
ΔF_a^m	Resistive axial force provided by a membrane
ΔF_a^{fp}	Buckling capacity of filter paper
G_s	Specific gravity
H_d	Drainage height
I_p	Plasticity index
K	Lateral stress ratio
K_O	Coefficient of lateral earth pressure at rest
K_{ONC}	Coefficient of lateral earth pressure at rest for NC soil
K_{fp}	Axial force per perimeter of filter paper
k_v	Vertical hydraulic conductivity
m	Exponent in the SHANSEP equation describing the change in normalized strength with OCR

n	Exponent describing the change in K_O with OCR
P_{fp}	Perimeter of filter paper
p'	Average effective stress, $\frac{1}{2}(\sigma'_a + \sigma'_r)$
p'_m, p'_{mc}	Mean effective stress, mean consolidation stress, $\frac{1}{3}(\sigma'_1 + 2\sigma'_3)$
q	Shear stress, $\frac{1}{2}(\sigma_a - \sigma_r)$ or equivalently $\frac{1}{2}(\sigma_1 - \sigma_3)$
q_u	Unconfined compressive strength
r^2	Regression coefficient
S	Normalized undrained strength for NC soil in SHANSEP equation
S_t	Strength sensitivity
S_σ	Stress sensitivity
s_u	Undrained shear strength
T_{95}	Time factor corresponding to 95% pore pressure equilibration in a specimen
t	Time, or thickness of membrane
t_p	Time to end of primary consolidation
t_{95}	time to 95% pore pressure equilibration in a specimen
U_v	Degree of [vertical] consolidation
u	Pore pressure
u_e	Excess pore pressure
u_s	Shear induced pore pressure
u_{sp}	Shear induced pore pressure at peak shear stress
v	specific volume
w	Water content
w_L	Liquid limit
w_p	Plastic limit

ε	Strain
ε_a	Axial strain
ε_f	Strain at peak shear stress, i.e. at failure
ε_v	Volume strain
φ'_p	Secant friction angle at peak shear strength
φ'_{mo}	Friction angle at maximum obliquity
$\rho_{0.5}$	The change in normalized strength across one log cycle of strain rate as a percentage of the normalized strength measured at a reference rate 0.5 %/hr
σ'_a, σ'_{ac}	Axial effective stress, axial consolidation stress
σ'_{ey}	Stress on the virgin compression curve of resedimented soil at the void ratio corresponding to yield of the intact soil
σ'_p	Preconsolidation pressure
σ'_r	Radial effective stress
$\Delta\sigma_r^m$	Resistive radial stress provided by a membrane
σ'_v	Vertical effective stress
σ'_{vo}	In situ vertical effective stress
σ'_{vy}	Vertical effective yield stress
σ_1, σ_2, σ_3	Major, intermediate and minor principal stresses
σ_{oct}	Octahedral stress, $\frac{1}{3}(\sigma_1 + 2\sigma_3)$ (same as total mean stress)
τ	Shear stress

1 INTRODUCTION

1.1 PROBLEM STATEMENT

The mechanical behaviour of soft sedimentary deposits, namely soils, is now relatively well understood for the range of stresses conventionally encountered in geotechnical engineering. Traditionally, the geotechnical engineering discipline has been focused on applications involving stresses less than say 1 to 2 MPa, with the result that much less is known about soil behaviour at higher stresses. Recently, however, there has been an increasing desire to gain a deeper understanding of behaviour at these higher stresses. This desire has been driven primarily by the petroleum industry for applications in shallow oil reservoir development. In particular, a better understanding of the mechanical behaviour of cohesive soils is necessary to reduce drilling costs associated with borehole instabilities in these materials. The behaviour of cohesive soils at high effective stresses involves a gradual transition between that of hard clay to that of unlithified or weakly lithified soft clay-shales and mudstones, these materials being the most abundant in the uppermost 5 km of the Earth's crust (Petley, 1999).

This thesis addresses one particular aspect of the triaxial testing of soil at high stresses which has not received adequate attention in the past. This is the issue of specimen end restraint. Previous investigations which have examined behaviour at high stresses through a program of laboratory triaxial testing have all involved the use of fixed ends in the triaxial device, that is to say that the ends of the specimen are restrained from radial deformation by rough porous stones. During shearing, end restraint causes so called dead zones to develop at the ends of specimens which are the result of non-uniform stresses and strains developed within the specimen. Since a triaxial specimen is assumed to be a uniform element of soil, these non-uniform stresses and strains detract from the elemental assumption. The problems associated with end restraint in triaxial testing can be minimized by using smooth end platens which allow for radial deformation at the ends of specimens. It is this approach of using smooth ends platens which has been adopted in the author's research in order to investigate the effects of end restraint on the interpretation of triaxial test results.

1.2 THESIS SCOPE AND OBJECTIVES

The research presented in this thesis has two main objectives. The first objective is to gain an improved understanding of the mechanical behaviour of cohesive soil at high consolidation stresses,

particularly as a function of stress history, i.e. overconsolidation ratio (OCR), and stress level. This is done by examining the work carried out by previous researchers in this area and by analyzing the results of a series of triaxial compression tests carried out by the author. Resedimented Boston Blue Clay (RBBC) was employed in the author's triaxial tests as the 'analogue' test material. RBBC is a soil resedimented in the laboratory from natural Boston Blue Clay, a low plasticity illitic clay.

As indicated by the title of this thesis, the second, primary, objective of the research is to investigate the significance of specimen end restraint in the triaxial testing of cohesive soil at high stresses. This is done by comparing the results of the author's triaxial tests performed using smooth end platens with the corresponding results of Abdulhadi (2009). Abdulhadi conducted an extensive investigation of the stress-strain-strength properties of RBBC through a program of triaxial testing with fixed ends. The comparison with Abdulhadi's results allows the relative importance of the issue of specimen end restraint to be established.

The work presented in this thesis represents one element of the wider research objectives of the UT GeoFluids Consortium, a joint venture between the Massachusetts Institute of Technology and the University of Texas at Austin. The high level objective of the GeoFluids group is "*to study the state and evolution of pressure, stress, deformation and fluid migration through experiments, theoretical analysis, and field study*". The author's research focuses solely on mechanical behaviour determined from laboratory testing. The results of the research will establish a baseline elemental mechanical behaviour which can support numerical modeling of field situations.

1.3 ORGANIZATION OF THE THESIS

This thesis is organized into six chapters, each of which has a separate and distinct function, as given below.

Chapter 2 provides the important background information relevant to the research. The aim is to establish an overall picture of the current level of knowledge regarding the high pressure mechanical behaviour of cohesive soil and the effects of specimen end restraint. The discussion is limited to the case of triaxial compression mode of shear. The effects of natural micro-structure, particularly cementation due to diagenesis, on the behaviour of cohesive materials at high stresses are discussed. The normalization of soil behaviour, in particular the SHANSEP normalization procedure, is also described.

Chapter 3 presents an overview of RBBC. The chapter summarizes the resedimentation procedure used to produce samples for testing and the index properties of the soil. A fairly extensive

discussion is also presented on the consolidation and undrained shear behaviour of RBBC as obtained from previous experimental studies. The soil has being studied extensively at MIT since the 1960's and a large database exists on its properties. Chapter 3 also provides comparisons with the corresponding behaviour of natural Boston Blue Clay.

Chapter 4 discusses the procedures and equipment used in the research. A particular emphasis is placed on describing the smooth end platens used in the triaxial device to reduce end restraint.

Chapter 5 presents the results of the triaxial tests carried out in the course of the research. The testing program consisted of K_O consolidated undrained triaxial compression (CK_OUC) tests performed at several different stress levels and OCRs. A comparison is made with the corresponding results obtained by Abdulhadi (2009) in order to examine the impact of specimen end restraint. The influence of increasing stress level on normalized shear behaviour is also presented. In addition, the consolidation behaviour of the soil as measured during the K_O consolidation phase of the triaxial tests is also summarized in this chapter.

Chapter 6 presents a summary of the results and the main conclusions which can be drawn from the research. Finally, recommendations for future work are presented.

2 BACKGROUND

2.1 INTRODUCTION

Although the mechanical behaviour of cohesive soils at conventional effective stresses commonly encountered in geotechnical engineering applications, below say 2 MPa, is relatively well understood and documented throughout the literature, considerably less is known about the behaviour of these soils at much higher stresses. Recent work by Abdulhadi (2009) involved an extensive experimental program to examine systematically the effective stress-strain-strength properties of resedimented clay as a function of both stress level and OCR for axial consolidation stresses (σ'_{ac}) up to 10 MPa. Above this stress level, however, there has been no similar experimental program previously carried out to examine systematically the behaviour of clay as a function of both stress level and OCR.

This chapter begins with a review of previous experimental studies carried out on the behaviour of both natural and resedimented hard clays in triaxial compression at high stresses. Particular attention is paid to the findings of Abdulhadi (2009).

In Section 2.3 emphasis is made on the effects of natural micro-structure, particularly cementation due to diagenesis, on the behaviour of cohesive soils at high stresses. These materials are often regarded as clay shales. The brittle-ductile transition in stress-strain response often experienced by these materials is discussed along with some basic models that have been proposed to define their behaviour.

Section 2.4 presents a review of our current understanding regarding the normalized behaviour of cohesive soils at high stresses. The SHANSEP normalization procedure and its applicability at high stresses is also discussed.

One of the main goals of the author's research is to examine the influence of specimen end restraint in triaxial testing. The last section of this chapter presents a discussion of this issue including the effects of using standard fixed ends on triaxial test results.

2.2 PREVIOUS STUDIES OF HARD CLAYS IN TRIAXIAL COMPRESSION

One of the earliest programs of triaxial testing at relatively high stresses is that of Bishop et al. (1965) on London Clay from Ashford Common for σ'_{ac} up to approximately 7.5 MPa. Boom clay has

been investigated by both Horseman et al. (1993) and Taylor and Coop (1993) for σ'_{ac} up to 5.4 MPa. Petley (1994) tested London Clay up to 30.1 MPa in an effort to define the form of the peak strength envelope. Marsden et al. (1992) conducted tests on Weald Shale and Fullers Earth up to 23 MPa and on London Clay up to 8 MPa with a view towards making correlations between petrophysical and mineralogical characteristics and the measured mechanical behaviour. Petley et al. (1993) tested Kimmeridge Clay up to 10.6 MPa and Eocene North Sea Shale up to 16 MPa and compared their undrained shear deformation behaviour with that of chalk. More recently, Gutierrez et al. (2008) tested Kimmeridge Clay up to 30 MPa and Barents Sea Shale up to 63 MPa to investigate normalized behaviour.

All of the studies mentioned above involved isotropically consolidated undrained triaxial compression (CIUC) tests on unweathered intact samples. Obtaining intact samples generally involves some sampling disturbance, even with the use of careful sampling procedures, and ideally large diameter or block samples should be used. However, this may often be too expensive or infeasible, as in the case of deep sampling or offshore exploration. Even more important, the use of intact samples rather than resedimented ones does not allow for control of the stress history, i.e. preconsolidation pressure (σ'_p), of the sample. As a result, intact samples with a high σ'_p require a large consolidation stress to reach the normally consolidated range while samples with a low σ'_p require the development of large strains in order to test at high stresses. Combined, these factors make a systematic investigation of the mechanical behaviour of any soil as a function of both stress level and OCR practically impossible. It is important to note that the above studies also involved isotropic consolidation of test specimens prior to shear. Unlike K_o consolidation which best mimics in situ conditions, isotropic consolidation is a very rare occurrence in nature and can produce a significantly different undrained strength. For consolidation to the same σ'_{ac}, isotropically consolidated specimens will generally have a higher undrained strength. This is due to the fact that, assuming $K_o < 1$, the mean effective stress prior to shearing will be larger, thereby producing a lower water content/void ratio and a higher undrained strength. On the other hand, due to the anisotropic micro-structure possessed by soil in a K_o condition, K_o consolidated specimens will generally exhibit a higher undrained strength than isotropically consolidated specimens when consolidated to the same mean effective stress. A compilation of a large variety soft clays in both intact and resedimented states by Belviso et al. (2001) illustrates the large difference in undrained strength which some clays exhibit depending on the laboratory consolidation procedure used. Isotropic consolidation can also produce a significantly misleading stress-strain response during shearing. For samples of resedimented clay and NC intact clay in particular, isotropic consolidation can result in a much larger strain to failure (ε_f) and a less distinct peak shear stress compared to samples subjected to K_O consolidation.

Amorosi and Rampello (2007) investigated the behaviour of Vallericca Clay, a structured stiff clay of marine origin from Italy using a series isotropically and anisotropically consolidated triaxial compression tests for σ'_{ac} up to 11 MPa and 6.75 MPa respectively. These tests were performed on intact samples, though some isotropically consolidated tests were also performed on resedimented samples for σ'_{ac} up to approximately 1.2 MPa. Specimens were sheared in both drained and undrained conditions. Figure 2-1 shows some typical effective stress paths in Cambridge stress space[1] for anisotropically consolidated intact specimens sheared undrained in both the normally consolidated (NC) and overconsolidated (OC) range. Amorosi and Rampello reported that, under both isotropic and anisotropic consolidation to stresses greater than σ'_p, major and irreversible damage to the soil's initial interparticle bonding (likely weak cementation) was produced. While significant changes to the initial soil fabric also occurred during isotropic consolidation to stresses beyond σ'_p, only minor changes to the soil's fabric were induced by anisotropic consolidation to stresses beyond σ'_p under nearly K_o conditions. It was found that, unlike for purely cemented soils, the natural fabric of the Vallericca Clay gave the intact specimens an undrained strength much higher than the resedimented counterparts which was not eliminated by consolidation to high stresses nor by shearing. This can be seen in Figure 2-2 where both drained and undrained shear stress paths of intact and resedimented specimens are plotted in specific volume ($v = 1+e$) versus p'_m space. The end points of the tests where constant shear stress was observed with continuous straining, i.e. critical state, are shown by circles for the intact specimens and by asterisks for the resedimented specimens. A single critical state line (CSL) can be defined for the intact specimens irrespective of their isotropic or anisotropic consolidation histories and of the maximum effective stress experienced prior to shearing. The critical states observed for resedimented specimens define a CSL significantly below the one relevant to the intact specimens, though characterized by the same slope $\lambda = 0.148$. Since the intact and resedimented CSLs were found to be parallel, it was concluded that over the stress range investigated, the natural Vallericca Clay does not tend to the reference state defined by the corresponding resedimented material. One possible reason for this occurrence may be that Vallericca Clay was found to contain a large proportion of microfossils, giving the clay a calcium carbonate content of about 30%. This could have resulted in the intact material possessing a strong natural micro-fabric which would have been destroyed by resedimentation, though not by shearing in the triaxial device.

One of the most comprehensive and systematic investigations of the mechanical behaviour of a clay for σ'_{ac} up to 10 MPa was carried out by Abdulhadi (2009) on RBBC[2] through a series of

[1] Cambridge stress space plots mean effective stress $p'_m = \frac{1}{3}(\sigma'_1 + 2\sigma'_3)$ versus deviatoric stress $(\sigma_1 - \sigma_3)$

[2] A more in-depth discussion of the general mechanical behaviour of RBBC is given in Chapter 3

CK_OUC tests. Some of the main findings of this investigation are summarized in Table 2-1, which shows the separate effects of varying OCR and stress level on the behaviour of RBBC. Regarding the effect of increasing OCR, the findings are in agreement with previous well established knowledge of behaviour of clays, e.g. Burland (1990) and Amorosi and Rampello (2007), as well as with previous work carried out on RBBC, e.g. Sheahan (1991), Santagata (1994) and Santagata (1998). The increase normalized undrained strength (s_u/σ'_{ac}) associated with increasing OCR is due to the dilative response of OC clay. As a result of dilation, OC samples tend to generate lower excess pore pressures and fail at an effective stress higher than the consolidation stress. On the other hand, NC samples exhibit entirely contractive behaviour during shear as positive excess pore pressures are produced and tend to fail at an effective stress much lower than the consolidation stress. Figure 2-3 shows effective stress paths for specimens of RBBC at OCRs 1, 2 and 4 in MIT stress space[3] normalized to the same σ'_p of 10 MPa. As shown in Figure 2-4, increasing OCR also leads to a more ductile response as the strain to failure increases and post-peak strain softening decreases. Increasing lateral stress ratio (K) and normalized undrained secant Young's Modulus (E_u/σ'_{ac}) with increasing OCR, as well as decreasing Skempton A parameter at failure (A_f) with increasing OCR, are also results that are to be expected for clay.

Unlike the effect of OCR, the effect of stress level on the mechanical properties of clay was previously less well established. Significantly, Abdulhadi (2009) found that increasing consolidation stress causes a reduction in normalized undrained strength. Figure 2-5 clearly illustrates the consistent trend of decreasing normalized strength with increasing stress level for each OCR which is more pronounced at lower stresses. This reduction in normalized strength corresponds with an increase in lateral stress ratio at the end of virgin consolidation (K_{ONC}) as stress level increases, as shown in Figure 2-6. Abdulhadi suggested that the association between normalized undrained strength and K_O is more pronounced in the NC clay than the OC clay since for the NC clay a relatively small shear stress increment is required to attain the peak stress state from the pre-shear stress state. At a given stress level, the stress paths for each OCR approach a common failure envelope at large strains, as shown in Figure 2-3 for σ'_p = 10 MPa. However, while the failure envelope at 10 MPa has a friction angle at maximum obliquity φ'_{mo} = 26.8° and normalized cohesion intercept c'/σ'_{am} = 0.032, the failure envelope at 0.2 MPa has φ'_{mo} = 33.7° and c'/σ'_{am} = 0.018. This implies a failure envelope having significant curvature. Moreover, it should be noted that while the secant friction angle at peak shear strength (φ'_p) decreases with increasing stress level for the OC clay, for the NC clay φ'_p is mostly unaffected by stress level. Increasing consolidation stress also produces a more ductile response as strain to failure increases and post-peak strain softening decreases for a given OCR, a behaviour illustrated in Figure 2-4. The normalized undrained secant

[3] MIT stress space plots $p' = \frac{1}{2}(\sigma'_a + \sigma'_r)$ versus $q = \frac{1}{2}(\sigma_a - \sigma_r)$

Young's Modulus also displays stress level dependence, decreasing in magnitude with increasing consolidation stress for each OCR tested, as illustrated in Figure 2-7. It can be seen from Figure 2-7 that the high pressure tests showed a larger strain range of linear behaviour than the low pressure tests. The reduction in normalized undrained strength with increasing stress level found by Abdulhadi (2009) is also discussed further in Section 2.4.2.

One might suspect that the decrease in normalized strength with stress level found by Abdulhadi (2009) would be associated with an increase in excess pore pressure (u_e) at failure. Significantly, however, Abdulhadi (2009) found that as consolidation stress level increases, the excess pore pressures generated during undrained shear decreased for each OCR tested. To isolate the pore pressure due to changes in shear stress alone, the shear induced pore pressure ($u_s = \Delta u - \Delta\sigma_{oct}$)[4] provides a better understanding of pore pressure generation during undrained shear as this essentially removes the effect of total stress path. Note that u_s is a soil property. Figure 2-8 shows the normalized shear induced pore pressure (u_s/σ'_{ac}) generation with strain for RBBC at OCRs 1, 2, and 4 at low and high stress levels (σ'_p = 0.2 and 10 MPa). In all cases the shear induced pore pressures initially increase indicating contractive behaviour. The NC clay remains contractive throughout shearing while the OCR = 2 clay changes to slightly dilative behaviour before contracting again with increasing strain. The shear induced pore pressures decrease beyond 0.5% strain for the OCR = 4 clay which ultimately displays dilative behaviour with continued shearing. As the stress level increases, the shear induced pore pressures decrease for the NC and OCR = 2 clay while for the OCR = 4 clay the pore pressures instead increase, i.e. become less negative.

Some of the very limited triaxial compression testing carried out on resedimented clays for σ'_{ac} higher than the 10 MPa achieved by Abdulhadi (2009) include William (2007), Yassir (1989), Berre (1992) and Bishop et al. (1975)[5]. William (2007) tested both resedimented and intact Bringelly Shale from Sydney for σ'_{ac} up to 60 MPa. However, these tests involved incremental isotropic consolidation of test specimens prior to drained shearing. Only a limited number of tests were performed on the resedimented material and the results are of little relevance to the author's research. Berre (1992) attempted to mimic the behaviour of intact natural clay shale using artificial shale produced in the laboratory by resedimentation. Mixtures of remolded Moum Clay and kaolinite were created so that their composition would be as close as possible to that of the natural clay shale. The mixture had a clay fraction of approximately 58%, w_L = 60% and I_p = 37%. Specimens were consolidated in an oedometer to σ'_p = 32 MPa before being unloaded and dismounted. Triaxial specimens were then

[4] Octahedral stress (σ_{oct}) is the same as total mean stress (p_m). For conventional triaxial compression testing where there is no change in cell pressure during shear, i.e. $\Delta\sigma_3 = 0$, u_s is simply equal to $\Delta u - \frac{1}{3}\Delta\sigma_a$

[5] Some of the findings of Bishop et al. (1975) are discussed in Section 2.4.2

cut from the oedometer specimen and reconsolidated anisotropically in the triaxial cell to σ'_{ac} = 20 MPa (corresponding to an OCR = 1.6) before being sheared undrained. A comparison of very limited results from triaxial tests performed on the resedimented material and on the natural clay shale shows that while the undrained strengths were somewhat similar for the two materials when compared at the same porosity, the stress-strain responses were very different. The resedimented material behaved in a purely ductile manner with ε_f of almost 5% while the intact natural clay shale behaved in a brittle manner with ε_f varying from 0.4% to 2.4% and increasing with stress level. It should be noted that ε_f of 5% is extremely large even for resedimented clay at an OCR of 1.6. In addition to the differences in stress-strain response, the resedimented specimens showed a pronounced barrel shape when dismounted from the triaxial cell after shearing with little sliding along a slip surface. On the other hand, for the intact natural specimens most of the displacements after the small strain failure took place along one or two very distinct slip surfaces. This type of shear deformation reported by Berre has also been found to occur in many other natural clay shales (e.g. Petley (1999) & Petley et al. (1993)). Berre concluded that the artificial clay shale may be considered as an uncemented version of the natural clay shale.

Yassir (1989) carried out an investigation into the undrained shear behaviour of several resedimented soils from mud volcanoes. A clay obtained from a mud volcano in Taiwan was tested for σ'_{ac} up to 68 MPa. This clay had a clay fraction of approximately 29%, w_L = 32% and I_p = 13%, resulting in a USCS classification of CL (low plasticity clay). Since it was obtained in a completely remolded state, it contained little or no cementation bonding. The samples tested were prepared by consolidating a vacuumed slurry in an oedometer to σ'_p = 2.45 MPa. Triaxial specimens were then trimmed from the oedometer specimen and reconsolidated in the triaxial cell to a consolidation stress higher than the batch σ'_p. All specimens were normally consolidated prior to undrained shear. A peak shear strength was not observed in any of the anisotropically consolidated tests and the clay behaved in a completely ductile fashion, maintaining maximum deviatoric stress without significant strain weakening for axial strains up to 16%, as shown in Figure 2-9. Note the large difference in stress-strain response for specimens TA and TF which were isotropically consolidated to σ'_{ac} = 50 and 5 MPa respectively compared to specimens TC, TD and TE which were anisotropically consolidated (with K = 0.6) to σ'_{ac} = 68, 20 and 34 MPa (p'_m = 50, 15 and 25 MPa) respectively. Figure 2-10 shows the corresponding undrained effective stress paths for the tests in Cambridge stress space. It can be seen that the shape of the stress paths followed by the anisotropically consolidated specimens is quite different from that typically expected for NC clay, e.g. by comparison with Figure 2-1 or Figure 2-3 for tests carried out by Amorosi and Rampello (2007) and Abdulhadi (2009) respectively. Similar to the findings of Abdulhadi (2009), Yassir reported a failure envelope having marked curvature, with φ'_{mo} (assuming c' = 0) decreasing from 26.1° for test TF

(σ'_{ac} = 5 MPa) to 22.6° for test TC (σ'_{ac} = 68 MPa). A line drawn through the end points of the tests at lower stresses in Figure 2-10 is used to illustrate the curvature of the failure envelope. Pore pressures increased initially during undrained shear after which they remained approximately constant, thereby indicating critical state having been achieved.

The normalized undrained shear strengths found by Yassir (1989) vary very little over the entire stress range investigated, ranging between just 0.24 to 0.25 for the anisotropically consolidated tests, with no clear trend with stress level. This is in contrast to the findings of Abdulhadi (2009) and may be related to the fact that Yassir used a constant K = 0.6 for all anisotropically consolidated tests. Recall that Abdulhadi employed K_O consolidation and found K_{ONC} to increase with increasing consolidation stress as normalized undrained strength decreased. Significantly, however, similar to the findings of Abdulhadi (2009), Yassir did find a clear decrease in normalized excess pore pressures with increasing consolidation stress. Figure 2-11 illustrates this trend for both the isotropically and anisotropically consolidated tests (keep in mind that Figure 2-11 plots excess pore pressure u_e normalized with respect to the pre-shear mean consolidation stress p'_o while Figure 2-8 by Abdulhadi (2009) plots shear induced pore pressure u_s normalized with respect to the pre-shear axial consolidation stress σ'_{ac}). The decrease in normalized excess pore pressures indicates an increasingly dilative shear response with increasing stress level. Yassir claimed that this is due to the decrease in void ratio as the clay consolidates. Yassir also concluded that there is strong evidence to suggest that the behaviour of a sediment changes with increasing stress level.

2.3 EFFECTS OF DIAGENETIC CEMENATATION ON BEHAVIOUR

2.3.1 Introduction

Diagenesis refers to chemical and mechanical processes which affect both the physical and mineralogical composition of sediments from the time of their deposition but prior to the onset of metamorphism. A common diagenetic process in clays involves the gradual breakdown of smectite to illite which is a well known occurrence in sedimentary basins. One of the most significant diagenetic processes which occurs in both cohesive and granular soils involves the cementation of soil particles from the precipitation of calcium carbonates, aluminum and iron hydroxides, silicates as well as other organic or inorganic compounds at interparticle contacts. Cementation is regarded as a form of natural micro-structure and can have a major effect on the properties of soils including void ratio, initial shear modulus, apparent preconsolidation and shear strength (Gutierrez et al., 2008). It is also regarded a possible cause of 'true' cohesion for soils. Cementation is a particularly important phenomenon influencing the behaviour of natural cohesive soils which exist at high in situ effective

stresses. Because of their diagenetic history, these materials are more difficult to characterize and their behaviour much more difficult to predict than soft clays.

2.3.2 Classification of Cohesive Materials

Before proceeding any further it is important to clarify the terminology used to describe and classify cohesive materials in general. The materials referred to in this section lie in a transitional regime between hard clay and soft ductile argillaceous rock. This transitional nature has lead to great confusion and researchers neither in soil mechanics, rock mechanics nor geology have succeeded in adopting a consistent classification scheme for these materials. For example, while one author may refer to a material simply as shale, others may refer to the same material as clay, clay shale or mudstone. For clarification, the following descriptions are given based on definitions suggested by Stokes and Varnes (1955):

Shale: A general term for lithified clays and silts which are *fissile* and break along planes parallel to the original bedding.

Clay shale: A shale that consists primarily of clay minerals.

Claystone: Now used mainly to designate clay which has become indurated by some means, e.g. due to cementation. It is the same as *clay rock* and is sometimes used to designate concretionary masses found in clay deposits. Unlike shale, claystone does not necessarily possess significant fissility.

Mudstone: Mudstone (sometimes mudrock) is a generic term for all fine-grained sediments and includes clay, silt, siltstone, claystone, shale and argillite. It should be used when there is doubt as to precise identification or when a deposit consists of a mixture of clay, silt and sand sized particles.

While the above descriptions are helpful, they are by no means definitions which all in the geology and engineering professions follow. A good review of the various geological and engineering classification schemes which have been proposed for cohesive materials over the years is given in William (2007). To add to complication, the terms clay and silt also have more than one definition:

Clay:

Definition 1: Under the USCS classification system, a soil whose Atterberg Limits (ASTM D4318) cause it to be plotted above the 'A' Line in the Casagrande Plasticity chart (Lambe and Whitman, 1969).

Definition 2: A soil which, by weight, more than 50 % of its particles are smaller than 0.002 mm

Definition 3: A soil consisting primarily of clay minerals, e.g. smectite, illite, kaolinite.

Silt:

Definition 1: A soil which, by weight, consists primarily of particles in the size range 0.075 -0.002 mm

Definition 2: A soil which, by weight, more than 50 % of its particles are smaller than 0.075 mm and whose Atterberg Limits cause it to be plotted below the 'A' Line in the Casagrande Plasticity chart.

It is therefore necessary for the author to adopt some reasonable terminology which can be used consistency throughout this literature review. Since the research presented in this thesis focuses on the mechanical behaviour of resedimented clay at relatively high stresses, this material will be regarded by the author as 'hard clay' (with clay being defined using Definition 1 above). This is in accordance with the classification scheme proposed by Terzaghi and Peck (1967) for clays exhibiting an undrained strength s_u > 0.2 MPa. The same designation will be used for natural clay subjected to high stresses but not possessing significant cementation, such as London Clay for example. In addition, uncemented clay subjected to densification under high pressures may also be referred to as a 'compaction shale' (H.H. Einstein, personal communication).

As mentioned previously, many of the past studies on the mechanical behaviour of cohesive materials at relatively high stress levels have been carried out on intact samples. These intact samples often possess varying degrees of cementation due to diagenesis and are usually referred to by the authors simply as shale or clay shale. While it is possible that many of these materials do possess significant fissility, it seems likely that some do not and would therefore be better classified generally as a mudstone. However, for the purpose of consistency and simplicity, the author will use the term 'clay shale' throughout this literature review when referring to these materials.

2.3.3 Apparent Preconsolidation

Cementation is often attributed to causing an increase in the preconsolidation stresses of sediments well above that caused by mechanical compression. In fact, for older sediments that have been subjected to high stresses as a result of burial at a great depth, diagenetic processes such as cementation can be a much more significant cause of overconsolidation than mechanical processes, e.g. due to increased overburden pressure. This increase in overconsolidation due to non-mechanical processes such as cementation is often referred to as 'apparent' or 'quasi' preconsolidation (Gutierrez et al., 2008). The ratio of the apparent preconsolidation stress to the

current in situ effective stress is sometimes called the yield stress ratio (YSR) rather than overconsolidation ratio (OCR). It should be noted that, apart from cementation, many other natural phenomenon may cause an apparent preconsolidation to develop in a soil such as ageing (often referred to as creep or secondary compression) or desiccation caused by evaporation or freezing (Ladd, 1985).

2.3.4 Stress-Strain Response during Shear

Diagenetic cementation also has a major effect on the stress-strain-strength properties of cohesive materials by imparting a significant stiffness and brittleness that would not otherwise exist. In comparison to the behaviour of OC resedimented clay as discussed earlier, OC clay shales at the same stress level exhibit an extremely brittle behaviour characterized by a well defined peak strength and large amounts of post-peak strain softening (Berre 1992, Horseman et al. (1993), Taylor and Coop (1993), Petley et al. 1993, Marsden et al. 1992). On the other hand, NC clay shales (i.e. produced by consolidating a clay shale well beyond its apparent preconsolidation stress) show a ductile response with a less well defined peak strength, much less post-peak strain softening and contractive behaviour similar to that exhibited by NC resedimented clay. Figure 2-12 shows normalized shear stress-strain responses for intact samples of Kimmeridge Shale and Barents Sea Shale subjected to CIUC tests by Gutierrez et al. (2008). The apparent preconsolidation stresses for the Kimmeridge Shale and Barents Sea Shale were estimated to be 22 MPa and 40 MPa respectively. The general trend seen in each case is that as the consolidation stress increases, i.e. OCR decreases, brittleness decreases as post-peak strain softening and stiffness are reduced.

The observed behaviour of clay shales described in the preceding paragraph can be attributed to a brittle-ductile transition in the stress strain response. This is a well known phenomenon in the field of rock mechanics (e.g. Paterson & Wong, 2005). Though less well understood for clay shales, work has been carried in this area as well as on the deformation and fabric changes induced in these materials due to high pressure consolidation and shear by Petley et al. (1993) and Petley (1999). Figure 2-13 illustrates conceptually the different types of stress-strain response observed in clay shales. At relatively low consolidation stresses the shear stress-strain response is brittle in nature with a distinct peak strength followed by strain softening to a post-rupture strength. Brittle failure occurs rapidly once the stresses at certain inter-particle contacts reach the bond strength and a de-bonding process is initiated. Failure of a triaxial specimen occurs along one or two very distinct slip surfaces, or failure planes, with large deformations occurring along these slip surfaces. The slip surfaces are seen to be at the centre of a shear zone in which the original bonded structure is progressively re-oriented causing the platy clay particles to become

increasingly aligned parallel to the surface. This realignment of clay particles increases with increasing shear strain. On the other hand, at higher stresses where the yield strength of the bonded structure has been exceeded during consolidation, the response is ductile with peak strength being maintained for the accumulation of large strains. The specimen deforms pervasively in a pronounced barrel shape with no slip surface generally being present. At intermediate stresses a transitional regime exists in which the response is a combination of ductile behaviour, during which a peak strength is maintained up to a certain strain, followed by brittle behaviour, during which failure and strain weakening occur. During the maintenance of peak strength the specimen undergoes pervasive micro-fracturing and is thus behaving in a ductile manner on the macro-scale and in a brittle manner on the micro-scale. Brittle failure occurs as a result of the creation of a single slip surface caused by the coalescence of micro-cracks formed during the ductile phase. Once this occurs the shear strength along the slip surface quickly drops to the post-rupture value (Petley, 1993). After increasing initially as deviatoric stress increases, pore pressures remain approximately constant during the ductile phase. An excellent example of the brittle-ductile transition experienced by two clay shales is given in Figure 2-12 (keep in mind that Figure 2-12 plots *normalized* shear stress versus axial strain).

2.3.5 Failure Envelopes

Factors such as natural micro-structure, OCR and stress level allow several failure envelopes to be defined for a cohesive material. Burland (1990) reviewed the behaviour of different natural and resedimented clays and indicated that the peak undrained strength of undisturbed natural clays is often significantly greater than that of the corresponding resedimented material at the same void ratio due to the effects of natural micro-structure. Burland concluded that four fundamental failure envelopes may be defined for clays: 1) a peak strength envelope defining brittle failure of undisturbed natural OC clays; 2) a post-rupture strength envelope representing the end of rapid post-peak strain softening of undisturbed natural OC clays; 3) an 'intrinsic' critical strength envelope defined by resedimented samples; and 4) a residual strength envelope reached only after very large strains. The four failure envelopes defined by Burland (1990) are shown in Figure 2-14. The peak strength envelope is curved, shows a cohesive intercept and lies above the intrinsic critical state envelope due to the influence of natural micro-structure possessed by undisturbed OC clay. On the other hand, undisturbed NC clay (i.e. natural clay which possesses no mechanical or apparent preconsolidation) will tend to fail on the intrinsic critical state envelope and then travel down this envelope. The intrinsic critical state envelope may be interpreted as a basic property independent of the undisturbed state of the material and can be viewed as providing a good basis for comparison of the properties of different clays. The post-rupture envelope can be seen to lie very close to the

intrinsic critical state envelope. After very large shear strains both undisturbed and resedimented clay will reach a common residual strength envelope as the platy clay particles become aligned parallel to a shear surface, such as can be attained in a ring shear device.

Petley (1999) reviewed the undrained shear behaviour of some resedimented and natural hard clays and clay shales and proposed an extension to the work of Burland (1990) to include the behaviour of these materials for mean consolidation stresses up to 50 MPa. The conceptual form of the failure envelopes proposed by Petley (1999) is shown in Figure 2-15 (it should be noted that what Petley (1999) refers to as the 'residual' strength envelope in Figure 2-15 is in fact the intrinsic critical state envelope under Burland's (1990) definition. A true residual strength envelope is not considered by Petley (1999)). The brittle failure envelope (i.e. the 'peak strength' envelope under Burland's terminology) is initially approximately linear with a cohesive intercept but reduces in gradient with increasing consolidation stress. This reduction in gradient is believed to be due to the brittle-ductile transition as micro-cracking prevents the material from reaching higher peak strengths during shear. The gradient of the brittle failure envelope eventually decreases such that it intersects the intrinsic critical state envelope at which point behaviour is purely ductile. The stress level at which these envelopes intersect will likely depend on the degree and strength of natural micro-structure which the material possesses as indicated by the magnitude of the [apparent] preconsolidation stress, with strongly structured soils showing a distinct peak strength up to relatively high stresses. After brittle failure the undisturbed material will strain weaken to the post-rupture envelope. The form of the post-rupture envelope is poorly understood and difficult to define but evidence suggests that it has non-linear form at high stresses. For relatively low consolidation stresses, undisturbed natural OC clays and clay shales do not reach the intrinsic critical state envelope except at large strains. However, at relatively high consolidation stresses, when many of the inter-particle bonds have been broken down and the material enters the NC range, the peak strength envelope coincides with the intrinsic critical state envelope. Based on the work of Yassir (1989), Petley concluded that the intrinsic critical state envelope is linear for mean consolidation stresses up to at least 50 MPa. However, as mentioned previously, Yassir (1989) found that slope of this envelope decreases slightly with stress level. Moreover, the findings of Abdulhadi (2009) now seem to give strong indication that the intrinsic critical state envelope is in fact also non-linear.

2.4 NORMALIZED BEHAVIOUR

2.4.1 Introduction

The Normalized Soil Parameter concept is based on the empirical observation that clay samples having a similar OCR but different consolidation stresses, and therefore different preconsolidation pressures, exhibit similar properties (e.g. undrained strength, shear induced pore pressures) when normalized with respect to the consolidation stress. This has led to the SHANSEP (Stress History and Normalized Soil Engineering Properties) design procedure developed by Ladd and Foott (1974). The Normalized Soil Parameter concept is also the basis for other frameworks which describe soil behaviour such as Critical State Soil Mechanics (Schofield and Wroth, 1968), or analytical models such as Modified Cam Clay (Roscoe and Burland, 1968) and MIT-E3 (Whittle and Kavvadas, 1994).

The SHANSEP normalization procedure is generally applied to undrained shear in triaxial compression (TC) and extension (TE), plain strain compression (PSC) and extension (PSE) and direct simple shear (DSS). Figure 2-16 shows typical results of a SHANSEP test program performed on AGS Plastic Marine Clay in TC, TE and DSS, which can be represented using an expression commonly referred to as the SHANSEP equation:

$$s_u/\sigma'_{vc} = S(OCR)^m \qquad \text{Equation 2-1}$$

where S is the undrained strength ratio for NC clay and m is the slope of the regression line. The difference in behaviour for the three modes of shearing is a reflection of the anisotropic nature of soil. Figure 2-17 from Ladd (1991) shows normalized undrained strengths (S values) in TC, TE and DSS as a function of plasticity for a large number of NC clays and silts. Note that axial stress in triaxial space now corresponds to vertical stress in the SHANSEP design procedure (where σ'_{vc} is vertical consolidation stress). The procedure should ideally only be applied to tests involving K_O consolidation. While the use instead of isotropic consolidation is generally believed to have a small impact on the measured undrained strength of intact OC specimens, for resedimented specimens or for intact specimens consolidated well into the NC range when the yield surface changes, K_O consolidation prior to shearing is especially important.

2.4.2 Effect of Stress Level on Normalized Strength

The underlying assumption of SHANSEP is that normalized behaviour is only dependent on OCR. Thus, while the pre-shear stresses used in the laboratory testing program may be different to the in situ stresses, the method predicts identical behaviour for a given OCR. However, the work of

Abdulhadi (2009) shows clearly that normalized properties can have a stress level dependence. Figure 2-18 by Abdulhadi illustrates the effect of stress level on the SHANSEP S and m parameters for RBBC in triaxial compression. Although the regression line for each stress level only contains three data points, excellent conformity of the data is illustrated by regression coefficient (R^2) values greater than 0.998 in each case. It can be seen that the S parameter decreases consistently with increasing consolidation stress from 0.314 at σ'_p = 0.2 MPa to 0.281 at σ'_p = 10 MPa. On the other hand, the m parameter varies only slightly, ranging from 0.770 to 0.738, and does not appear to be dependent on stress level. This observation would seem to indicate that the effect of increasing stress level on undrained strength is the same for all OCR. A value of 0.314 for the S parameter is consistent with results obtained previously by other researchers who investigated RBBC in triaxial compression at low stresses, e.g. Sheahan (1991) and Santagata (1994). However, the m parameter reported by Abdulhadi (2009) is slightly higher than previously quoted values. This is believed to be due the fact that values of m in the past were determined by matching data points from tests at different stress levels (i.e. higher OCR tests were consolidated to higher values of σ'_p). It could be said that while the effect of stress level on the SHANSEP parameters is relatively small in the range of stresses commonly encountered in geotechnical engineering (see Figure 2-17 for perspective on how S changes due to plasticity and mode of shear), over a much wider range of stresses it becomes more significant. Recall from Section 2.2 that increasing stress level also affects normalized stiffness and normalized shear induced pore pressures, as shown in Figure 2-7 and Figure 2-8 respectively.

The above finding by Abdulhadi (2009) of a reduction in normalized strength with increasing stress level can also be seen by studying work carried out on resedimented clay by other researchers. Moniz (2009) performed CK_OUE triaxial tests for σ'_{ac} up to 2 MPa and Ahmed (1990) performed a series of CK_OUDSS tests for σ'_{ac} up to 1.2 MPa. Both studies were carried out on NC RBBC and consistent trends of decreasing normalized strength with increasing stress level were also observed in these modes of shear.

As mentioned previously, one of the earliest programs of triaxial testing at relatively high stresses is that of Bishop et al. (1965) who conducted CIUC tests on London Clay for σ'_{ac} up to approximately 7.5 MPa. While the vast majority of these tests involved the use of intact block samples, a limited number of tests were also carried out on resedimented samples for comparative purposes. The tests on the resedimented clay were carried out in the NC range and it was found that while the undrained strength ratio for the low pressure tests varied from 0.22 to 0.24, it reduced to 0.20 for the highest pressure test. It should be kept in mind that these numbers should not be regarded as SHANSEP S parameters due to the use of isotropic consolidation. The failure envelope

for the resedimented clay (i.e. the intrinsic critical state envelope under Burland's (1990) definition) was also found to possess marked curvature, with φ'_{mo} decreasing from 21° in the low pressure range to 16.1° in the high pressure range (assuming c' = 0).

Bishop et al. (1975) conducted a series of high pressure CIUC tests on NC resedimented London Clay for σ'_{ac} up to 62.1 MPa. The tests were carried out to determine the effect of negative pore pressure on the strength of clay. This was done by comparing the results of conventional CIUC tests (referred to as confined tests by Bishop et al.) with tests where the cell pressure was removed under undrained conditions prior to shearing, thereby producing negative pore pressure but keeping the same consolidation stress (referred to as unconfined tests by Bishop et al.). Figure 2-19 shows a graph of undrained strength plotted against consolidation stress where the slope of the graph is equal to the undrained strength ratio. Disregarding the results for the unconfined tests, a definite reduction in the slope of the graph at high consolidation stresses for the confined tests indicates a decreasing normalized undrained strength. Once again, however, due to the isotropic consolidation of specimens, the slope of the graph at a given point should not be regarded as the SHANSEP S parameter. It should also be pointed out that these tests were conducted without back-pressure and as a result full saturation of the specimens prior to shearing is not certain. Pore pressure measurements were not taken during the tests and so the undrained pore pressure response of the clay is unknown. In addition, the specimens were sheared very quickly at an axial strain rate of 2% per minute. Combined, these factors reduce the relevance of the tests to the research presented in this thesis.

Jones (2010) performed a series of CK_OUC triaxial tests on Resedimented Ugnu Clay from Northern Alaska for σ'_{ac} up to 10 MPa. Figure 2-20 shows the variation in normalized undrained strength of the soil with stress level at OCR = 1. It can be seen that there is a relatively consistent trend of decreasing normalized undrained strength with increasing stress level (the results of the test at σ'_{ac} = 0.69 MPa would appear to be anomalous). Similar to Abdulhadi (2009), Jones reported that the decrease in normalized strength of the soil corresponds to an increase in the pre-shear K_{ONC} with increasing consolidation stress. In addition, the intrinsic failure envelope of the clay was found to have significant curvature, with φ'_{mo} decreasing from 35.1° at σ'_{ac} = 0.2 MPa to 23.6° at σ'_{ac} = 9.8 MPa (assuming c' = 0).

It is important to keep in mind that the results mentioned above from Moniz (2009), Ahmed (1990), Bishop et al. (1965), Bishop et al. (1975) and Jones (2010) were all limited to the NC range of the soils tested. Only Abdulhadi (2009) examined the effect of stress level on normalized strength in the OC range.

2.4.3 SHANSEP versus Recompression

It is important to distinguish between using SHANSEP as a *normalization* procedure, i.e. demonstrating that clays at the same OCR display similar normalized properties, and the SHANSEP *reconsolidation* technique used in the laboratory to create a desired stress history prior to shearing. The SHANSEP reconsolidation technique is illustrated in Figure 2-21. The desired stress history is achieved by K_O consolidation well past the in situ σ'_p into the virgin compression range to a new maximum stress 1.5 - 2 greater than σ'_p (points A and B in Figure 2-21). For OCRs greater than unity, the specimen is mechanically overconsolidated by K_O swelling (points C and D in Figure 2-21). The SHANSEP reconsolidation technique is applicable to clays that are close to being normally consolidated or have been mechanically overconsolidated (i.e. possess a true preconsolidation as opposed to only an apparent preconsolidation) and maintain the same basic structure once consolidated beyond the in situ σ'_p. The method is therefore ideal for resedimented samples. However, the method is not applicable to sensitive clays or clay shales possessing significant cementation since laboratory consolidation past the in situ σ'_p will result in a significant destruction of natural micro-structure. For these materials the undrained strength measured using the SHANSEP technique will be much lower than the in situ value (Ladd, 1991).

Another common reconsolidation procedure used to determine in situ shear strengths from laboratory testing is the Recompression technique (Bjerrum, 1973). As illustrated in Figure 2-21, this technique involves laboratory K_O reconsolidation of an intact specimen back to the in situ vertical effective stress (σ'_{vo}) before shearing. However, due to sampling disturbance, the water content of the intact specimen reconsolidated to σ'_{vo} will invariably be somewhat lower than the in situ value, thereby resulting in an overestimation of the in situ strength. The validity of the technique therefore depends on the degree of sampling disturbance which the sample was subjected to and the resulting water content reduction during laboratory reconsolidation. As such, the technique is favoured more if large diameter or block samples are available. Recompression should never be used for samples close to being normally consolidated since the significant reduction in water content at $\sigma'_{vo} \sim \sigma'_p$ would give unrealistic strength results. The technique is more appropriate for sensitive and cemented materials whose structure would be destroyed if the SHANSEP reconsolidation procedure were used. The Recompression technique is also more appropriate for highly overconsolidated samples since the larger pressures required by the SHANSEP technique in the laboratory may make it difficult to employ. In addition, evidence suggests that, when compared to Recompression, the use of the SHANSEP reconsolidation technique may result in an underestimation of the stiffness of natural OC clay, as shown in Figure 2-22 for Boston Blue Clay.

2.4.4 Normalized Behaviour of Clay Shales

Gutierrez et al. (2008) attempted to apply the SHANSEP normalization procedure to clay shales. Data on 25 different natural clay shales having varying degrees of cementation was compiled and it was concluded that SHANSEP may be applicable to these materials. Figure 2-23 shows the SHANSEP normalization procedure applied to four individual clay shales. All of the shales included in the study have a clay content greater than 50% based on clay mineralogy and the values of porosity range from 62.5% for Fuller's Earth to about 15% for Barent's Sea Shale. Due to the highly anisotropic mechanical behaviour of clay shales caused by their distinct lamination and fissility, Gutierrez et al. highlighted that the results were strictly limited to the case of triaxial compression with the axial stress normal to the direction of bedding.

It is important to note that Gutierrez et al. (2008) only applied the normalization aspect of SHANSEP. Since the SHANSEP reconsolidation technique would be entirely inappropriate to apply to intact specimens of natural clay shales possessing significant diagenetic cementation, Recompression was used to reconsolidate the test specimens prior to shearing in all cases. However, as mentioned previously, Recompression will result in an overestimation of undrained shear strength for NC and low OCR samples due to a reduction in water content caused by sampling disturbance. In addition, unlike true Recompression which requires K_O consolidation, the majority of the tests compiled in the study by Gutierrez et al. (2008) likely involved isotropic consolidation with only limited testing involving K_O or even anisotropic consolidation. While the use of isotropic consolidation in the laboratory is generally believed not to have a major impact on the measured undrained strength of intact samples in the OC range, where the majority of the tests were indeed performed, the effect of isotropic consolidation would certainly more pronounced in the NC range. Although Gutierrez et al. claim a good correlation between normalized undrained strength and OCR, thereby confirming the applicability of SHANSEP, the quoted R^2 values would seem to indicate that the correlation is by no means as good as for uncemented clays. In addition, the SHANSEP S parameters quoted for various clay shales, e.g. in Figure 2-23, are very much larger, and the m parameters vary over a much wider range, than values typically quoted for soft clays, e.g. by Ladd and Foott (1974). It is likely that to some extent this is due to the combined effects of sampling disturbance and isotropic consolidation. Both of these influences are more pronounced in the NC range, thereby reducing the validity of both the measured SHANSEP S parameter as well as the m parameter.

Interestingly, Gutierrez et al. (2008) concluded from the study that the normalization of undrained strength is valid regardless of the cause of the preconsolidation of the material. Thus, the normalized behaviour predicted by SHANSEP can be used without the need to determine the separate contributions of mechanical overconsolidation and diagenetic cementation on the apparent

preconsolidation stress. The term preconsolidation stress σ'_p could therefore be used without regard to the underlying mechanism causing overconsolidation and it is this definition of preconsolidation stress which Gutierrez et al. (2008) used to define all quoted values of OCR. This is in contrast to Burland (1990) who recommended that the term yield stress, or more precisely vertical yield stress σ'_{vy}, be used while the term preconsolidation pressure should be reserved for situations where the magnitude of such a pressure can be established by geologic means.

2.5 SPECIMEN NON-UNIFORMITY IN TRIAXIAL COMPRESSION

2.5.1 Introduction

One of the major shortcomings of the conventional triaxial test is stress and strain non-uniformity through the specimen during shearing. As a triaxial specimen is sheared axially in either drained or undrained compression, radial strains are produced as the specimen increases in cross-sectional area. However, due to end restraint caused by using fixed ends, i.e. the ends of the specimen are restrained from radial deformation by rough porous stones, these radial strains are not uniform throughout the height of the specimen. Radial strains are greatest in the middle of the specimen and zero at the ends. Since a triaxial specimen is assumed to be a uniform element of soil, these non-uniform radial strains detract from the elemental assumption. Figure 2-24 shows how conical 'dead' zones (Rowe and Barden, 1964) are created within which end restraint affects the stress state. This influence is greatest at the ends and decays with increasing distance from the ends. The middle third of the specimen is believed to be largely unaffected by end restraint (assuming no pore water migration occurs), has the most uniform stress state and is where the axial and radial stresses most closely duplicate the corresponding applied stresses. In a conventional triaxial apparatus pore pressures measured in the base of the specimen are in the dead zone.

Based on elastic analysis (Poulos and Davis, 1974), the effect of end restraint caused by fixed ends on the stress state in a triaxial specimen is shown diagrammatically using Mohr's Circles of stress in Figure 2-25. During shearing, end restraint increases the confining stress σ_3 near the ends which results in a higher total octahedral stress and a lower maximum shear stress. Depending on the pre-shear stress history of the soil, this results in a different pore pressure response being produced at the ends than at the middle of the specimen in undrained tests. Pore pressure gradients are therefore setup which in turn can lead to pore water migration between the ends and middle of the specimen. In the case of drained tests, the non-uniform stress state caused by end restraint may cause significant changes in the measured volume change behaviour, especially in the case of highly dilatant materials. End restraint could also encourage the development of slip surfaces in a

triaxial specimen. The effects of specimen non-uniformity on undrained triaxial compression results are discussed further below.

2.5.2 Implications of Specimen Non-Uniformity in Undrained Triaxial Compression

(i) *Pore pressure measurements*

The increase in total octahedral stress $\Delta\sigma_{oct}$ produced by end restraint will result in a corresponding increase in pore pressure equal to $B\Delta\sigma_{oct}$, where B is Skempton's pore pressure parameter (Skempton, 1954). For NC clay the decrease in shear stress at the ends will, however, also result in a lower shear induced pore pressure. As a result, the difference between pore pressures at the middle and at the ends of the specimen is minimized by compensating effects for NC clay. On the other hand, for heavily OC clay the decrease in shear stress at the ends will instead result in a higher shear induced pore pressure, and a potentially much larger pore pressure may be generated at the ends as compared to the middle of the specimen. Since pore pressures are generally measured at the base of a triaxial specimen, the misleadingly high pore pressures measured for OC clay lead to reported values of c' that are too high and values of φ'_{mo} that are too low. It should be noted, however, that the measured s_u is hardly affected (Germaine and Ladd, 1988).

Barden and McDermott (1965) have shown that, in addition to axial pore pressure gradients, significant radial pore pressure gradients can also occur at the base of large diameter triaxial specimens. However, these radial pressure gradients are generally less significant than the axial pressure gradient, this being especially true if the triaxial specimen has a height to diameter ratio of 2 or more.

(ii) *Pore water migration*

One obvious solution to the problem of pore pressure gradients setup during shearing of a triaxial specimen with end restraint is to run the test at a sufficiently slow strain rate such that pore pressure equalization can occur throughout the specimen. However, while such an approach will result in the correct determination of the failure envelope defined by c' and φ'_{mo}, pore pressure equalization requires that pore water must redistribute within the specimen as it flows from the ends towards the middle. As a result, because stress-strain characteristics are predominantly controlled by the material in the middle portion of the specimen (Germaine and Ladd, 1988), the increase in water content in this region will lead to a lower (and incorrect) s_u. This is a particular problem for heavily OC clays where significant pore water migration occurs due to the higher pore pressure

gradients setup within a specimen. Richardson and Whitman (1963) observed a classic case of such migration in CIUC tests on OCR = 16 specimens of high plasticity resedimented Mississippi Valley Alluvial Clay. In slow tests pore water migration occurred such that the water content in the middle of the specimens was significantly higher than at the ends when measured after the tests, as shown in Figure 2-26.

In order to measure the strength parameters of a heavily OC clay using a conventional triaxial apparatus with fixed ends, one is therefore required to run tests at both slow and fast strain rates. A fast strain rate prevents significant pore water migration which allows for the correct measurement of s_u but an incorrect measurement of c' and φ'_{mo}. Tests with a slow strain rate, where pore water migration occurs, are then required to obtain correct values of c' and φ'_{mo}. This is illustrated in Figure 2-27 by Germaine and Ladd (1988).

Whether or not a test can be regarded as 'slow' or 'fast' depends on the strain rate used relative to the rate at which pore pressures can equilibrate within the specimen. The rate of pore pressure equilibration in turn depends on the drainage conditions and geometry of the specimen as well as the on coefficient of consolidation of the soil. The classic work in this area is that of Bishop and Henkel (1962) who propose the following theoretical relationship to ensure 95% pore pressure equilibration within specimens during undrained shearing:

$$t_{95} = \frac{T_{95} H_d^2}{c_v} \qquad \text{Equation 2-2}$$

where: t_{95} = time to the point of concern in the test. This is generally taken to be the point of peak shear strength

c_v = is the vertical coefficient of consolidation of the soil

H_d = the drainage height of the specimen

T_{95} = time factor corresponding to 95% equilibration of pore pressures. For the case of end drainage only T_{95} = 1.67

In general, therefore, a test can be regarded as slow if the undrained shear strength is reached after t_{95}.

It is also important to keep in mind that, as will be discussed in Chapter 3, strain rates in of themselves can also play a significant role in the undrained shear behaviour of soil. However, for simplicity, the current discussion is restricted to the hypothetical case of rate-independent soil.

(iii) *Development of slip surfaces*

Slip surfaces, as mentioned previously in Section 2.3.4, are planes of concentrated strain which often form in triaxial specimens and almost always in OC specimens. In compression tests the formation of a slip surface is influenced by the boundary conditions as well as localized areas of weakness within intact specimens. The location of slip surfaces can vary but they generally intersect one or both ends of the specimen. Interpretation of results from tests in which slip surfaces occur is a matter of uncertainty since, once a slip surface develops, the complexity of the stress and strain fields around it then makes analyzing the specimen as a simple element practically impossible. Analysis of data relative to the slip surface must consider various complications such as localized membrane and filter paper resistance, changes in the contact area along the slip surface and the influence of lateral loading on both the specimen and piston. Results obtained prior to the visible formation of a slip surface are generally assumed to be reasonable when computed using the assumption of a uniform strain field. However, it is likely that a slip surface begins to develop long before becoming visible, raising doubts as to at what point the specimen began to significantly deviate from a condition of uniform strain. It is also not clear if the development of a slip surface significantly changes the strength or effective stress parameters measured prior to its visible formation (Germaine and Ladd, 1988).

As discussed in Section 2.3, it is generally believed that during shearing NC clay should deform in a homogenous fashion without the development of slip surfaces. However, in the experimental program carried out by Abdulhadi (2009) on RBBC it was found that while the low pressure CK_OUC tests on NC clay involved only bulging of the specimens with no discernable strain localization, tests carried out for $\sigma'_{ac} > 4$ MPa were found to form slip surfaces. Figure 2-28 shows a picture of 2 NC RBBC specimens after shearing illustrating the different modes of failure for the low and high pressure tests. It is interesting to note, however, that no significant change in the observed undrained shear behaviour could be detected between tests in which slip surfaces did and did not develop. Amorosi and Rampello (2007) tested anisotropically consolidated Vallericca clay for σ'_{ac} up to 6.75 MPa and reported slip surfaces occurring in NC specimens. Several experimental methods including the observation of measurements from local strain transducers, comparing the output from internal and external load cells as well as comparing pore pressures measured at the base and mid-height of specimens, allowed the onset and full development of slip surfaces to be examined. Amorosi and Rampello found that for the OC specimens strain localization began prior to the peak strength being reached, with a slip surface intersecting the specimen boundaries at the point corresponding to the peak strength. For the NC specimens on the other hand, strain localization did not begin until the peak strength had been reached and proceeded with subsequent strain softening. Complete development of a slip surface was achieved only when the failure envelope had been

reached. These results are illustrated in Figure 2-1. Burland (1990) reported slip surfaces occurring in NC specimens of anisotropically consolidated kaolin which were subjected to undrained shear at conventional low stresses. Local strain transducers were used on the specimens and, similar to the findings of Amorosi and Rampello (2007), it was found that a slip surface would not develop fully until well after the peak strength had been reached and the failure envelope had been encountered. This is in contrast to the behaviour of OC specimens of Todi Clay for which Burland reported that the full development of a slip surface coincided with the peak strength. Unfortunately, Abdulhadi (2009) did not employ any experimental techniques to examine the development of slip surfaces in specimens during shearing.

The experimental studies mentioned above by Abdulhadi (2009), Amorosi and Rampello (2007) and Burland (1990) were carried out using conventional triaxial apparatuses with fixed ends (i.e. rough porous stones) and the results contradict previous knowledge regarding the deformation behaviour of NC clay (e.g. Petley et al. 1993, Berre 1992). It is possible that the non-uniform straining of triaxial specimens with end restraint may have encouraged the development of slip surfaces which would not be expected to occur had the specimens been sheared in a completely uniform fashion. Saada and Townsend (1981) refer to tests carried out on sand by Raju et al. (1972) who found that while a well-known failure plane develops in specimens of dense sand tested in compression using fixed ends, no such plane occurred if smooth ends were used. Raju et al. concluded from the study that the occurrence of this failure plane was not a property of the soil but was instead a result of the triaxial testing method used. Rowe and Barden (1964) also came to a similar conclusion, stating that the more uniform development of dilation provided using by smooth ends in drained tests results in a tendency towards multiple failure surfaces and general plastic failure, rather than the pre-mature development of a predominant slip surface.

2.5.3 Smooth End Platens

The problem of triaxial specimen non-uniformity during shearing can be prevented by using frictionless ends. Although a true frictionless condition can never actually be achieved in a triaxial cell, several researchers have used variations of smooth end platens (sometimes referred to as lubricated end platens) in order to reduce the radial stresses acting between the end platens and the specimen, thereby minimizing the intensity of the dead zones. If smooth end platens are completely effective in eliminating non-uniformities, the specimen will deform as a right cylinder and no pore pressure gradients will be generated. Table 2-2 by Germaine and Ladd (1988) summarizes the main reasons for and against using smooth ends as opposed to conventional fixed ends. While smooth ends can minimize specimen non-uniformity, they are routinely not used in most soil mechanics

laboratories. The primary practical reasons against their use are that they involve only radial specimen drainage, thereby tending to increase the time required for consolidation, as well as requiring a more complicated and timely equipment setup. The primary technical reason against the use of smooth ends is their tendency to increase system compliance at the ends leading to a less stiff system response. This is an important factor for small strain measurements in the elastic region. However, this problem can be avoided through the use of on-specimen strain transducers (Germaine and Ladd, 1988).

A review of the many variations of smooth end platens developed by researchers over the years is given in Sheahan (1991). Rowe and Barden (1964) ran tests on samples of weathered shale in an effort to examine different end platen designs and their impact on base pore pressure measurements and pore water migration. As shown in Figure 2-29, design 1 involved a steel base platen and perspex top cap, both of which were the same size as the specimen. The base pore pressure device responded almost immediately to changes in cell pressure, pore water migration was measureable and the specimens were barrel shaped at large strains. For design 2, grease was applied to the end platens of design 1 and circular membrane discs with radial slits were placed between the specimen and end platens. In this case, the base pore pressure device responded more slowly to cell pressure changes, little pore water migration was observed and at large strains the specimens remained cylindrical, buckled sideways or failed due to an end expanding. For design 3, enlarged perspex end platens were used with grease and membrane discs. Filter paper extended ~1 cm up the side of the specimen and wrapped around the base platen to a ceramic disc underneath. The measured pore pressure response in this setup was intermediate between that of designs 1 and 2, the large strain behaviour was the same as in design 2 and pore water migration was minimal.

Barden and McDermott (1965) used a variation of design 3 above by utilizing the grease and membrane discs but adding a dowel in the top platen to prevent sideways buckling as well as adding a mid-height pore pressure probe. Tests were carried out on large, partially saturated specimens of laboratory compacted clays using both fixed and smooth ends. It was concluded that the use of smooth ends markedly reduced axial and radial pore pressure gradients for axial strains up to 20% even under fast strain rates. Pore water migration as well as barreling of specimens were also minimized. A design similar to that used by Barden and McDermott (1965) was used initially by Sheahan (1991). However, Sheahan found that during K_o consolidation the grease was being squeezed out leaving a frictional interface between the latex membrane discs and brass end platens. The grease and membrane discs were therefore abandoned and the soil specimen was simply placed in direct contact with the end platens. The design of the end platens used by Sheahan (1991) is discussed further in Chapter 4.

Olsen and Campbell (1964) found no reduction in the degree of bulging in specimens of kaolin when using smooth ends compared to fixed ends but did measure a drop in φ'_p and u_s. Duncan and Dunlop (1968) noticed that, compared to tests with fixed ends, tests with smooth ends produced a lower value of E_u (likely due to system compliance at the ends), a higher ε_f and a small decrease in strength. Bishop et al. (1965) carried out a limited number of tests on London Clay from the Ashford Common site using smooth ends for comparison with the tests conducted using fixed ends. While the tests with smooth ends showed a slight drop in u_s, the effective strength parameters were not found to be significantly altered. Germaine and Ladd (1988) recommended the use of smooth ends when reliable data at large strains (say $\varepsilon_a > 15\%$) is required or for obtaining reliable pore pressure data with minimal pore water migration when testing highly overconsolidated soils at OCR > 6.

Parameter	Effect of Increasing OCR at a given σ'_{ac}	Effect of increasing σ'_{ac} at a given OCR
s_u/σ'_{ac}	increases	decreases (more pronounced at low OCR)
K_o	increases	increases
ε_f	increases	decreases
φ'_p	increases	decreases for OC, ~ no change for NC
φ'_{mo}	~ no change	decreases
u_e and u_s	decreases	decreases for OCR=1 and 2 but increases for OCR=4
A_f	decreases	increases
E_u/σ'_{ac}	increases	decreases

Table 2-1: Summary of the main findings of Abdulhadi (2009) for CK_OUC test program

Frictional Ends		Lubricated Ends	
Reasons For	Reasons Against	Reasons For	Reasons Against
• East set-up procedures	• Nonuniform stress and strain	• Improves uniformity at *all* strain levels	• More difficult to assemble
• Simple, efficient drainage	• Nonuniform excess pore pressure	• Reduces strain rate effects	• Reduces small strain precision
• Stiff apparatus for axial strain measurement	• Water migration	• Reduces uncertainty in area correction	• Increases consolidation time
• Simple cell geometry	• Larger strain rate effect	• Essential for large strain behavior	
	• Formation of rupture surfaces		

Table 2-2: Summary of reasons for and against fixed ends and smooth ends (Germaine and Ladd, 1988). Note that Germaine and Ladd refer to fixed ends as 'frictional' and smooth ends as 'lubricated'

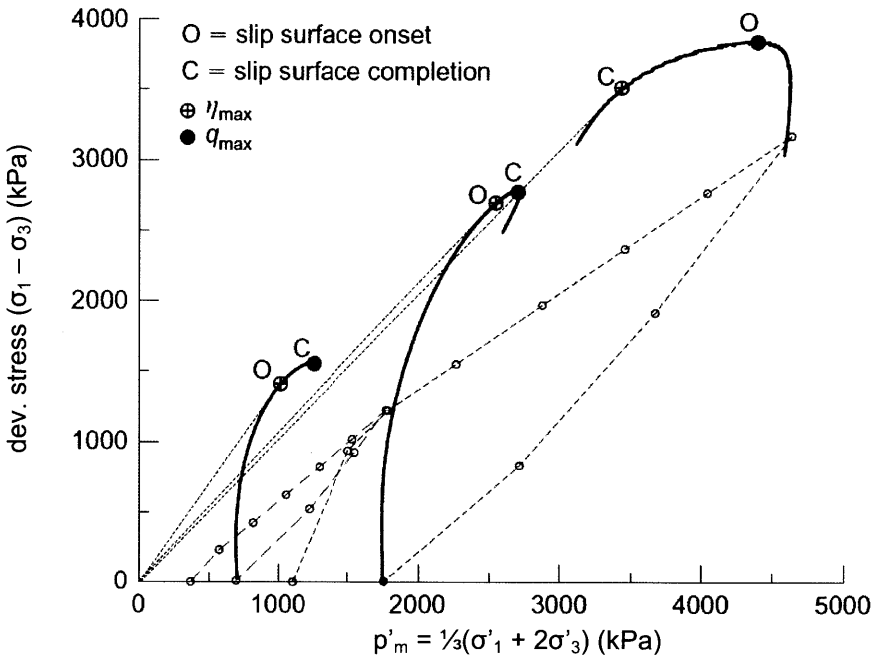

Figure 2-1: Effective stress paths (Cambridge stress space) in undrained triaxial compression for Vallericca Clay. The onset and development of slip surfaces in specimens is also shown (Amorosi and Rampello, 2007)

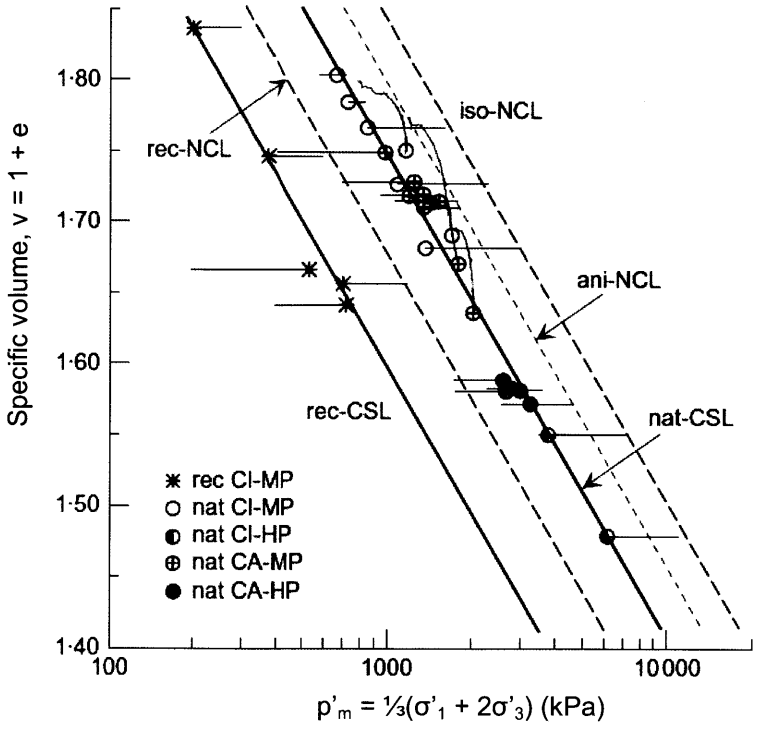

Figure 2-2: Virgin compression and critical state conditions for intact and resedimented specimens of Vallericca Clay (Amorosi and Rampello, 2007)

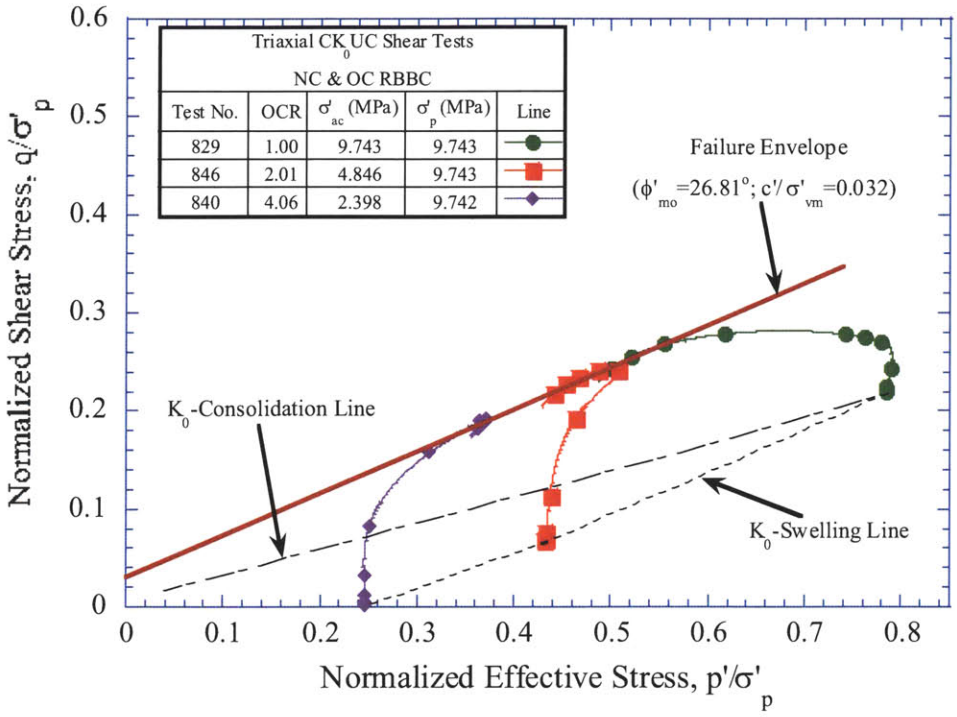

Figure 2-3: Normalized effective stress paths (MIT stress space) for RBBC at OCRs 1, 2 and 4 from CK_OUC triaxial tests with σ'_p = 10 MPa (Abdulhadi, 2009)

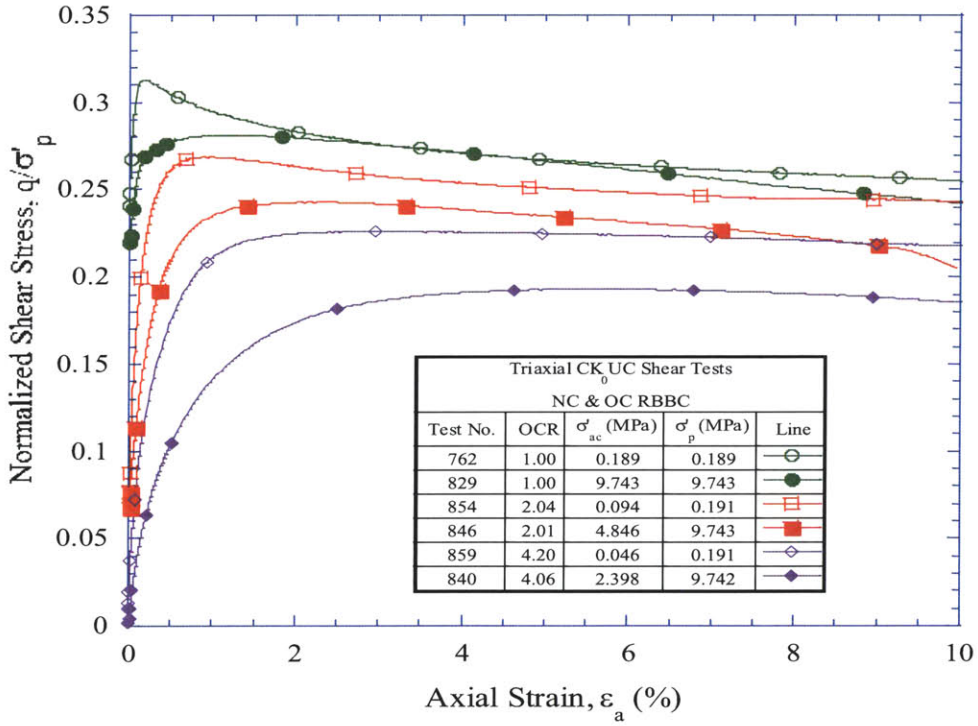

Figure 2-4: Normalized shear stress-strain responses for RBBC at OCRs 1, 2 and 4 from CK_OUC triaxial tests with σ'_p = 0.2 and 10 MPa (Abdulhadi, 2009)

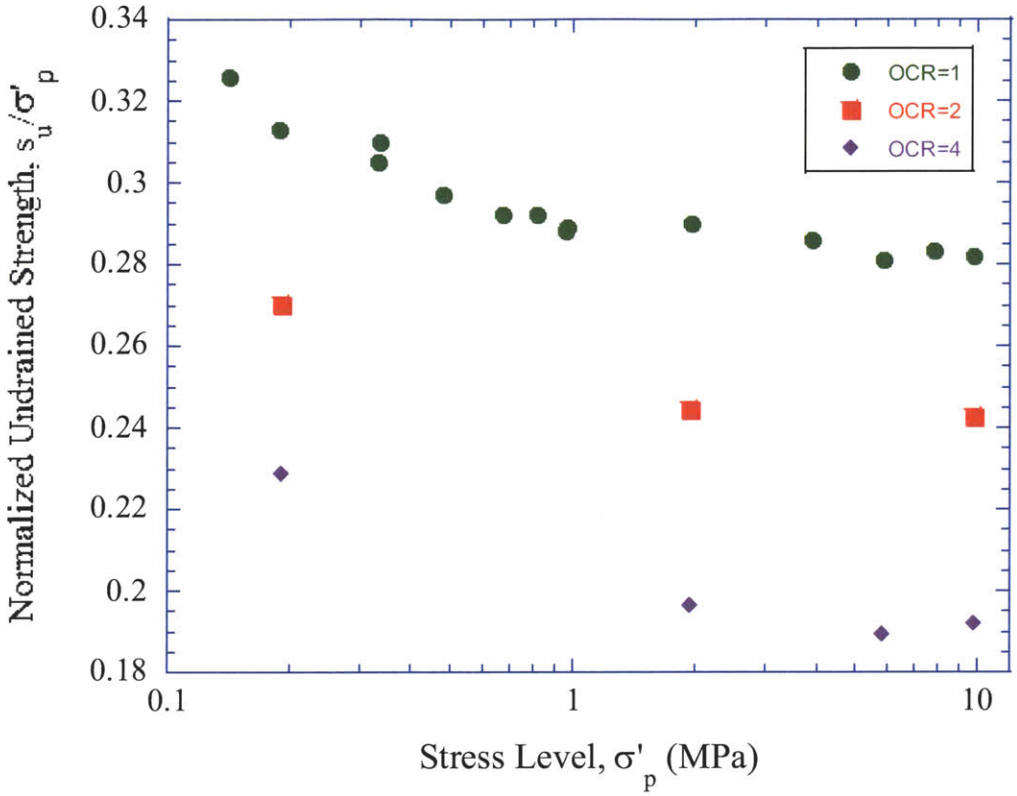

Figure 2-5: Variation in normalized undrained strength with stress level for RBBC at OCRs = 1, 2 and 4 from CK_OUC triaxial tests (Abdulhadi, 2009)

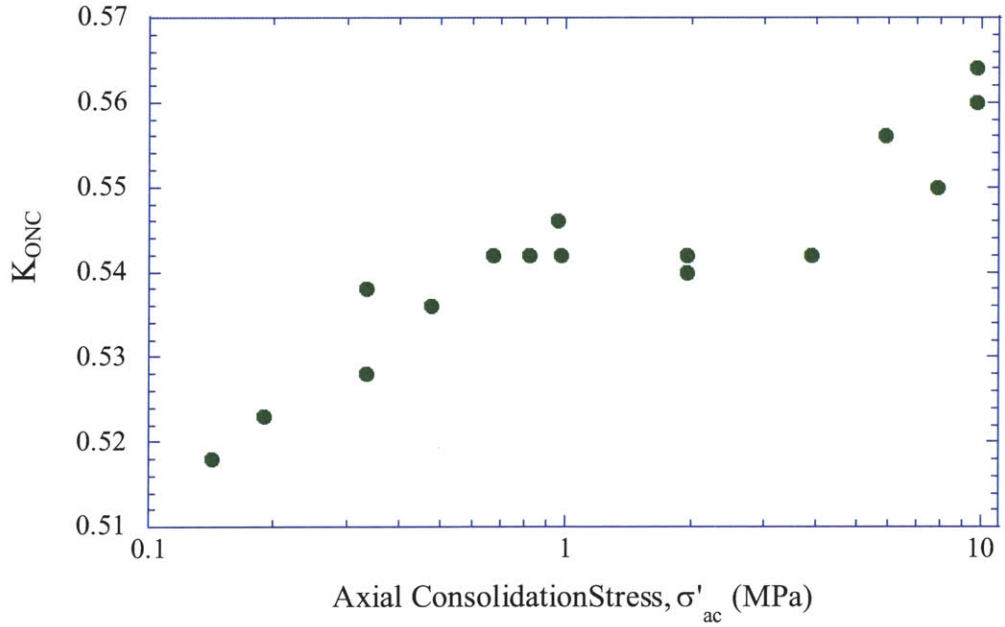

Figure 2-6: Lateral stress ratio at the end of virgin consolidation (K_{ONC}) versus stress level for RBBC from CK_OUC triaxial tests (Abdulhadi, 2009)

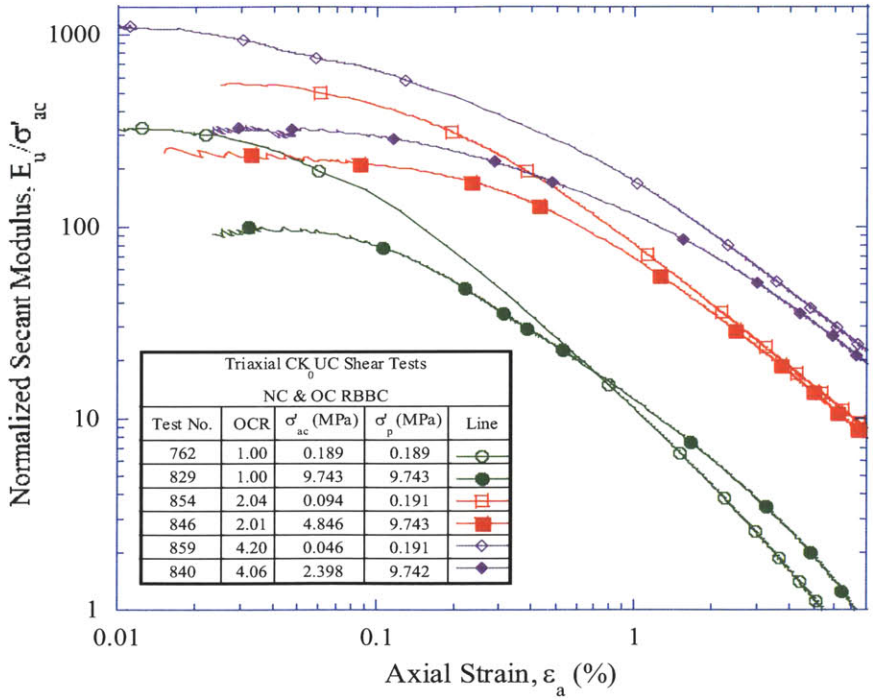

Figure 2-7: Normalized undrained secant Young's modulus versus axial strain for RBBC at OCRs 1, 2 and 4 from CK_OUC triaxial tests with σ'_p = 0.2 and 10 MPa (Abdulhadi, 2009)

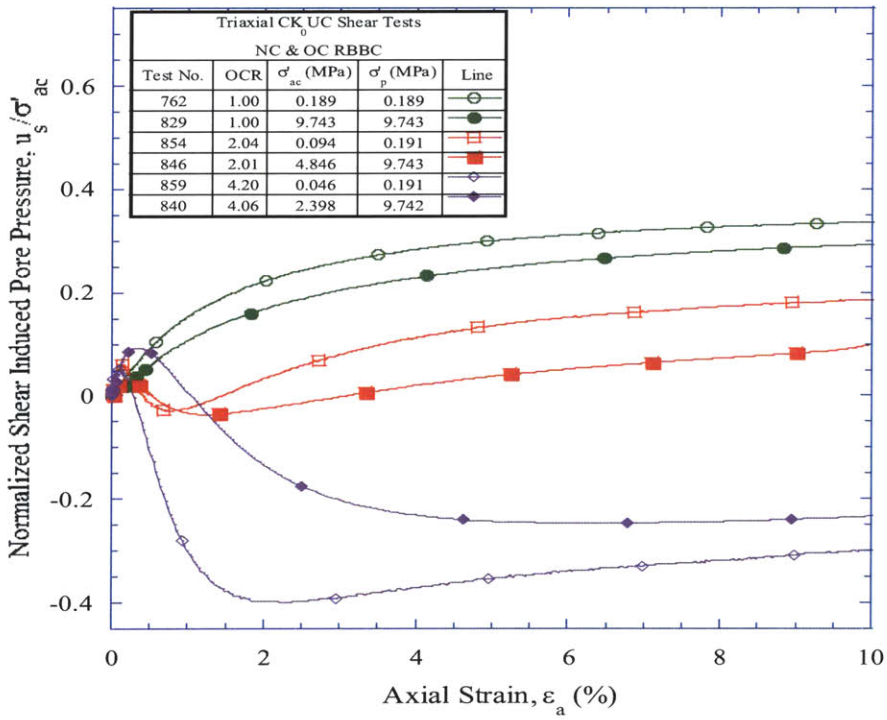

Figure 2-8: Normalized shear induced pore pressure versus axial strain for RBBC at OCRs 1, 2 and 4 from CK_OUC triaxial tests with σ'_p = 0.2 & 10 MPa (Abdulhadi, 2009)

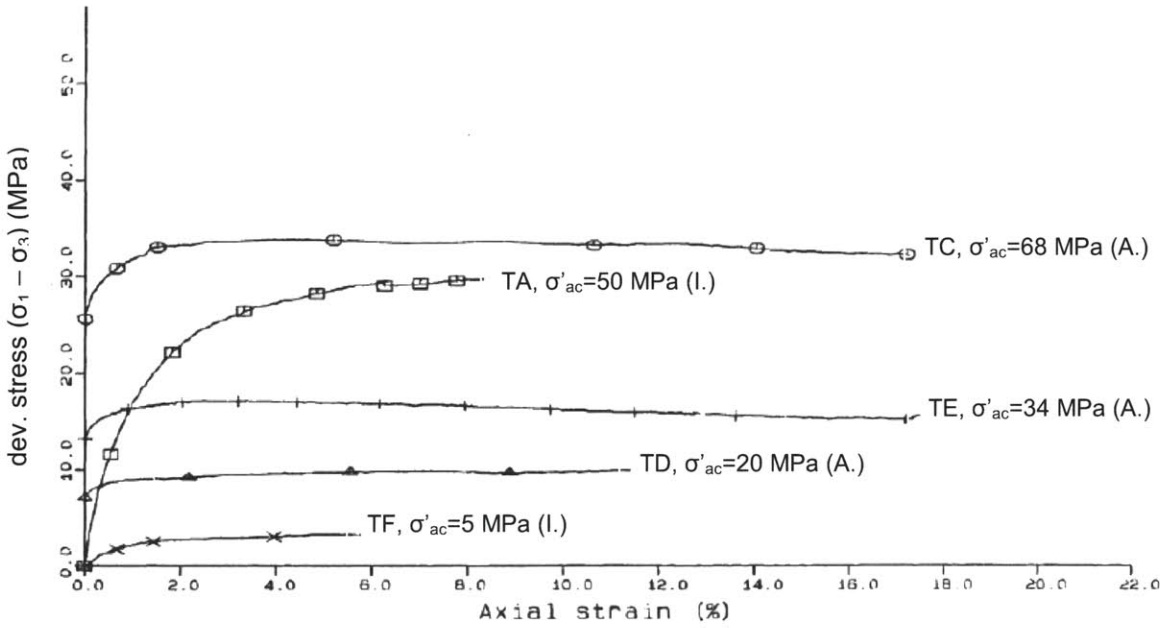

Figure 2-9: Deviatoric stress-strain response during undrained triaxial compression for a NC mud volcano clay (Yassir, 1989)

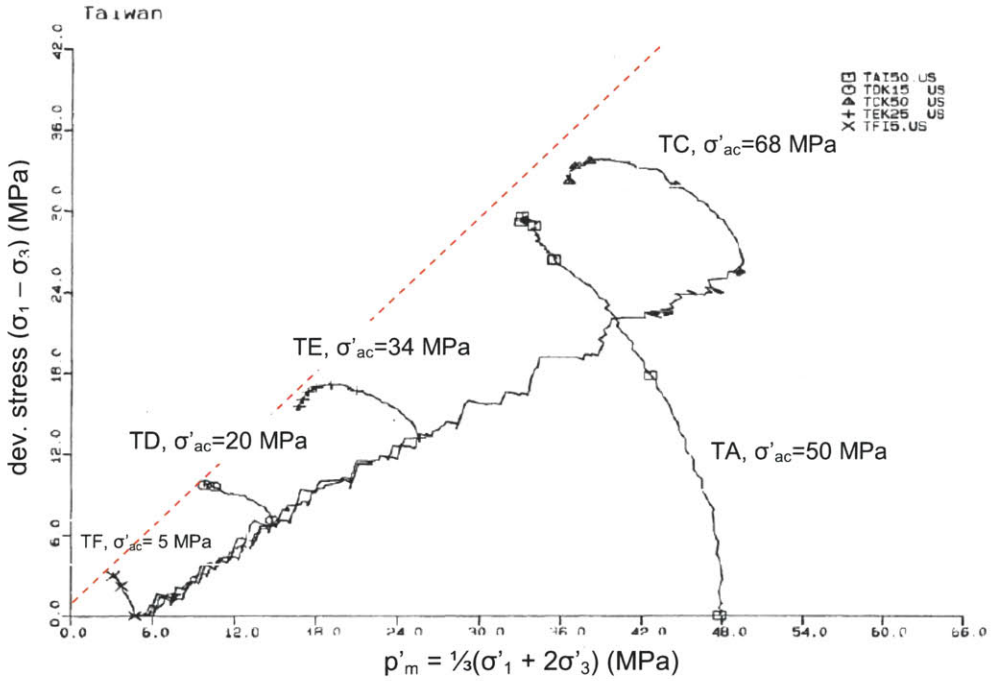

Figure 2-10: Effective stress paths (Cambridge stress space) in undrained triaxial compression for a NC mud volcano clay (Yassir, 1989). The dashed red line is added to illustrate possible curvature of the failure envelope

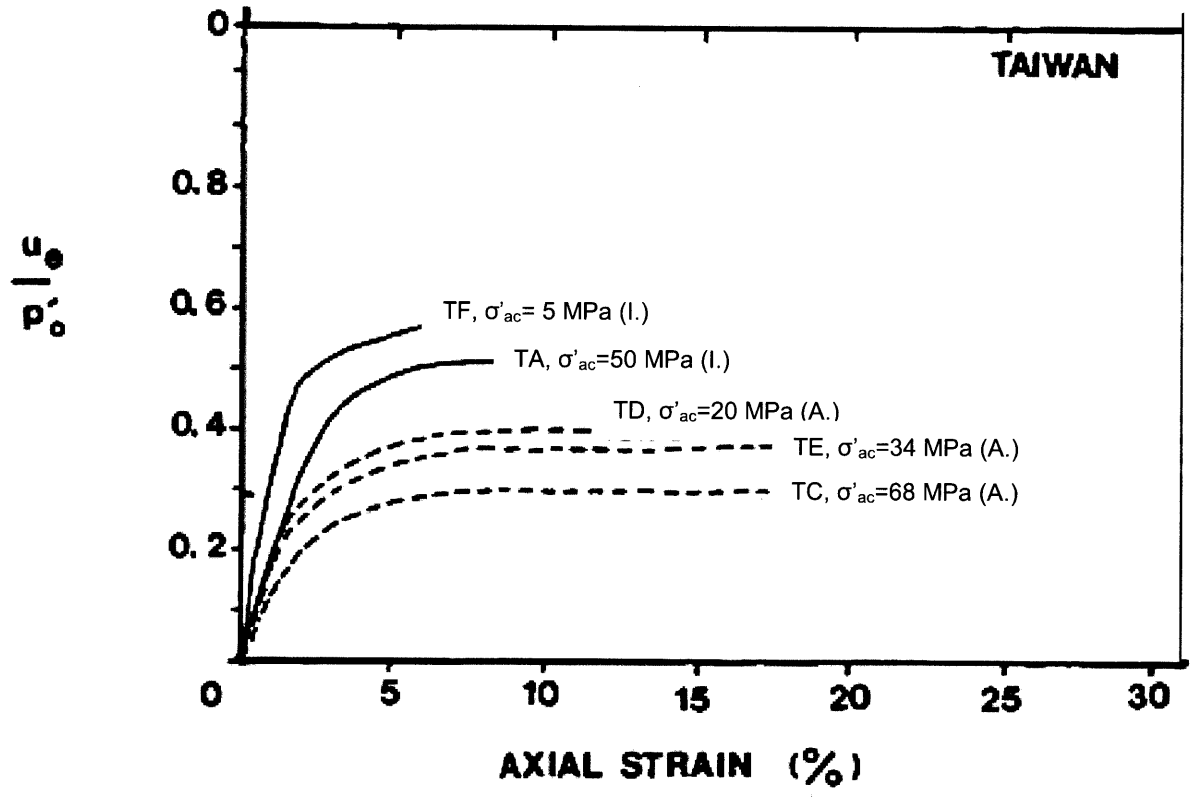

Figure 2-11: Normalized excess pore pressure (u_e/p'_o) versus axial strain during undrained triaxial compression for a NC mud volcano clay (Yassir, 1989)

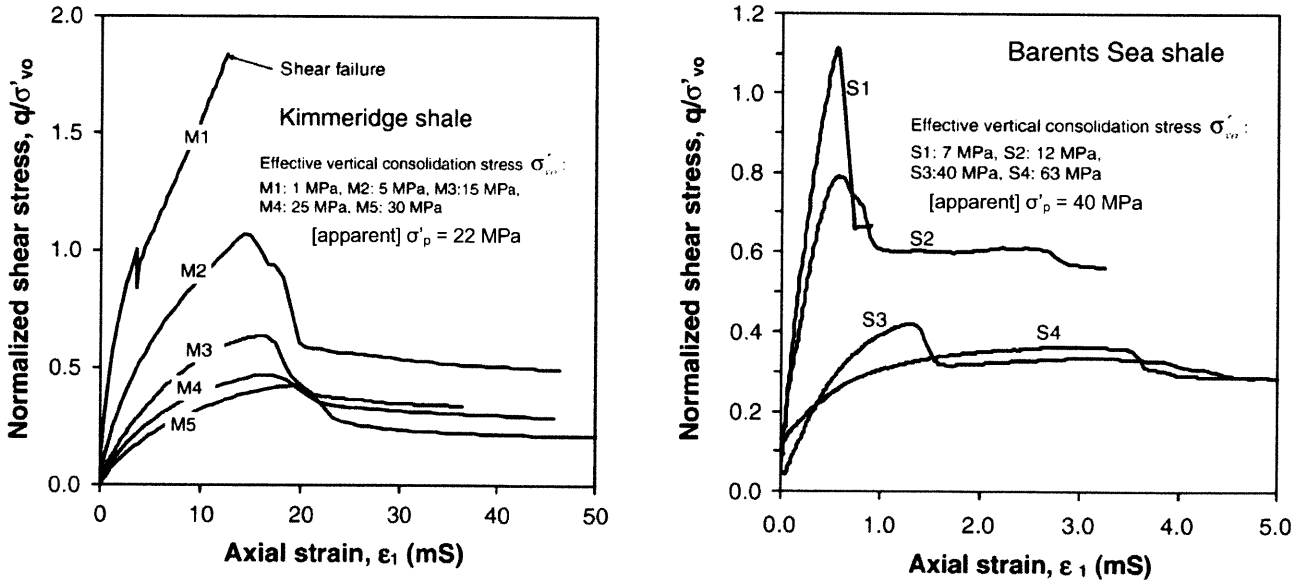

Figure 2-12: Normalized shear stress versus axial strain for CIUC tests on Kimmeridge Shale and Barents Sea Shale. Note that strain is given millistrain, mS (Gutierrez et al., 2008)

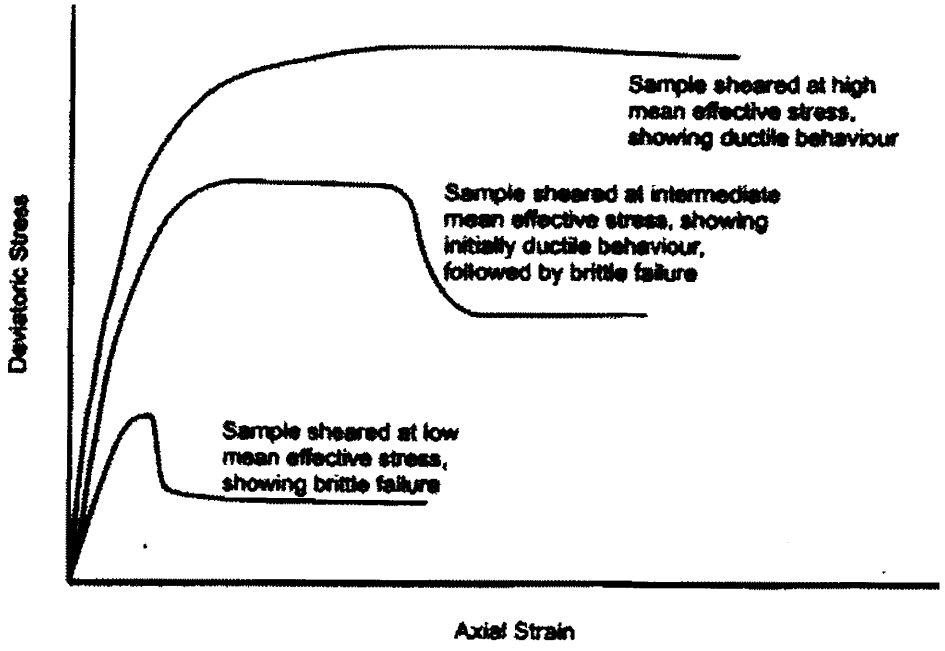

Figure 2-13: General forms of stress-strain response for clay shales (Petley, 1999)

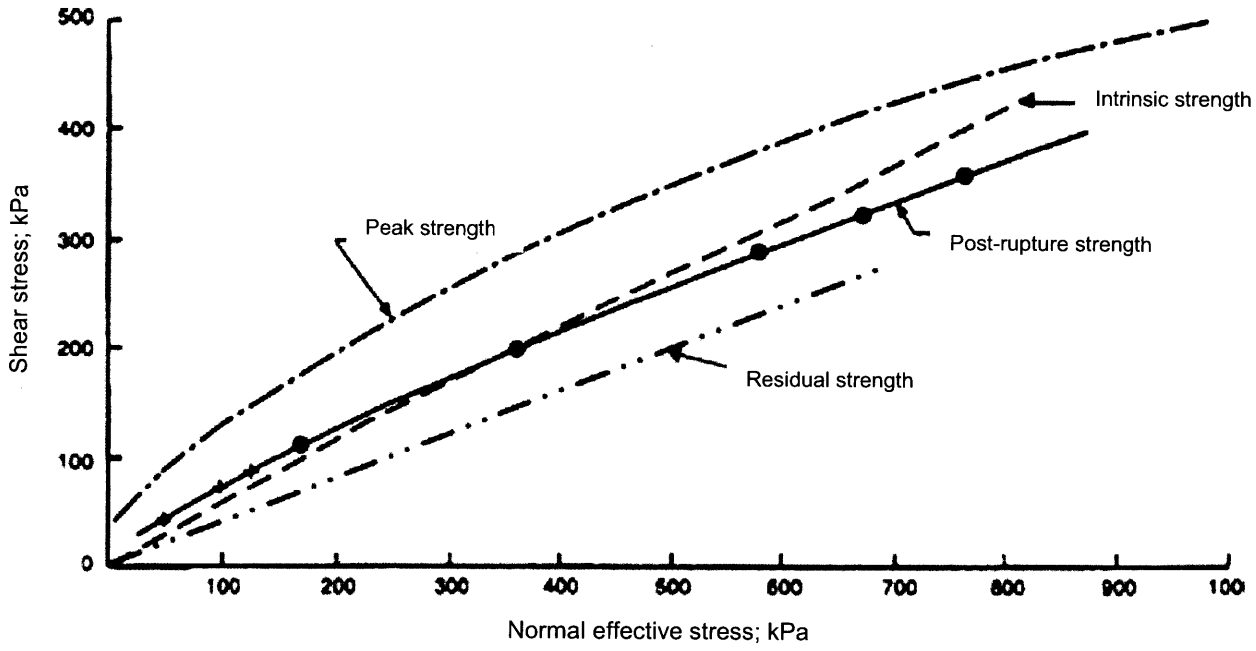

Figure 2-14: Conceptual form of failure envelopes for clays by Burland (1990) (taken from Abdulhadi, 2009)

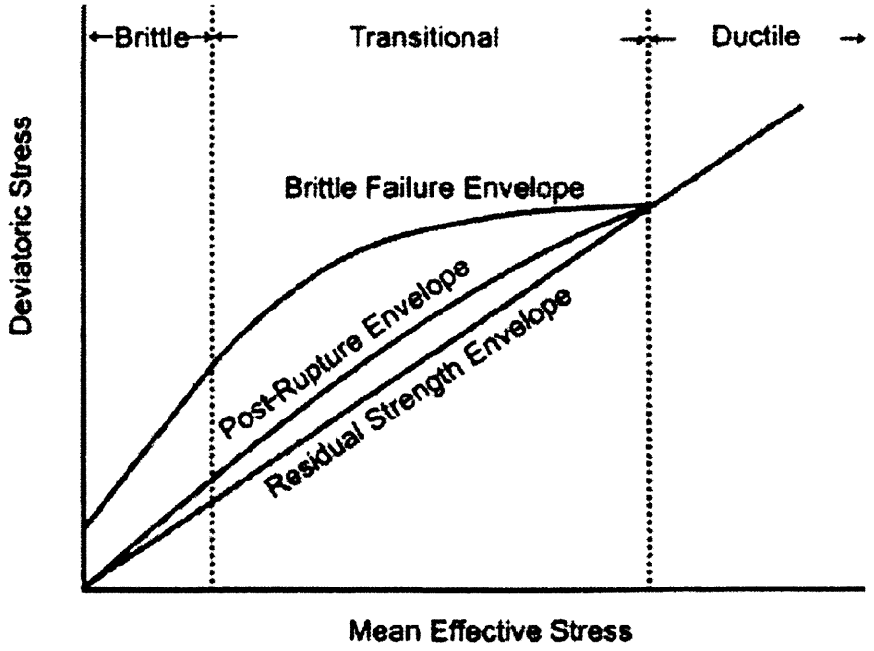

Figure 2-15: Conceptual form of failure envelopes for hard clays and clay shales (Petley, 1999)

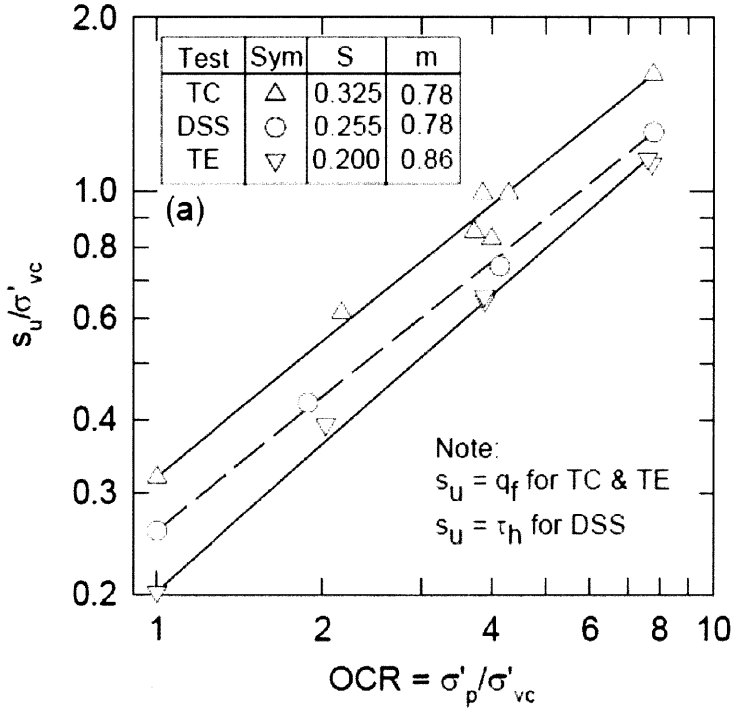

Figure 2-16: Normalized undrained shear strength versus OCR for a SHANSEP test program on AGS Plastic Marine Clay (Koutsoftas & Ladd, 1985)

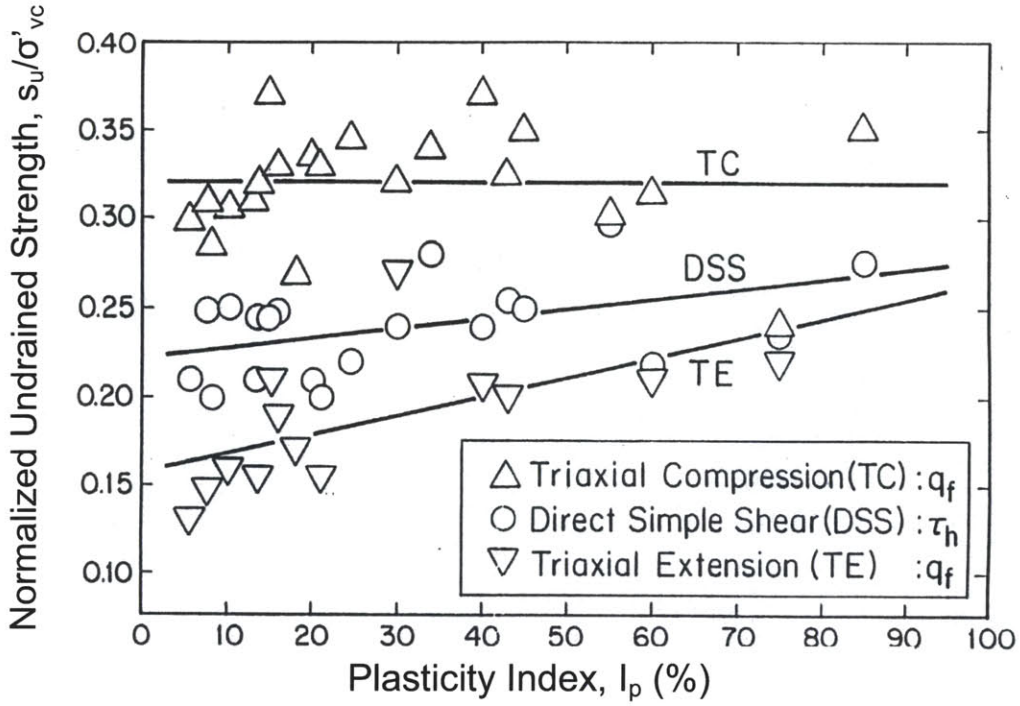

Figure 2-17: Normalized undrained strengths in TC, TE and DSS as a function of plasticity from CK_OU tests on NC clays and silts (Ladd, 1991)

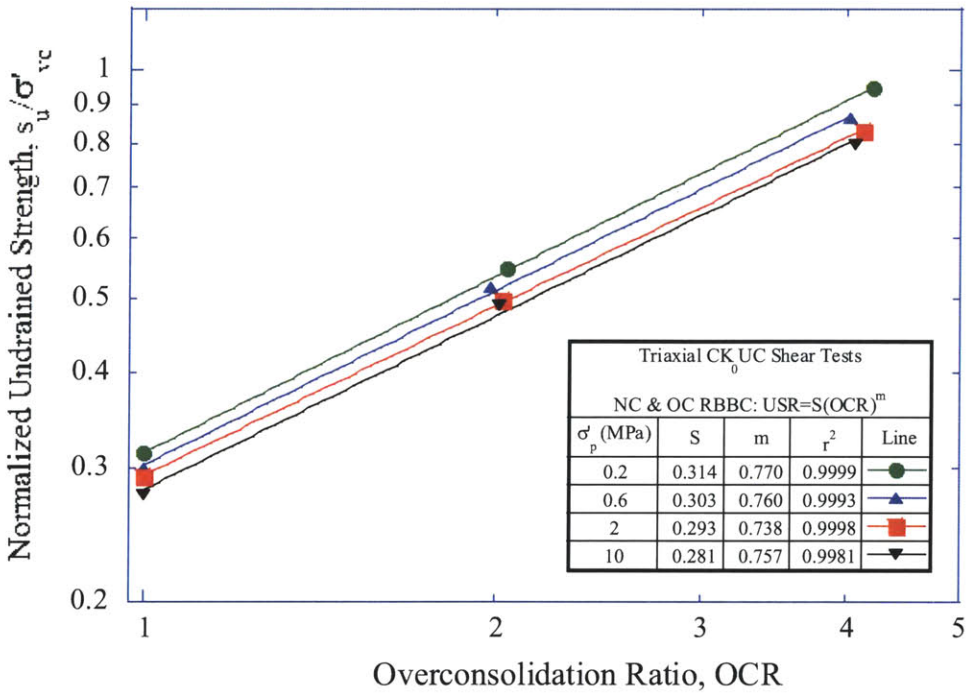

Figure 2-18: Effect of stress level on the SHANSEP S and m parameters for RBBC in triaxial compression (Abdulhadi, 2009)

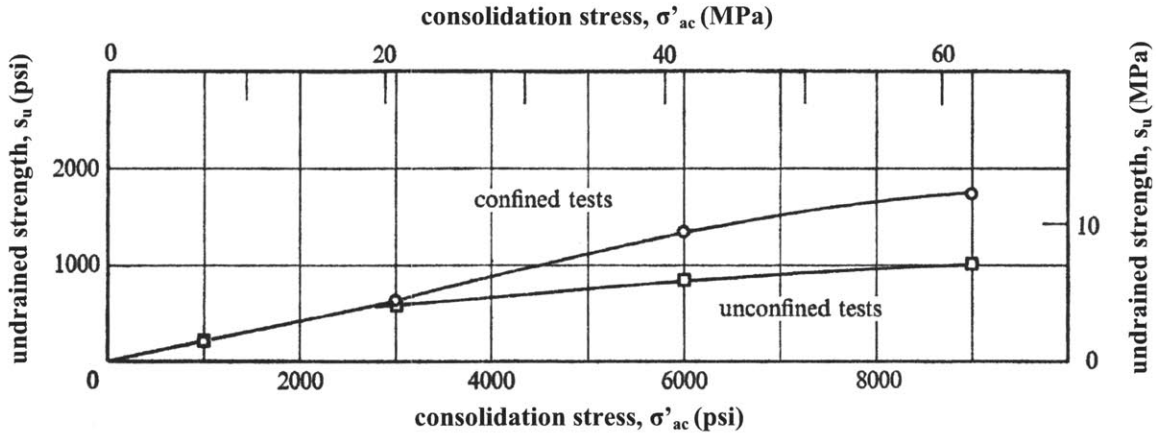

Figure 2-19: Relationship between undrained strength and consolidation stress for CIUC tests performed on resedimented London Clay. Where a number of tests were performed at a particular stress the average value is plotted (Bishop et al., 1975)

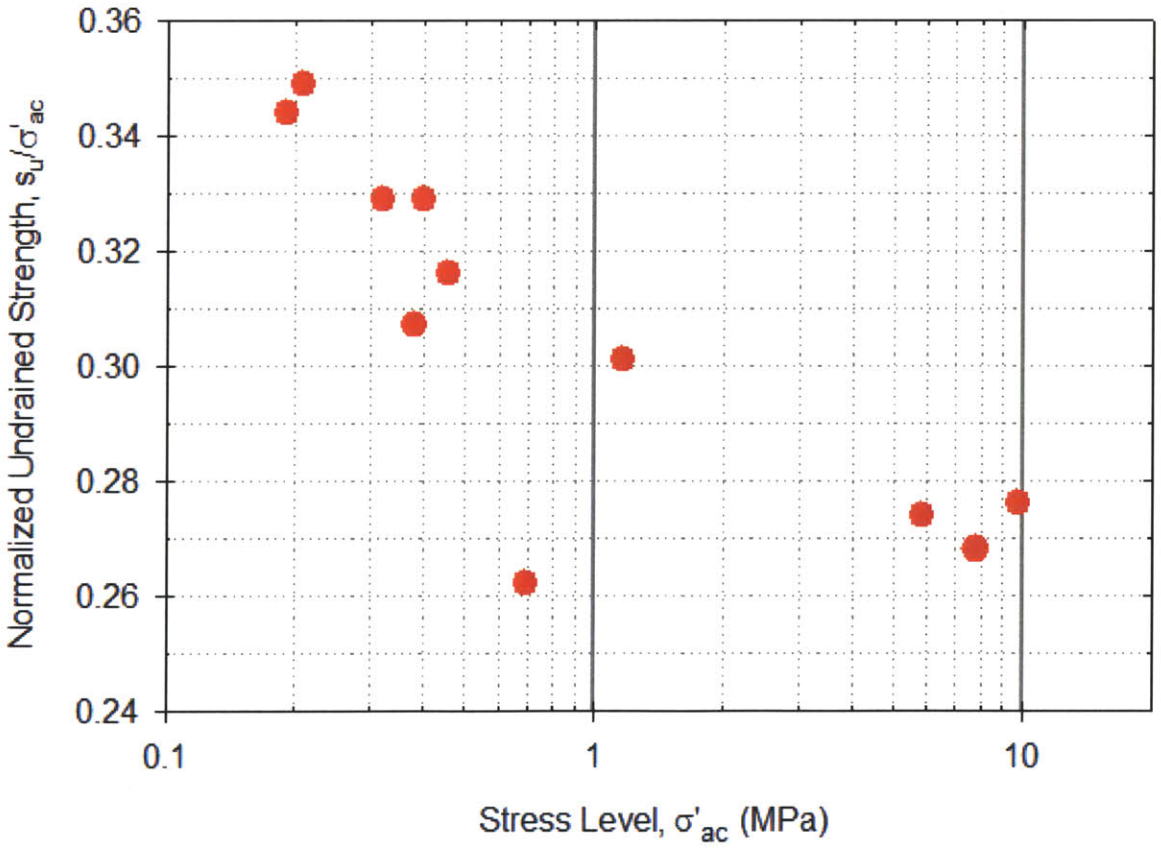

Figure 2-20: Variation in normalized undrained strength with stress level for Resedimented Ugnu Clay at OCR = 1 from CK_OUC triaxial tests (Jones, 2010)

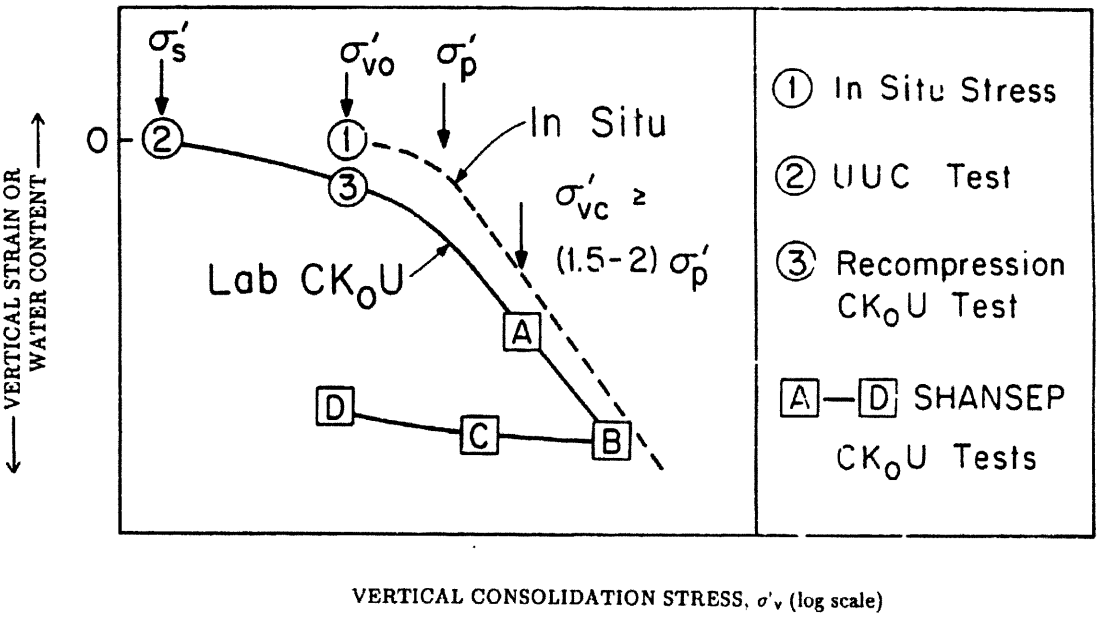

Figure 2-21: Reconsolidation procedures for laboratory CK_oU testing (Ladd, 1991)

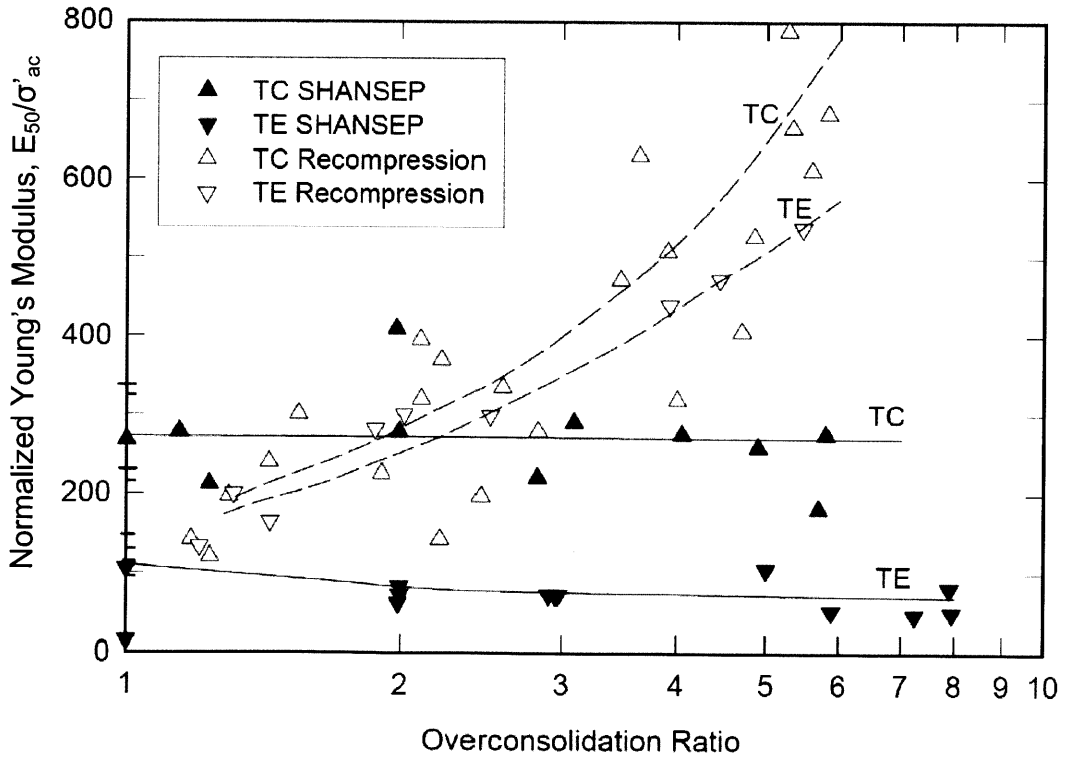

Figure 2-22: Effect of laboratory reconsolidation procedure on measured stiffness for Boston Blue Clay (Ladd et al., 1999)

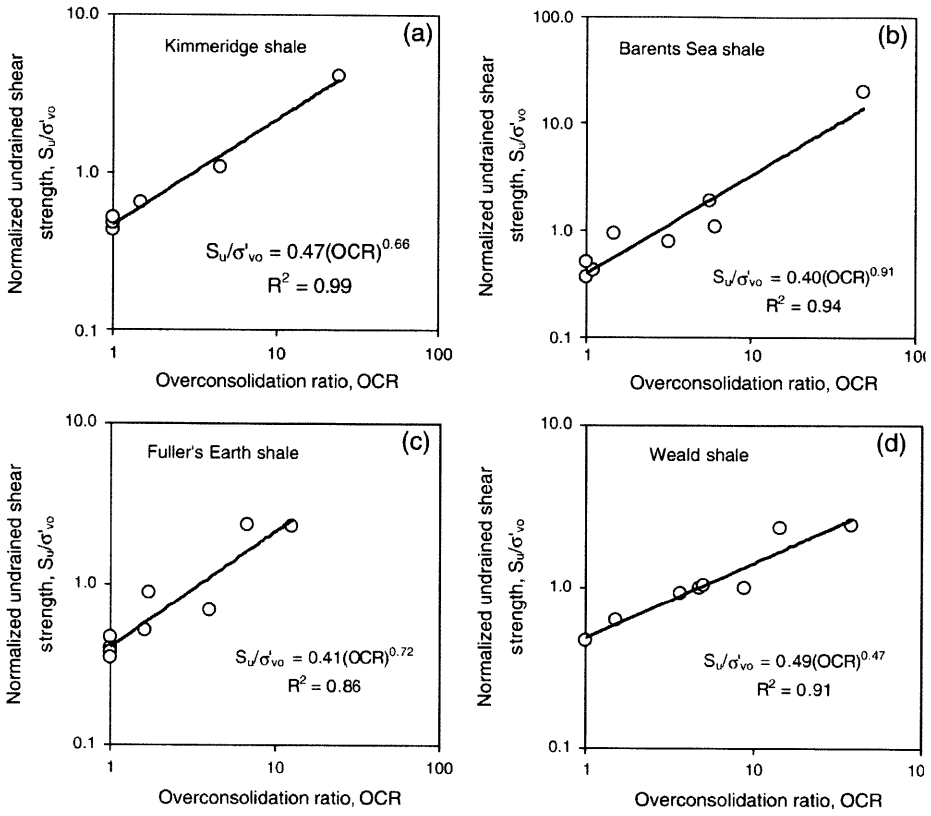

Figure 2-23: Normalized undrained shear strength versus OCR for four clay shales (Gutierrez et al., 2008)

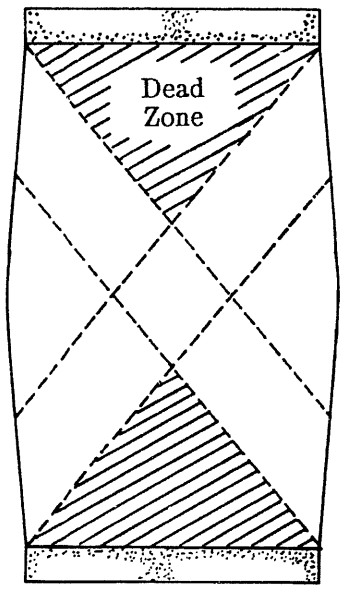

Figure 2-24: Location of conical 'dead' zones in a fixed end triaxial specimen (Rowe and Barden, 1964)

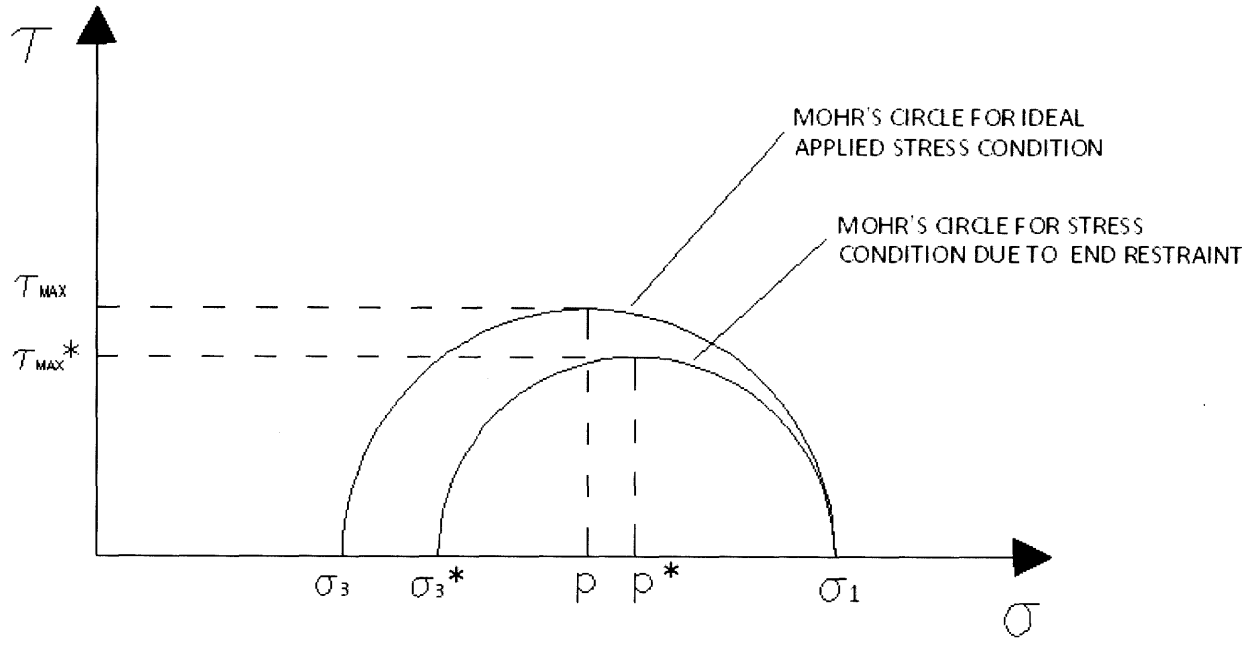

Figure 2-25: Effect of end restraint caused by fixed ends on the stress state in a triaxial specimen. Stresses at the ends which are altered from the corresponding applied stresses are denoted by an asterisk

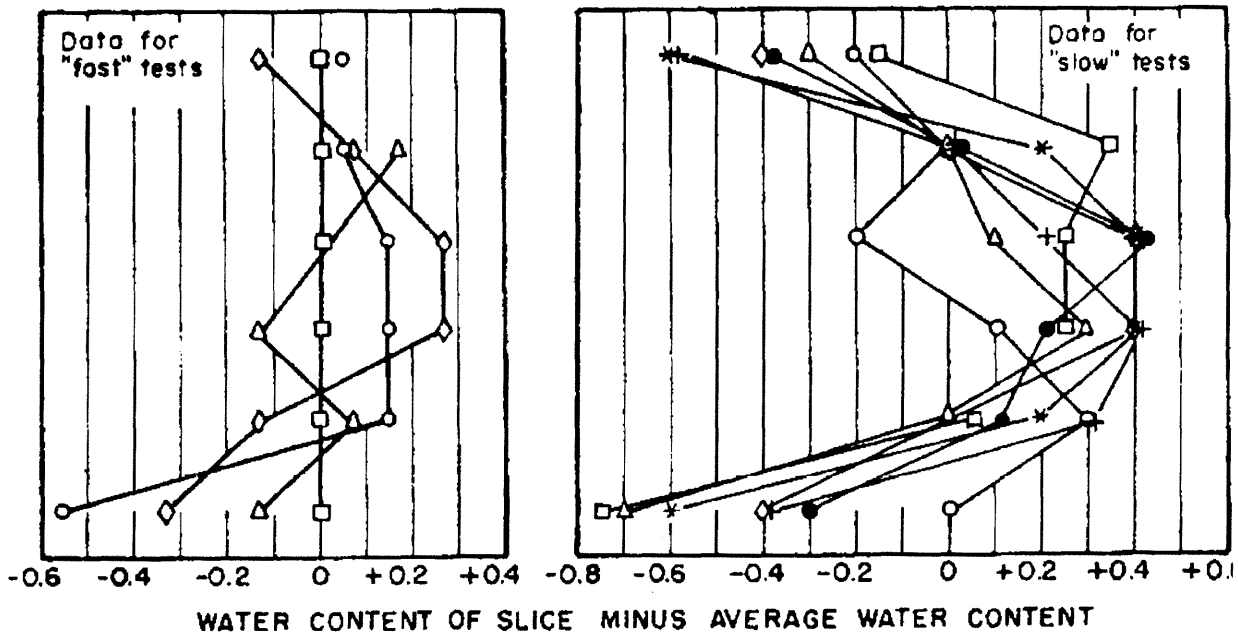

Figure 2-26: Post-shear water content distribution (%) in CIUC test specimens of resedimented Mississippi Valley Alluvial Clay at OCR = 16 (Richardson and Whitman, 1963). Each symbol represents a separate test

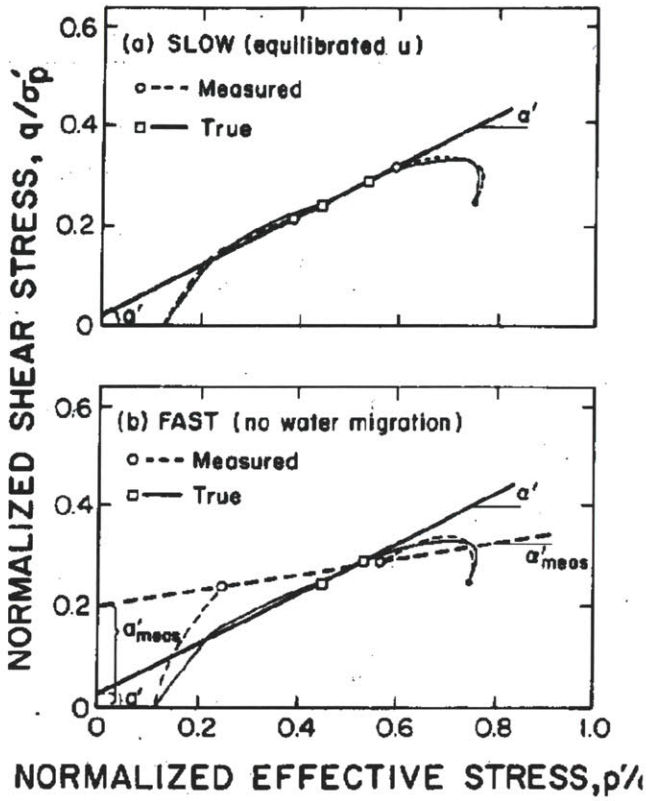

Figure 2-27: Hypothetical stress paths for slow and fast undrained triaxial compression tests on rate-independent cohesive soil where fixed ends are used (Germaine and Ladd, 1988)

Figure 2-28: A picture of NC RBBC specimens after CK_OUC tests showing a bulging mode of failure for the low pressure test (TX757, σ'_{ac} = 0.67 MPa) and a slip surface for the high pressure test (TX829, σ'_{ac} = 9.74 MPa) (Abdulhadi, 2009)

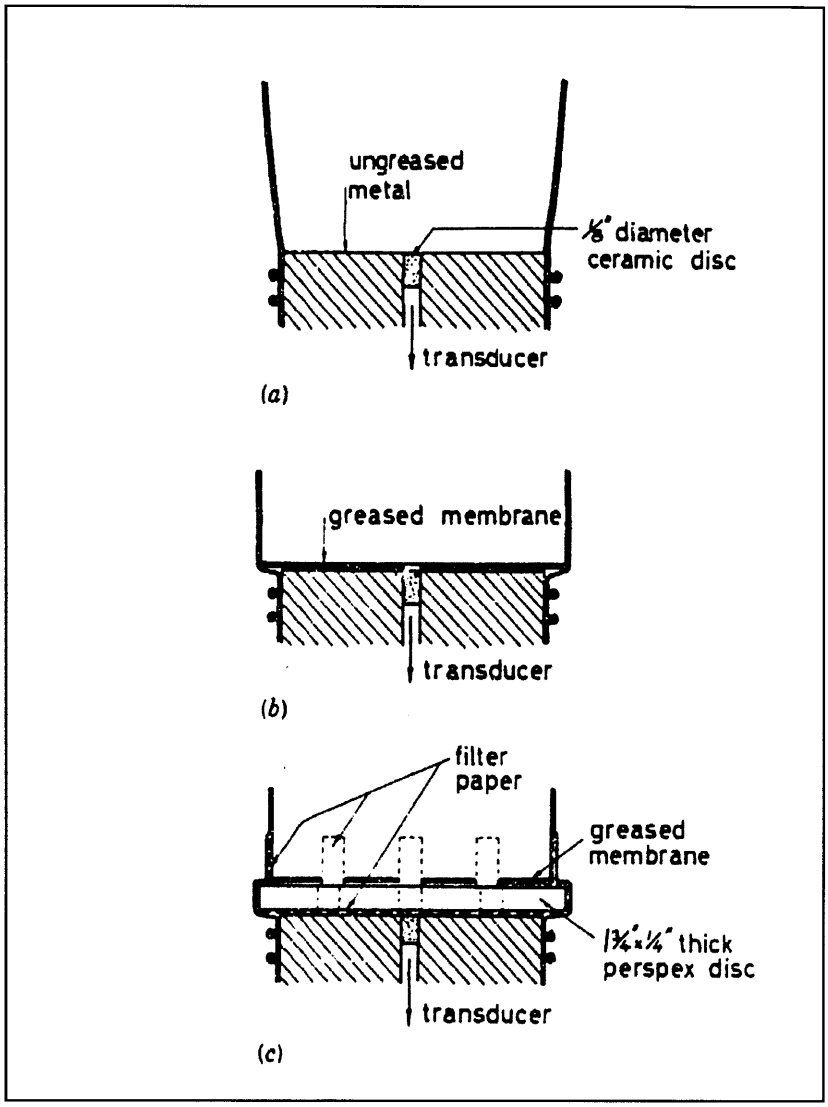

Figure 2-29: End platen designs (Rowe and Barden, 1964): (a) design 1; (b) design 2; (c) design 3

3 RESEDIMENTED BOSTON BLUE CLAY

3.1 INTRODUCTION

This chapter presents an overview of Resedimented Boston Blue Clay (RBBC), the analog test material employed in the author's experimental program. RBBC is a soil resedimented in the laboratory from natural Boston Blue Clay, an illitic clay of low sensitivity and a USCS classification of CL (low plasticity clay). RBBC has being studied extensively at MIT since 1961 and a large database exists on its properties. The soil has several attractive features which make it an ideal reference material for research purposes. Its engineering properties are very similar to many natural uncemented clays, including stress-strain-strength anisotropy, low to medium sensitivity, significant strain rate dependency and typical consolidation characteristics. In addition, the resedimentation process eliminates variability among samples and produces uniform specimens with well-defined one-dimensional consolidation histories and complete saturation. Along with its virtually infinite local supply, these key characteristics have made the soil an ideal research material to investigate fundamental aspects of soil behaviour without having to take into account the wide variability of natural soils. The well-defined and repeatable behaviour of RBBC has also made it an asset in the development and proofing of new laboratory testing equipment as well as the modification of existing equipment.

Table 3-1 summarizes the research performed on RBBC since the 1960's (extended from Santagata, 1998) and also provides a large proportion of the history of soil mechanics research at MIT in the last 50 years in the area of clay behaviour. Laboratory resedimentation at MIT was pioneered by Wissa (1961) who designed the first apparatus for the production of large batches of clay. However, it was Bailey (1961) who first resedimented BBC to examine the effect of salt concentration on undrained strength. It can be seen from Table 3-1 that RBBC has been used in both laboratory element tests as well as model tests. The extensive study of the behaviour of RBBC at MIT is also strongly linked to the development of soil models. Three generalized constitutive models formulated at MIT, MIT-E1 (Kavvadas, 1982), MIT-E3 (Whittle and Kavvadas, 1994) and MIT-S1 (Pestana, 1994), have all been validated using the wide database for RBBC.

Natural Boston Blue Clay consists of glacial outwash deposited in a marine environment about 12,000 to 14,000 years ago in the period immediately following deglaciation of the Boston basin (Kenney, 1964). It is present throughout the Boston area varying in thickness from 20 to 40 m. A stiff overconsolidated crust (OCR = 2 – 5) forms the upper 12 to 20 m of the deposit while underneath

the clay is close to normally consolidated (Santagata, 1998). Although the depositional and general characteristics of BBC are fairly similar throughout most of the Boston area, some variability can be expected in clay retrieved from different locations, and thus in the resedimented version produced from these different natural sources. The index properties of the clay can vary slightly depending on several factors including particle size distribution, pore fluid chemistry and mineralogy. These properties can also change at a given location as a function of depth.

The origin of the natural material used to produce RBBC defines the batch series (see Table 3-1) and to this day BBC has been obtained from five different locations. However, the BBC obtained from the most recent location has not yet been processed and as such only four series of RBBC exist. No exact record of the origin of Series I or II BBC is available. Series III was obtained by augering from a depth of about 23 m during construction of a parking garage near Kendall Square close to the east side of the MIT campus. The material used in the author's research is from Series IV which was obtained in 1992 from the base of an excavation for MIT's Biology Building (Building No. 68). Approximately 2500 kg of BBC was excavated at a depth of about 12 m where the OCR of the clay varied from 1.3 to 4.3 (Berman, 1993). The clay was processed as described in Section 3.2.2 and the resulting dry powder stored for future use.

The procedures and equipment used to resediment BBC have undergone dramatic modification through the years since the practice first began in the early 1960's. Until recently, RBBC was batched in large quantities to produce soil cakes. These soil cakes were trimmed into smaller pieces depending on project requirements which were then stored for use in individual tests. For Series I RBBC the batches were numbered following no consistent method and often on a project by project basis. Starting from Series II all batches have been numbered sequentially starting from 100, 200 and 400 for Series II, III and IV respectively. Beginning with Abdulhadi (2009), however, RBBC has been batched in much smaller quantities where each consolidometer is used to produce individual test specimens. This methodology is now used to resediment all clay at MIT, be it Boston Blue Clay or otherwise. It should be noted that since this approach requires a much larger number of smaller batches, the batch numbers are not given in Table 3-1. The procedures and equipment used by the author to produce specimens of RBBC for different types of tests are described in Section 3.2. The consolidation characteristics of the clay during resedimentation are also examined in this section along with an evaluation of the effectiveness of the author's resedimentation methods.

Since RBBC has been studied at MIT for almost 50 years, a considerable database exists on its index and engineering characteristics. Section 3.3 presents index properties for RBBC including grain size distribution, Atterberg limits, specific gravity and salt concentration data. These data are important to verify that the soil from a new source exhibits characteristics similar to those of the soil

previously used. A comparison is then made with typical known index properties of natural BBC. Finally, information is also presented on the known effects of salt concentration on the index properties of RBBC.

Section 3.4 reviews the consolidation characteristics of RBBC including compressibility parameters, lateral stress ratio, secondary compression, the coefficient of consolidation and flow properties as obtained from CRS (Constant Rate of Strain) and triaxial testing. Again, a comparison with the corresponding behaviour of natural BBC is made.

Section 3.5 presents a brief discussion of the undrained shear behaviour of RBBC. The discussion is limited to the case of triaxial compression, as it is only in this mode of shear that the author has carried out testing and obtained results. The undrained shear behaviour of RBBC in triaxial compression at high stresses has been examined by Abdulhadi (2009) and the results have already been discussed in Chapter 2. As such, Section 3.5 presents only a limited discussion of aspects of undrained shear behaviour which have not previously been discussed in Chapter 2 but are still relevant to the research presented in this thesis. In particular, stiffness, strain rate sensitivity, the effect of lateral stress ratio on undrained strength, the behaviour of natural Boston Blue Clay and the effect of salt concentration on behaviour are discussed.

3.2 THE PROCESS OF RESEDIMENTATION

3.2.1 Introduction

Batches of RBBC are prepared by one-dimensionally consolidating a dilute slurry of BBC in a rigid-walled cylindrical container referred to as a consolidometer. The early method of resedimentation (e.g. Ladd and Varallyay, 1965) produced partially saturated samples which could only be subsequently saturated using a 200 kPa back-pressure. This became a critical issue when RBBC was used in the directional shear cell by Germaine (1982) since the clay specimens could not be back-pressure saturated in this device. Germaine therefore substantially revised the resedimentation technique to produce fully saturated and uniform samples with a salt concentration of 16 g/l. Further modifications were later introduced by Seah (1990) who improved the layout of the system to increase productivity, modified the technique for extrusion of the soil cake from the consolidometer and implemented remote data acquisition to provide continuous monitoring of the consolidation process. As mentioned previously, Abdulhadi (2009) introduced a substantially different approach by preparing individual batches for each test specimen, as opposed to producing large soils cakes which were subsequently divided into smaller pieces as had been done in the past. The approach of preparing individual batches for each test specimen dramatically reduces the load

which must be applied to achieve a particular batch preconsolidation pressure, a critical issue for samples which need to be batched to high stresses.

3.2.2 Resedimentation Procedure

For the author's experimental program the approach of preparing individual batches for each test specimen was used. However, due to the various types of tests performed which require slightly different resedimented samples to be produced, different variations of resedimentation equipment have been utilized. Regardless of this, the basic procedure for resedimentation remains the same and can be divided into four main stages: powdering, deposition, consolidation, sample extrusion and preparation. These stages are described below.

(i) Powdering

The natural BBC (Series IV) obtained from the ground was first softened with tap water and mixed into a thick slurry. The slurry was then passed through a #10 ASTM standard sieve (opening size of 2 mm) to remove all non-natural material, gravel, coarse sand and large shell fragments before being oven-dried at 60°C. The oven-dried material was then ground to 95% passing a #100 ASTM standard sieve (opening size of 0.15 mm) by the Sturtevant Company using a roller mill. Finally, the material was manually randomized by several blending operations before being stored in sealed 40 gallon drums (Cauble, 1996).

(ii) Deposition

After retrieving the desired mass of BBC powder from storage it is mixed thoroughly with water using an electric blender to produce a homogenous slurry without lumps at a water content of 100%. Except for tests in which the effect of salt content on consolidation behaviour is examined, the pore fluid consists of distilled water with salt (NaCl) added to achieve a concentration of 16 g/l. Salt is added as a flocculent to minimize segregation of the soil particles during sedimentation and to achieve a soil fabric similar to that of natural BBC, a marine illitic clay. Note that the slurry water content of 100% is over twice the liquid limit of the clay (45 ~ 48 %) and results in a workable yet stable slurry with no free water present at the surface. The slurry is then vacuumed (under 20 inches Hg) to get rid of any entrapped air using the setup shown in Figure 3-1. The flask used to vacuum the slurry has two lines. One line is connected to the vacuum pump while the second line is used to pull the slurry from the adjacent container. The slurry is effectively de-aired as it drops into the vacuum flask. Following vacuuming, the de-aired slurry is carefully placed in a consolidometer from bottom to top using a funnel in such a manner as to minimize entrapment of air bubbles. Prior to

pouring the slurry, the inside wall of the consolidometer is lubricated with a thin film of either silicon oil or high viscosity vacuum grease. This lubrication minimizes side wall friction during consolidation and also aids in the extraction of the clay from the consolidometer.

(iii) Consolidation

The slurry is loaded incrementally in a consolidometer, which has double drainage, using a load increment ratio $\Delta\sigma_a/\sigma_{ao} = 1$. Each load increment is maintained at least until the end of primary consolidation as determined by the Casagrande log time method. After the desired maximum axial stress, i.e. preconsolidation pressure σ'_p, has been achieved, the resedimented sample is rebounded to an OCR of 4 using a load increment ratio of -0.75. At OCR = 4 the clay is close to hydrostatic effective stress conditions, i.e. $K_o \sim 1$, and the shear strains due to sample extrusion from the consolidometer are minimized, as confirmed by the work of Santagata (1994). As a result, the degree of sample disturbance which RBBC specimens are subjected to is minimal. A more in depth description of the equipment used during the consolidation stage of resedimentation is given in Section 3.2.3.

(iv) Extrusion and Preparation

After resedimentation in the consolidometer is completed, the sample is removed and prepared for testing. Advantage is taken of the lubricant on the interior wall of the consolidometer to minimize disturbance of the clay and reduce the force required for extrusion. Samples prepared for triaxial tests at a low consolidation stress have a low σ'_p and it is possible to extrude the samples manually. These samples are subsequently trimmed to the required diameter for testing using a wire saw and mitre box with the last portion of trimming being performed using a razor blade. Trimmed material is taken for water content measurements. Once the sample is reduced to the required diameter it is placed in a mold and the ends are cut off to achieve the required height of the test specimen and to ensure that the two ends of the specimen are parallel. The pieces cut off the ends are also taken for water content measurements. Finally, the ends of the specimen are smoothed down using a razor blade.

RBBC samples prepared for high pressure triaxial testing are consolidated to $\sigma'_p = 2$ MPa and require a hydraulic jack for extrusion, even with lubricant on the inside wall of the consolidometer. However, because these samples are consolidated using a consolidometer with the same inside diameter as the final triaxial specimen, it is not necessary to trim the extruded samples to a smaller diameter. In this case it is only necessary to trim the ends to achieve the required specimen height.

3.2.3 Equipment

Two somewhat different types of consolidometer have been employed to produce samples of RBBC for the author's research. Table 3-2 summarizes the dimensions and characteristics of the samples produced using the two types of consolidometers, referred to as Type I and Type II, along with the typical dimensions of the large diameter soil cake produced in the past. Both types of consolidometer consist of the same basic structure involving a cylindrical acrylic tube in which the clay consolidates between top and bottom porous stones. Nylon filter fabric is placed between the porous stones and the clay. A thin film of silicon oil is used to lubricate the inside of the tubes in order to reduce the friction acting between the tube walls and the sample. During each consolidation increment axial deformation can be measured using an electronic displacement transducer (LVDT) in order to establish the end of primary consolidation as well as to gain information on consolidation properties during resedimentation.

Consolidometer Type I is used to produce samples for triaxial tests performed at a low consolidation stress. All samples are consolidated to σ'_p = 0.25 MPa. The basic setup of the consolidometer is illustrated in Figure 3-2. A bottom piston topped with a porous stone and filter fabric is placed inside a 30 cm long smooth acrylic tube of either 4.09 or 4.39 cm inside diameter (corresponding to Type I (a) or (b) respectively in Table 3-2). The bottom portion of the tube is submerged in a bath filled with water of the same salt concentration as that of the pore fluid of the clay (i.e. generally 16 g/l except for tests where the effect of salt content on consolidation behaviour is examined). Load is applied to the sample through a top piston which rests on the top porous stone. Clamps are used to ensure that the entire setup is maintained vertical during the consolidation process. For the first series of load increments up to 0.032 MPa the load is applied by simply stacking weights on the top piston. For higher loads the weights are placed on a hanger which in turn transfers load to the top piston, as shown in Figure 3-2. When the consolidometer is initially set up the acrylic tube rests on a spacer of approximately 3 cm height which in turn sits on the base of the water bath. However, at the point when the method of load application is changed to the hanger system, this spacer is removed. This allows the sample to strain from both ends (i.e. as is achieved in a floating ring oedometer), thereby halving the amount of side wall friction which the sample is subjected to. RBBC samples prepared in consolidometer Type II require approximately 3 weeks to produce.

Consolidometer Type II is used to produce samples for high pressure triaxial testing. It has a smooth acrylic tube of 30 cm height and an inside diameter equal to that of a triaxial specimen, i.e. 3.45 cm, thereby eliminating the need to trim the final resedimented sample to a smaller diameter prior to placement in the triaxial cell. The setup of the consolidometer is almost identical to that of Type I described above and shown in Figure 3-2. Once again side wall friction is halved by allowing

the sample to deform from both ends. However, unlike samples prepared in Type I which are only consolidated to σ'_p = 0.25 MPa, samples prepared in Type II are consolidated to σ'_p = 2 MPa. Given a cross sectional area of 9.35 cm^2, this requires a maximum load of 1870 N to be applied to the sample. As this is greater than the capacity of the hanger system on which dead weights are placed, a pneumatic actuator is used to apply the higher loads. Once the sample is consolidated to 0.25 MPa it is transferred to the pneumatic actuator for further consolidation up to σ'_p = 2 MPa. The transfer from the hanger system to the pneumatic actuator is performed rapidly to prevent significant swelling of the sample. A load equal to what was reached in the hanger system (i.e. 0.25 MPa) is also initially applied in the pneumatic actuator for at least 24 hours before the next increment (0.5 MPa) is applied. Samples prepared in consolidometer Type II for high pressure triaxial testing require a little over a month to produce.

3.2.4 Consolidation Behaviour during Resedimentation

The time required to reach the end of primary consolidation (t_p) for each load increment during the resedimentation process depends on the drainage height of the sample as well as on c_v. Several days are generally required to reach t_p for the first few load increments, though this reduces significantly at higher stresses as the drainage height becomes shorter and, as will be discussed in Section 3.4.5, c_v increases. For example, approximately only 3 hours is required to reach t_p for the 1 to 2 MPa load increment in consolidometer Type II. For each consolidometer type, Figure 3-3 shows typical[6] settlement-(log)time curves for the 16 to 32 kPa load increment. The value of t_p (obtained using the Casagrande log-time method) is about 12 hours in each consolidometer. The corresponding settlements are 1.01 cm and 1.09 cm in Types I and II respectively. For the same load increments Figure 3-4 shows normalized settlement-(log)time curves where degree of consolidation U_v is plotted against t/t_p for samples in each consolidometer compared with what is predicted by Terzaghi's theory of one-dimensional consolidation. It can be seen that the theory tends to slightly over-predict the settlement at a given time until t_p is approached.

The water content and height of a sample measured upon extrusion from the consolidometer can be used to back-calculate the void ratio of the clay at the end of each load increment during the resedimentation process. Figure 3-5 shows compression curves obtained during the resedimentation of samples in e-logσ'_{ac} space. Samples with a batch preconsolidation of 0.25 MPa were prepared in Type I consolidometers while those with a batch preconsolidation pressure of 2 MPa were prepared in Type II consolidometers. Each solid dot on the curves represents the conditions at the end of each

[6] The consolidation behaviour for samples prepared in each type of consolidometer was almost identical and therefore only 'typical' results from representative batches are presented here

load increment. Overall, the measured compression curves demonstrate the very good repeatability involved in the resedimentation process. It should be kept in mind that the end points for each load increment include varying amounts of secondary compression. As such, properties such as compression ratio (CR), compression index (C_c), coefficient of consolidation (c_v), and hydraulic conductivity (k_v) are better obtained from the results of CRS tests and are discussed in Section 3.4.

For comparison, Figure 3-5 also includes the compression curve obtained from a typical CRS test performed by Abdulhadi (2009). The slight offset that can be seen in the resedimentation compression curves relative to the virgin compression curve measured in the CRS test is almost certainly due to the effects of side wall friction in the consolidometers. Side wall friction of course reduces the actual stress imposed on the soil sample relative to the target stress level and appears to effect samples prepared in both types of consolidometer equally. As will be discussed in Chapter 5, yield stresses observed during the reconsolidation of specimens in the triaxial device are observed to be considerably lower that the batch preconsolidation pressures which are supposedly applied during the resedimentation process. Side wall friction in the consolidometers is believed to have contributed to this.

3.2.5 Evaluation of Specimen Uniformity

The uniformity and quality of RBBC samples produced by the large diameter (30 cm) consolidometers used in the past were evaluated by Germaine (1982) and Seah (1990). Uniformity of individual batches was examined by measuring the variation of water content throughout the sample, utilizing X-ray diffraction pattern methods as well as air dry vertical and radial slices to check for stratification. Results from all these procedures verified that the batches were indeed uniform. As shown in Table 3-2 however, the height to diameter and surface area to cross sectional area ratios of samples produced using consolidometers Type I and II are much higher at the end of batch consolidation compared to those of the large diameter samples produced in the past. This will exaggerate the effects of side wall friction for samples prepared in consolidometers Type I and II. As well as reducing the actual stress imposed on the soil, side wall friction encourages sample non-uniformity during resedimentation in both the axial and radial directions and may create a slightly smeared outer layer. It should be kept in mind, however, that the impact of side wall friction on samples prepared in consolidometers Type I and II is limited to some extend by allowing the samples to consolidate from both ends, as described in Section 3.2.3.

Following the SHANSEP reconsolidation procedure (as described previously in Chapter 2), the effects of side wall friction imposed during the resedimentation process, or indeed any other

disturbance effects caused by extrusion from the consolidometer, should be effectively eliminated following K_o consolidation in the triaxial device to stresses much higher than the batch preconsolidation pressure. This ensures that any specimen non-uniformity is eliminated prior to undrained shearing in the triaxial device. Confirmation of this has been shown by Abdulhadi (2009) who compared the consolidation and shear results of two CK_oUC tests on RBBC where one specimen was prepared in a Type II consolidometer while the second specimen was prepared in a consolidometer of 6.35 cm inside diameter (actually a modified oedometer) and was trimmed prior to triaxial testing. The results of the two tests are presented in Figure 3-6 and Figure 3-7 (note that Abdulhadi refers to the Type II consolidometer as 'Plexi.' and the larger consolidometer as 'Stnd.'). Both specimens were consolidated to the same target stress in the consolidometers (σ'_{ac} = 0.1 MPa) and in the triaxial apparatus (σ'_{ac} = 0.35 MPa). Figure 3-6 shows the compression curves obtained during the K_o consolidation phase of the triaxial tests. At the final consolidation stress of σ'_{ac} = 0.35 MPa the two specimens have an almost identical void ratio, but slightly different values of K_o and axial strain. Note that the compression curve exhibited by the specimen prepared in consolidometer Type II has a yield stress which would appear to be significantly less than the preconsolidation of 0.1 MPa which was supposedly applied during resedimentation and that the yield stress is also quite poorly defined. In addition, the initial void ratio of the specimen is notably higher than that possessed by the specimen prepared in the larger diameter consolidometer. These observations could reasonably be attributed to an increase in side wall friction occurring in the Type II consolidometer. As shown in Figure 3-7, however, the undrained shear stress-strain responses for both tests are almost identical, with both tests having the same strain to peak, undrained strength and shear resistance at large strains. Since the consolidation and shear behaviour measured by Abdulhadi (2009) for RBBC at low stresses agrees very well with that measured by previous researchers who tested specimens trimmed from large diameter soil cakes, it is concluded that the additional side wall friction which specimens prepared in small diameter consolidometers are subjected to during resedimentation has a negligible effect on undrained shear behaviour, provided that the SHANSEP reconsolidation procedure is adopted.

3.3 INDEX PROPERTIES

3.3.1 Introduction

The properties of natural BBC vary throughout the Boston area even though the basic mineralogy and depositional history of the clay are believed to be the same. Each time new material is acquired from a natural source for resedimentation it is therefore necessary to perform several index tests to verify that the clay is sufficiently similar to that previously used for research at MIT.

Due to the long history of resedimentation of BBC at MIT, a large database exists on its index properties. Table 3-3 summarizes the specific gravity (G_s), Atterberg limit, clay fraction and salt concentration values reported by researchers for Series I, II and III RBBC while Table 3-4 shows the data for Series IV.

It can be seen from Table 3-3 and Table 3-4 that index properties vary somewhat considerably between the different series. Results from Series Ia in particular show significant deviation from the later series. The clay fraction of the soil varies from 35 to 60 %. Specific gravity for all series lies in the range of 2.75 to 2.81. Excluding data from Series Ia, the plasticity index (I_p) ranges from 16 to 26 % and this is mainly due to variations in the liquid limit (w_L) from 33 to 48 % as the plastic limit (w_p) only varies from 18 to 25 %. Despite this scatter in Atterberg limits, the USCS classification for all RBBC series is CL. Except for RBBC prepared by the author and Bailey (1961) to examine the effect of salt content on soil properties, salt concentration remains in the range of 8 to 24 g/l.

The index properties specific to Series IV RBBC, which is used in the author's research, are summarized below. A comparison is then made with typical known index properties of natural BBC. Finally, information is presented on the known effects of salt concentration on the index properties of RBBC.

3.3.2 Index Properties of Series IV RBBC

The first course of index testing on Series IV RBBC was carried out by Cauble (1996) with the most recent being performed by Abdulhadi (2009). Figure 3-8 by Abdulhadi shows the grain size distribution of Series IV BBC powder obtained using the hydrometer test (ASTM Standard D422). The graph shows that the clay has an average fine fraction (% passing #200 ASTM standard sieve) greater than 98% and an average clay fraction (% less than 2 μm) of 56%. These results agree well with those of Cauble (1996) who measured a fine fraction and clay fraction of 98% and 58±1.2% respectively.

Atterberg limit tests performed by Abdulhadi (2009) gave w_p = 23.5±1.1 %, w_l = 46.5±0.9 % and I_p = 22.7±1.2 % and are almost identical to the values reported by Cauble (1996). Liquid limits were determined using the Casagrande cup and plastic limits were determined using the rolling method (ASTM Standard D4318). Figure 3-9 shows liquid limits and plasticity indexes for RBBC Series IV plotted on a Casagrande plasticity chart, confirming its USCS classification as a low plasticity clay CL.

Specific gravity tests (ASTM Standard D854) were carried out on a specimen of RBBC which had previously been used in a CK_oUC triaxial test with σ'_{ac} = 10 MPa. Specific gravity tests were performed on the triaxial specimen in order to investigate whether any permanent change in the value of G_s results from consolidation to relatively high stresses. However, the value of G_s was measured to be 2.778±0.001 which, as can be seen from Table 3-3 and Table 3-4, is a typical value in the mid-range of those previously quoted for RBBC, though is slightly lower than the value of 2.81 quoted by Cauble (1996) and Abdulhadi (2009). Bishop et al. (1975) stated that, on the basis of purely elastic behaviour, a maximum increase in G_s for clay particles would be approximately only 0.2 - 0.3 % at a consolidation stress of 62 MPa. It is therefore concluded that that no adjustment in the value of G_s with stress level is necessary for the author's experimental program.

As will be discussed below, the pore fluid of natural BBC contains salt which varies in concentration as a function of both location and depth. The salt content of BBC Series IV dry powder used for resedimentation was measured using the conductivity method and calibrated against a KCL standard. The salt content was found to be 2.68±0.05 g per kg of dry powder. At an in situ water content of say 40 %, this would correspond to 6.70±0.12 g per litre of pore fluid.

Cauble (1996) determined the organic content of Series IV BBC powder to be 4.4% by combustion (ASTM D2974). No other data on organic content is available for RBBC.

3.3.3 Index Properties of Natural Boston Blue Clay

An extensive experimental investigation of the properties of natural BBC was carried out by Berman (1993). BBC from the construction site of Building 68 on the MIT campus was used in the investigation and significantly this is also the natural source for RBBC Series IV. This allows for a reasonable comparison to be made between the index properties of the natural BCC and the corresponding properties of RBBC Series IV described above. The stratigraphy of the Building 68 site is shown in Figure 3-10. The layer of BBC has an average thickness of 20 m, the top 10 – 12 m being an overconsolidated crust below which the clay is close to normally consolidated. Salt concentration decreases through the top 10 m of BBC from about 20 g/l to about 5 g/l and remains almost constant at 5 g/l throughout the remainder of the deposit. The presence of salt in the clay is due to it being deposited in a marine environment, with subsequent leaching (caused by artesian pressures in the underlying glacial till) having reduced the salt concentration in the clay from that of seawater (35 g/l). Specific gravity for BBC at the Building 68 site was found to be 2.793±0.025. The pH of the clay was found to remain in the neutral range with values from 6 to 8 throughout the deposit (Berman, 1993).

Figure 3-11 by Berman (1993) shows the grain size distribution profile for the layer of BBC at the Building 68 site obtained from 16 hydrometer tests. Although the distribution varies considerably throughout the deposit, there is no consistent trend with depth. The clay fraction can be seen to vary from 40 to 53 %, the percentage of silt sized particles varies from about 37 to 49 % while the percentage of non-fines (i.e. sand and gravel) is typically 5 to 10 %.

The results of Atterberg limit tests performed by Berman (1993) show significant scatter with w_p = 24.7±3.2 %, w_L = 36.8±8.6 %, and I_p = 15.5±6.2 %. These are average values for the 20 m BBC deposit obtained from 29 tests. Berman also noted that there is a trend for I_p to decrease with depth. The value of w_p for the Building 68 site compares well with values for BBC from 8 other sites on the MIT campus as well as with other locations in the Boston area. However, Berman noted that the value of w_L, and therefore also I_p, is considerably lower than previously quoted values for BBC.

3.3.4 Effects of Salt Concentration

Bailey (1961) investigated the effects of salt content on the index properties of Series Ia RBBC by comparing samples produced at concentrations of 35 g/l and 2-3 g/l. Table 3-5 summarizes the results. As expected, salt content has little effect on the measured values of clay fraction, specific gravity and plastic limit. However, also as would be expected, a higher salt content increases the liquid limit, thereby increasing the plasticity of the clay. The activity of the clay is also seen to be increased by a higher salt content. It should be pointed out that the increase in liquid limit from 30 to 34.7 % reported by Bailey (1961) is relatively modest for such a large increase in salt concentration. This may be explained by examining some of the results of Green (1956) who investigated the effect of salt content on the Atterberg limits of BBC. The BBC used by Green was washed thoroughly during preparation and contained a negligible initial amount of salt. The data shown in Table 3-6 illustrates that the first few g/l of NaCl has a profound effect on the liquid limit. However, for concentrations greater than about 5 g/l the effect becomes significantly reduced. Again, salt concentration can be seen to have little effect on the plastic limit. These results help to explain the small increase in liquid limit observed by Bailey (1961) since the most pronounced effect of salt on the liquid limit may already occurred at a concentration of just 2-3 g/l. In addition, the very small variation in liquid limit reported for RBBC Series IV by various researchers in Table 3-4 could be attributed to the fact that the salt concentration of the clay only varied from about 10-13 g/l.

3.4 ONE-DIMENSIONAL CONSOLIDATION BEHAVIOUR

3.4.1 Introduction

There is a large amount of data available on the one-dimensional consolidation behaviour of RBBC derived from incremental oedometer, CK_oUDSS and CRS tests as well as from the K_o consolidation stage of triaxial tests. However, with the exception of Abdulhadi (2009) who investigated one-dimensional consolidation behaviour for σ'_{am} up to 10 MPa, previous studies were confined to relatively low stresses with σ'_{am} up to approximately only 1 MPa. This section therefore focuses primarily on the consolidation behaviour of RBBC Series IV reported by Abdulhadi (2009), though comparisons will also be made will the corresponding behaviour of RBBC observed by previous researchers for lower stresses as well as with natural BBC. The RBBC used in previous investigations has generally had a salt concentration in the range of 10 to 20 g/l, and usually about 16 g/l.

3.4.2 Compression Curves and Compressibility Parameters

Figure 3-12 from Abdulhadi (2009) shows compression curves for RBBC Series IV for σ'_{ac} up to 10 MPa in conventional e-logσ'_{ac} space and demonstrates the exceptional repeatability of RBBC. The figure includes curves obtained from the K_O consolidation triaxial tests along with a compression curve obtained from a typical CRS test. The K_O algorithm used for the consolidation stage of triaxial testing at the MIT Geotechnical Engineering Laboratory works by continually adjusting cell pressure in order to ensure zero radial strain as the specimen is being strained axially at a constant rate. It can be seen from Figure 3-12 that the curves from the two types of tests agree very closely. The compression curves are characterized by a well defined yield at the batch preconsolidation pressure, with the triaxial tests having σ'_p of either 0.1 MPa or 1 MPa and the CRS tests having σ'_p of 0.1 MPa. The agreement in behaviour observed for the two types of tests also indicates that the axial strain rate of 0.15 %/hr employed during the K_O consolidation stage of the triaxial tests was sufficiently slow to prevent unreasonably large excess pore pressures from being generated in specimens.

For the CRS tests performed by Abdulhadi (2009) the slope of the virgin consolidation line was found to be slightly non-linear and 'S-shaped'. The virgin compression ratio ($CR = \Delta\varepsilon_a/\Delta\log\sigma'_a$) was found to decrease from about 0.18 – 0.2 at σ'_a = 0.2 MPa to 0.13 at σ'_a = 0.2 MPa, with the rate of decrease reducing with stress level. The value of CR at low pressures is consistent with prior studies on RBBC, e.g. Ahmed (1990), Sheahan (1991), Seah (1990) and Santagata (1994). However, the value of CR reported by Abdulhadi for higher stresses is lower than any value previously quoted. The swelling ratio (SR) is approximately an order of magnitude smaller than CR

and increases with OCR. Values of SR are determined by connecting compression curve points at the end of loading (after allowing for secondary compression) and at the end of unloading. As OCR increases from 1 to 4, Abdulhadi reported SR increasing from 0.012 to 0.015. These values for SR, as well as the trend with OCR, are consistent with previous studies. For example, Ahmed (1990) reported SR increasing from 0.011 at an OCR of 2 to 0.019 at an OCR of 8.

Slightly different compression parameters were derived by Abdulhadi (2009) from triaxial tests. The value of CR varied from 0.147 to 0.168 over the stress range of 0.15 to 10 MPa. However, unlike in the CRS tests, there is no clear trend for CR to vary with stress level and the compression curves appear to remain approximately (log)linear throughout the entire virgin compression range. Abdulhadi found no reason to justify this [apparent] difference in behaviour observed between the CRS and triaxial tests. Values of SR derived from triaxial tests varied from 0.011 – 0.022 and showed a similar trend of increasing with OCR.

3.4.3 Lateral Stress Ratio

Figure 3-13 shows the variation in K_O with axial stress during the consolidation stage of triaxial tests performed by Abdulhadi (2009). The graph shows that K_O decreases in the OC range until σ'_p is reached (0.1 MPa or 1 MPa) and then plateaus to a fairly stable value of K_{ONC} once in the NC range. It should be noted that this trend for the change in K_O during consolidation is slightly different to that found in previous studies, e.g. Sheahan (1991) and Santagata (1994). Figure 3-14 shows the typical trend for the change in K_O with axial stress during the consolidation phase of triaxial tests performed on RBBC Series III by Santagata (1994). It can be seen that K_O decreases during the initial loading to a value lower than K_{ONC} before increasing again. Once consolidated well into the virgin compression range, K_{ONC} remains fairly constant. This plunge in K_O just before reaching the preconsolidation pressure was observed in all tests performed by Santagata (1994) but in none of the tests performed by Abdulhadi (2009). Abdulhadi hinted that this could possibly be due to either the different resedimentation procedures or different series of RBBC adopted in each study.

In addition to the different trend for the change in K_O during consolidation described above, Abdulhadi (2009) also reported significant differences in the magnitude of K_{ONC} compared to prior investigations. As mentioned previously in Chapter 2 (and illustrated in Figure 2-6), Abdulhadi reported that K_{ONC} increased consistently with stress level from 0.518 at σ'_{ac} = 0.15 MPa to 0.564 at σ'_{ac} = 10 MPa. The value of K_{ONC} at low stresses is consistent with previous studies on RBBC Series III and IV. For example, Seah (1990) found K_{ONC} = 0.522±0.005, Santagata (1994) reported K_{ONC} varying from 0.44 to 0.52 and Force (1998) obtained K_{ONC} = 0.52±0.01. However, the value of 0.564

for K_{ONC} found by Abdulhadi (2009) at σ'_{ac} = 10 MPa is considerably higher than anything previously reported for RBBC. The change in K_{ONC} with stress level reported by Abdulhadi is certainly significant and this is especially so given the fact that the value of K_{ONC} prior to shearing may dramatically affect the undrained strength of the clay, as will be discussed further in Section 3.5.3.

Prior studies using CK_OU triaxial tests (e.g. Sheahan, 1991 and Santagata, 1994) and lateral stress oedometer devices (O'Neill, 1985) have found that the variation in K_O with OCR for RBBC can be well described using the following empirical equation:

$$K_O = K_{ONC}(OCR)^n \qquad \text{Equation 3-1}$$

where $n \sim 1-\sin\varphi'_{mo}$. For triaxial tests performed at MIT, specimens which need to be unloaded into the OC range prior to shearing are usually subjected stress path swelling by employing Equation 3-1 to compute the pre-shear value of K_O at the desired OCR.

3.4.4 Secondary Compression

The largest sets of data on the secondary compression behaviour of RBBC are provided by Sheahan (1991) and Cauble (1993) based on CK_oU and CK_oUDSS triaxial tests respectively. For NC RBBC both Cauble and Sheahan report a rate of secondary compression $C_{\alpha\varepsilon} = \Delta\varepsilon_a/\Delta\log t$ of 0.0028±0.0005, thereby resulting in a $C_{\alpha\varepsilon}/CR$ (or $C_{\alpha e}/C_c$) ratio of 0.0173±0.0042. Seah (1990) obtained a slightly higher $C_{\alpha\varepsilon}/CR$ ratio of 0.02 from a series of incremental oedometer tests. It should be noted that these results for $C_{\alpha\varepsilon}/CR$ are well below the range of 0.04±0.01 quoted by Mesri and Castro (1987) for a variety of inorganic soft clays and are also on the low side compared to data reported by O'Neill (1985) for RBBC Series II of 0.036±0.004.

In accordance with the constant C_α/C_c ratio concept develop by Mesri and Castro (1987), the rate of secondary compression for OC RBBC is about an order of magnitude smaller than that of the NC clay.

3.4.5 Coefficient of Consolidation and Hydraulic Conductivity

Figure 3-15 shows the variation in c_v for NC RBBC as obtained from three CRS tests performed by Abdulhadi (2009). The results were interpreted using the standard linear theory. For each CRS test σ'_p = 0.1 MPa. The figure also includes values of c_v measured during the process of batching samples for triaxial and other shear tests. It can be seen that there is a clear trend for c_v to increase with increasing consolidation stress, rising from a minimum of approximately 0.0005 cm^2/s

at 0.002 MPa to 0.003-0.006 cm^2/s at σ'_{ac} = 10 MPa. For σ'_{ac} above approximately 1 MPa the trend is less obvious. The significant increase in c_v from very low to high stresses found by Abdulhadi (2009) was not previously reported for RBBC as prior studies did not involve a wide enough stress range. However, the magnitude of c_v and the trend with stress level is consistent with previous results in the stress range 0.1 – 1 MPa, e.g. Force (1998). It should be kept in mind that the rate of pore pressure equilibration in specimens during the undrained shear phase of triaxial tests is influenced by c_v of the soil. In the NC range the increase in c_v with stress level would indicate that the historical axial strain rate of 0.5 %/hr employed for the undrained shear phase of triaxial tests performed at the MIT Geotechnical Engineering Laboratory should also appropriate at relatively high consolidation stresses. Data on c_v for OC RBBC is more scarce, though Force (1998) reports values of 0.010 – 0.015 cm^2/s at σ'_{ac} < 0.1 MPa based on the results of CRS tests. The significantly higher c_v for the OC soil compared to the NC soil is expected, given its lower compressibility at the same stress level.

The reduction in vertical hydraulic conductivity (k_v) with decreasing void ratio, and therefore increasing consolidation stress, obtained from Abdulhadi's CRS tests and batching is shown in Figure 3-16. It can be seen that k_v reduces from approximately 1 x 10^{-6} cm/s at e = 1.85 (corresponding to σ'_{ac} = 0.0005 MPa) to about 3 x 10^{-9} cm/s at e = 0.53 (corresponding to σ'_{ac} = 10 MPa). The value of $C_k = \Delta e/\Delta \log k$ varies with stress level as it decreases from about 0.90 at low consolidation stresses (below approximately 0.01 MPa) to about 0.32 at higher stresses (above approximately 1 MPa). Once again, while C_k in the stress range 0.1 – 1 MPa is in good agreement with previous results for RBBC Series IV, the values of C_k found by Abdulhadi (2009) at much lower and much higher stresses are outside the range of previously reported values.

The ratio C_C/C_k is important for examining the consolidation behaviour of clays as it determines whether the rate of consolidation, as indicated by c_v, will increase or decrease with increasing stress level. For C_C/C_k < 1 the value of c_v becomes larger with increasing consolidation stress while for C_C/C_k > 1 the opposite is the case. The variation in C_C/C_k with stress level found in CRS tests performed by Abdulhadi (2009) is shown in Figure 3-17. The measured values of C_C/C_k can be seen to lie in the range of about 0.6 – 1.2. As mentioned above and illustrated in Figure 3-15, c_v rises in the NC range for σ'_{ac} up to approximately 1 MPa, beyond which the change in c_v is less conclusive. This variation in c_v can be explained by examining Figure 3-17, where it can be seen that for σ'_{ac} below approximately 1 MPa the ratio of C_c/C_k is certainly less than 1 while for higher stresses C_c/C_k remains at about 1. It is also important to note that the conventional Terzaghi theory of one-dimensional consolidation assumes that C_c/C_k = 1.

Force (1998) examined the effect of axial strain rate on consolidation behaviour measured in CRS devices. The strain rates investigated ranged from very slow, at just 0.07 %/hr, to very fast, at 12.71 %/hr. Force noted that the amount of excess pore pressure generated increases with increasing strain rate in an approximately linear manner, while the ratio of excess pore pressure to total axial stress (u_e/σ_a) varies from 0.2% to 30%. The compression curves tend to fall within a narrow band with the faster tests tending to shift very slightly to the right with a corresponding small increase in σ'_p. Values of c_v agree well once the soil is in the NC range and, with the exception of the fastest test, the measured hydraulic conductivity was hardly affected by the strain rate.

3.4.6 Consolidation Behaviour of Natural Boston Blue Clay

Figure 3-18 shows compression curves obtained from two CRS tests performed on specimens of natural BBC in e-logσ'_{ac} space. For comparative purposes the curve from a typical CRS test (CRS912) performed on RBBC by Abdulhadi (2009) is also included in the figure. The BBC specimens were taken from tube samples obtained during a drilling program in the Killian Court area of the MIT campus in June 2010. The tests were run by Ms. Lauren Biscombe. CRS1153 was performed on sample S1 obtained from a depth of 14.5 m. CRS1154 was performed on Sample S2 obtained from a depth of 17 m. The in situ vertical effective stresses for Samples S1 and S2 were estimated to be 0.14 and 0.16 MPa respectively[7]. It can be seen from Figure 3-18 that the compression curves of the BBC specimens show a well defined yield point corresponding to the preconsolidation pressure of the clay. Using the strain energy method (Becker et al., 1987) σ'_p was calculated to be 0.46 MPa and 0.3 MPa for samples S1 and S2 respectively, resulting in an in situ OCR of 3.3 and 1.9 respectively. It should be noted that the higher σ'_p and lower in situ void ratio for shallower Sample S1 is due to this sample having been taken from a upper desiccated crust of the BBC layer. Figure 3-18 illustrates that the compression behaviour of BBC is very similar to that of the corresponding resedimented material. As can be expected for a natural clay, however, the void ratios of samples S1 and S2 at σ'_p are higher than the corresponding void ratio on the virgin compression line of the resedimented material at the same stress, thereby indicating the presence of a slightly stronger structure in the in situ soil (Burland, 1990). Once samples S1 and S2 are both consolidated into the NC range their compression curves converge and an almost identical stress-void ratio state is attained. At this point the curves appear to begin converging with the RBBC compression curve. At the highest stress of 2.6 MPa achieved in two tests on the intact samples, the

[7] These effective stresses are based on assuming hydrostatic groundwater conditions with a watertable at 2 m depth (Germaine, personal communication), as well as a total unit density for the soil of 18 kN/m^3

compression curve for Sample S1 lies on the curve for RBBC while Sample S2 still maintains a slightly higher void ratio than the resedimented material.

Figure 3-19 shows the variation in CR and SR with stress level as measured for samples S1 and S2. It can be seen that CR for both BBC samples increases significantly after σ'_p is reached and achieves a peak value (CR_{max}) of approximately 0.20 and 0.18 for samples S1 and S2 respectively. CR for both samples then reduces and approaches that of RBBC, which also shows a slight but consistent decrease with increasing stress. As expected, the value of SR for BBC is approximately an order of magnitude smaller than CR and increases significantly with OCR. The variation in SR alone for samples S1 and S2 is shown in Figure 3-20. It can be seen that SR for both samples is almost identical and increases from about 0.012 at σ'_{ac} = 2.6 MPa (OCR = 1) to about 0.038 at σ'_{ac} = 0.1 MPa (OCR = 26). At OCR = 10 SR was found to be 0.035 and 0.034 for samples S1 and S2 respectively. The corresponding value for RBBC was measured to be 0.029. Figure 3-21 by Berman (1993) summarizes CR and SR data for BBC at the Building 68 site, as well as various other locations around the MIT campus including the Materials Centre (13), the Student Centre (W20), CAES (9), Solar House (W74), Hayden Library (14S) and the Nuclear Physics Lab (16/56). The CR values quoted by Berman are values of CR_{max} and the values of SR correspond to unloading over one log stress cycle, i.e. at OCR = 10. The average CR_{max} for all locations given in Figure 3-21 is 0.178±0.036 above El.-45 ft (-13.7 m) and 0.172±0.045 below El.-45 ft. The values of CR_{max} for samples S1 and S2 obtained from Killian Court lie within the standard deviation of values from these other locations. However, as can be seen from Figure 3-21, the values of SR found for samples S1 and S2 at OCR = 10 are on the high side when compared to previously quoted values for other locations around the MIT campus. The collective data represented in Figure 3-21 yields SR = 0.029±0.006 above El.-45 ft and 0.022±0.008 below El.-45 ft. Berman (1993) noted that the SR data from the Building 68 site may be questionable as sufficient pore pressure dissipation did not occur at the end of consolidation by allowing for an adequate period of secondary compression.

Cotecchia and Chandler (2000) define stress sensitivity $S_\sigma = \sigma'_{vy}/\sigma^*_{ey}$, where σ'_{vy} is the consolidation stress corresponding to 'gross yield' of the clay, i.e. the real or apparent preconsolidation stress, and σ^*_{ey} is the corresponding stress on the virgin consolidation curve of the resedimented material at the same void ratio. Based on an examination of the consolidation and strength behaviour of many soils in both intact and resedimented states, Cotecchia and Chandler proposed that, for all practical purposes, stress sensitivity is almost equal in magnitude to strength sensitivity, i.e. $S_\sigma = S_t$, where S_t in this case is defined as the ratio of the undrained strength of the undisturbed clay after consolidation to σ'_p to that of the resedimented clay normally consolidated to

the same void ratio[8]. Therefore, by definition $S_\sigma = S_t = 1$ for resedimented clay. Table 3-7 compares values of S_σ and S_t for various clays in an intact state. By analyzing the compression curves shown in Figure 3-18 and applying the same approach to BBC, the value of S_t for natural BBC would be approximately only 1.27. The calculations used to derive this value are given in Table 3-8. Though based on the results of only two tests, it can be seen from Table 3-7 that when compared to other natural clays (none of which would be regarded as quick) a value of S_t = 1.27 for BBC is exceptionally low. This observation certainly serves to promote the use of RBBC as an analogue test material.

Figure 3-22 shows the variation in c_v with stress level for BBC samples S1 and S2. Only values of c_v for which the ratio u_e/σ_a was less than 0.2 are shown (during the initial loading and final unloading the u_e/σ_a ratio was often greater than 0.2 and as such some c_v data in the recompression range and all of the data in the unloading range is omitted from Figure 3-22). It can be seen that the change in c_v with stress level is very similar for both BBC samples. For sample S1, c_v decreases from a maximum value of about 0.0040 cm^2/s in the OC range to a minimum of 0.0016 cm^2/s at σ'_{ac} = 1 MPa. Beyond this point, c_v increases again with increasing stress to reach 0.0020 cm^2/s at σ'_{ac} = 2.6 MPa. For sample S2, c_v decreases from a maximum value of about 0.0045 cm^2/s in the OC range to a minimum of 0.0016 cm^2/s at σ'_{ac} = 0.5 MPa. Once again c_v increases with stress to reach 0.0024 cm^2/s at σ'_{ac} = 2.6 MPa. The trend for c_v to increase with stress level in the NC range is explained by examining Figure 3-23, where it can be seen that the ratio C_c/C_k for BBC remains considerably less than 1 within the stress range investigated. For comparison, Figure 3-22 also shows the change in c_v with stress for NC RBBC. For various locations around the MIT campus Berman (1993) quoted an average c_v = 0.0014±0.0007 cm^2/s for NC BBC. The trend for c_v to increase with stress level in the NC range was also noticed by Berman, who reported an average C_c/C_k ratio of 0.71 for BBC at the Building 68 site. For OC BBC the data from the MIT campus shows more scatter, with values of c_v generally ranging from about 0.002 to 0.009 cm^2/s, depending on the location and test program. In general, c_v for a soil would be expected to be an order of magnitude or so greater in the OC range than in the NC range, so the quoted values of c_v for OC BBC could be regarded as being relatively low.

The value of K_O for BBC was investigated by Berman (1993) for the Building 68 site based on data from the one-dimensional consolidation stage of triaxial tests performed using the MIT automated triaxial system. It was found that K_O decreases during the initial loading within the OC range until approximately the overburden stress is reached, beyond which it increases again. Once

[8] Keep in mind that this is not the typical definition of sensitivity S_t, which is usually defined as the ratio of peak shear strength to the large strain residual shear strength at the same water content (Terzaghi and Peck, 1967)

consolidated into the NC range K_O either remains approximately constant or shows a slight continuous increase. This is similar to the behaviour of RBBC reported by several researchers as discussed previously (e.g. Sheahan, 1991 and Santagata, 1994). The value of K_{ONC} found by Berman showed wide variation and ranged from 0.51 to 0.60 with no clear trend with depth. Berman noted that this range for K_{ONC} is consistent with previous data for BBC from South and East Boston. When compared to the value of K_{ONC} for RBBC at corresponding low stresses as discussed previously, K_{ONC} for BBC is somewhat higher, though is similar to what was obtained by Abdulhadi (2009) for RBBC at high stresses. The same relationship linking the increase in K_O with OCR for RBBC given in Equation 3-1 was also found to apply to BBC. The value of n recommended by Berman for BBC is equal to 0.45.

3.5 UNDRAINED SHEAR BEHAVIOUR IN TRIAXIAL COMPRESSION

3.5.1 Introduction

Considerable knowledge exists on the undrained shear behaviour of RBBC as a function of stress history and stress system. However, apart from the work of Abdulhadi (2009), previous experimental studies have been confined to investigating behaviour under stresses conventionally encountered in geotechnical engineering, with consolidation stresses generally no higher than about 1 MPa being employed. As a result, this section presents only a limited discussion of the undrained shear behaviour of RBBC in triaxial compression reported from previous studies, focusing on aspects of this behaviour which are still important in relation to the research presented in this thesis and have not already been discussed in Chapter 1, i.e. such as the work of Abdulhadi (2009). In particular, stiffness, strain rate sensitivity, the effect of lateral stress ratio on undrained strength and the effect of salt concentration on behaviour are discussed. When employing a laboratory manufactured soil to pursue fundamental research it is important that its behaviour is representative of a natural soil. Therefore, a brief comparison is also made between the undrained shear behaviour of RBBC and natural BBC in triaxial compression at low stresses.

3.5.2 Stiffness

Santagata (1998) used on-specimen displacement transducers with a high resolution in order to gain information on the stiffness of RBBC at very small strains. Figure 3-24 plots the results of Santagata's tests at OCR's 1, 2, 4 and 8 where initial (maximum) Young's modulus E_{uMAX} in undrained triaxial compression is plotted against mean consolidation stress p'_{mc} on log scales. Mean consolidation stress accounts for changes in both void ratio and axial consolidation stress, both of

which in turn influence initial stiffness. It can be seen from Figure 3-24 that the OC data fall within a narrow range, distinct from the NC results. Based on the results of her tests, Santagata proposed the following relationship linking initial stiffness of RBBC to axial consolidation stress and void ratio for all OCR's:

$$E_{uMAX} = 270e^{-2.45}\sigma'_{ac}{}^{0.43} \text{ (MPa)} \qquad \text{Equation 3-2}$$

Santagata (1998) also indicated that the E_u does not exhibit perfect normalized behaviour, even when examined over a relatively small range of low stresses, with E_u/σ'_{ac} tending to decrease with increasing stress level. This in consistent with the findings of Abdulhadi (2009) discussed in Chapter 2 where a substantial decrease in E_u/σ'_{ac} was found over a wider stress range.

Figure 3-25 shows the strain to undrained failure versus OCR as reported by Abdulhadi (2009). As expected for an uncemented soil, the strain to failure increases substantially with increasing OCR and, as discussed previously in Chapter 2, increases with stress level at a given OCR.

3.5.3 Impact of Lateral Stress Ratio

As discussed previously in Chapter 2, Abdulhadi (2009) found a consistent increase in the value of K_{ONC} with increasing stress level and this corresponds with a decrease in normalized undrained strength with increasing stress level. Santagata (1994) also found a similar correlation for RBBC Series III. Figure 3-26 illustrates the decrease in normalized undrained strength with increasing pre-shear lateral stress ratio for NC RBBC as obtained from tests performed by both Sheahan (1991) and Santagata (1994) in the stress range 0.2 – 0.6 MPa. It should be noted that Figure 3-26 includes results from triaxial tests involving K_o consolidation as well as from tests involving stress path consolidation with a prescribed value of K. These stress path tests were carried out specifically to check the validity of the relationship outside the range of experimental variability in K_{ONC}.

3.5.4 Strain Rate Sensitivity

The undrained shear behaviour of RBBC discussed so far (including the behaviour discussed in Chapter 2) corresponds to the behaviour measured using an axial strain rate of 0.5 %/hr. The time dependent behaviour of RBBC during undrained shearing has been investigated by Sheahan (1991), who tested RBBC Series III. The triaxial apparatus used in this study had smooth

ends and the pore pressure was measured at the specimen mid-height. Behaviour was investigated at four different strain rates: 0.05, 0.5, 5 and 50 %/hr. The effect of strain rate on the normalized shear stress-strain response of NC RBBC is shown in Figure 3-27 for strains up to 2%. The figure shows that increasing the strain rate from 0.05 to 50 %/hr increases normalized strength from about 0.30 to 0.37. Initial stiffness and the degree of post-peak strain softening both increase considerably with increasing strain rate, though strain to failure appears to be unaffected by strain rate. The corresponding stress paths given in Figure 3-28 show that φ'_p increases significantly with increasing strain rate while φ'_{mo} is rate independent. The shear induced pore pressures tend to be suppressed with increasing strain rate, as illustrated in Figure 3-29. For OC RBBC similar trends are observed, though the increases in undrained strength and stiffness with increasing strain rate are less pronounced. A unique failure envelope is reached at large strains independent of strain rate and OCR.

The effect of strain rate on undrained strength is summarized in Figure 3-30 for OCR's 1, 2, 4 and 8. The number in parentheses on the graph refers to $\rho_{0.5}$, the change in normalized strength (s_u/σ'_p) across one log cycle of strain rate expressed as a percentage of the normalized strength measured at a reference rate 0.5 %/hr. In general, it can be seen that strain rate sensitivity decreases with increasing OCR, especially at slow strain rates. The increase in undrained strength with increasing strain rate results from a combination of two factors: a higher frictional resistance at peak strength (as indicated by φ'_p) and the suppression of shear induced pore pressures. Both of these mechanisms act to increase the undrained strength of RBBC at OCR's 1 and 2, while only lower shear induced pore pressures are responsible for any increase in strength at higher OCR's. The effect of strain rate on the SHANSEP parameters is summarized in Figure 3-31. An increase in strain rate causes S to increase and m to decrease, since increasing strain rate increases undrained strength with this increase being less pronounced at higher OCR's.

In Chapter 2 it was discussed that a 'slow' test can generally be regarded as one in which 95% pore pressure equilibration occurs prior to undrained strength being reached. Recall the theoretical relationship given in Equation 2 – 2 by Bishop and Henkel (1962) for determining t_{95}:

$$t_{95} = \frac{T_{95} H_d^2}{c_v}$$

Assuming a conservative value of c_v = 0.01 cm^2/s for OC RBBC (Force, 1998), a H_d of 3.6 cm (at the end of consolidation for two-way drainage of a standard sized triaxial specimen) and T_{95} = 1.67, then a value of 36 minutes is computed for t_{95}. For the historical strain rate of 0.5 %/hr used for RBBC at MIT, t_{95} = 36 minutes requires a minimum ε_f = 0.3 %. Since OC RBBC generally fails at strains much

greater than 0.3 % (see Figure 3-25), a rate of 0.5 %/hr is deemed to be sufficiently slow. For NC RBBC on the other hand, assuming an average c_v = 0.003 cm^2/s yields a minimum ε_f = 1.0 % and, as demonstrated in Figure 3-25, NC RBBC specimens which have been K_O consolidated often fail at strains less than 1.0 %, particularly at low stresses. However, given the fact that relatively small pore pressures are generated in NC soil prior to failure, and the fact that pore pressure gradients are minimized by compensating effects for NC soil (as discussed in Chapter 2), it is strongly believed that there is not sufficient opportunity for non-negligible pore gradients to develop in NC specimens prior to failure when a strain rate of 0.5 %/hr is adopted. It is concluded that the historical MIT strain rate of 0.5 %/hr is sufficiently slow to ensure reasonable pore pressures equilibration in RBBC specimens during undrained shearing.

3.5.5 Effect of Salt Concentration

The effect of salt concentration on the undrained shear behaviour of RBBC has been investigated by Bailey (1961). Bailey performed an extensive series of CIUC triaxial tests on samples of RBBC Series Ia prepared at salt concentrations of 2-3 g/l and 35 g/l. The samples at 2-3 g/l and 35 g/l salt concentration were produced using initial batch water contents of just 51% and 72% respectively (which are quite low given the current resedimentation practice at MIT of preparing clay slurries at 100% water content). It was found that the friction angle of the clay is reduced by decreasing salt concentration. For the clay at 35 g/l salt concentration φ'_{mo} and φ'_p were found to be 30.5° and 26.5° respectively, while for clay at a concentration of 2-3 g/l these values reduce to 28° and 24.5° respectively (assuming c' = 0). The pore pressure at failure was also found to reduce with decreasing salt concentration as indicated by a decreasing value of A_f. Bailey reported that, at the same water content, the undrained shear strength of the clay with 35 g/l of salt is twice the undrained strength of the clay with 2-3 g/l of salt. However, the consolidation pressure of the clay with 35 g/l of salt is also about twice the consolidation pressure of the clay with 2-3 g/l of salt for the same water content. Combined, these two factors compensate each other with the result that, at the same consolidation stress, the undrained strength of the clay was found to be unaffected by salt concentration. Bailey also noted that salt content appears to have no impact on the initial stiffness of the clay. It should be kept in mind that, as mentioned previously in Section 3.3, the liquid limit of RBBC is most affected by the first few g/l of salt. If the same applies to shear behaviour then the most pronounced effect of salt may already occurred at a concentration of just 2-3 g/l.

3.5.6 Natural Boston Blue Clay

In order for a true comparison to be made between the undrained shear behaviour of a natural soil and the corresponding resedimented material, the comparison should be based on the results of Recompression[9] tests performed on the intact natural material. Berman (1993) carried out five CK_oUC Recompression tests on intact tube samples of natural BBC which were obtained from the Building 68 site on the MIT campus. The five tests were performed on samples taken at varying depths with in situ vertical effective stresses σ'_{vo} ranging from 0.11 MPa to 0.24 MPa and in situ OCRs ranging from 1.35 to 4.3. Berman also compared the results of these tests with those of previous Recompression tests carried out on samples obtained from beneath the site of the CAES building on the MIT campus as well as from a site in South Boston. The general shear behaviour of intact natural BBC was shown to be very similar to that of the resedimented material. For example, like the behaviour of RBBC, increasing OCR for natural BBC causes a consistent increase in s_u/σ'_{ac}, E_u/σ'_{ac} and ε_f as well as a decrease in the degree of post-peak strain softening. Somewhat different effective strength parameters were found for BBC at the Building 68 site when compared to RBBC however. From the results of her Recompression tests, Berman quoted an average $\varphi'_{mo} = 21.9°$ and $c'/\sigma'_p = 0.054$ ($r^2 = 0.904$). In comparison, the large database of SHANSEP tests on RBBC at low stresses from Sheahan (1991) and Santagata (1994) gives $\varphi'_{mo} = 31°$ and $c'/\sigma'_p = 0.011$ ($r^2 = 0.97$). The very low friction angle quoted by Berman (1993) may be due to her interpretation of a particularly high normalized cohesion intercept for the natural material. However, a much larger database of 28 Recompression tests performed on natural BBC from a site in South Boston (de La Beaumelle, 1991) gives average values of $\varphi'_{mo} = 29°$ and $c'/\sigma'_p = 0.044$ ($r^2 = 0885$). These values of effective strength parameters are much more similar to those of RBBC and are likely to be more representative of natural BBC.

Regarding the undrained strength of natural BBC, Berman (1993) quoted average SHANSEP S and m parameters in triaxial compression of 0.27 and 0.73 respectively ($r^2 = 0.971$). In comparison, the database of SHANSEP tests on RBBC at low stresses from Sheahan (1991) and Santagata (1994) yields average S and m parameters of 0.33 and 0.71 respectively. Once again, however, Recompression tests carried out on natural BBC from South Boston give results more similar to the resedimented material, with S and m parameters of 0.30 and 0.68 respectively (Estabrook, 1991). The lower S parameter measured in the Recompression tests on natural BBC is somewhat unexpected, as it is typically believed that Recompression tests should overpredict the normalized undrained strength of NC soil when compared to SHANSEP tests. The lower value of S for BBC compared to RBBC may be attributed to notably higher values of K_{ONC} measured for the natural material. As discussed in Section 3.5.3, higher values of K_O can lead to a significant

[9] The Recompression reconsolidation technique (Bjerrum, 1973) has been described in Chapter 2

decrease in the undrained strength of NC soil. It should also be pointed out that, unlike the tests carried out on the tube samples of BBC obtained from the Building 68 site, the tests carried on the soil from South Boston were performed on specimens taken from both tube and block samples. Interestingly, Estabrook (1991) reported that of the tests carried on the South Boston material, tests performed at low OCR on specimens taken from tube samples yielded lower normalized undrained strengths than specimens taken from block samples.

Series	Year	Researcher	Topic	Tests Performed
I	1961	Bailey	Effect of salt concentration on undrained shear behavior	-
	1963	Jackson	Thixotropy	Triaxial
	1964	Varallyay	Influence of stress system on undrained strength	Triaxial
	1965	Ladd	Use of pressure transducer to measure soil pressure	-
	1965	Preston	Sample disturbance	Triaxial
	1966	Braathen	Disturbance effects on undrained strength	Triaxial
	1967	Dickey	Development of plane strain device	Plane Strain Device
	1967	Rixner	Behavior in plane strain at OCR 1, 2 &4	Plane Strain Device
	1968	Bovee	Behavior in plane strain at OCR 1, 2 &4	Plane Strain Device
	1970	Kinner	Behavior of strip footings during undrained loading	Model footing tests
II	1982	Germaine	Cross-anisotropic behavior at OCR 4	DSC, Triaxial
	1984	Bensari	Stress-strain and yielding behavior	Triaxial
	1985	O'Neill	Anisotropy of Thixotropic clay	DSC, Triaxial
	1986	Fayad	Volumetric and undrained behavior	Triaxial
	1987	Malek	Behavior under cyclic loading	DSS
III	1988	Walbaum	Investigation of sample disturbance	DSS
	1988	Sheahan	Modification of computer controlled triaxial apparatus	Triaxial
	1989	DeGroot	Behavior in undrained multidirectional DSS at OCR 1	DSS
	1990	Ahmed	Normalized behavior in DSS	DSS
	1990	Seah	Anisotropy at OCR 1	DSC
	1991	Ting	Performance of sand drains	Model testing
	1991	Sheahan	Time dependent material	Triaxial
	1992	Ortega	Computer automation of DSS	DSS
	1993	Cauble	Cyclic and post-cyclic behavior in simple shear	DSS
	1994	Santagata	Simulation of sampling disturbance in soft clays using triaxial tests	Triaxial
IV	1994	Sinfield	Simulation of sampling and effects on compression and shear	CRS, Triaxial
	1996	Cauble	Behavior of model suction caisson	Model Caisson
	1998	Santagata	Pre-failure behavior	Triaxial
	1998	Force	Strain rate selection in triaxial tests	CRS
	2000	Gonzalez	Investigation of CRS consolidation	CRS
	2009	Abdulhadi	Stability of Boreholes	Triaxial, Model BH
	2009	Moniz	Normalized behaviour in triaxial extension	Triaxial
	2011	Casey	Effect of specimen end restraint	Triaxial
	2011	Adams	Comparison of lab permeability measurement techniques	CRS

Table 3-1: Overview of previous studies performed using RBBC (extended from Santagata, 1998)

Consolidometer	Specimen Dimensions (cm)		Height to Diameter Ratio	Surface Area (i.e. side area) (cm^2)	Cross Sectional Area (cm^2)	Surface to Cross Section Area Ratio
	Diameter	Height				
Type I (a)	4.09	11	2.7	141.3	13.1	10.8
(b)	4.39	11	2.5	151.7	15.1	10.0
Type II	3.45	11	3.2	119.2	9.3	12.8
Large Consolidometer	30.5	12.5	0.4	1197.7	730.6	1.6

Table 3-2: Dimensions and area ratios of consolidometer specimens at the end of resedimentation

Year	Researcher	Series	Source Batch	G_s	w_l	w_p	I_p	Clay Frac. <2μm (%)	Salt (g/l)
1961	Bailey	Ia	MIT	2.77	30.0	17.5	12.5	40	2-3
			1139		34.7	17.7	17.0		35
1963	Jackson				36.2	19.5	16.7		16.7
1964	Varallyay		S4		32.6	19.5	13.1		
			S5		33.3	20.4	12.9	35	16.8
			S6		32.8	20.3	12.5		16.0
1965	Ladd, R.S.	Ib		2.77	45	22	23		16
1965	Preston		S1	2.77	45.6	23.4	22.2	35	24
1966	Braathen		S2	2.77	45.4	23.1	22.3		22
1967	Dickey				34.5	23.9	19.6		
1970	Kinner		100	2.78	43.5	19.6	23.9	50	
			150		43.5	19.6	23.9		
			200		38.1	17.8	20.3	52	8
			300		39.7	21.6	18.1		10
			400		39.4	21.3	18.1	52	10
			800		41.5	19.5	22.0	48	16
			900		41.2	18.7	22.5	54	16
			1000		41.1	19.5	22.6	58	16
			1100		42.0	20.6	21.4		16
			1200		40.2	18.6	21.6	48	16
			M101		40.7	19.6	21.1	52	
			M104		40.3	19.6	20.7		
			M107		41.3	19.6	21.7		
			M200		42.3	18.5	23.8	52	
			M400		39.8	18.9	20.9	47	
1971	Ladd et al.		160	2.78	38.1	17.8	20.3		8
			1300		42.1	22.1	20.0		16
			1500		43.8	20.6	23.2		16
1984	Bensari	II	105	2.75	47.6	23.3	24.3		16
			111	2.75	47.1	24.9	22.2		16
1985	O'Neill		105-112	2.78	41.3	22.1	19.2	52	16
1989	Seah	III	200-207	2.78	45.2	21.7	23.5	58	16
1991	Sheahan		210,214, 216		45.6	21.4	24.2		
1993	Cauble		217-218	2.78	37.0	21.3	15.7		
1994	Santagata		219-220		40.4	20.9	19.5		

Table 3-3: Index properties of RBBC Series I, II and III (Cauble, 1996)

Year	Researcher	Batch	w_l (%)	w_p (%)	I_p (%)	G_s	Clay fraction (%)	Salt g/L
1994	Zriek	powder	46.4	22.5	23.9	2.78	60.1	
1994	Sinfield	powder	47.0	23.8	23.2	2.79		
		402	46.8	22.4	24.4			
		403	47.2	23.3	23.9			
1996	Cauble	powder				2.81		
		401	46.7	21.8	24.9			
		404	47.4	21.9	25.5			10.4
		405	45.2	22.1	23.1			10.0
		406	45.0	22.6	22.4		57.6	12.5
		407	44.6	23.0	21.6		57.8	13.1
		408	44.7	23.9	20.8		58.7	10.1
		409	45.4	24.0	21.4		56.8	13.0
		410	46.6	25.0	21.6			13.4
		411	46.7	24.5	22.2		56.9	10.2
		413	45.5	24.3	21.2			9.7
		414	46.3	24.3	22.0			12.0
		415	46.1	24.7	21.4			10.5
		416	46.7	24.0	22.7			12.9
		417	47.2	24.5	22.7			13.2
1998	Santagata	418						
		419	47.8	23.3	24.5			
1998	Force	420	45.2	22.6	22.6			
2009	Abdulhadi	powder	46.5	23.5	23.0	2.81	56.0	11.1

Table 3-4: Index properties of RBBC Series IV (extended from Santagata, 1998)

salt concentration	2-3 g/l	35 g/l
liquid limit, w_L	30.0%	34.7%
plastic limit, w_p	17.5%	17.7%
plasticity index, I_p	12.5%	17.0%
clay fraction (< 2 μm)	40%	40%
activity, A	0.31	0.42
specific gravity, G_s	2.77	2.77

Table 3-5: Index Properties of RBBC Series Ia (batch no. MIT 1139) at low and high salt concentrations (Bailey, 1961)

salt concentration (g/l)	liquid limit, w_L (%)	plastic limit, w_p (%)	plasticity index, I_p (%)
1	33	22	11
3*	45	22	23
5	49	22.5	26.5
20	53	24	29
36	52	25	27

* interpolated

Table 3-6: Atterberg limits of BBC as a function of salt concentration (Green, 1956)

Clay	Stress Sensitivity, S_σ ($\sigma'_{vy}/\sigma^*_{ey}$)	Strength Sensitivity, S_t
Bothkennar	6	7.3
Todi	2.25	2.3
Boom	1.5	1.5
Vallericca	2.47	2.5
Pappadai	3.5	3.2
London	> 2	2.1

Table 3-7: Values of stress sensitivity and strength sensitivity as defined by Cotecchia and Chandler (2000) for various clays in an intact state

BBC Sample	Test no.	σ'_p (σ'_{vy}) (MPa)	σ^*_{ey} of RBBC (MPa)	Stress Sensitivity, S_σ ($\sigma'_{vy}/\sigma^*_{ey}$)
S1	CRS1153	0.46	0.39	1.18
S2	CRS1154	0.3	0.22	1.36
			Average	1.27

Table 3-8: Calculation of sensitivity for natural BBC based on the method of Cotecchia and Chandler (2000)

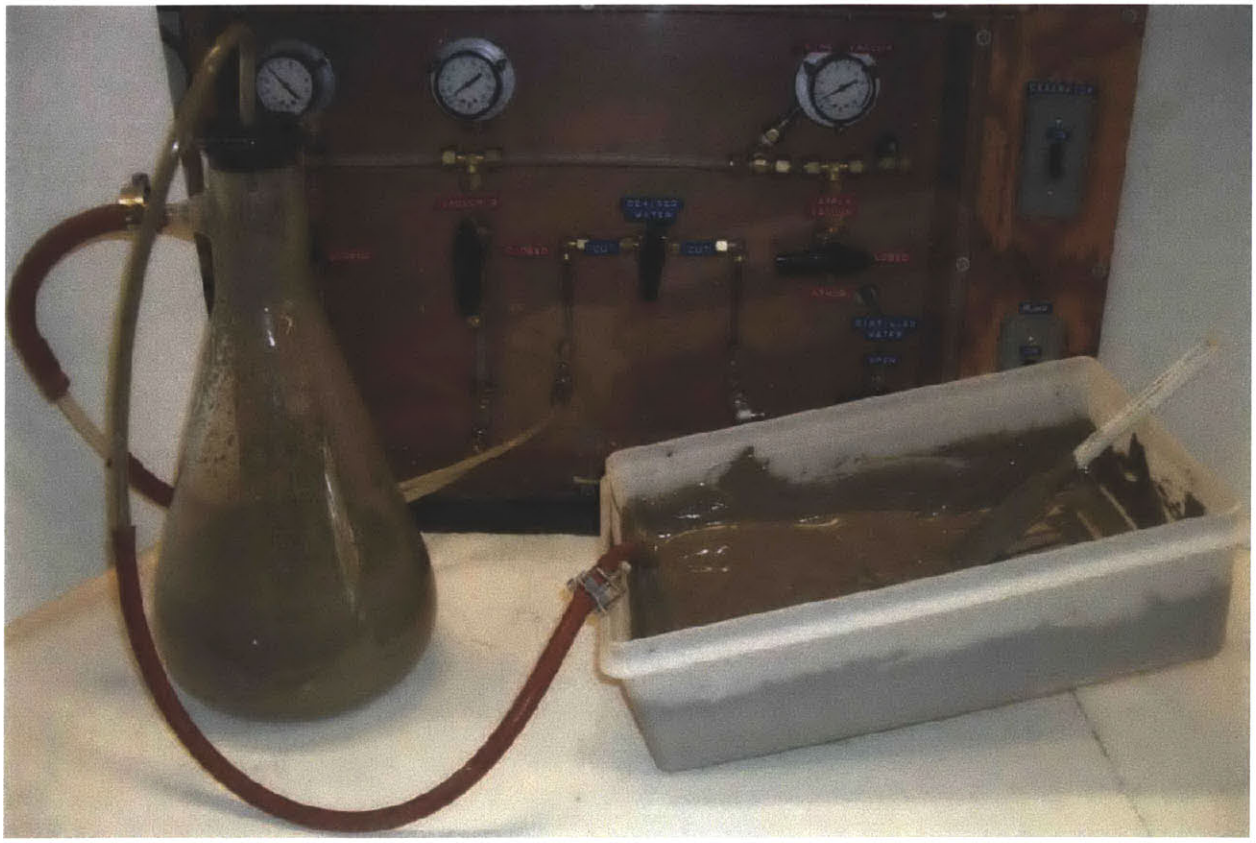

Figure 3-1: Vacuum setup used to de-air RBBC slurry

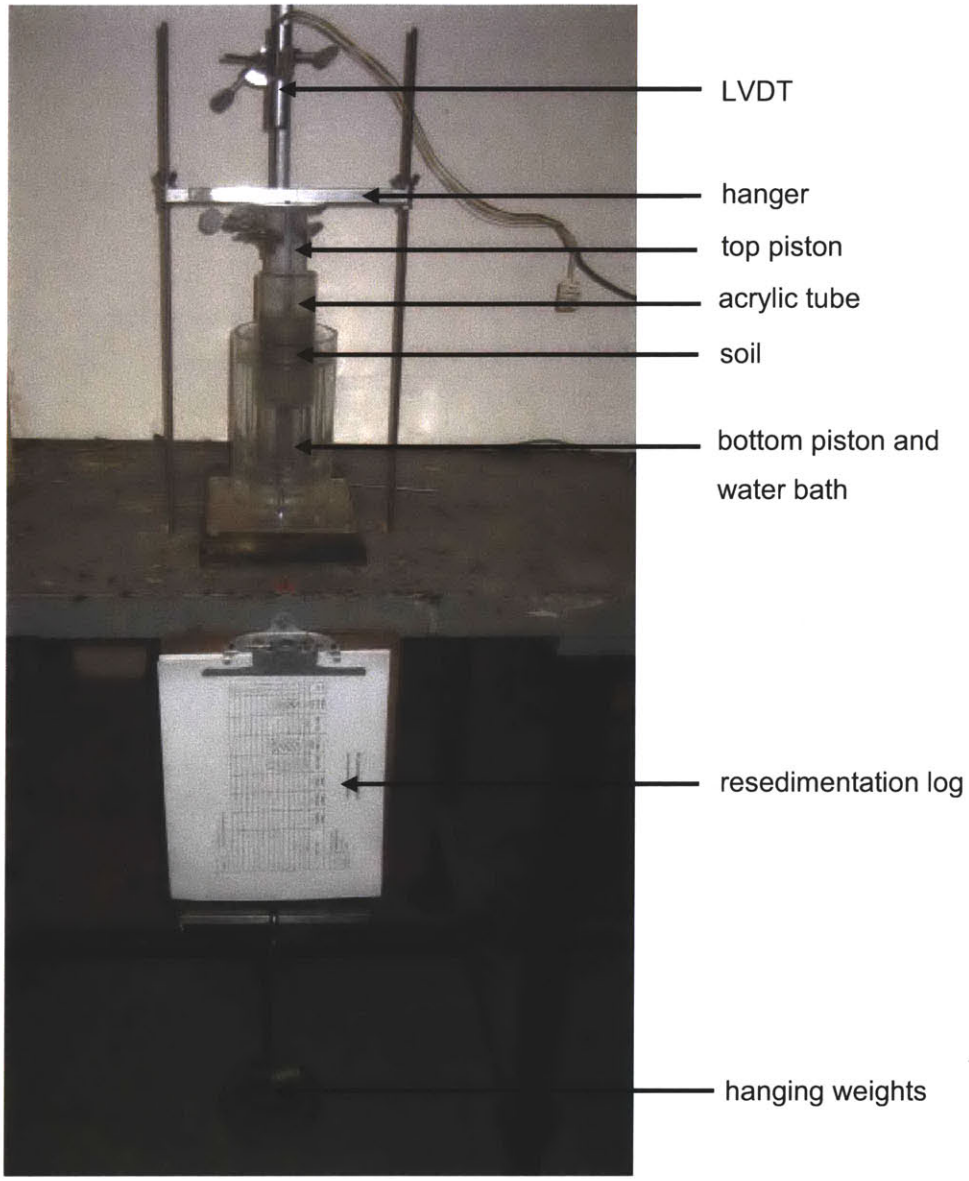

Figure 3-2: Setup of consolidometer Type I (almost identical to that of Type II)

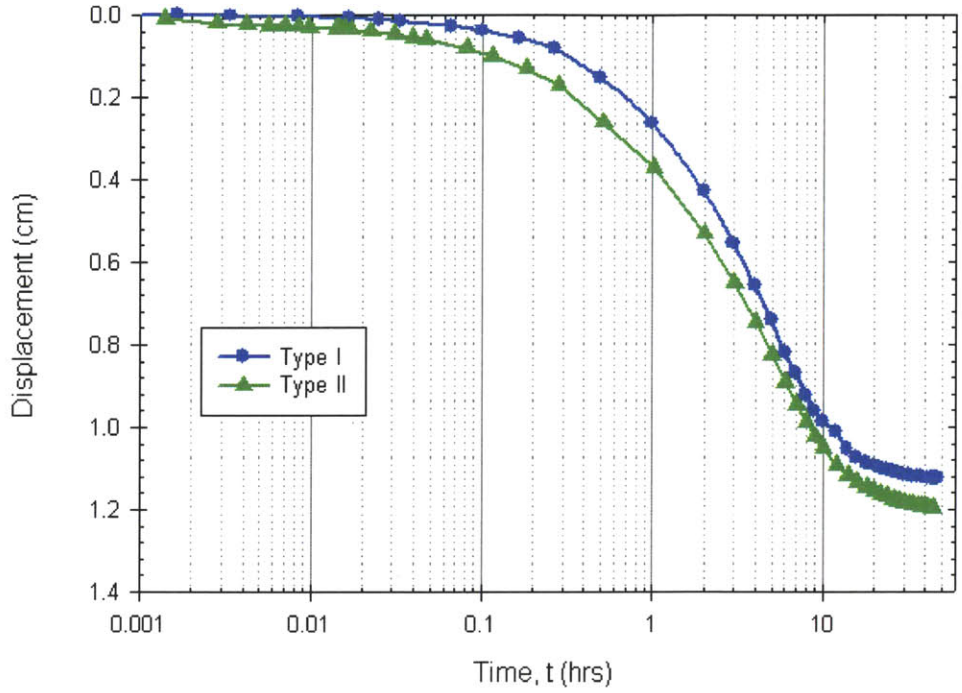

Figure 3-3: Typical settlement-(log)time curves for load increments applied to RBBC samples prepared in each type of consolidometer

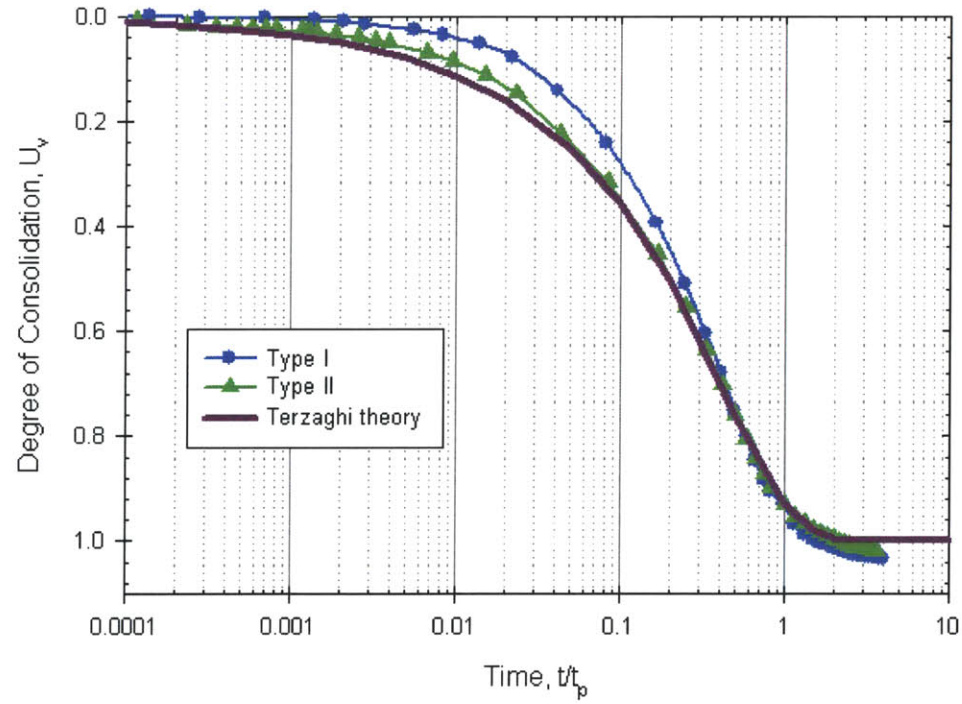

Figure 3-4: Typical normalized settlement-(log)time curves for load increments applied to RBBC samples prepared in each type of consolidometer compared with what is predicted by Terzaghi's theory

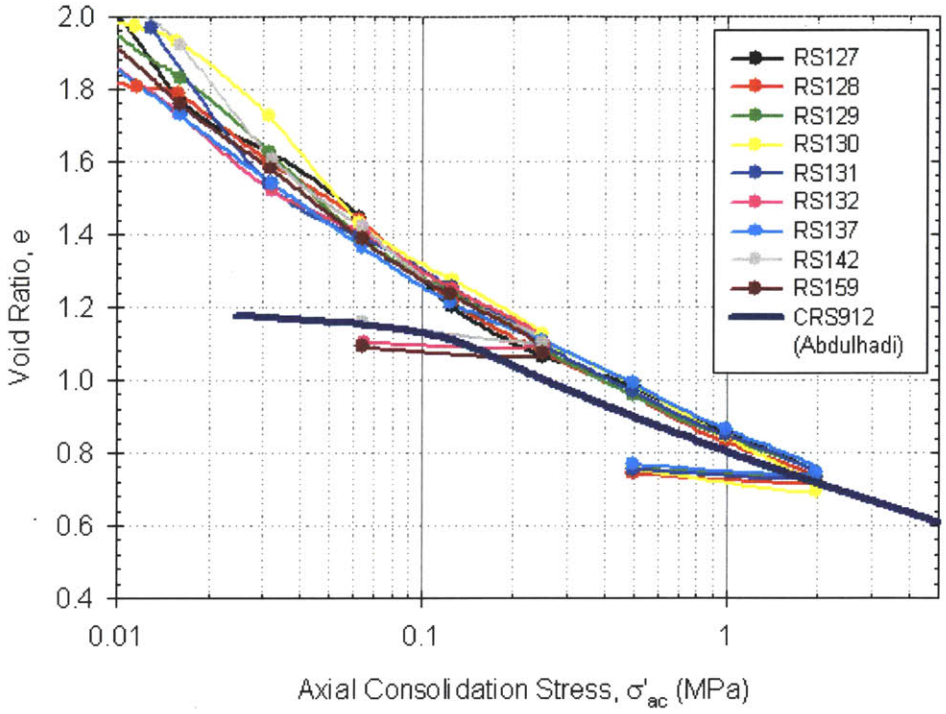

Figure 3-5: One-dimensional compression behaviour measured during the resedimentation of RBBC samples as well as during a typical CRS test on RBBC

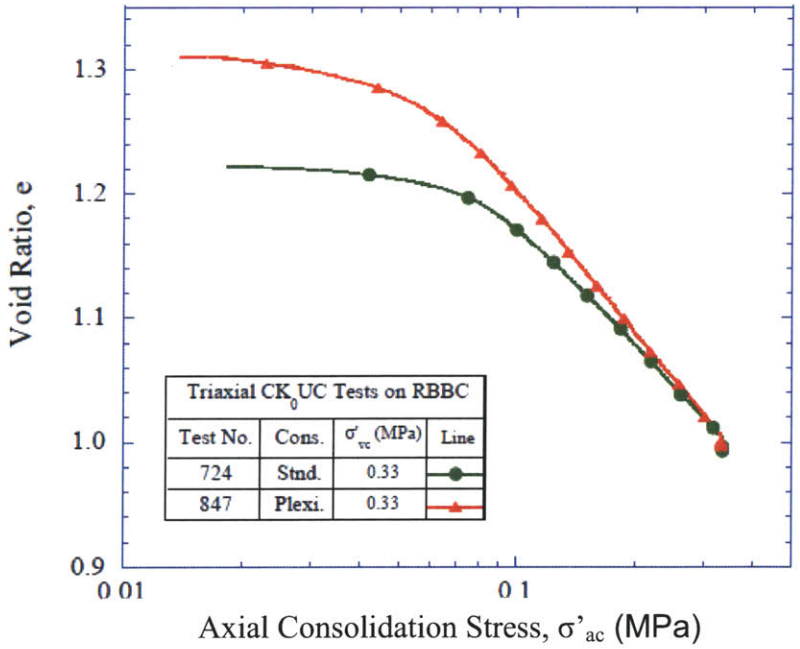

Figure 3-6: Comparison of compression behaviours measured during the K_o consolidation phase of triaxial tests for RBBC samples prepared in a Type II consolidometer ('Plexi.') and in a larger diameter consolidometer ('Stnd.') (Abdulhadi, 2009)

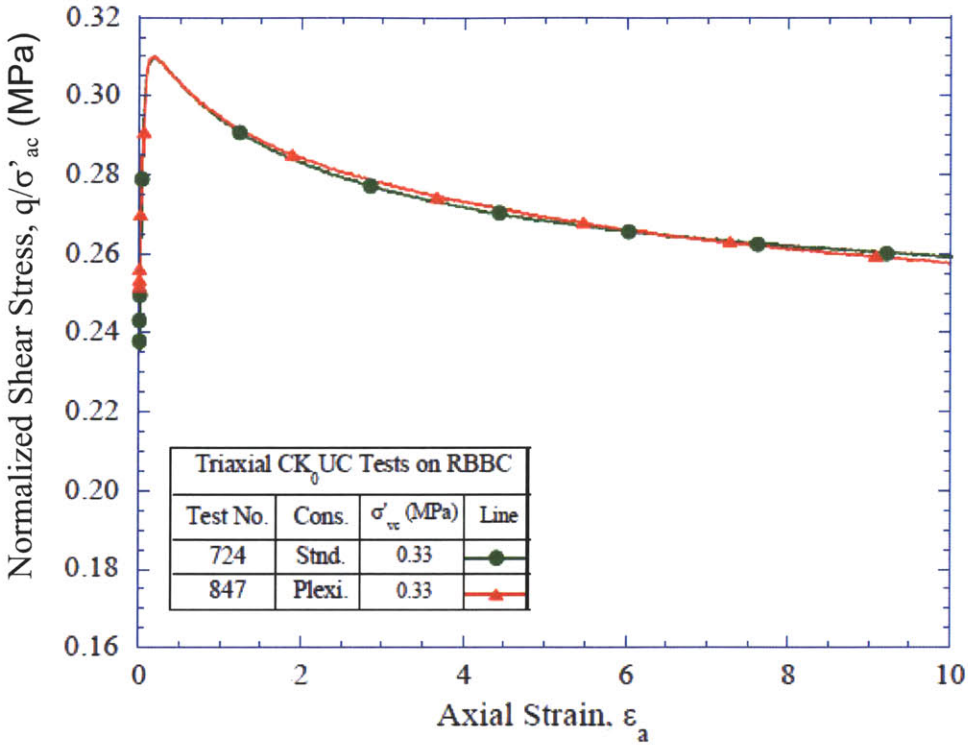

Figure 3-7: Comparison of shear stress-strain responses measured during the undrained shear phase of triaxial tests for RBBC samples prepared in a Type II consolidometer ('Plexi.') and in a larger diameter consolidometer ('Stnd.') (Abdulhadi, 2009)

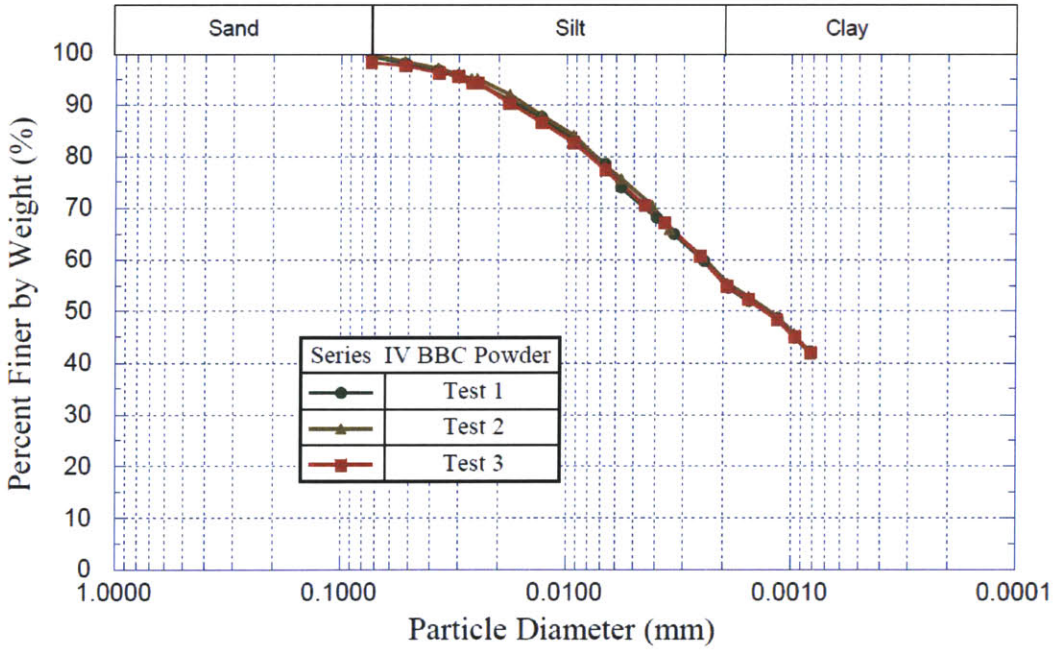

Figure 3-8: Grain size distribution for Series IV BBC powder as obtained from hydrometer tests (Abdulhadi, 2009)

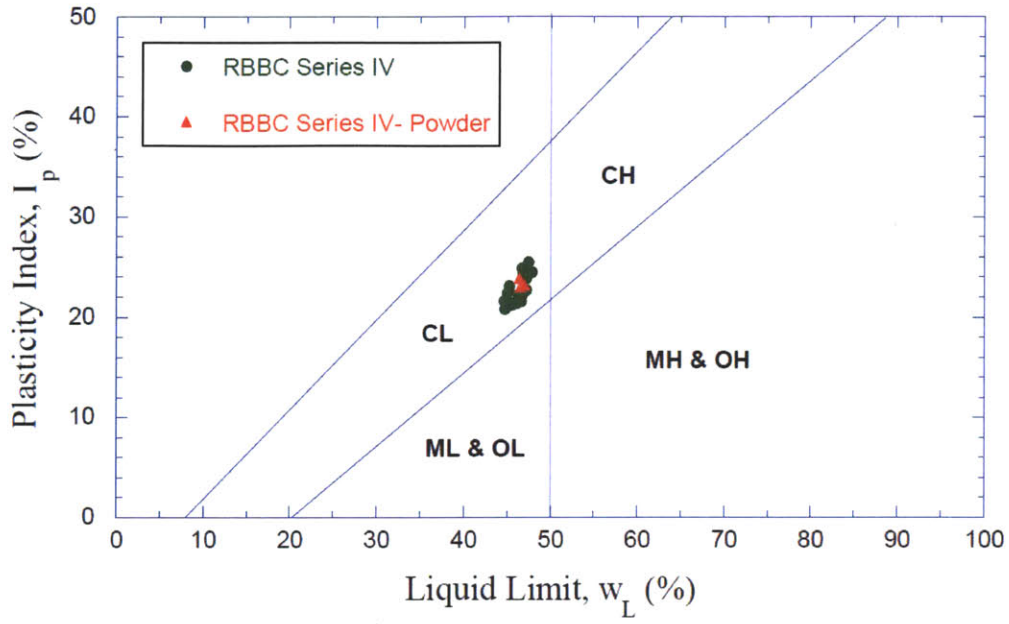

Figure 3-9: Casagrande plasticity chart showing results from Atterberg limit tests on RBBC Series IV (Abdulhadi, 2009)

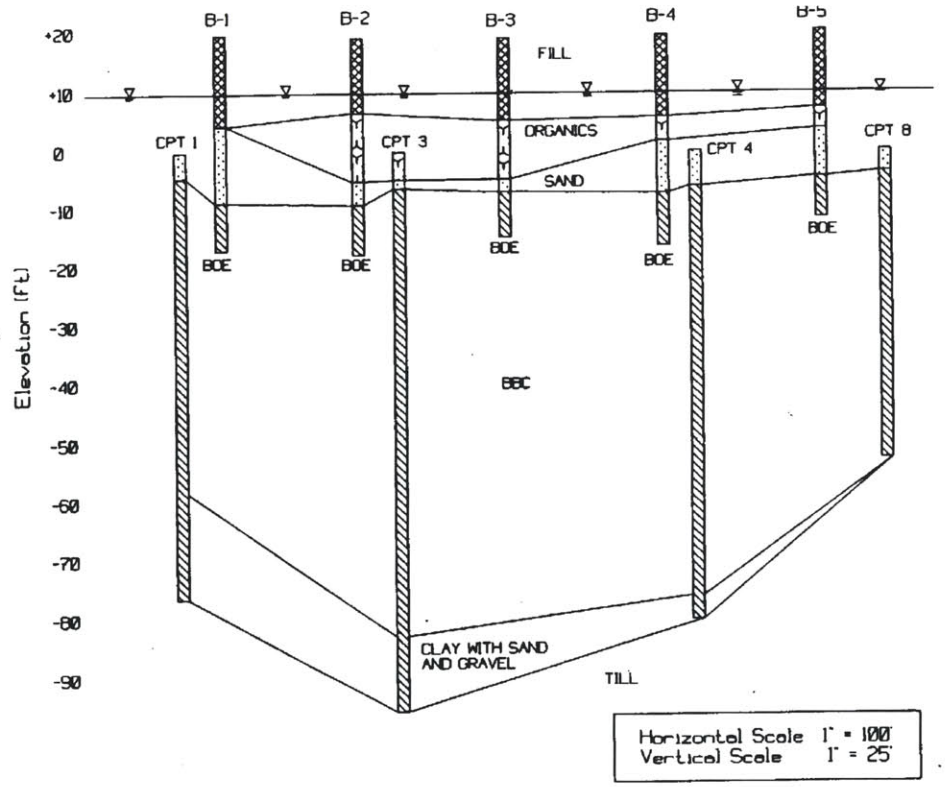

Figure 3-10: Stratigraphy at the Building 68 site. The ground surface is at El.+20 ft. (Berman, 1993)

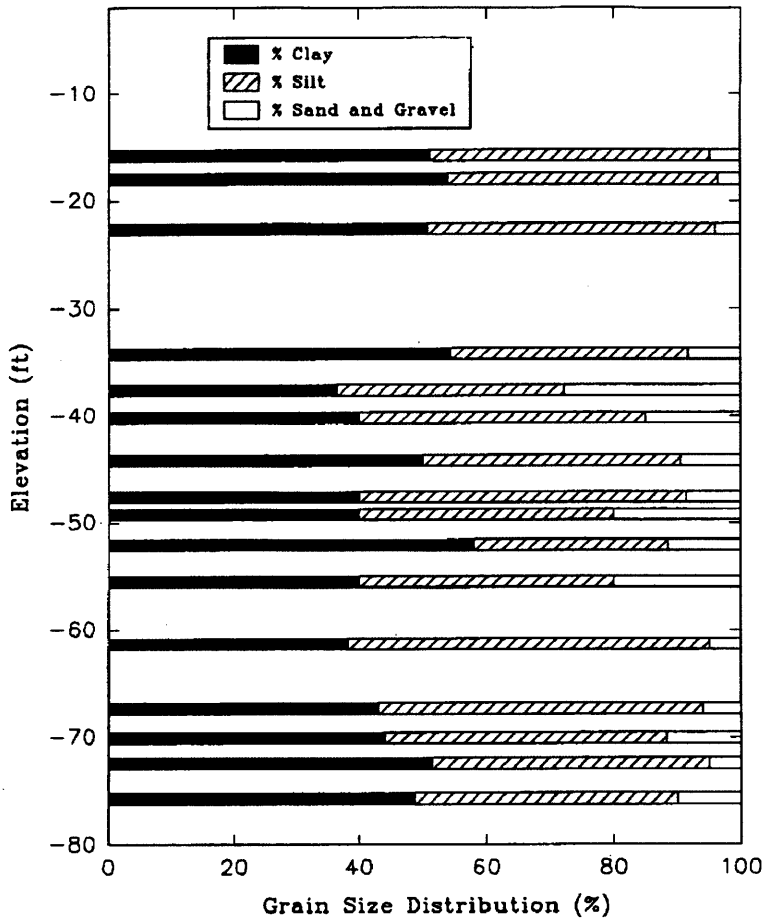

Figure 3-11: Grain size distribution profile for the layer of BBC at the Building 68 site. The ground surface is at El.+20 ft. (Berman, 1993)

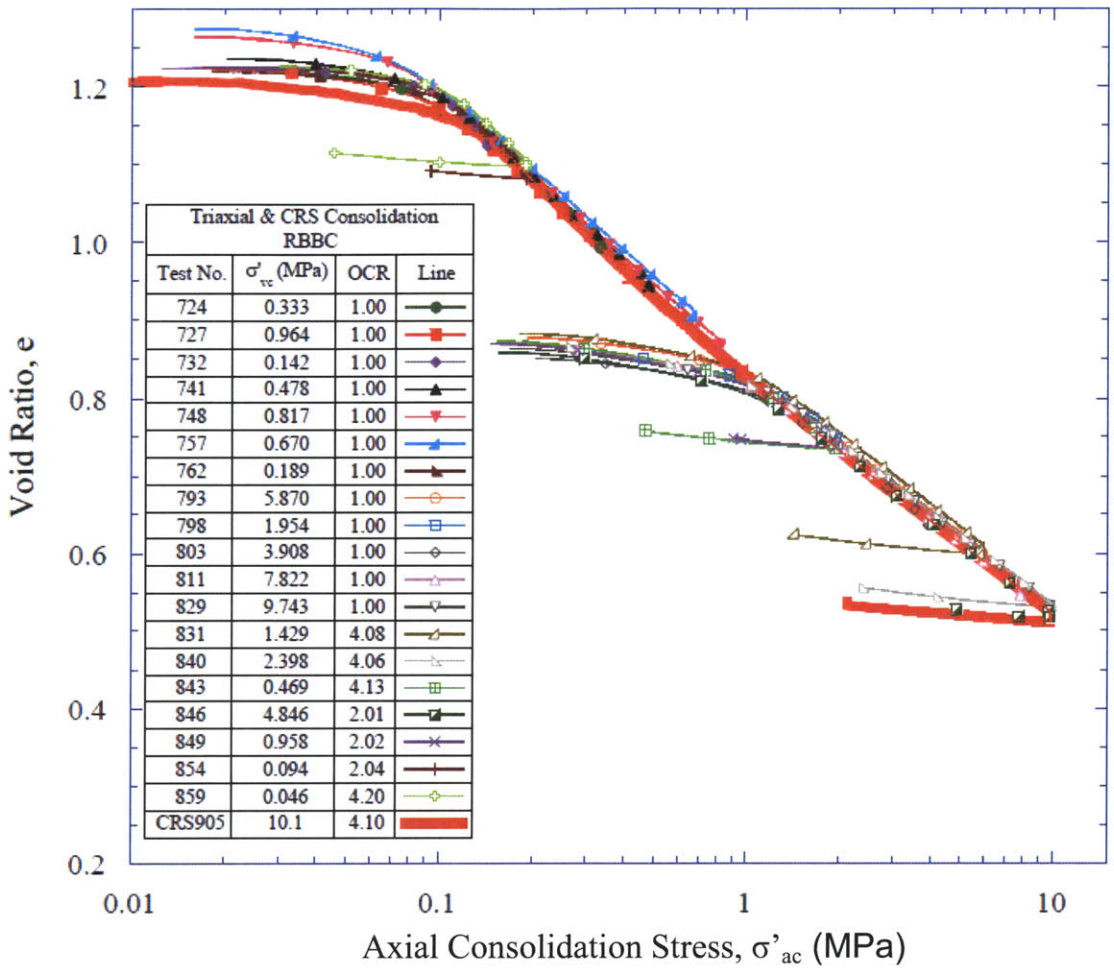

Figure 3-12: One-dimensional compression behaviour of RBBC as obtained from triaxial tests and a typical CRS test (Abdulhadi, 2009)

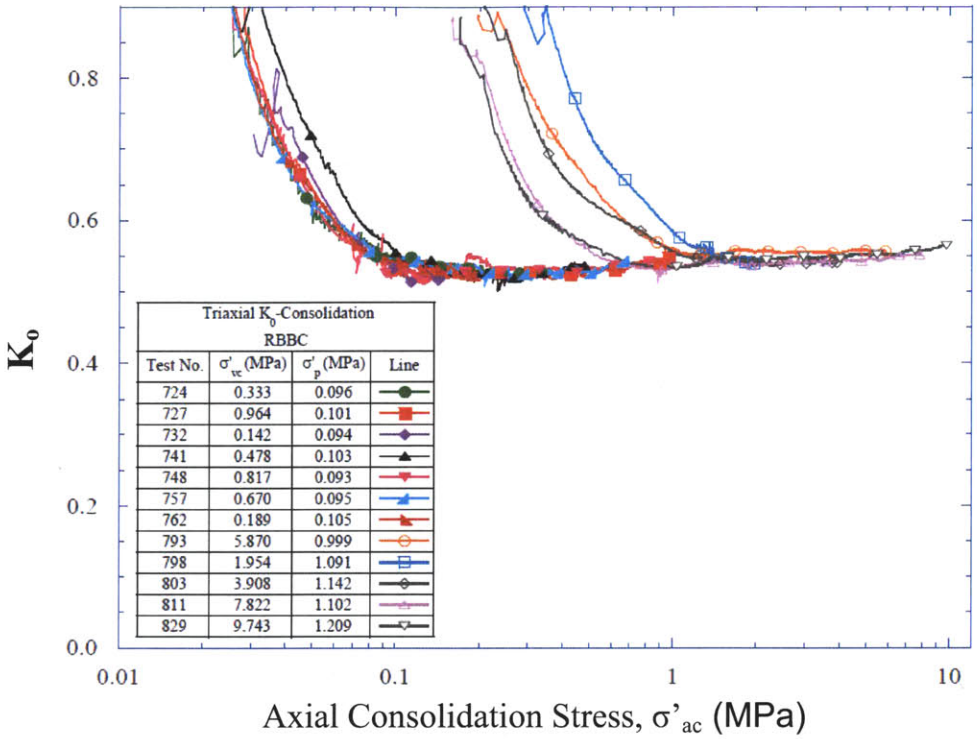

Figure 3-13: The variation in K_O with stress level for RBBC Series IV as measured during the consolidation stage of triaxial tests (Abdulhadi, 2009)

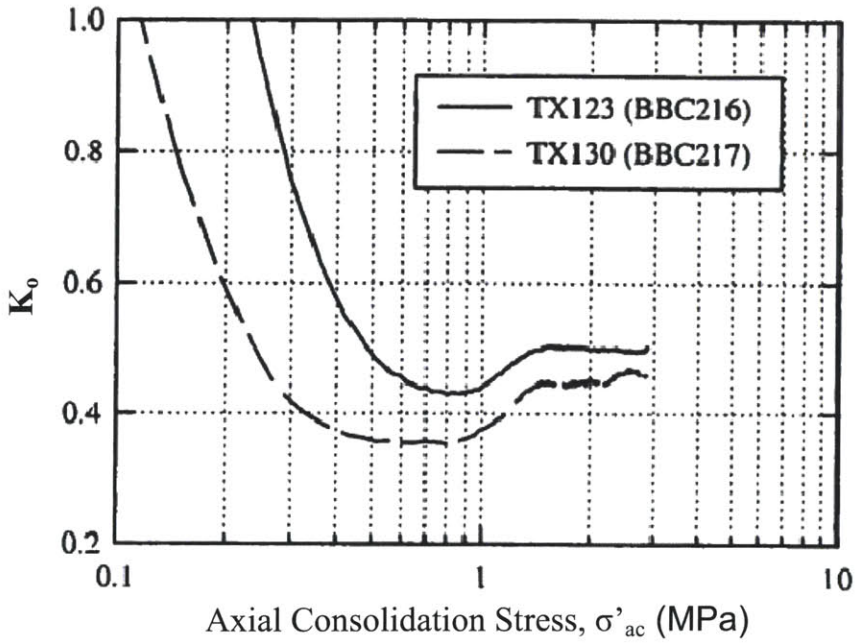

Figure 3-14: K_o versus stress level for RBBC Series III as measured during the consolidation stage of triaxial tests (Santagata, 1994)

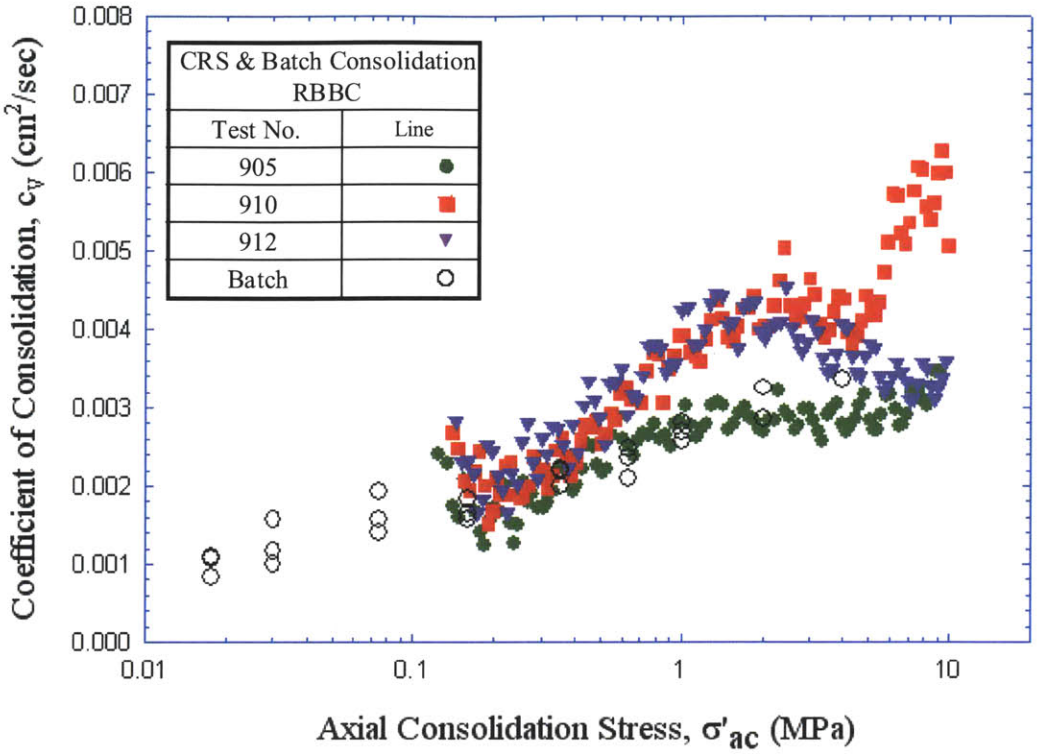

Figure 3-15: Coefficient of consolidation versus stress level for NC RBBC as obtained from CRS tests as well as from the consolidation stage of batching (Abdulhadi, 2009)

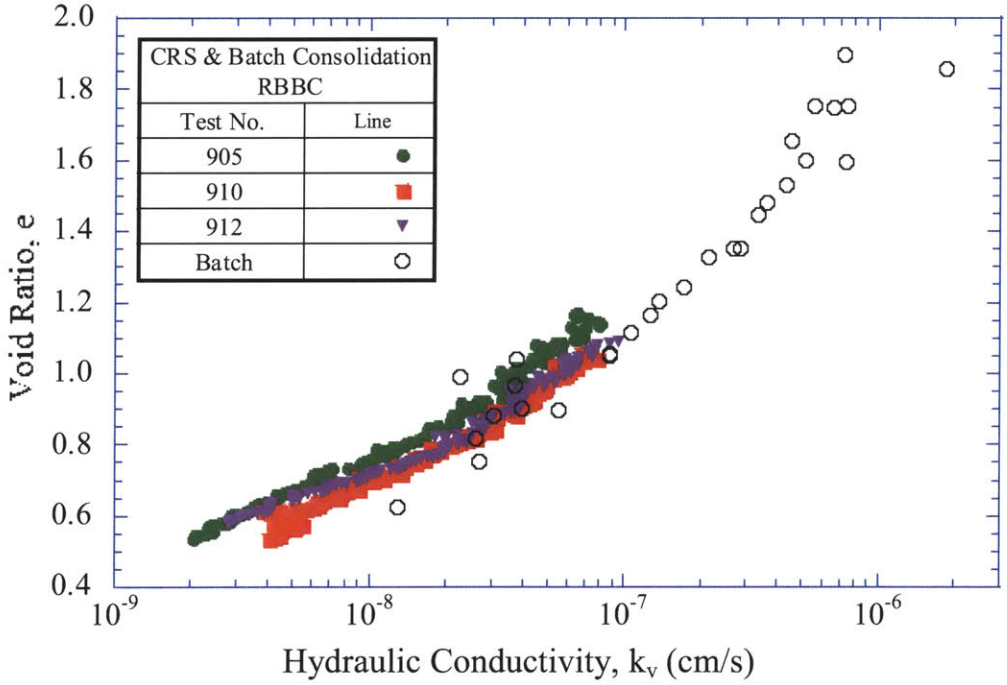

Figure 3-16: Void ratio versus hydraulic conductivity for RBBC as obtained from CRS tests as well as from the consolidation stage of batching (Abdulhadi, 2009)

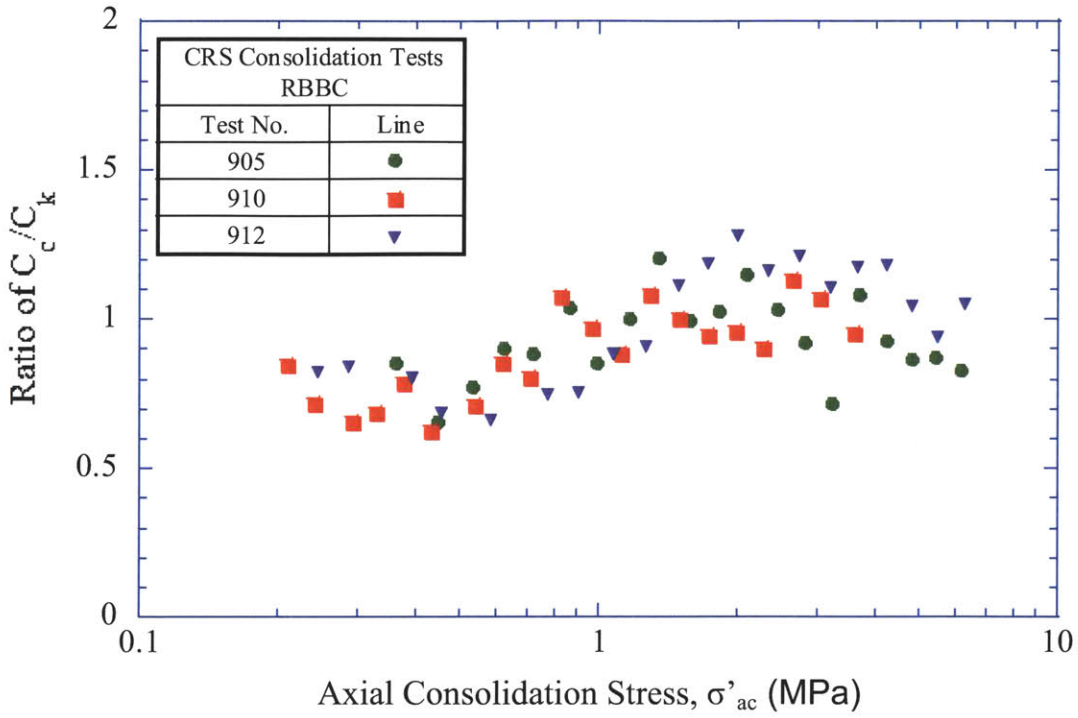

Figure 3-17: Ratio of C_c/C_k versus stress level for RBBC as obtained from CRS tests (Abdulhadi, 2009)

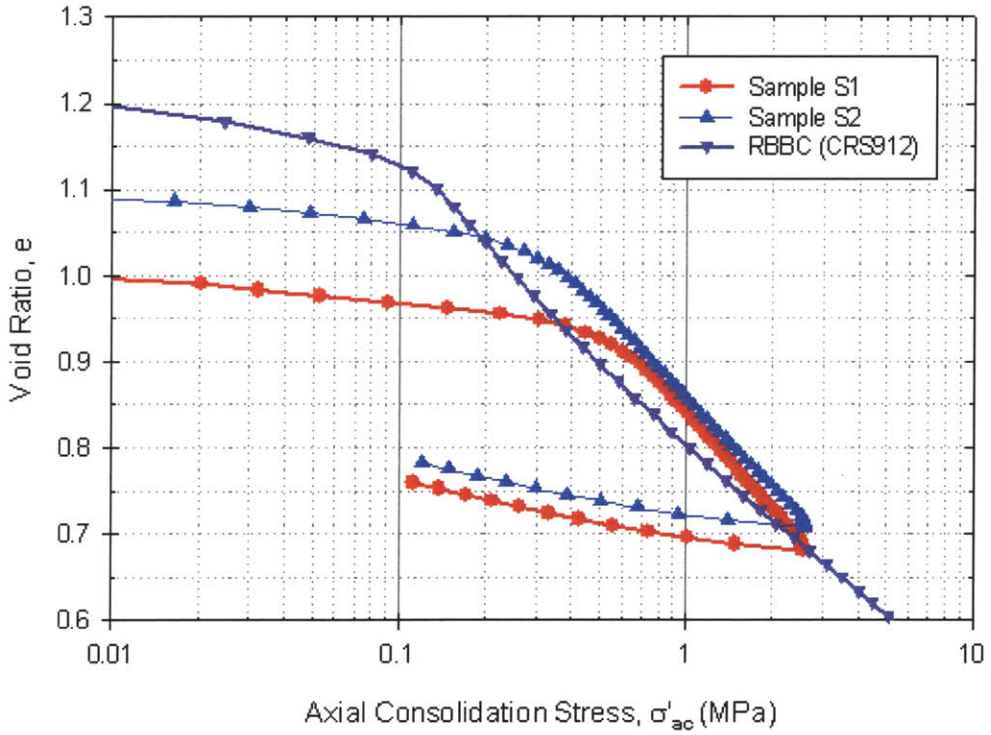

Figure 3-18: One-dimensional compression behaviour of natural BBC (Samples S1 and S2) compared to that of RBBC as obtained from CRS tests

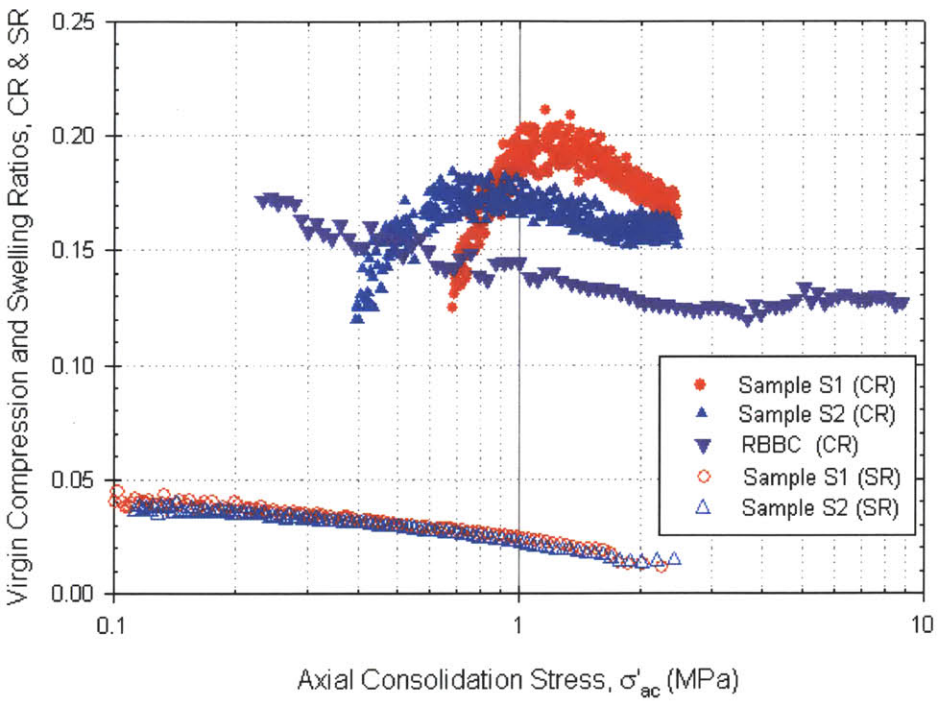

Figure 3-19: Variation in virgin compression ratio and swelling ratio with stress for natural BBC (Samples S1 and S2) and RBBC as obtained from CRS tests

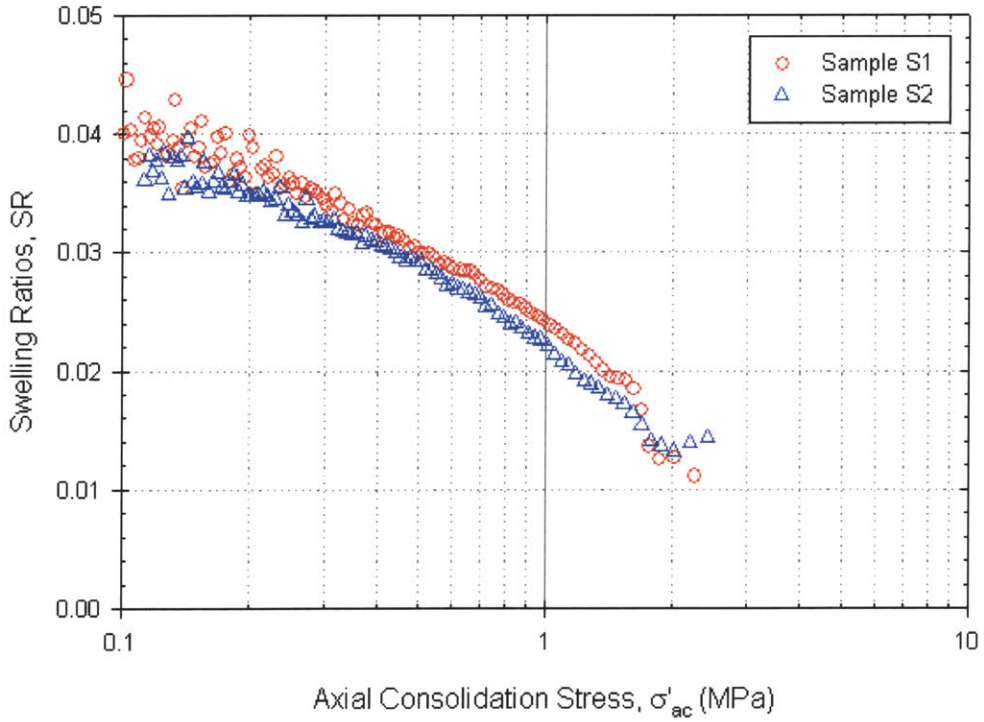

Figure 3-20: Variation in swelling ratio for natural BBC (Samples S1 and S2) as obtained from CRS tests

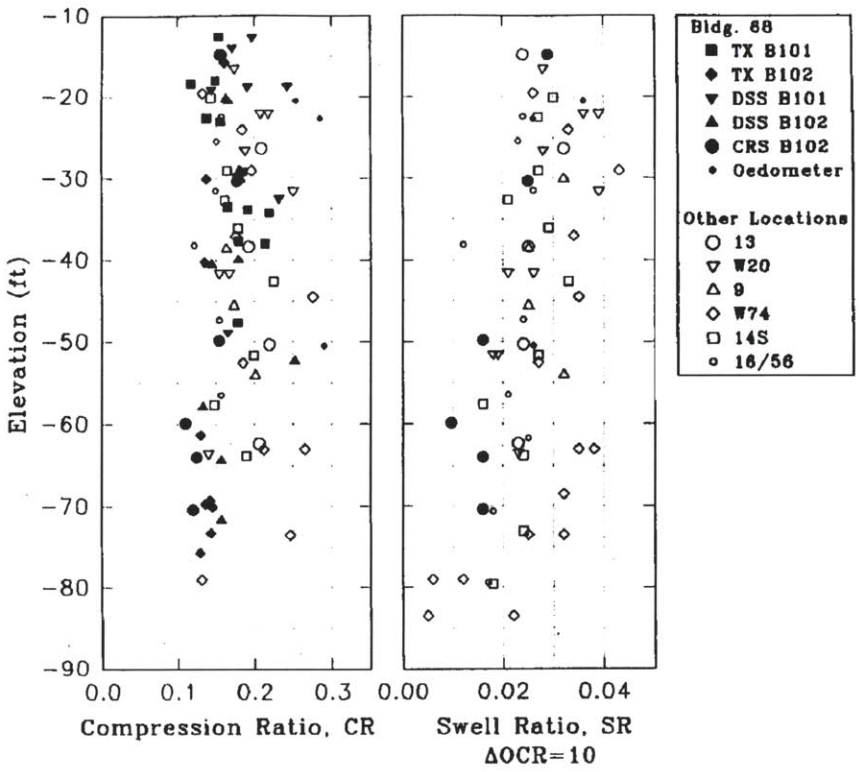

Figure 3-21: Values of compression ratio and swelling ratio for BBC at the Building 68 site as well as at various other locations around the MIT campus (Berman, 1993)

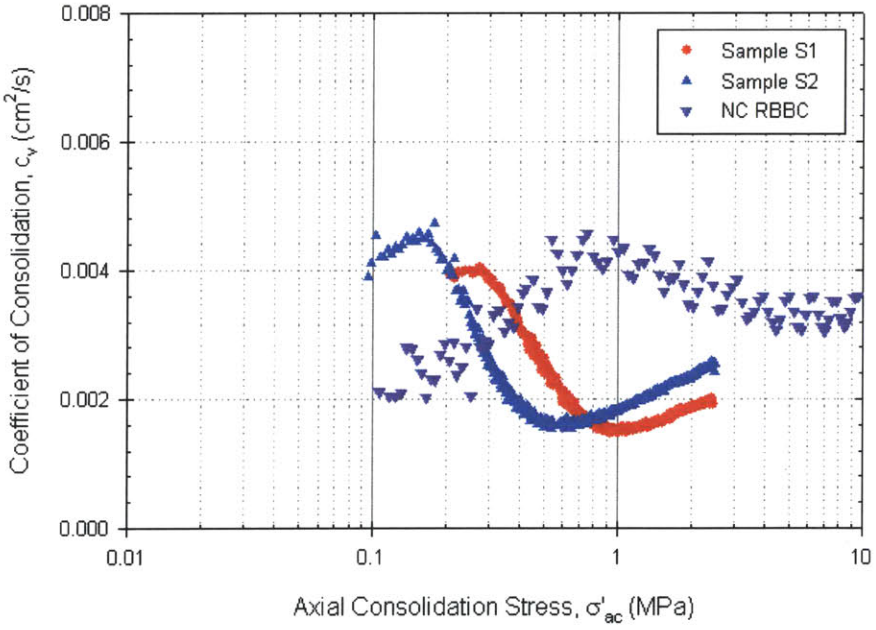

Figure 3-22: Variation in the coefficient of consolidation for natural BBC (Samples S1 and S2) compared to that for NC RBBC as obtained from CRS tests

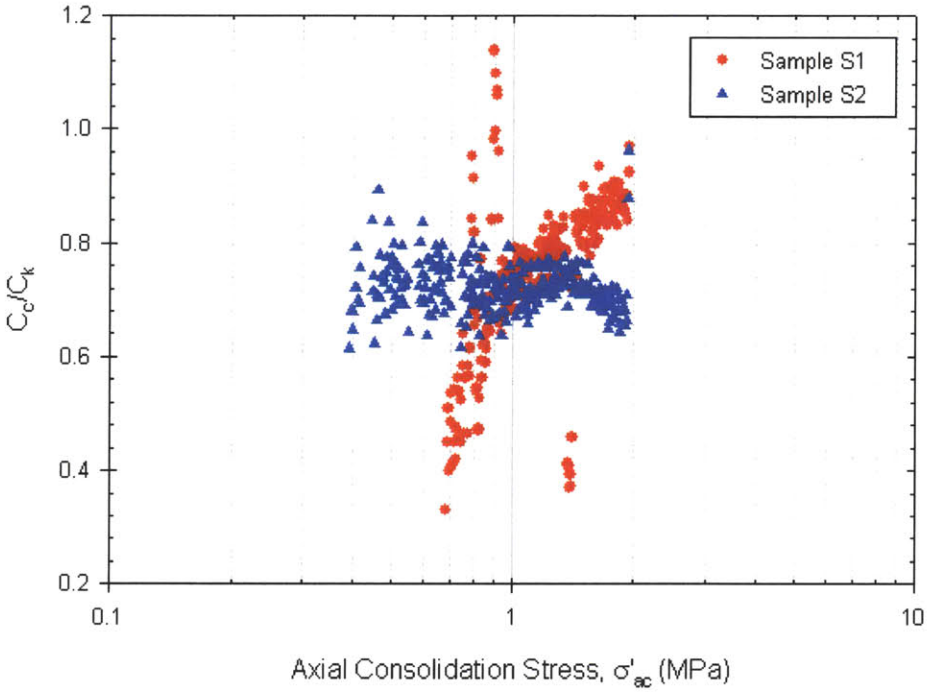

Figure 3-23: Ratio of C_c/C_k versus stress level for natural BBC (Samples S1 and S2) as obtained from CRS tests

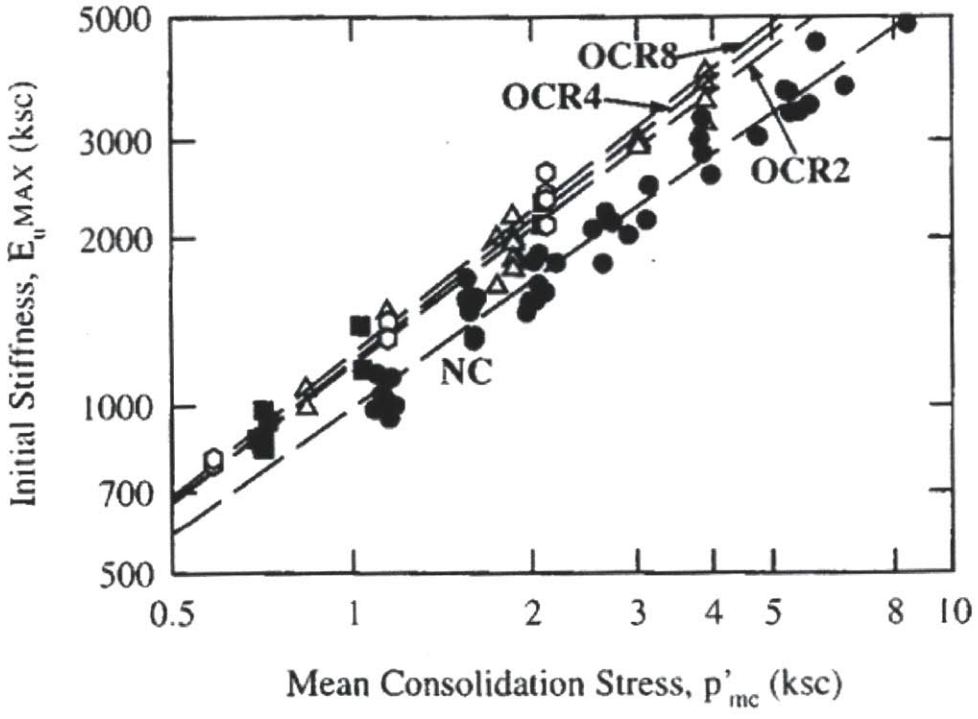

Figure 3-24: Relationship between initial stiffness of RBBC and mean consolidation stress in undrained triaxial compression (Santagata, 1998)

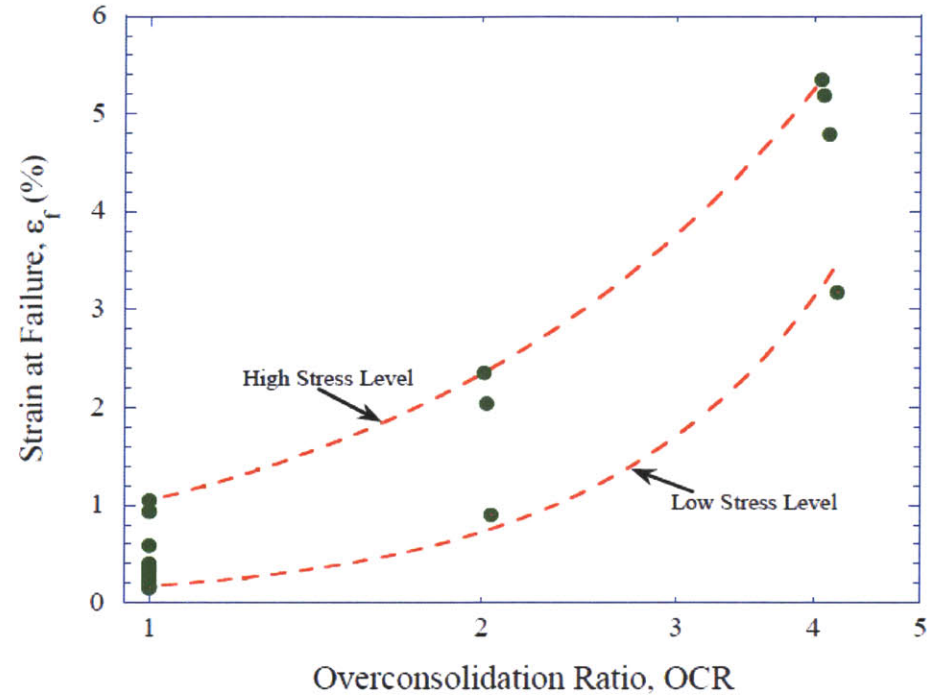

Figure 3-25: Strain to failure for RBBC as a function of OCR and stress level as obtained from CK_OUC tests (Abdulhadi, 2009)

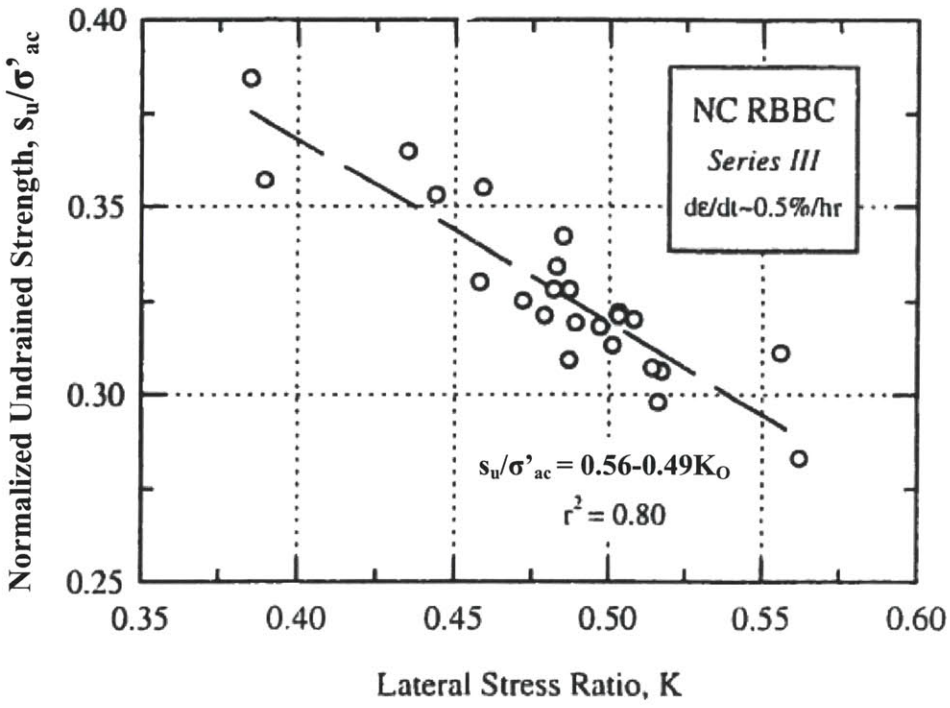

Figure 3-26: Normalized undrained strength versus pre-shear lateral stress ratio as obtained from CKUC tests on NC RBBC (Santagata, 1994)

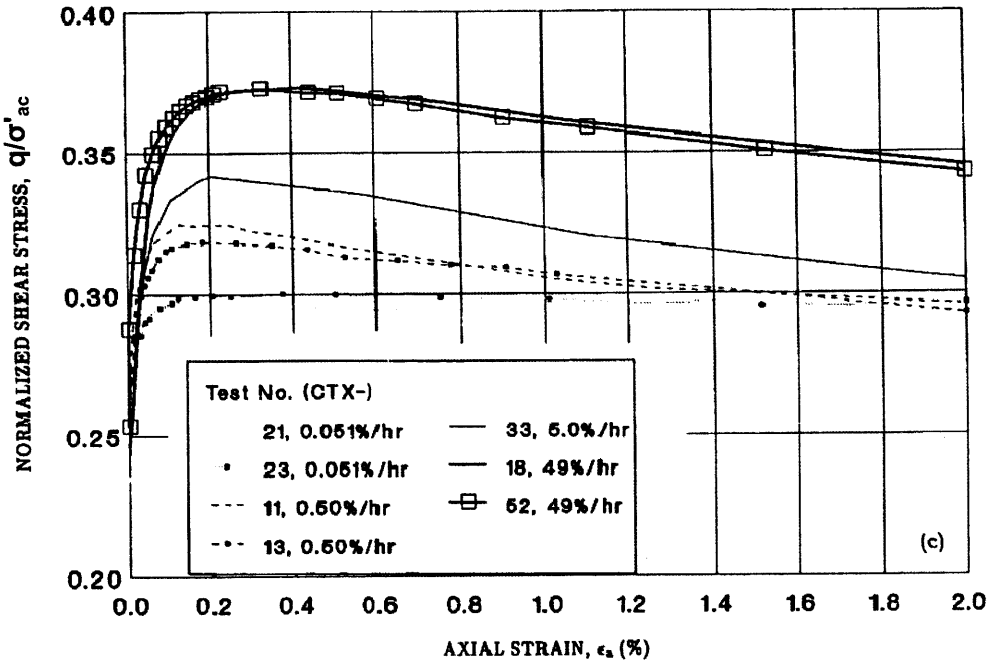

Figure 3-27: Effect of strain rate on the normalized shear stress-strain response of NC RBBC as obtained from CK_OUC tests (Sheahan, 1991)

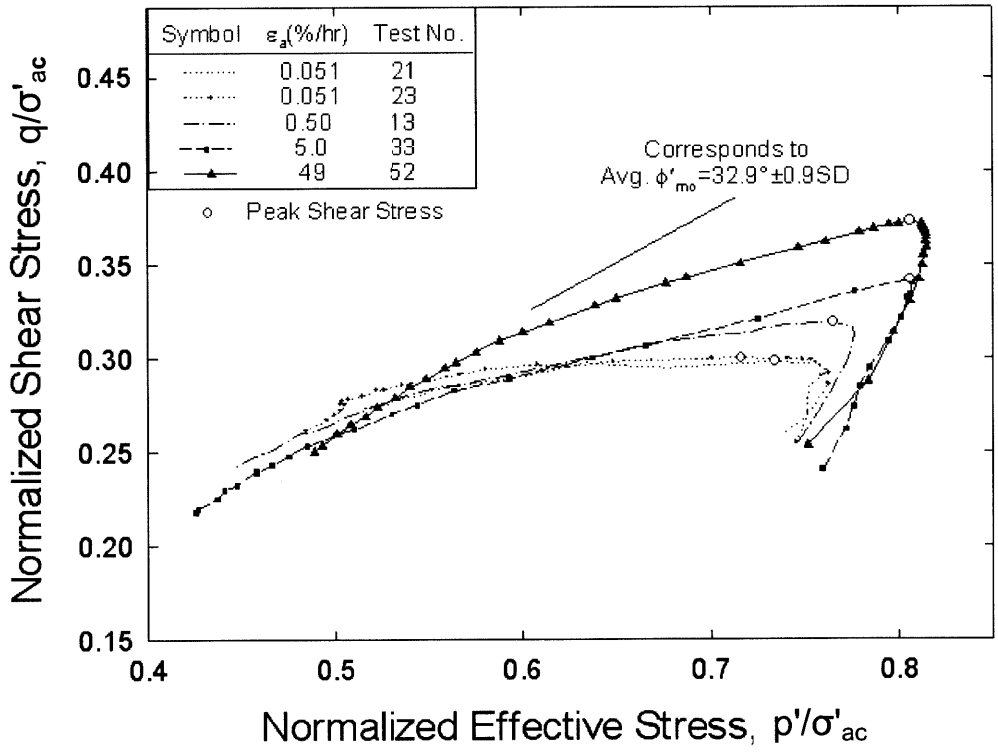

Figure 3-28: Effect of strain rate on the normalized effective stress paths of NC RBBC as obtained from CK_OUC tests (Sheahan, 1991)

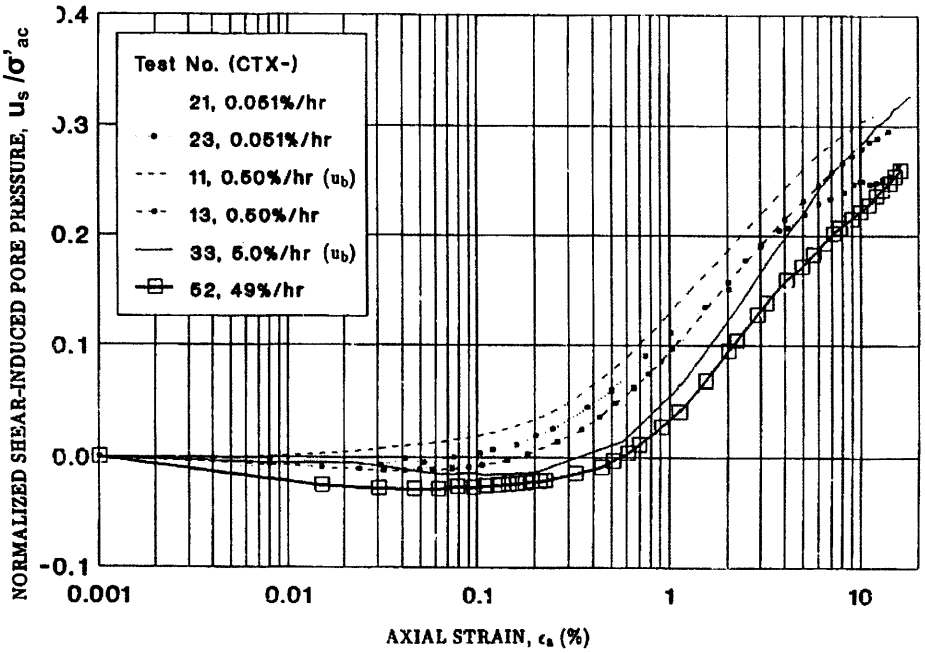

Figure 3-29: Effect of strain rate on the normalized shear induced pore pressures generated in NC RBBC as obtained from CK_OUC tests (Sheahan, 1991)

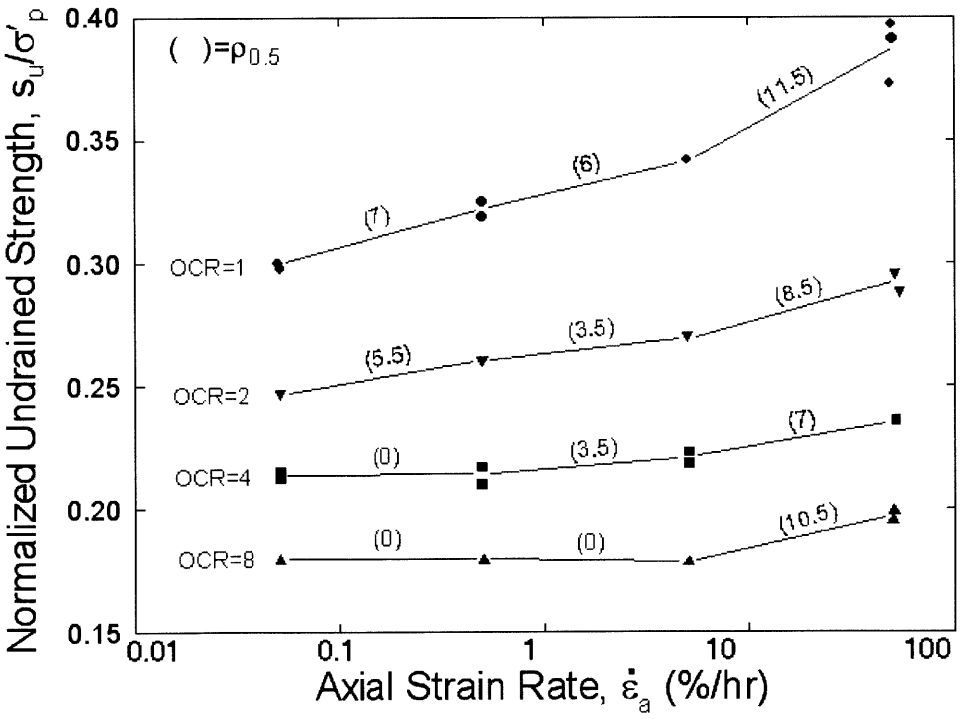

Figure 3-30: Effect of strain rate on the normalized undrained strength of RBBC as obtained from CK_OUC tests (Sheahan, 1991)

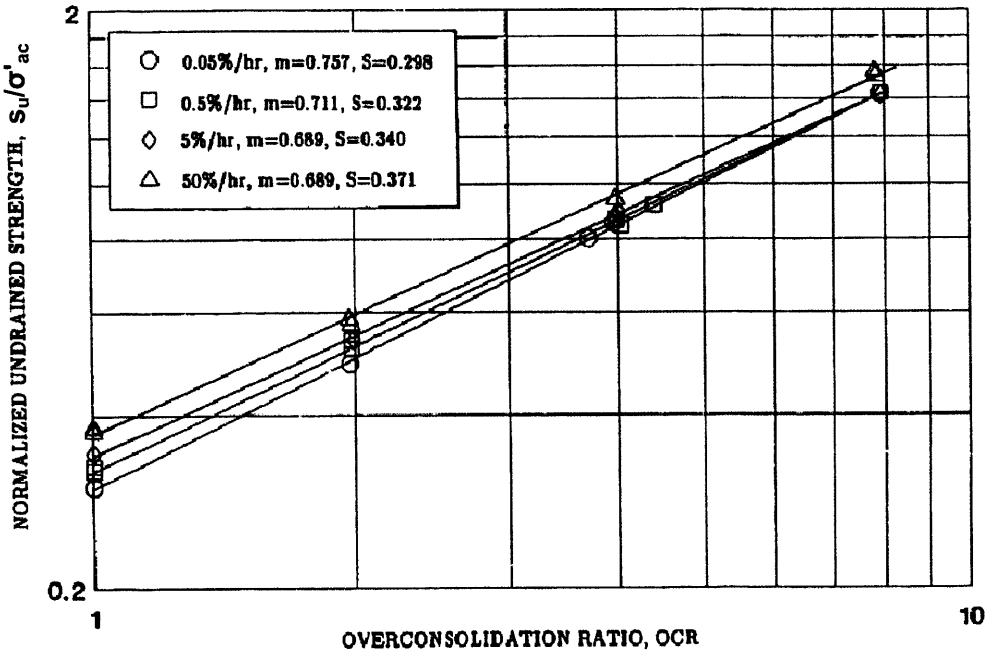

Figure 3-31: Effect of strain rate on the SHANSEP parameters as obtained from CK_OUC tests (Sheahan, 1991)

4 EQUIPMENT AND PROCEDURES

4.1 INTRODUCTION

This chapter describes the equipment and procedures used in the triaxial testing program performed in the course of the research. The tests were performed using an MIT automated stress path triaxial cell. Automation allows for higher quality results as well as for a dramatic reduction in labour. Section 4.2 provides a description of the triaxial testing system. Section 4.3 describes more specifically the design of the smooth end platens used in the triaxial device. The control hardware and software which allows for automation of testing is already well described by previous researchers (e.g. Sheahan, 1991) and therefore will not be repeated in this chapter. The procedures adopted in the testing program are described in Section 4.4.

4.2 TRIAXIAL TESTING SYSTEM

Figure 4-1 shows a general schematic of the standard automated triaxial testing system used in the MIT Geotechnical Engineering Laboratory. The system incorporates seven basic components: the triaxial cell itself; a load frame for axial load application; Pressure Volume Actuators (PVAs); a motor control box containing the drivers for the motors; a personal computer to run the control software; a power supply for the transducers and a data acquisition system.

The specific triaxial cell used for the author's tests was developed originally by Anderson (1991) and later used by Da Re (2000) for the testing of frozen and unfrozen sand specimens. These tests on sand employed the use of smooth end platens and as a result no modification of the triaxial cell was necessary for the author's testing program. The cell accommodates standard sized triaxial specimens of 3.55 cm diameter and a height of 8.1 cm. Figure 4-2 shows a schematic of the cell from Da Re (2000). It has a steel chamber which encloses the soil specimen, base pedestal, floating top cap, top and bottom drainage lines and a compact shear beam load cell of 8.9 kN (2000 lb) capacity (note that Figure 4-2 shows on-specimen displacement transducers which were not used in the author's tests). The use of an internal load cell is essential as it eliminates the complication of having to account for piston friction at the O-rings, a major problem associated with the use of an external load cell. Axial load is applied to the specimen through a 2.54 cm diameter hardened steel piston which enters the top of the chamber through a double O-ring seal. Piston movement is continuously monitored by an externally mounted LVDT (Linear Variable Differential

Transformer). The bottom of the load cell mates with the floating top cap by means of an alignment device. All drainage lines are made of copper tubing, rather than plastic, to minimize system compliance. The top drainage line is also coiled to accommodate axial shortening which occurs during the consolidation and shear phases of tests. Table 4-1 summarizes the properties of the transducers used with the triaxial cell. Values of resolution and stability given in Table 4-1 are based on characteristics of the central data acquisition system. For axial and volume strain engineering values of resolution and stability are also based on specimen dimensions.

Cell pressure is applied to the triaxial specimen using low viscosity silicone oil (Dow-Corning '200 fluid', 20 centistokes). The oil is transparent, non-toxic, and does not degrade the seals or latex membranes used in testing. Silicone oil was initially used instead of water because unlike water the oil does not permeate through membranes over long periods of testing. A second important benefit of the use of silicone oil is that is electrically non-conductive, thereby allowing electronic devices such as a load cell or strain gauge to be located inside the cell chamber.

The triaxial testing system employs the use of 3 PVAs. The PVAs have a maximum pressure capacity of approximately 14 MPa. One PVA is used to apply cell pressure and it is the pressure capacity of this PVA that limits the stress level which can be attained in triaxial tests, since the triaxial cell itself can withstand higher cell pressures. A second PVA is used to apply back-pressure to the soil specimen. Volume change of the specimen is monitored using an LVDT mounted on the piston of the back-pressure PVA. Both cell and back-pressures are measured using 6.9 MPa (1000 psi) diaphragm type gauge pressure transducers. A third PVA is connected directly to an 89 kN (10 ton) hydraulic load frame (note that in Figure 4-1 axial load is provided by means of a mechanical load frame and therefore a third PVA is not included in the diagram). The load frame uses the fluid pressure generated by the PVA to apply axial load to the specimen in the cell. The same silicone oil used to apply cell pressure is also used for the hydraulic load frame in order to minimize problems associated with corrosion.

The triaxial cell and PVA's are housed in a temperature controlled environmental enclosure, as shown in Figure 4-3. Constant temperature is maintained within the enclosure by means of a light bulb which is turned off and on by a mercury contact switch. The enclosure itself, along with the remainder of the components shown in Figure 4-1, is located in an air-conditioned laboratory.

The triaxial system used in the research is automated using control hardware and software custom developed at the MIT Geotechnical Engineering Laboratory. The automated system was first developed by Sheahan (1991) for low pressure triaxial testing. Essentially, measurement of test variables such as force and displacement is performed by transducers located both inside and

outside the triaxial cell (e.g. load cell, LVDTs). The output from the transducers is read by a computer which runs a control program written in QBASIC. This control program is capable of performing all aspects of a triaxial test from initial pressure-up to shearing. The program compares the actual measurements from the transducers with the target values and determines the corrective action required to reduce the difference between the two values. The necessary corrective action is then conveyed to the PVA motors which adjust pressure, axial displacement, etc. accordingly. This closed-loop feedback control therefore uses direct measurements of test variables in an iterative scheme to enable continuous test control. A central data acquisition system is used to record all test variables for future analysis. The details of the control hardware and software and the data acquisition are already well documented (e.g. Sheahan,1991) and therefore will not be discussed in this chapter.

4.3 SMOOTH END PLATENS

The smooth end platens used in the author's triaxial tests are similar to those used by Sheahan (1991). The design of the smooth end platens adopted by Sheahan is shown in Figure 4-4. The left side of the figure shows an exploded view of the arrangement of membranes, O-rings and filter paper strips. The top cap and base pedestal are made of brass. In both the top cap and base pedestal a 6 mm porous stone is held in place by a threaded cap. The threaded cap is removable to enable cleaning of the porous stone. The base cap has a 3 mm diameter center hole to accommodate a base pore pressure measurement stone and the top cap has a small dowel pin at the center. The purpose of the dowel is to prevent the specimen from sliding sideways during testing. The base cap center hole narrows and extends through the threaded section, connecting to a drilled hole in the permanent base. This hole leads out to a pressure transducer supported on the triaxial cell base. Radial drainage is provided by vertical filter paper strips which extend from the ends of the specimen to the porous stones. As shown in Figure 4-4, Sheahan also utilized mid-height pore pressure measurement.

Sheahan (1991) had initially adopted an end platen design similar to that used by Barden and McDermott (1964) (described in Chapter 2, Section 2.5.3.) involving greased membrane discs with radial slits placed between the end platens and the specimen. However, Sheahan found that during K_O consolidation the grease was being squeezed out, leaving a frictional interface between the latex membrane discs and brass end platens. The greased membrane discs were therefore abandoned and the soil specimen was simply placed in direct contact with the end platens. Dry teflon spray was instead applied to the end platens, though Sheahan reported that little difference could be detected between tests in which the teflon spray was and was not used.

The design of the smooth end platens adopted in the author's research is shown in Figure 4-5. An exploded view of the membranes, filter paper strips and O-rings is given for clarity. The base pore pressure measurement stone used by Sheahan is replaced with a dowel pin. Pore pressure is measured by connecting a pore pressure transducer to the bottom drainage line. The pressure transducer is placed close to the specimen at the cell base so as to minimize system compliance. Radial drainage is provided by 16 vertical filter paper strips each of 6 mm width. The porous stones are relatively coarse, high permeability stones made from 54 grit vitrified bond stone.

Two latex membranes (0.3 mm think) are used to seal the soil specimen from the cell fluid. Abdulhadi (2009) found that leakage occurs if condoms are used at cell pressures greater than about 3 MPa (condoms being the conventional way of sealing specimens at low pressures). For consistency, latex membranes were used for all of the tests carried out by the author. Leakage through the latex membranes was not observed even in the high pressures tests.

As will be discussed in Chapter 5, the smooth ends adopted in the author's research were not entirely successful in allowing a triaxial specimen to deform in a completely uniform fashion. A thin film of silicone lubricant spray was applied to the top and bottom platens in an effort to increase lubrication at the ends. Given that Sheahan found greased membranes discs to be ineffective in providing end lubrication for his tests which were carried out at stresses less than 1 MPa, with the grease being squeezed out, it is certain that the same would have occurred in the author's tests carried out at much higher stresses. Similar to the finding of Sheahan (1991), however, it is believed that the silicone spray likely provided little additional lubrication. In one test a thin sheet of teflon was instead placed between the end platens and the specimen. No discernable increase in lateral spreading at the ends could be detected for this test and approach was not used in any later tests.

4.4 TEST SETUP AND PROCEDURES

Test setup takes place on a mobile cart. Before the specimen is prepared for testing, narrow membrane strips, approximately 1 cm wide, are placed over the porous stones (referred to as 'membrane protectors' in Figure 4-5). These pieces of membrane serve to prevent the rough porous stones from puncturing the outer membranes. The piece of membrane covering the base porous stone also allows the vertical filter paper strips to now be held in place around the base pedestal. At this stage the RBBC sample is extruded from the consolidometer and prepared for placement in the triaxial cell. The resedimentation process and procedures carried out to prepare test specimens for placement in the triaxial device are described in detail in Chapter 3 and will not be repeated here. Once prepared, the test specimen is placed in direct contact with the brass base platen, a small

dowel pin being pushed into the specimen in order to keep it centralized on the platen and prevent it from moving out of place during setup. The top cap is then placed on the specimen. Both the top and base platens are coated with a thin film of silicone lubricant spray prior to the specimen being put in place.

At this stage the filter paper strips are tucked under the piece of membrane covering the top porous stone. This point in the setup is shown in Figure 4-6. Note that the figure also shows two narrow strips of membrane at the top and bottom of the specimen which are used to keep the filter paper strips tucked in against the specimen during setup. The first (inner) latex membrane is then placed over the specimen using a membrane stretcher connected to a vacuum. The membrane is sealed with two O-rings at both the top and bottom. The outer membrane is then placed and a third O-ring is positioned between the first two at both the top and bottom (the arrangement of the O-ring seal is illustrated on the left side of Figure 4-4). The top drainage line, which spirals around the specimen, is then connected at the cell base and top cap. Throughout the whole process an alignment device is used to keep the specimen and top cap perfectly aligned with the base pedestal.

The steel cell chamber is now placed over the specimen. The load cell is brought into contact with the top cap and the external LVDT attached. The whole cell is moved into the load frame and the chamber filled with silicone oil. The cell oil is then pressurized, which is done to prevent the specimen from swelling once the drainage lines are flushed with water. The magnitude of the cell pressure needed to prevent the specimen from changing volume at this time (so that it neither swells nor consolidates) was determined mostly by trial and error to be equal to about 0.4 MPa for specimens which had been batched to σ'_p = 2 MPa and about 0.05 MPa for specimens batched to σ'_p = 0.25 MPa. The drainage lines are vacuumed (under approximately 20 inches Hg) to remove air before being flushed with water. The pore pressure transducer is then placed and the drainage valves closed. At this point a further isotropic increment of cell pressure is applied. This increment of cell pressure is generally equal to 0.2 MPa for specimens which had been batched to σ'_p = 2 MPa and 0.05 MPa for specimens batched to σ'_p = 0.25 MPa.

The specimen is allowed to equilibrate overnight and the following day the sampling effective stress is recorded. The specimen is then back-pressure saturated while holding the sampling effective stress constant. At the end of back-pressure saturation a B-value check is performed using a cell pressure increment of 0.025 MPa. Typically, a back-pressure of 0.5 MPa is more than sufficient to ensure saturation of the drainage system. A B-value greater than at least 0.95 is generally taken to indicate saturation of the drainage system. Occasionally, lower B-values may warrant an increased back-pressure.

All triaxial tests involve K_O consolidation of specimens to stresses at least two times higher than the batch preconsolidation pressure. The K_O consolidation algorithm used to control the triaxial testing system ensures zero radial strain of the specimen by continuously adjusting cell pressure to keep volume and axial strains equal. At the end of virgin consolidation, specimens are allowed at least 24 hrs of [drained] secondary compression before either being swelled into the OC range or sheared undrained. Backlash of the load frame upon load reversal complicates the use of the K_O algorithm for swelling. As a result, swelling of specimens into the OC range is done by using a prescribed stress path with a target lateral stress ratio corresponding to the desired pre-shear OCR. This target lateral stress ratio (and therefore radial effective stress) is computed using Equation 3-1 as given in Chapter 3. Again, secondary rebound of OC specimens is allowed prior to undrained shearing. A constant axial strain rate of 0.15 %/hr is used during virgin consolidation while a constant axial strain rate of 0.05 %/hr is used during swelling (though a rate of 0.10 %/hr had originally been used for swelling). These rates are sufficiently slow to prevent non-negligible excess pore pressures from developing in specimens.

Before undrained shearing is carried out a leak check is performed by closing the drainage valves and monitoring the pore pressure. Provided no internal or external leak is detected, the specimen is sheared undrained using an axial strain rate of 0.5 %/hr in compression mode of shear. Shearing is ended after about 13 – 16 % axial strain.

The raw test data is analyzed using a QBASIC computer program. The program converts the transducer voltages recorded by the central data acquisition system into engineering values of axial displacement, volume change, cell and pore pressures, which are in turn used to compute effective stresses and strains. The analytical procedure followed by the program is described in more detail in Sheahan (1991). The computation of axial and radial stresses involves two important corrections, as given below:

(i) Membrane Correction (Berre, 1985)

Account must be taken of the fact that, during both consolidation and shearing, the two latex membranes which seal the soil specimen offer resistance to axial shortening as well as resistance to the radial stress imposed via the cell pressure. The resistive axial force (ΔF_a^m) and resistive radial stress ($\Delta \sigma_r^m$) offered by each membrane are computed from elasticity theory as follows:

$$\Delta F_a^m = \pi D_i E t \left(\varepsilon_a + \frac{2}{3} \varepsilon_v \right)$$

$$\Delta \sigma_r^m = \frac{4Et}{D_i} \left(\frac{\varepsilon_v}{3} \right)$$

where: D_i = initial specimen diameter

E = Young's modulus of rubber, taken to be 1.4 MPa

t = thickness of the latex membrane, taken to be 0.3 mm

ε_a = axial strain of the specimen (based on initial specimen height)

ε_v = volume strain of the specimen (based on initial specimen volume)

When analyzing the test data ΔF_a^m is subtracted from the axial force applied to the specimen as measured by the load cell while $\Delta\sigma_r^m$ is subtracted from the radial stress applied to the specimen via the cell pressure. The latex membranes have an unstretched diameter only slightly smaller than the initial diameter of the specimen and as such no correction is necessary to account for initial stretching of the membranes when they are first placed on the specimen.

(ii) Filter Paper Correction (Bishop and Henkel, 1962)

Sixteen 6 mm wide vertical filter paper strips are used to provide radial drainage in the triaxial tests, resulting in 91 % coverage of the initial specimen circumference. The following correction is applied to account for the buckling capacity (ΔF_a^{fp}) of the filter paper:

$$\Delta F_a^{fp} = K_{fp} P_{fp} (\varepsilon_a / 0.02)$$

where: K_{fp} = axial force per perimeter of filter paper (taken to be 0.16 kg/cm)

P_{fp} = perimeter of filter paper (taken to be 10.16 cm)

Buckling of the filter paper strips is assumed to occur after ε_a = 2 % (based on initial specimen height) and as such the maximum possible value of ΔF_a^{fp} = 1.63 kg (15.9 N). When reducing the test data, ΔF_a^{fp} is subtracted from the axial force applied to the specimen as measured by the load cell.

It should be kept in mind that, due to the relatively high consolidation stresses achieved in the triaxial tests, the above corrections have only a slight impact on the computed radial and axial stresses.

4.5 STRAIN RATE DURING VIRGIN CONSOLIDATION

The author used a constant axial strain rate of 0.15 %/hr during K_O virgin consolidation, which is the same as that used by Abdulhadi (2009). However, the specimen drainage conditions used in the two experimental programs are very different, as Abdulhadi used standard end drainage through porous stones while the author employed radial drainage using vertical filter paper strips. In order to confirm that the strain rate of 0.15 %/hr is sufficiently slow to prevent excess pore pressures

from developing during the consolidation phase of the author's tests, a test (TX1057) was carried out whereby the strain rate was varied during consolidation. If it were the case that the strain rate of 0.15 %/hr is too fast, then pore water would not flow quickly enough from the specimen to prevent the build-up of excess pore pressures. As a result, volume strain of the specimen would be measured to be too low and the K_O algorithm used to control the triaxial testing system would increase the cell pressure in an effort to force the volume strain of the specimen to equal the applied axial strain. This would cause a misleadingly high value of K_O to be measured during consolidation. If the axial strain rate were decreased then the build-up of excess pore pressure would be reduced and the measured K_O would decrease closer to its true value. Figure 4-7 shows the variation in K_O during the consolidation phase of test TX1057 where the axial strain rate was varied between 0.10 to 0.20 %/hr. Note that the test specimen had a batch σ'_p = 2 MPa. It can clearly be seen from Figure 4-7 that varying the strain rate has no effect on the measured K_{ONC}. This observation serves to indicate that the axial strain rate of 0.15 %/hr used by the author is sufficiently slow to prevent the development of non-negligible excess pore pressures during the consolidation stage of triaxial tests.

Measurement	Device	Calibration Factor	Range	Resolution	Stability
Axial Strain	LVDT (external)	3.295 cm V/V	3 cm	±0.00075% (0.1 mV)	±0.0075% (1 mV)
Volume Strain	LVDT	22.078 cm^3 V/V	45 cm^3	±0.00050% (0.1 mV)	±0.0050% (1 mV)
Cell Pressure	Pressure Transducer	345.4 MPa V/V	6.9 MPa	62.8 Pa (0.001 mV)	628 Pa (0.01 mV)
Pore Pressure	Pressure Transducer	347.0 MPa V/V	6.9 MPa	63.1 Pa (0.001 mV)	631 Pa (0.01 mV)
Axial Load	Internal Load Cell	291.89 kN V/V	8.9 kN	0.053 N (0.001 mV)	0.53 N (0.01 mV)

Note: Values of resolution and stability are based on characteristics of the central data acquisition system. For axial and volume strain engineering values of resolution and stability are also based on specimen dimensions.

Table 4-1: Properties of transducers used with the triaxial cell.

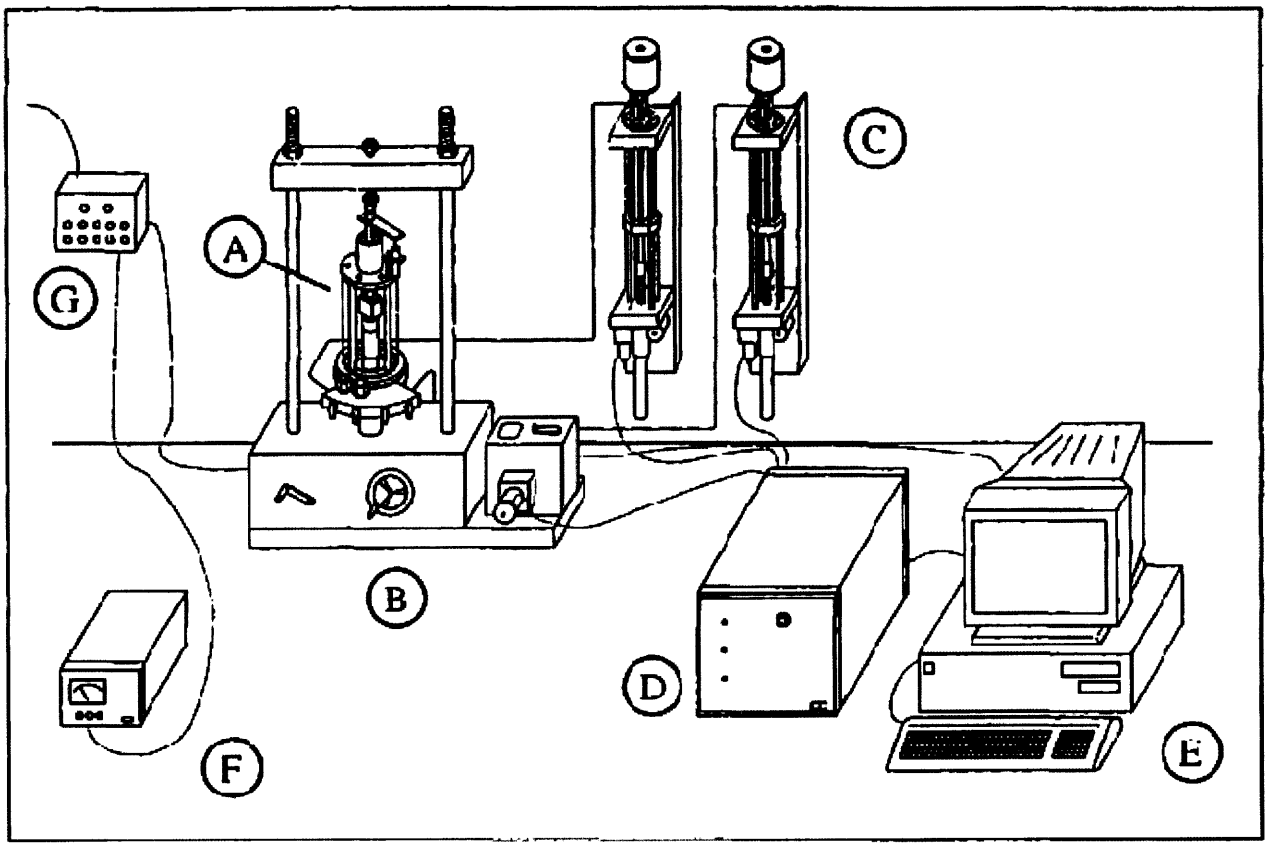

A - Triaxial Cell
B - Load Frame
C - Pressure/Volume Controllers
D - Motor Control Box
E - Personal Computer
F - DC Power Supply
G - Data Acquisition Channels

Figure 4-1: Schematic of the standard automated triaxial testing system used in the MIT Geotechnical Engineering Laboratory (from Santagata, 1998)

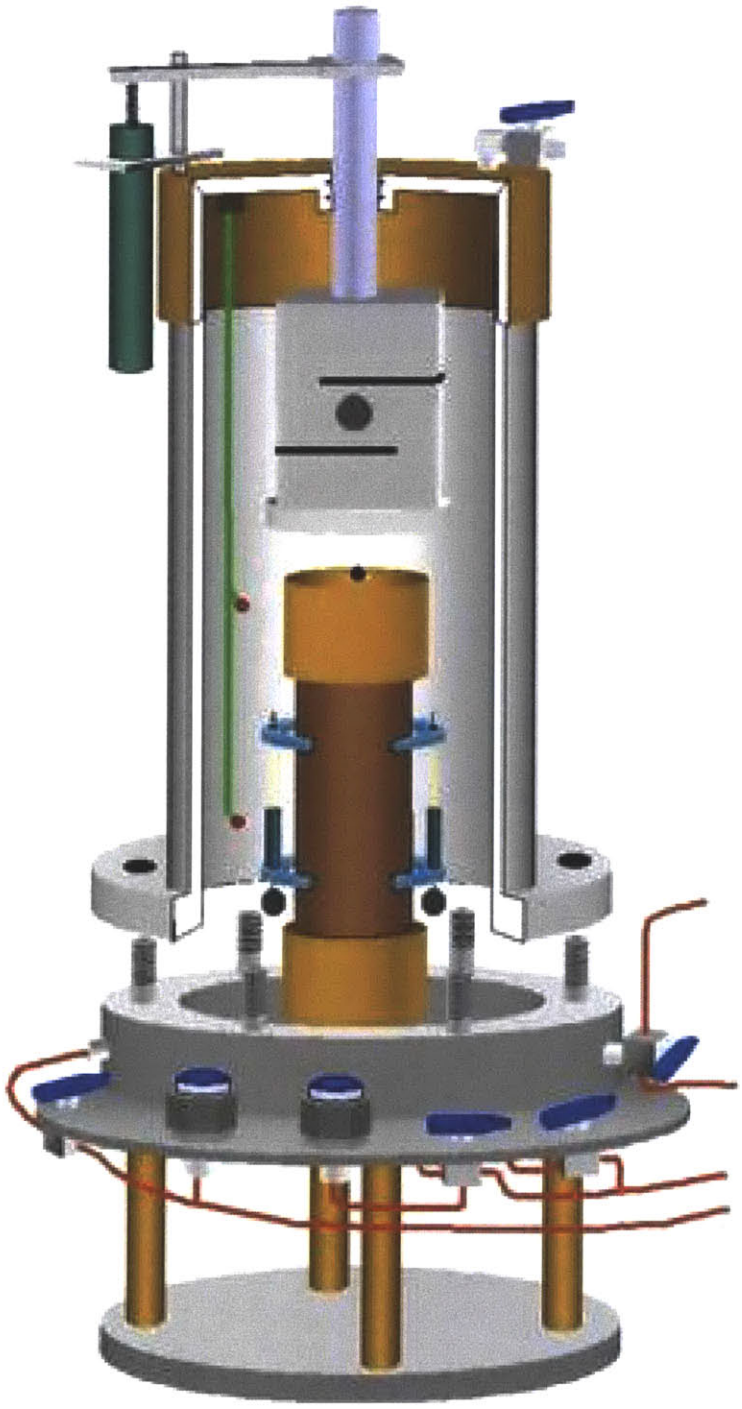

Figure 4-2: Schematic of triaxial cell (Da Re, 2000). Note that the figure shows on-specimen displacement transducers which were not used in the author's tests

Figure 4-3: Triaxial cell and PVA's in the environmental enclosure

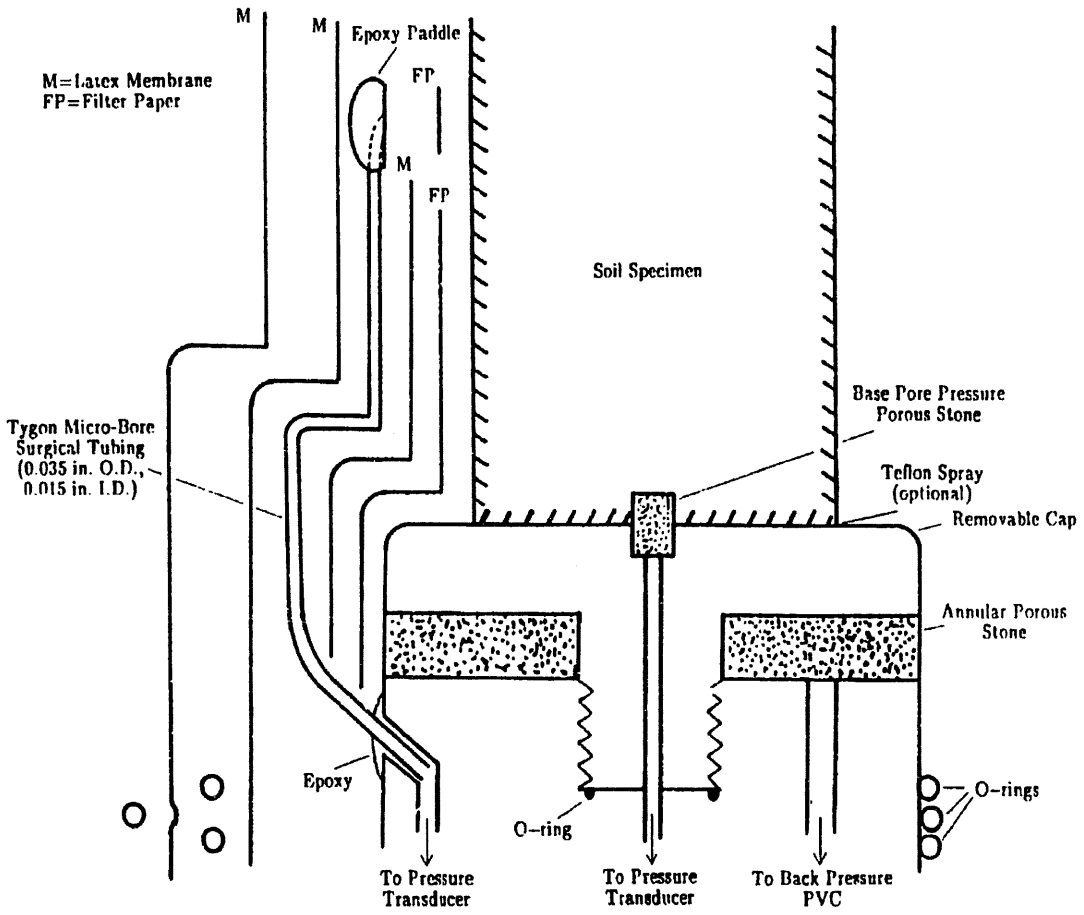

Figure 4-4: Design of smooth end platens used by Sheahan (1991)

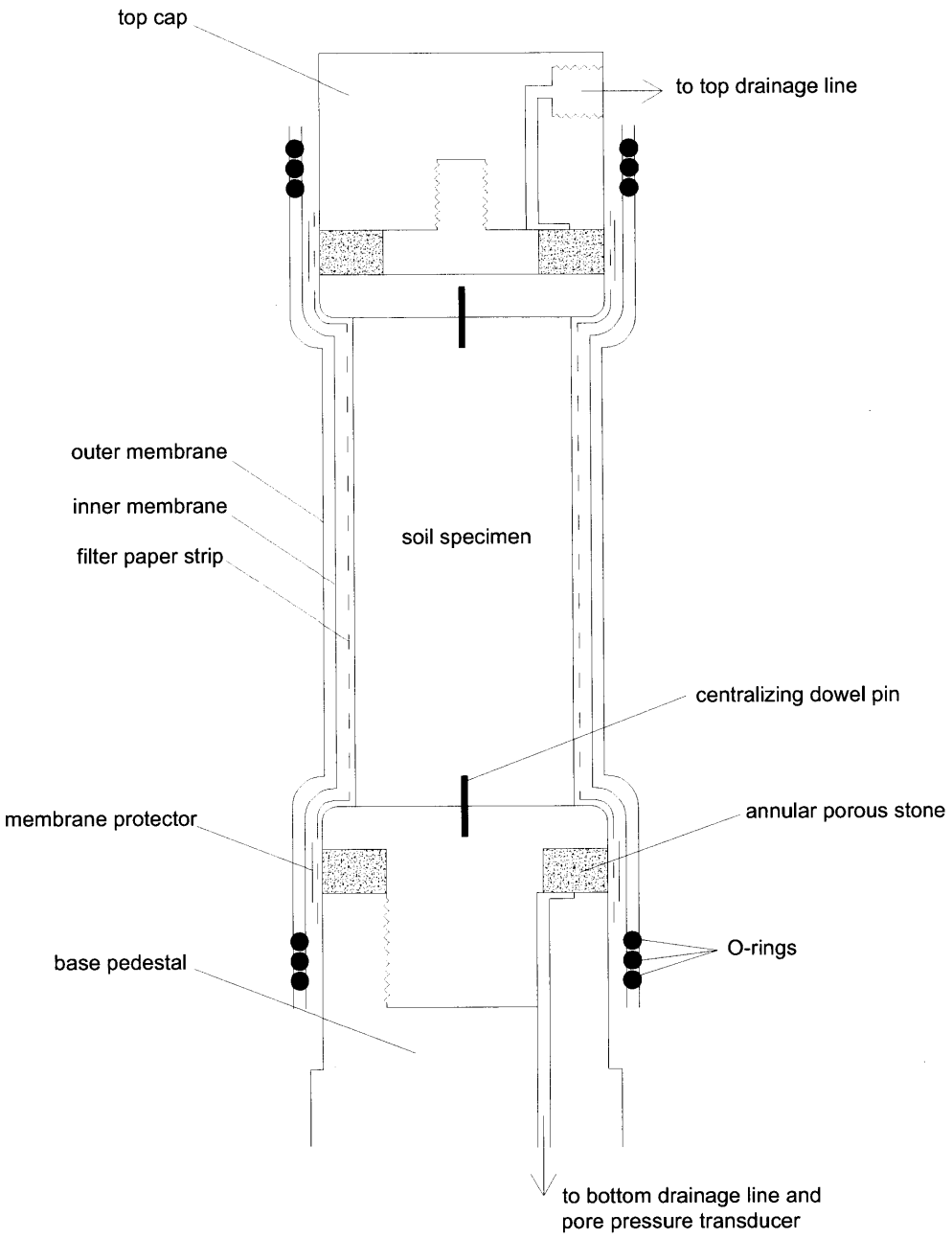

Figure 4-5: Cross-section of specimen setup

Figure 4-6: Test setup at the point at which filter paper strips have been positioned around the specimen but before the membranes are placed. The alignment device can be seen to keep the specimen and top cap in place

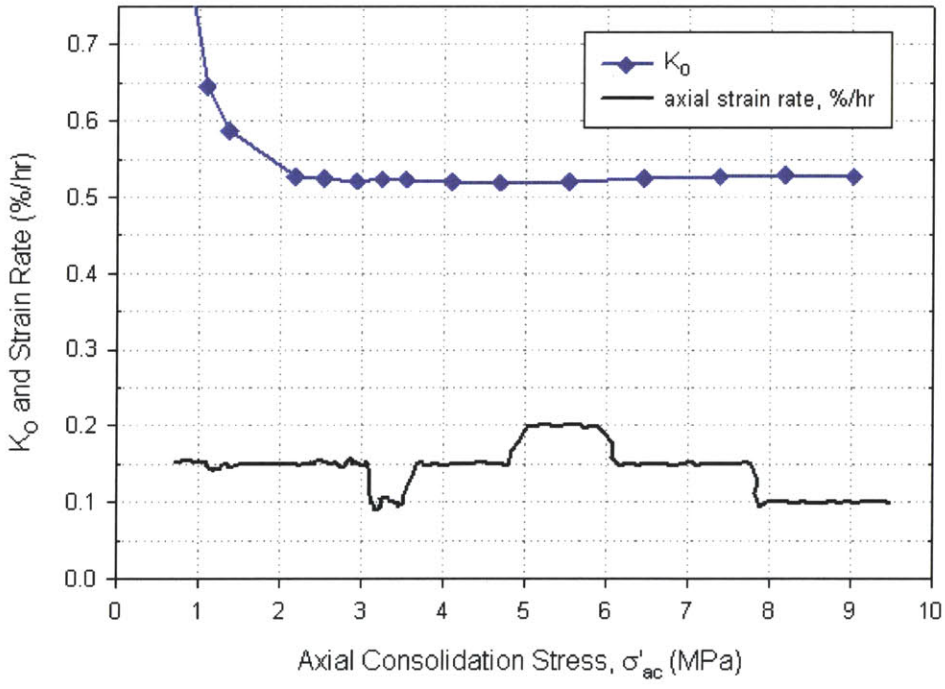

Figure 4-7: The variation in K_O with stress level as measured during the consolidation stage of a triaxial test in which the axial strain rate is varied

5 TRIAXIAL TEST RESULTS

5.1 INTRODUCTION

This chapter presents the results of the experimental program carried out to investigate the effects of end restraint in the triaxial testing of cohesive soil at high consolidation stresses. The impact of specimen end restraint on triaxial test results is examined by comparing the results of CK_OUC tests carried out by the author, who used smooth end platens in the triaxial device, with those of Abdulhadi (2009) who used conventional fixed ends. The author's experimental program has involved 14 CK_OUC triaxial tests with maximum axial consolidation stresses ranging from about 0.6 to 10 MPa. Behaviour is examined at three well-defined OCRs of 1, 2 and 4. All tests involve triaxial compression mode of shear. Of the 14 tests carried out, 6 developed problems either during or at the end of consolidation or during shearing. Only relevant consolidation data for these tests is therefore reported. Problems encountered include control program malfunction, external leaks, and membrane failure.

The results obtained from the K_O consolidation stage of triaxial tests are presented in Section 5.2. In particular, the section summarizes measured compression behaviour and the variation in K_O observed during consolidation.

Section 5.3 presents results from the undrained shear phase of triaxial tests. An in-depth comparison is made with the corresponding undrained shear results of Abdulhadi (2009) who used fixed ends in the triaxial device.

5.2 ONE-DIMENSIONAL CONSOLIDATION BEHAVIOUR

5.2.1 Introduction

All triaxial tests carried out involved K_O consolidation of RBBC specimens in the triaxial device to stresses at least two times higher than the applied batch preconsolidation pressure. For each test with a successful consolidation phase, Table 5-1 summarizes the test number, batch number and applied batch σ'_p, initial phase relations of the specimen (w_c and e_o), conditions at maximum consolidation stress (σ'_p and K_{ONC}) as well as pre-shear consolidation conditions (σ'_{ac}, OCR, e and K). For one test, TX1042, a significant portion of the data for the consolidation portion of the test was lost. As a result, this test is not included in Figure 5-1, Figure 5-2 or Figure 5-3.

Sections 5.2.2 and 5.2.3 discuss the compression behaviour and variation in K_O measured during the consolidation phase of triaxial tests respectively.

5.2.2 Compression Behaviour during Triaxial Consolidation

Figure 5-1 and Figure 5-2 show compression curves obtained during the K_O consolidation stage of triaxial tests in e-σ'_{ac} and e-logσ'_{ac} space respectively. For comparison, the figures also include the compression curve obtained during a typical triaxial test performed by Abdulhadi (2009). Apart from the results of one test, TX1030, it can be seen that the compression behaviour shows excellent repeatability and compares very well with that measured by Abdulhadi. The test TX1030 is a clear outlier, though the reason for the different behaviour observed for this test could not be established and the void ratio results are believed to be anomalous. The overall good repeatability found between the author's results and those of Abdulhadi is encouraging, especially given that the author employed only radial drainage of test specimens through filter paper strips while Abdulhadi employed standard [double] end drainage through porous stones. It can be concluded that the axial strain rate of 0.15 %/hr used by both researchers during virgin consolidation is sufficiently slow to prevent non-negligible excess pore pressures from developing in specimens. In addition, the results of a test (TX1057) described in Chapter 4 in which the axial strain rate was varied during consolidation also support this conclusion.

The compression curves display log-linearity throughout almost the entire range of virgin consolidation, with CR remaining at about 0.15 to 0.16 for most tests. For tests involving shearing in the OC range, values of SR were determined by connecting the compression curve points at the end of loading (after allowing for secondary compression) and at the end of unloading. This is referred to as a secant swelling ratio. For test TX1034 a relatively flat swelling curve was obtained, resulting in a calculated SR of just 0.020. The lack of swelling observed for the specimen is believed to have been caused by the use of an axial strain rate of 0.10 %/hr during unloading. While a rate of 0.10 %/hr was adopted by Abdulhadi (2009) using standard end drainage, the rate appears to be too fast when only radial drainage is provided. This is thought to have resulted in the misleadingly high undrained shear strength being measured for test TX1034, as will be discussed further in Section 5.3.4. For subsequent tests involving shearing in the OC range an axial strain rate of 0.05 %/hr was used during swelling. Tests TX1040, TX1046 and TX1057 had pre-shear OCRs of 2.0, 4.2 and 3.95 respectively and values of secant SR were calculated to be 0.021, 0.025 and 0.024 respectively (keep in mind that SR increases with OCR, so the lower value of 0.021 for TX1040 is reasonable given the lower OCR). As expected, these values of SR are almost an order of magnitude smaller than the average values of CR for the tests.

It can be seen from Figure 5-2 that the yield stresses of the compression curves appear to be considerably lower than the preconsolidation pressures which were supposedly applied during the resedimentation process. Tests TX1036 and TX1046 were performed on specimens which were batched to an applied σ'_p = 0.25 MPa while the remainder of the tests were performed on specimens batched to an applied σ'_p = 2 MPa (test TX846 by Abdulhadi was performed on a specimen batched to σ'_p = 1 MPa). The yield points of the compression curves are also quite poorly defined, making the interpretation of the actual specimen σ'_p difficult. These observations can reasonably be attributed to friction acting between the soil sample and the sides of the consolidometer during resedimentation. The maximum stress imposed on the sample during resedimentation, i.e. the target batch σ'_p, will be equal the applied stress at the top and bottom of the sample (since the sample is allowed to consolidate from both ends, as described in Chapter 3) but will be reduced by side-wall friction with increasing distance away from the ends. During reconsolidation in the triaxial device the middle of the specimen therefore yields at stresses lower than the target batch σ'_p, with yielding occurring progressively from the middle of the specimen towards the ends as the applied stress increases. This results in the low and poorly defined preconsolidation pressures being observed for reconsolidation in the triaxial device. A small amount of disturbance caused by the extrusion of samples from consolidometers may also contribute to a lesser extent. However, following the SHANSEP reconsolidation technique[10], any impact which these effects would have on undrained shear behaviour is eliminated following K_O consolidation in the triaxial device to stresses much higher than the batch preconsolidation pressure. This issue has been discussed in more detail in Chapter 3.

5.2.3 K_O during Triaxial Consolidation

Figure 5-3 shows the change in K_O during consolidation as measured in the triaxial tests. For clarity, the figure plots axial consolidation stress on a log scale and omits changes in K_O observed during the swelling of specimens into the OC range. The repeatability of the measured K_O values between tests is admittedly quite poor when compared to what was achieved by Abdulhadi (see Figure 3-13). The general trend observed in each test (except TX1030) is consistent however. K_O decreases in the OC range before reaching a fairly stable value for virgin consolidation. Note that in some tests a small deviator force was being applied to the specimen at the start of consolidation and as a result K_O can be seen to be start at a value significantly less than 1 for these tests in Figure 5-3. The trend of the change in K_O observed for consolidation in the triaxial device is the same as that reported by Abdulhadi, though is somewhat different to what was reported by previous researchers.

[10] The SHANSEP reconsolidation technique is described in Chapter 2

Sheahan (1991) and Santagata (1994), both of whom used RBBC Series III in their experimental programs, found that K_O decreased in the OC range to a value lower than K_{ONC} before increasing again. The K_O trend observed by previous researchers such as Sheahan and Santagata was discussed previously in Chapter 3 and illustrated in Figure 3-14. Abdulhadi hinted that the different K_O trends observed could possibly be due to either the different resedimentation procedures or different series of RBBC adopted in the studies.

Once again, test TX1030 can be seen to be a clear outlier in the data. As shown in Figure 5-3, K_O for test TX1030 drops to a very low value of about 0.38 at σ'_{ac} = 0.4 MPa before increasing again to reach a reasonable value of 0.56 prior to shearing at σ'_{ac} = 9.8 MPa. It should be kept in mind that test TX1030 was performed on an RBBC specimen with had been batched to an applied σ'_p = 2 MPa.

5.3 UNDRAINED SHEAR BEHAVIOUR

5.3.1 Introduction

This section presents results from the undrained shear phase of the triaxial tests. Of the 8 tests in which successful shear phases were conducted, 3 tests had a pre-shear OCR of 1, 1 test had a pre-shear OCR of 2 and 4 tests had a pre-shear OCR of 4. A comparison is made with corresponding results obtained by Abdulhadi (2009) so that the impact of specimen end restraint on triaxial test results can be examined. Shearing was performed at a constant axial strain rate of 0.5 %/hr in all tests. For each test with a successful undrained shear phase, Table 5-2 summarizes the test number, pre-shear consolidation conditions (σ'_{ac}, OCR and K), as well as pertinent stress-strain parameters measured during shearing (ε_f, s_u, φ'_p, φ'_{mo}).

Sections 5.3.2, 5.3.3 and 5.3.4 present the undrained shear results for OCRs 1, 2 and 4 respectively. In Section 5.3.5 the results for all OCRs are combined and compared at a given stress level. Finally, in Section 5.3.6 the effectiveness of the smooth ends used by the author to prevent end restraint during shearing is evaluated.

It is important to keep in mind when being presented with the results of this section that, as was discussed in Chapter 3, the strain rate of 0.5 %/hr used in Abdulhadi's tests with fixed ends is considered to be sufficiently slow to allow pore pressure equilibration in RBBC specimens during

undrained shearing. That is, in terms of conventional end restraint theory[11] Abdulhadi's tests would be regarded as 'slow'.

5.3.2 Behaviour at OCR = 1

Figure 5-4 shows shear stress-strain responses ($q = (\sigma_1 - \sigma_3)/2$ vs. ε_a) measured during undrained shearing for three triaxial tests performed at different stress levels at OCR = 1. Smooth end platens were used in each test. As expected, undrained strength increases with increasing consolidation stress. In each test a peak strength is reached at a relatively small strain followed by strain softening, a behaviour which would be expected for a normally consolidated soil. Figure 5-5 shows the same three tests given in Figure 5-4 but this time the shear stress measured in each test has been normalized with respect to the pre-shear axial consolidation stress. For comparison, the corresponding results obtained at the same stress levels by Abdulhadi using fixed ends are also shown in Figure 5-5. It can be seen that there is a trend of decreasing normalized undrained strength with increasing consolidation stress. The stress-strain response also becomes more ductile with increasing stress level as ε_f increases and the degree of post-peak strain softening is reduced. These trends are observed regardless of specimen end condition. If we now compare the results of the tests with smooth and fixed ends, it is seen that at a given stress level the undrained strength measured using fixed ends is consistently lower than that measured using smooth ends. Figure 5-6 presents the same test results as Figure 5-5 but only for axial strains up 2 % and may demonstrate more clearly the decrease in s_u/σ'_{ac} and increase in ε_f with increasing consolidation stress.

Figure 5-7 plots curves of normalized undrained secant Young's modulus (E_u/σ'_{ac}) versus axial strain on log scales for the tests with smooth and fixed ends. The measurement of axial displacement in the tests was performed using an external LVDT and thus the measured stiffnesses are only considered reliable for ε_a above about 0.05 %. In general, Figure 5-7 illustrates that the soil exhibits strong non-linearity and that yielding occurs at small strains. The decrease in stiffness is particularly marked once the soil reaches failure as post-peak strain softening begins to occur. For both smooth and fixed end tests there is a consistent decrease in the initial (maximum) stiffness with increasing consolidation stress. Increasing stress level also tends to produce a larger strain range of initial linear behaviour. At strains greater than about 0.1 % the curves of normalized stiffness converge. In addition, it can be seen from Figure 5-7 that, at a given stress level, the initial stiffness measured in a smooth end test is slightly higher than the initial stiffness measured in a fixed end test. However, this is believed to be due to measurement errors for $\varepsilon_a < 0.05$ % rather than

[11] End restraint theory is discussed in detail in Chapter 2

representing a true soil behaviour, since specimen end condition should have very little impact on measured initial stiffness.

Figure 5-8 plots the normalized shear induced pore pressures (u_s/σ'_{ac}) measured in the tests performed with smooth and fixed ends. The small strain pore pressure response is shown more clearly in Figure 5-9 for $\varepsilon_a < 2$ %. The positive shear induced pore pressures generated during shearing are indicative of the contractive behaviour of NC soil. Comparing the tests with smooth and fixed ends, it can be seen that while the tests with fixed ends show a consistent decrease in u_s/σ'_{ac} with increasing stress level, this trend is only observed in the smooth end tests at strains less than about 1 %. In fact, while the highest pressure test performed with smooth ends shows shear induced pore pressures initially becoming slightly negative, at large strains u_s/σ'_{ac} is found to be slightly larger than for the lower pressure tests.

Combining stress-strain and pore pressure data, Figure 5-10 plots the effective stress paths for the tests with smooth ends. The stress paths are drawn in normalized MIT q-p' space, i.e. $(\sigma_a - \sigma_r)/2\sigma'_{ac}$ versus $(\sigma'_a + \sigma'_r)/2\sigma'_{ac}$. Abduhadi's fixed end tests are omitted from the figure for clarity. The general shape of the effective stress path measured for each test remains the same. The generation initially of low shear induced pore pressures causes the stress path to rise somewhat vertically. A clear yield point is then reached, after which the generation of large shear induced pore pressures causes the effective stress to decrease and the stress path to travel to the left before reaching the large strain Mohr-Coulomb failure envelope. For test TX1030, the generation initially of a small negative shear induced pore pressure (as shown in Figure 5-9) causes the effective stress path for this test to travel slightly to the right prior to yield. Consistent with what was observed in Figure 5-6, the low pressure test reaches a greater normalized shear strength than the higher pressure tests. However, the large strain secant friction angle measured in each test is similar, with an average φ'_{mo} = 30.7° (exact values of φ'_{mo} for each test are given in Table 5-2). At low stress the yield point of the stress path coincides with peak shear strength. However, at higher stresses the point of peak shear strength occurs further down the stress path and does not coincide with the yield point, i.e. peak shear strength occurs at a lower effective stress. The reductions in both normalized shear stress and effective stress at failure with increasing stress level explains why the secant friction angle at peak shear strength (φ'_p) varies very little with stress level, remaining in the range of 23.5° to 24.0° for the three tests, as given in Figure 5-10. This is consistent with the finding of Abdulhadi for when fixed ends are used.

The different starting points for each of the effective stress paths shown in Figure 5-10 is due to different pre-shear values of K_{ONC}. Consistent with what was reported by Abdulhadi, K_{ONC} was found to increase with increasing consolidation stress. It is very likely that this increase in K_{ONC} is

linked to the decrease in normalized undrained strength with stress level, since, as discussed in Chapter 3, increasing pre-shear lateral ratio decreases the undrained strength of RBBC. Figure 5-11 shows the relationships between normalized undrained strength and pre-shear K_{ONC} for NC RBBC found in the experimental programs of the author, Abdulhadi (2009) and Santagata (1994). While a trend of decreasing s_u/σ'_{ac} with increasing K_{ONC} is observed in each case, regression analyses on the test results yield quite different equations relating s_u/σ'_{ac} to K_{ONC} for each experimental program. Note that Figure 5-11 excludes the individual test results of Santagata (1994), though this data is shown in Figure 3-26. While the relationships quoted by Santagata and Abdulhadi are derived from a large number of individual tests, the relationship determined for the author's experimental program is derived from only the results of three tests and is therefore believed to be less reliable. It should be kept in mind that Santagata's equation is based on results from triaxial tests performed on RBBC Series III, with some tests involving K_O consolidation and others involving stress path consolidation with a prescribed value of K. It is also worth mentioning that the negative correlation between s_u/σ'_{ac} and K_{ONC} is somewhat counter-intuitive. For a given σ'_{ac}, void ratio reduces with increasing K. As a result, one might expect undrained strength to *increase* with increasing K. The reason for the observed increase in strength with decreasing K is not fully understood.

5.3.3 Behaviour at OCR = 2

Only one test, TX1040, was performed using smooth ends at OCR = 2. The test was carried out at σ'_{ac} = 4.89 MPa (σ'_p = 9.78). Figure 5-12 shows the shear-stress strain behaviour measured in the test compared with what was measured at the same stress level by Abdulhadi using fixed ends. It can be seen that the two tests display almost identical responses, including very similar undrained strengths and strains to failure. As expected, RBBC at OCR = 2 shows a much more ductile behaviour compared to that of the NC soil described above, exhibiting significantly less strain softening. Figure 5-13 plots the normalized undrained secant Young's modulus versus strain for the tests. Again, almost identical stiffnesses are measured for both tests.

Figure 5-14 shows the normalized shear induced pore pressures generated in the test with smooth ends compared to those generated when fixed ends are used. Here, unlike the stress-strain responses, the two tests demonstrate considerably different behaviour. For the test with fixed ends a positive u_s is initially generated. After a relatively small strain of 0.2 % pore pressures then begin to decrease and a minimum u_s/σ'_{ac} of about -0.04 is reached just before the undrained strength is attained. The pore pressures subsequently increase for the remainder of the test and are still rising when the test is ended. Substantially different behaviour is exhibited in the test performed with smooth ends, with negative shear induced pore pressures being generated from the very beginning.

A minimum u_s/σ'_{ac} = -0.09 is reached and once again this occurs just before failure of the specimen. Shear induced pore pressures subsequently increase for the remainder of the test. The different pore pressure responses measured for the two tests is consistent with what is predicted by end restraint theory. The decrease in maximum shear stress which is produced at the ends of a specimen when fixed ends are used can result in a higher shear induced pore pressure overall in an OC specimen.

Normalized effective stress paths for the tests are shown in Figure 5-15. Despite the fact that the ultimate shear strengths measured in the two tests are almost identical, the higher pore pressures measured in the test with fixed has resulted in the effective stress path for this test being pushed to the left. At large strains the secant friction angle measured in each test is practically the same, with an average φ'_{mo} = 29.9°. For each test the undrained strength is attained at a value of φ'_p slightly below φ'_{mo}.

5.3.4 Behaviour at OCR = 4

Tests were performed at two different stress levels using smooth end platens at OCR = 4. One relatively high stress test (TX1057) was carried out at σ'_{ac} = 2.47 MPa (σ'_p = 9.78 MPa) while a lower stress test (TX1042) was carried out at σ'_{ac} = 0.47 MPa (σ'_p = 1.94 MPa). Figure 5-16 shows the shear stress-strain responses measured in these tests compared to the corresponding results obtained using fixed ends by Abdulhadi. It can be seen that fairly similar stress strain responses are observed for the tests, though at a given stress level the undrained strength measured using smooth ends is marginally higher than that measured with fixed ends. In addition, normalized undrained strength can be seen to decrease with increasing stress level regardless of specimen end condition. Figure 5-17 plots the normalized undrained secant Young's modulus versus strain as measured in the tests. For the tests with fixed ends initial normalized stiffness can be seen to decrease with increasing stress level, similar to what was observed at OCR = 1. On the other hand, for the tests with smooth ends the effect of stress level on the normalized stiffness is less noticeable.

Figure 5-18 plots the normalized shear induced pore pressures measured in the tests performed with smooth and fixed ends. Similar to what was observed at OCR = 2, the tests with smooth ends show notably lower values of u_s/σ'_{ac} at any given strain. The effect of stress level on the normalized shear induced pore pressures is less obvious. The tests with fixed ends show u_s initially becoming positive before subsequently decreasing and becoming negative, similar to the OCR = 2 behaviour. A slight positive u_s is also generated initially for the test with smooth ends at σ'_{ac} = 0.47 MPa. For the higher stress test with smooth ends a negative u_s is generated from the very beginning

of shear. However, after about 0.15 % strain u_s shows a slight increase before decreasing again. For strains greater than about 1 % the pore pressure response is very similar to that observed for the lower stress test with smooth ends. This small strain pore pressure behaviour exhibited in the higher stress test with smooth ends is somewhat bizarre and has not previously been reported at OCR = 4. At large strains stress level appears to have little to no effect on the measured u_s/σ'_{ac}.

Normalized effective stress paths are shown in Figure 5-19. The higher pore pressures measured in the tests with fixed ends have resulted in the effective stress paths for these tests being pushed to the left. The small strain pore pressure behaviour observed for the higher stress test with smooth ends, as discussed above, has resulted in the stress path for this test possessing a slightly unique shape. For all tests the average [secant] φ'_{mo} = 31.2°. At OCR = 4 peak undrained strength typically occurs on the failure envelope. This is indicated by values of φ'_p close to or equal to φ'_{mo} for all tests performed.

As mentioned previously, 4 tests were carried out using smooth ends at OCR = 4. However, only the results of two of these tests have been discussed in detail. The reason for this is that two tests were performed with smooth ends at each stress level. At the higher stress level of σ'_{ac} = 2.5 MPa, the results of the first test carried out (TX1034) were suspected to be unrepresentative. As discussed in Section 5.2.2, the strain rate used during the swelling portion of test TX1034 is believed to have been too fast, resulting in insufficient drainage and the development of negative excess pore pressures within the specimen. Once the specimen was subjected to undrained conditions these negative excess pore pressures would not have been able to dissipate, thereby causing misleadingly low pore pressures to be measured during the undrained shear phase of the test. Since the shear response was believed to be unrepresentative, a second test, test TX1057, was carried out in order to obtain more reliable results (it is the results of this test that were discussed in the preceding paragraphs). Figure 5-20 compares the normalized effective stress paths for tests TX1034 and TX1057. The low pore pressures measured in test TX1034 have resulted in the stress path being pushed well to the right and, because the stress path reaches failure further up the failure envelope, a particularly high s_u/σ'_{ac} of 0.913 is measured. In order to confirm the results of the low stress test with smooth ends (TX1042), a duplicate test (TX1046) was carried out with the same pre-shear conditions. Figure 5-21 compares the normalized effective stress paths measured for these two tests. The results obtained in each test are very consistent, though the undrained strength measured in TX1046 is somewhat low. Due to their similarity and to avoid unnecessary complication, the results of test TX1046 were not discussed in the preceding paragraphs.

5.3.5 Behaviour at OCRs 1, 2 and 4

In this section a comparison is made between the undrained shear behaviour measured using smooth and fixed ends at OCRs 1, 2 and 4. The comparison is made for tests with the same σ'_p of approximately 9.8 MPa, which corresponds to the highest stress level achieved in the experimental programs of both the author and Abdulhadi (2009). Figure 5-22 and Figure 5-23 compare shear stress-strain and pore pressures responses respectively as measured at each OCR. It is important to point out that, while in the preceding sections stresses and pore pressures were normalized with respect to pre-shear axial consolidation stress, in this section behaviour at different OCRs is compared by normalizing with respect to the preconsolidation pressure, i.e. maximum past axial consolidation stress, of the test specimen. The general trends observed in Figure 5-22 and Figure 5-23 are consistent with the predictions of standard end restraint theory: the use of fixed ends results in a lower undrained shear strength as well as the generation of higher shear induced pore pressures. The almost identical stress-strain behaviour measured using smooth and fixed ends at OCR = 2 could be said to be somewhat inconsistent with the overall trend. Combining the stress-strain and pore pressure responses, Figure 5-24 shows the effect of specimen end condition on the form of the effective stress path at each OCR. At OCR = 1 the use of fixed ends results in a relatively small increase in shear induced pore pressures, with the effect that the stress path is not dramatically altered. On the other hand, for OC soil, the notably higher pore pressures measured in the tests with fixed ends results in the effective stress paths for these tests being pushed well to the left. Regardless of specimen end condition, at large strains a common failure envelope is reached with an average [secant] $\varphi'_{mo} = 30.2°$.

Figure 5-25 shows the normalized undrained secant Young's modulus versus strain as measured in the same tests. Initial undrained stiffness, when normalized with respect to σ'_p, does not appear to be significantly affected by OCR. However, the NC soil can be seen to exhibit stiffness degradation much more rapidly as shearing progresses than the OC soil. At large strains the curves of normalized stiffness for the OC soil converge, distinct from those of the NC soil. These trends are observed regardless of specimen end condition.

As discussed previously in Chapter 3, Santagata (1998) used on-specimen displacement transducers with a high resolution in order to gain information on the stiffness of RBBC at extremely small strains. Santagata performed tests at OCRs 1, 2, 4 and 8, though only for low stresses less than 1 MPa. Based on the results of her tests, Santagata proposed a unique relationship linking initial (maximum) stiffness of RBBC to axial consolidation stress and void ratio for all OCR's. Recall that this relationship was given in Equation 3–2:

$$E_{uMAX} = 270e^{-2.45}\sigma'^{0.43}_{ac} \text{ (MPa)}$$

Figure 5-26 plots values of E_{uMAX} normalized with respect to void ratio as measured in the tests performed by both the author and Abdulhadi versus stress level. It can be seen that at a given stress level there is a lot of scatter in the measured normalized stiffness. This is somewhat expected given the fact that both the author and Abdulhadi employed the use of an external LVDT to measure axial displacements, with the result that measured stiffnesses can only be considered reliable for ε_a greater than about 0.05 %. Since values of E_{uMAX} were measured at strains less than 0.05 %, and often as low as 0.01 %, a lot of scatter in the data could be anticipated. In addition, it can be seen from Figure 5-26 that there appears to be no effect of either OCR or specimen end condition on the normalized stiffness. Again, these observations should be expected as the effect of OCR is eliminated from the data by normalizing stiffness with respect to void ratio and the use of smooth versus fixed ends should have little to no impact on initial stiffness.

For comparison, Figure 5-26 also includes the relationship proposed by Santagata (1998) extrapolated for σ'_{ac} up to 10 MPa. Santagata found that RBBC typically exhibits stiffness degradation at strains less than 0.01 %. For NC RBBC, in particular, yielding can begin at strains as low as 0.001 %. As a result, the values of E_{uMAX} obtained by the author and Abdulhadi using external displacement measurement are generally much lower than those measured by Santagata at a given stress level.

Figure 5-27 shows the decrease in secant friction angle with increasing consolidation stress. The figure includes data from the tests performed by the author and Abdulhadi (2009), as well as from CK_OUC tests carried out by Sheahan (1991) at a strain rate of 0.5 %/hr. Note that the trend in friction angle is much more consistent when stress level is taken in terms of σ'_p rather than σ'_{ac}. This is because at large strains, i.e. on the failure envelope, specimens (at different OCRs) with the same σ'_p reach effective stresses that are much more similar than specimens with the same σ'_{ac}. Since Abdulhadi's tests with fixed ends could be regarded as 'slow', specimen end condition should have no impact on the measured φ'_{mo}. Figure 5-27 shows that this would in fact appear to be the case. In addition, the figure shows no dependence of φ'_{mo} on OCR. The data presented in Figure 5-27 indicates an intrinsic failure envelope[12] having significant curvature.

Figure 5-28 presents the variation in normalized undrained strength with stress level at OCRs 1, 2 and 4 as measured in tests performed with smooth and fixed ends. Except for the NC test at σ'_p = 0.6 MPa which was performed by the author, the tests with smooth ends performed at low stress with σ'_p < 1 MPa were carried out by Sheahan (1991). At each OCR there is a generally consistent trend of lower undrained strengths being measured at a given stress level in tests with fixed ends, though it could be said that the error in the measured undrained strength associated with

[12] The intrinsic failure envelope (Burland, 1990) is discussed in Chapter 2

the use of fixed ends is relatively small. Normalized undrained strength can be seen to decrease consistently with increasing consolidation stress at each OCR regardless of specimen end condition.

The decrease in normalized undrained strength with increasing stress level, as well as the reduced undrained strength measured in tests performed with fixed ends, are both associated with the generation of higher shear induced pore pressures. Figure 5-29 and Figure 5-30 show the correlations between normalized peak undrained strength (s_u/σ'_p) and the normalized shear induced pore pressures at peak undrained strength (u_{sp}/σ'_p) for OCRs 1 and 4 respectively. The figures include data from both the author's tests and the tests of Abdulhadi. At OCR = 2 shear induced pore pressures are much smaller in magnitude than at OCR 1 or 4 and a correlation with s_u is therefore more difficult to detect. Both Figure 5-29 and Figure 5-30 illustrate a relatively consistent trend of decreasing s_u/σ'_p with increasing u_{sp}/σ'_p. In addition, the trend does not depend on specimen end condition. At OCR = 1 the increase in u_{sp} causes φ'_p to be reached at a lower peak shear strength, i.e. s_u. For OC soil the increase in u_{sp} causes φ'_{mo} to be reached at a lower s_u.

The impact of the variations in measured undrained strength due to stress level and specimen end condition, as described above, on the SHANSEP S and m parameters is summarized in Figure 5-31. As indicated in Figure 5-31, axial stress in triaxial space now corresponds to vertical stress in the SHANSEP design procedure. As discussed in Chapter 2, since Abdulhadi (2009) was the first to clearly show a consistent trend of decreasing normalized undrained strength with increasing consolidation stress, he was also the first to express the SHANSEP parameters as a function of stress level. Abdulhadi found that increasing stress level decreases normalized undrained strength by approximately the same degree at each OCR. As a result, S decreases while m remained fairly constant with increasing stress. At a stress level of σ'_p = 9.8 MPa, a regression analysis on Abdulhadi's test results at OCRs 1, 2 and 4 yields S = 0.286 and m = 0.730 [13]. When a regression analysis is performed on the author's test results obtained using smooth ends at σ'_p = 9.8 MPa, slightly higher values of 0.290 and 0.742 are obtained for S and m respectively. On the other hand, Sheahan's (1991) test results obtained using smooth ends at σ'_p = 0.6 MPa produce a higher S value of 0.315 and an m value of 0.730. The higher value of S for Sheahan's tests is expected given the lower consolidation stress.

At sufficiently large strains soil reaches a critical state whereby shearing progresses without any change in pore pressure (or volume in the case of drained conditions), effective stress or shearing resistance. Figure 5-32 shows the effective stresses at the end of shearing for the tests

[13] It should be noted that Abdulhadi (2009) actually quoted values of 0.281 and 0.757 for S and m respectively, as given in Figure 2-18. However, a re-analysis of his test results by the author yields the values of 0.286 and 0.730

performed by the author and Abdulhadi in e-logp'$_m$ space. The figure excludes the results of test TX1030 where the pre-shear void ratio was calculated to be uncharacteristically low (as shown in Figure 5-1). A regression line through the points representing the effective stresses at the end of the tests yields the critical state line. According to critical state soil mechanics theory this line should be parallel to the virgin consolidation line of the soil when plotted in e-logp'$_m$ space. Figure 5-32 includes compression curves obtained during K_O virgin consolidation for two typical triaxial tests. It can be seen that the virgin consolidation line of RBBC is in fact reasonably parallel to the critical state line for the soil. Although a unique critical state line is plotted in Figure 5-32, it can be seen that, at a given void ratio, the tests performed with smooth ends generally appear to reach a critical state at a slightly lower effective stress than the tests performed with fixed ends. It is suspected that two factors could be causing this. Firstly, in the author's tests with smooth ends undrained shearing was generally carried out to a slightly higher axial strain, say by 1 or 2 %, than in Abdulhadi's tests. Secondly, at large strains a more uniform stress state should exist in test specimens sheared using smooth ends, thereby causing a slightly different, and more accurate, interpretation of critical state to be achieved.

Figure 5-33 shows the same data as in Figure 5-32 but also includes the shear stresses measured at the end of the tests. A regression line through the points representing the shear stresses at the end of the tests yields the critical state line for shear stress. Similar to the case for effective stress, the tests performed with smooth ends typically to reach a critical state at a slightly lower shear stress than the tests performed with fixed ends for a given void ratio.

5.3.6 Evaluation of the Smooth End Platens

Since the research focuses on the effects of end restraint caused by the use of fixed ends on triaxial shear results, it is important to evaluate the effectiveness of the smooth ends used by the author to prevent end restraint. One way in which this can be done is by examining the geometric uniformity of test specimens after shearing. To this end, Sheahan defined the area uniformity ratio (AUR) as:

$$AUR = \frac{A_{parabolic} - A_{measured}}{A_{parabolic} - A_{cylindrical}} \qquad \text{Equation 5-1}$$

where $A_{parabolic}$ is the area computed using a parabolic area correction.

For an undrained test $A_{parabolic}$ is defined as (Germaine and Ladd, 1988):

$$A_{parabolic} = A_o \left\{ -0.25 + \frac{\sqrt{25 - 20\varepsilon_a - 5\varepsilon_a^2}}{4(1 - \varepsilon_a)} \right\}^2 \qquad \text{Equation 5-2}$$

and $A_{cylindrical}$ is the cylindrical area correction for an undrained test:

$$A_{cylindrical} = A_o(1/(1 - \varepsilon_a)) \qquad \text{Equation 5-3}$$

In both equations, A_o is the pre-shear specimen area and ε_a is the strain at the end of shearing. The value of $A_{measured}$ is obtained by directly measuring the specimen area at the end of the test after load removal. The AUR is a scale of specimen uniformity which is zero when the specimen follows a parabolic shape and unity if it deforms as a right cylinder. The ratio removes the effect of different tests having different values of ε_a. In a fixed end test the parabolic area correction predicts no change in specimen area at the ends but bulging in the middle. If smooth ends are completely effective in eliminating end restraint then a specimen should deform as an ideal right cylinder during shearing, i.e. radial deformation should be equal along the entire height of the specimen, as predicted by the cylindrical area correction.

At the end of each test carried out using smooth ends a calipers was used to take several measurements of specimen diameter. The average diameter was then computed for the top, middle and bottom of the specimen and this average diameter was in turn used to compute $A_{measured}$ and the AUR. Table 5-3 gives values of AUR for the top, middle and bottom of specimens. The table presents mixed results. For the top and bottom of specimens AUR values typically fall in the range of 0.2 to 0.5, indicating that the smooth ends do allow some lateral spreading but not enough to ensure right cylinder deformation. AUR values at specimen mid-height show greater variation, ranging from -0.56 to 1.23. A negative AUR, measured at specimen mid-height for tests TX1030 and TX1031, implies that the measured area is greater than that predicted by the parabolic area correction and indicates excessive bulging at mid-height. Overall, the average AUR values for all the tests would indicate that the smooth end platens were partially effective in allowing specimens to deform in a uniform fashion. This is consistent with the finding of Sheahan (1991) who used a very similar end platen design for his tests, as was discussed in Chapter 4. Based on the computed AUR values, the parabolic area correction was used in the analysis of all tests performed with smooth ends (the same area correction was applied by Sheahan in his triaxial compression tests).

Sheahan (1991) proposed a partial explanation as to why smooth ends were not entirely successful in allowing right cylinder deformation which may also be applicable to the author's tests.

As illustrated in Figure 5-34, cell pressure acting on the membranes and filter strips between the edge of the end platen and the specimen creates a frictional force which may constrain the membranes and filter strips from moving freely across the end platen. As a result, the specimen may be prevented from expanding at the ends as completely as it would if there were no frictional resistance.

It should be kept in mind that some of the scatter in the computed AUR values between tests could be attributed to inaccuracies in the measurements of final specimen diameter. Small errors in the measured diameter, on the order of fractions of a millimeter, can have a significant impact on the computed AUR. Such inaccuracies could be anticipated, even when an average of several caliper measurements is taken for each specimen location.

Slip surfaces were not found to develop in any of the triaxial tests performed using smooth ends, even for tests performed in the OC range. In contrast, for the test program carried out by Abdulhadi (2009) it was found that while the low pressure triaxial tests on NC RBBC involved only bulging of specimen with no discernable strain localization, tests carried out for $\sigma'_{ac} > 4$ MPa were found to form slip surfaces during shearing. For OC specimens Abdulhadi reported slip surfaces occurring at much lower stresses.

Test no.	Batch no.	Batch σ'_p (MPa)	Initial w_c (%)	Initial e_o	At Max Stress σ'_p (MPa)	At Max Stress K_{ONC}	Pre-Shear σ'_{ac} (MPa)	Pre-Shear OCR	Pre-Shear e	Pre-Shear K
TX1027	RS126	2	27.8	77.3	9.723	0.586	*external leak developed during shear*			
TX1030	RS127	2	27.2	75.6	9.783	0.560	9.783	1	0.447	0.560
TX1031	RS128	2	26.5	73.7	5.859	0.523	5.859	1	0.550	0.523
TX1032	RS129	2	27.1	75.3	8.233	0.526	*control program malfunction prior to shear*			
TX1034	RS130	2	27.2	75.7	9.785	0.602	2.445	4.00	0.508	1.000
TX1035	RS131	2	27.1	75.3	9.771	0.529	*control program malfunction prior to shear*			
TX1036	RS132	0.25	39.3	109.3	0.557	0.493	0.557	1	0.872	0.493
TX1040	RS137	2	27.4	76.2	9.776	0.556	4.885	2.00	0.517	0.744
TX1042	RS138	1	30.9	86.0	1.938	0.557	0.469	4.13	0.731	1.000
TX1046	RS162	0.25	39.3	109.3	1.930	0.582	0.462	4.18	0.740	1.000
TX1057	RS168	2	27.6	76.7	9.782	0.525	2.474	3.95	0.518	0.992

Table 5-1: Summary of triaxial consolidation results

Test no.	Pre-Shear σ'_{ac} (MPa)	Pre-Shear OCR	Pre-Shear K	During Undrained Shearing s_u (MPa)	During Undrained Shearing s_u/σ'_{ac}	During Undrained Shearing ε_f (%)	During Undrained Shearing ϕ'_p (°)	During Undrained Shearing ϕ'_{mo} (c'=0) (°)
TX1030	9.783	1	0.560	2.837	0.290	1.09	23.6	30.3
TX1031	5.859	1	0.523	1.693	0.289	0.60	23.5	30.9
TX1034	2.445	4.00	1.000	2.232	0.913	3.96	28.9	30.3
TX1036	0.557	1	0.493	0.173	0.310	0.12	24.0	30.8
TX1040	4.885	2.00	0.744	2.364	0.484	2.46	27.2	29.7
TX1042	0.469	4.13	1.000	0.384	0.819	6.25	30.5	30.9
TX1046	0.462	4.18	1.000	0.359	0.777	7.04	30.9	31.2
TX1057	2.474	3.95	0.992	1.989	0.804	6.56	30.7	30.8

Table 5-2: Summary of triaxial shear results

Test	OCR	AUR_{top}	AUR_{middle}	AUR_{bottom}
TX1030	1	0.55	-0.62	0.56
TX1031	1	0.79	-0.05	0.36
TX1034	4.00	0.59	0.55	0.31
TX1036	1	0.43	0.18	0.21
TX1040	2.00	0.22	0.10	0.26
TX1042	4.13	0.36	0.69	0.09
TX1046	4.18	0.06	1.18	0.18
TX1057	3.95	0.42	0.05	0.25
Average		0.43	0.26	0.28

Table 5-3: AUR values computed for the end of shearing

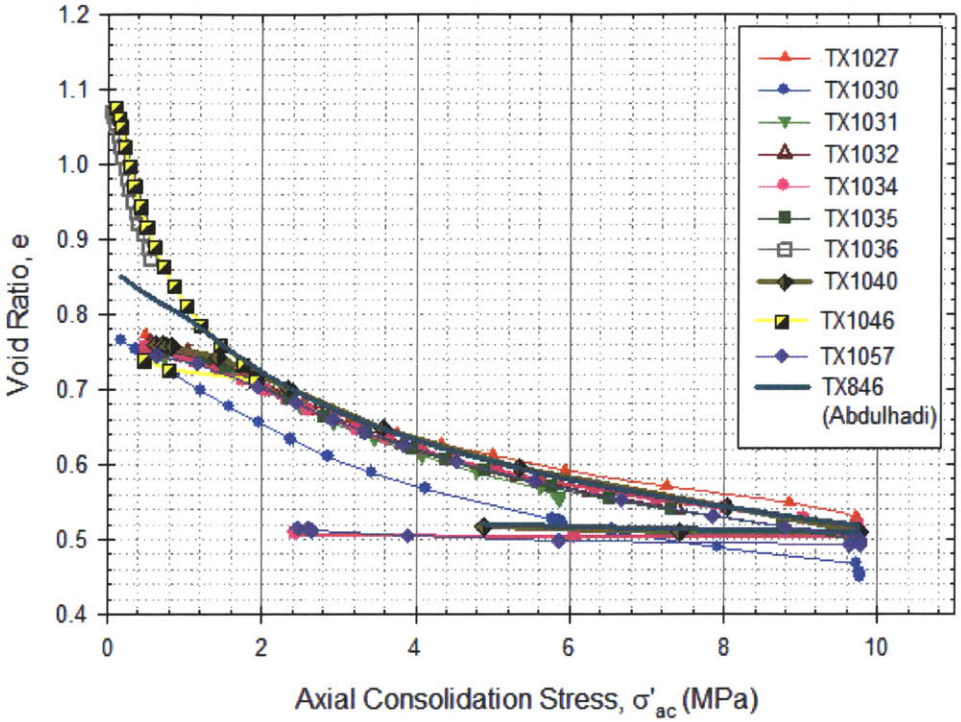

Figure 5-1: One dimensional compression behaviour as measured during the K_O consolidation stage of triaxial tests (in e-σ'_v space)

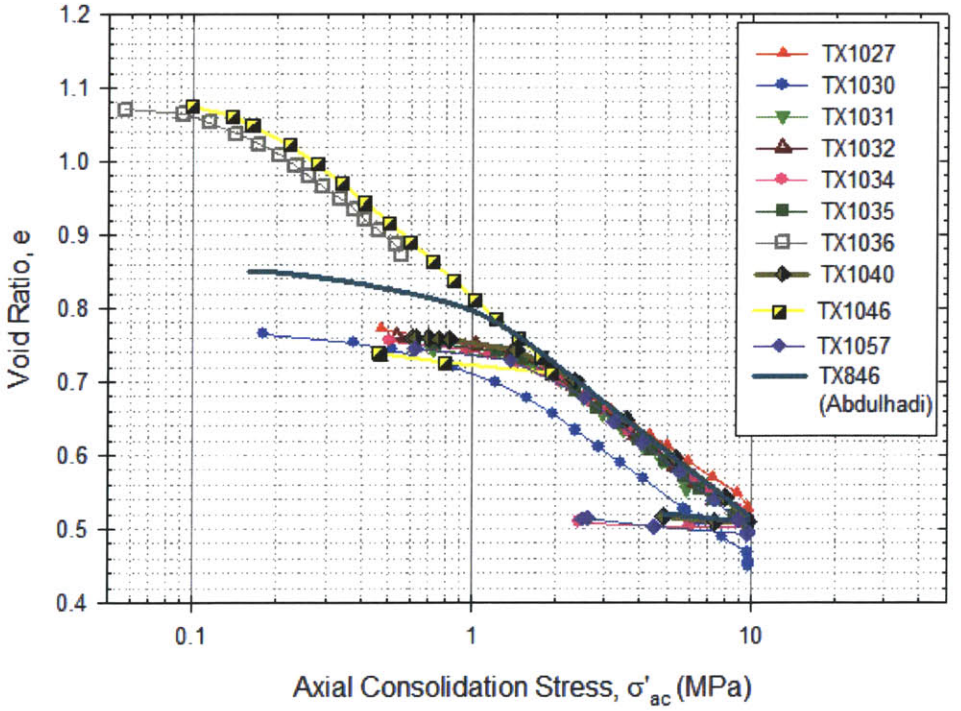

Figure 5-2: One dimensional compression behaviour as measured during the K_O consolidation stage of triaxial tests (in e-logσ'_v space)

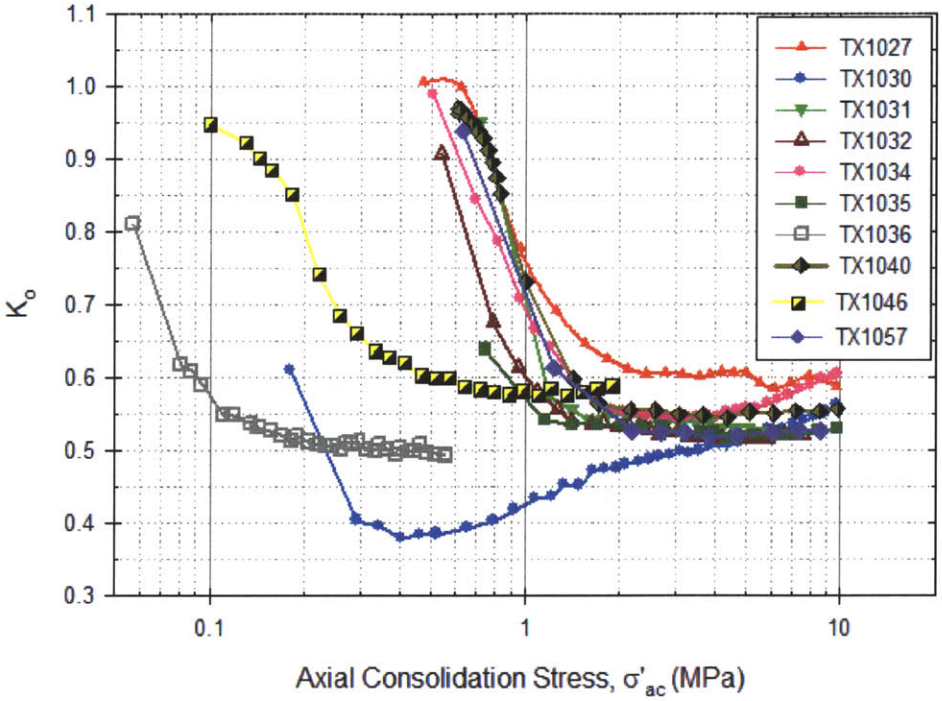

Figure 5-3: The variation in K_O with stress level as measured during the consolidation stage of triaxial tests

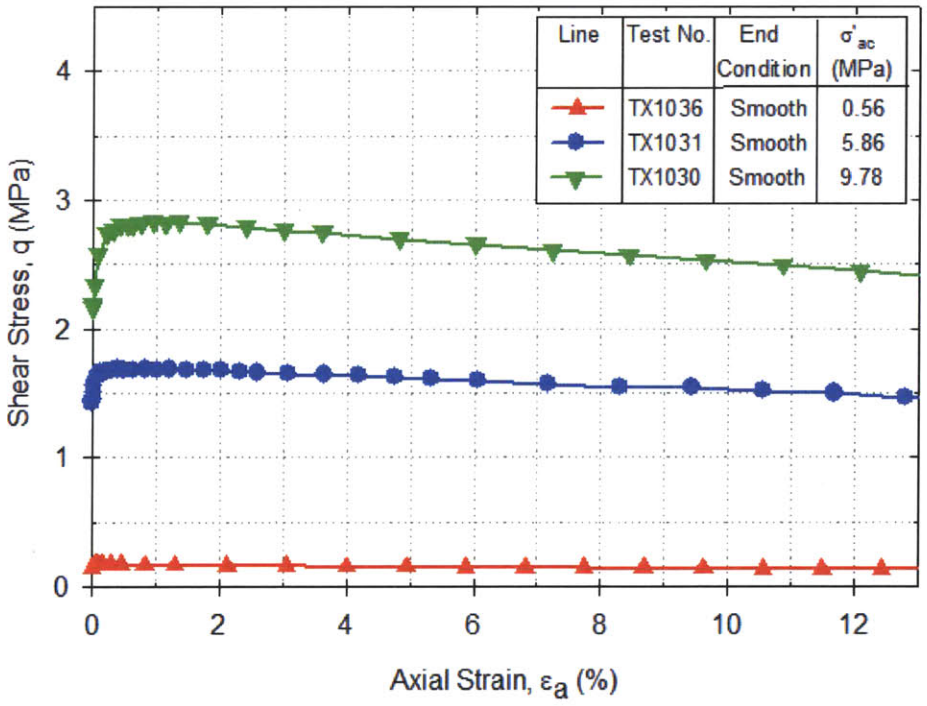

Figure 5-4: Stress-strain responses measured during undrained shearing for tests performed with smooth ends at OCR = 1

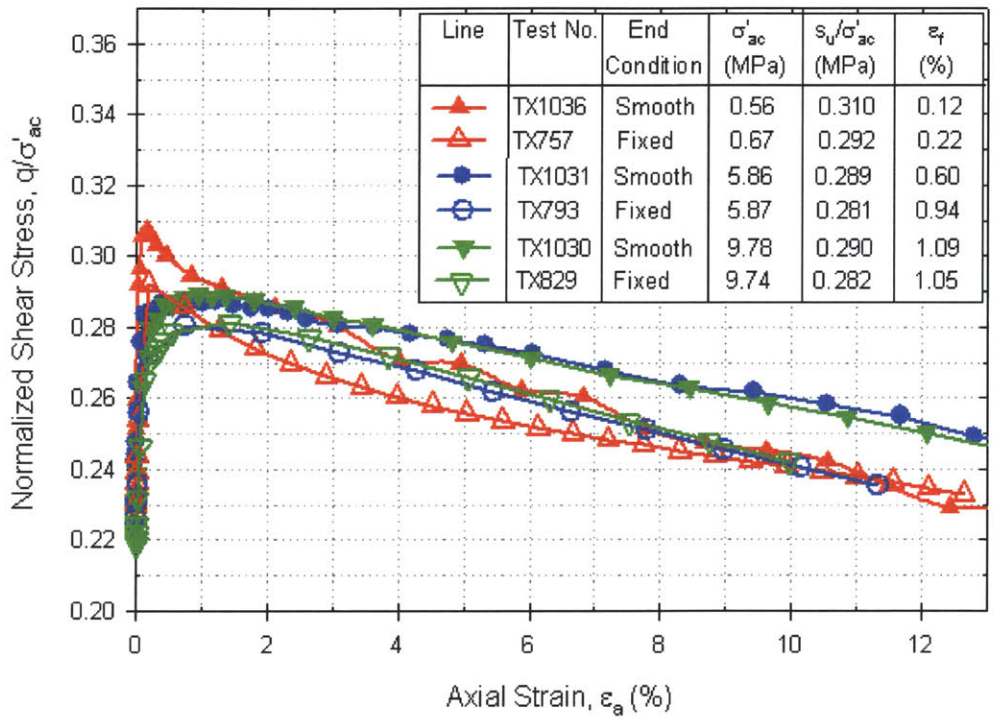

Figure 5-5: Normalized stress-strain responses measured during undrained shearing for tests performed with smooth and fixed ends at OCR = 1

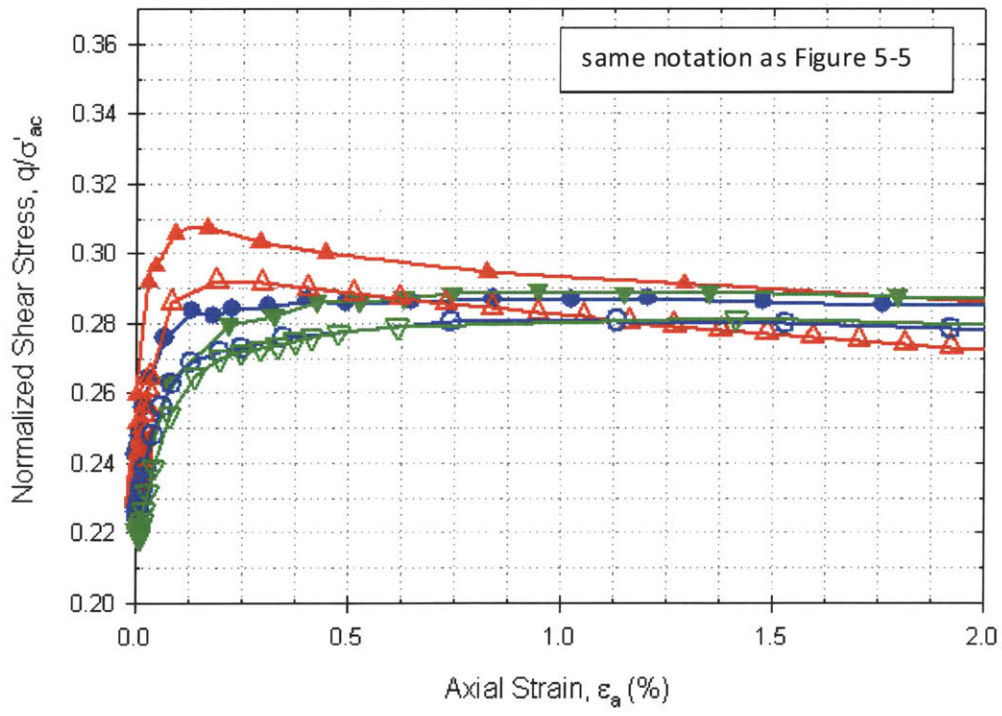

Figure 5-6: Normalized stress-strain responses (at small strains) measured during undrained shearing for tests performed with smooth and fixed ends at OCR = 1

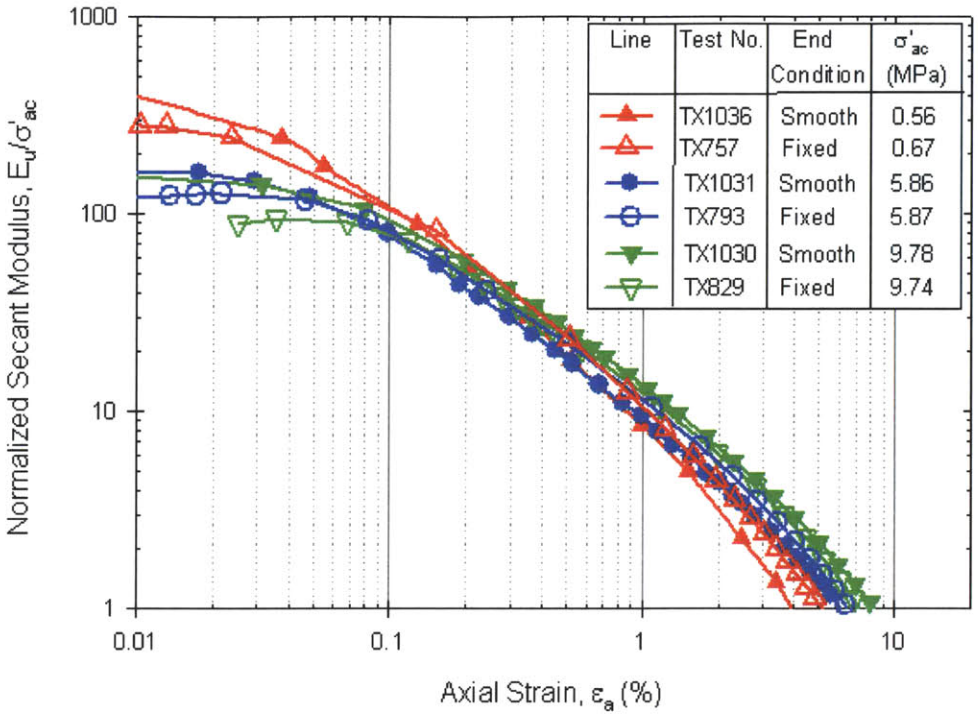

Figure 5-7: The variation in normalized secant Young's modulus with axial strain measured during undrained shearing for tests performed with smooth and fixed ends at OCR = 1

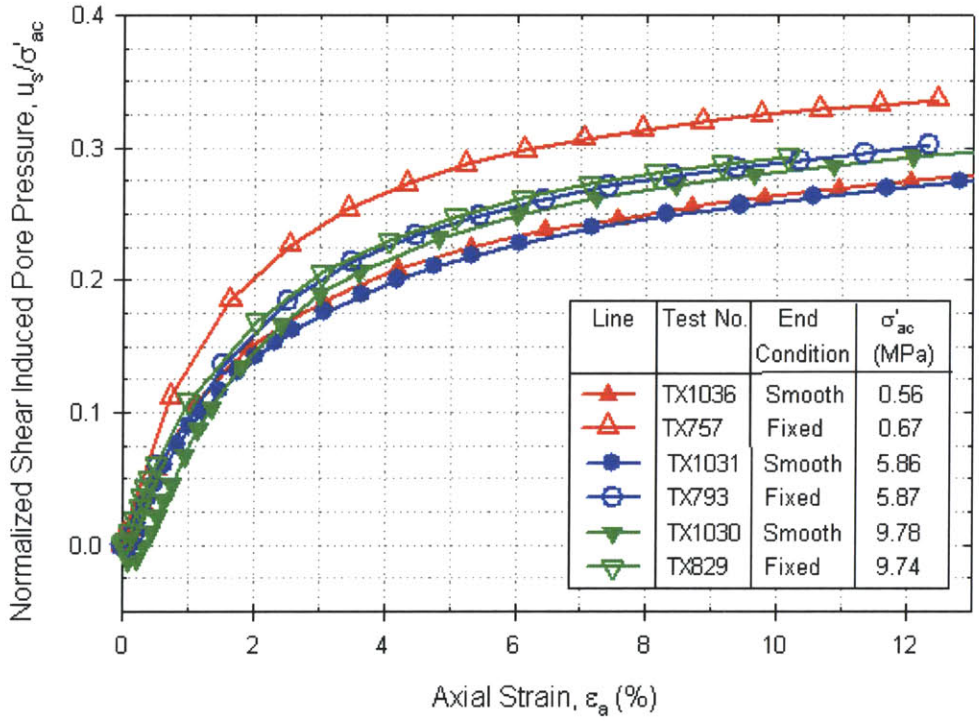

Figure 5-8: Normalized shear induced pore pressures measured during undrained shearing for tests performed with smooth and fixed ends at OCR = 1

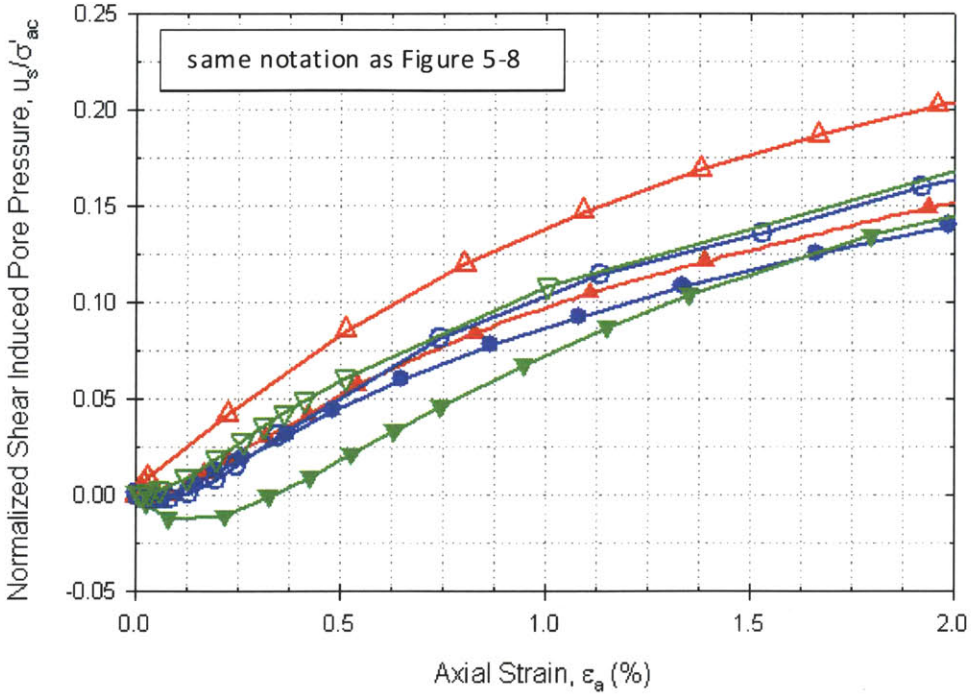

Figure 5-9: Normalized shear induced pore pressures (at small strains) measured during undrained shearing for tests performed with smooth and fixed ends at OCR = 1

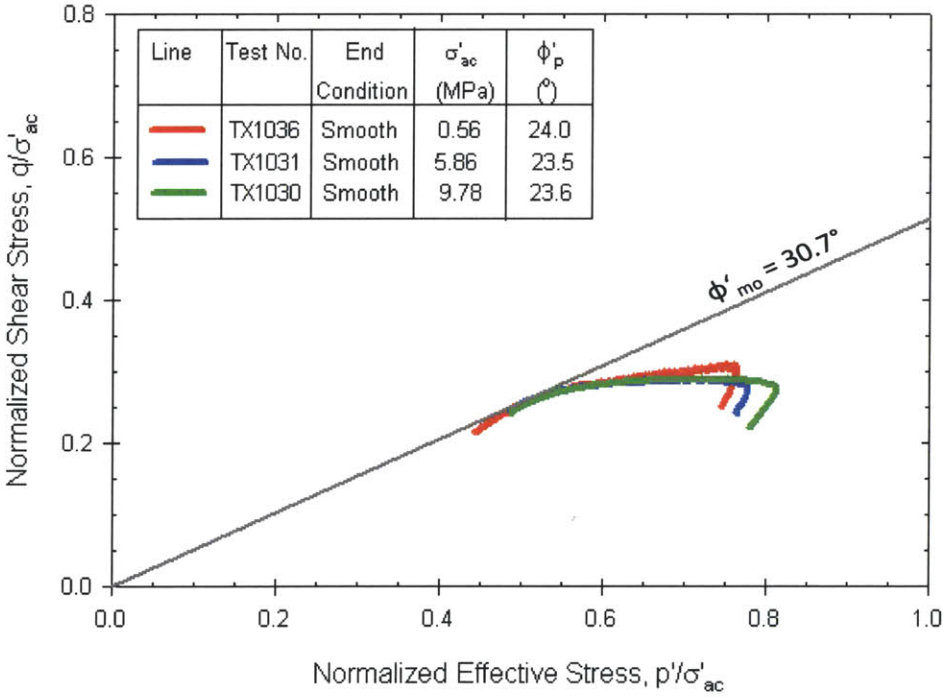

Figure 5-10: Normalized effective stress paths measured during undrained shearing for tests performed with smooth ends at OCR = 1

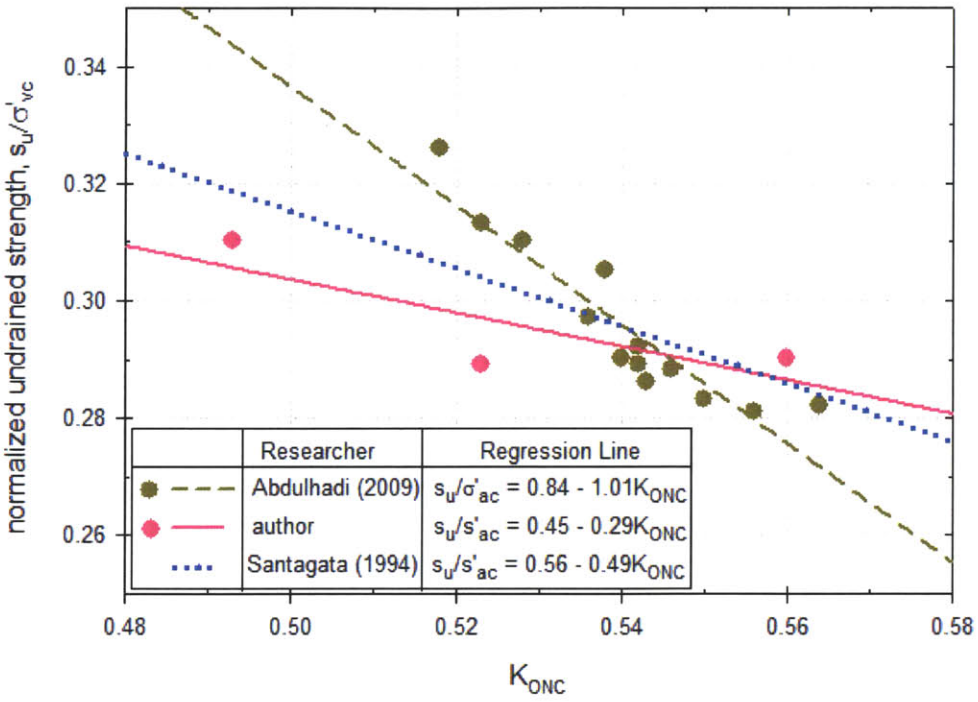

Figure 5-11: Relationship between normalized undrained strength and pre-shear K_O for NC RBBC as found in the experimental programs of the author, Abdulhadi (2009) and Santagata (1994)

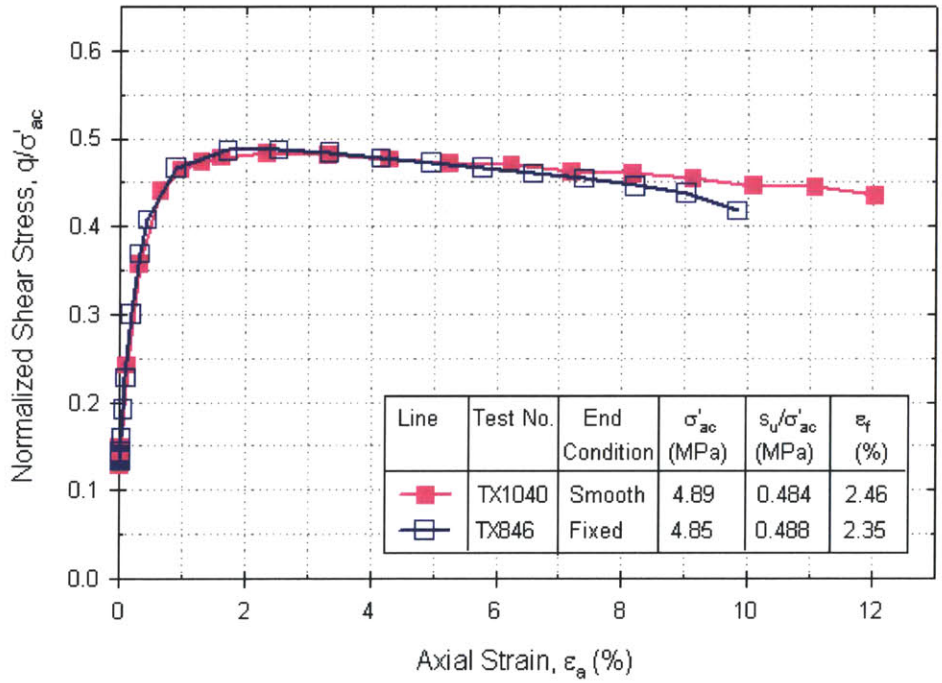

Figure 5-12: Normalized stress-strain responses measured during undrained shearing for tests performed with smooth and fixed ends at OCR = 2

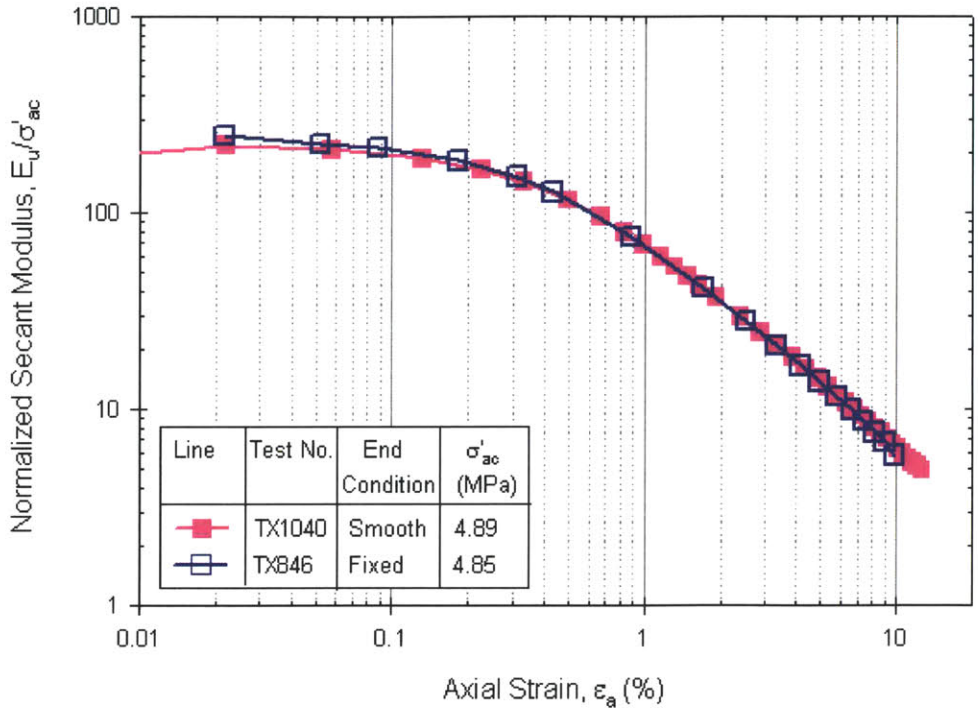

Figure 5-13: The variation in normalized secant Young's modulus with axial strain measured during undrained shearing for tests performed with smooth and fixed ends at OCR = 2

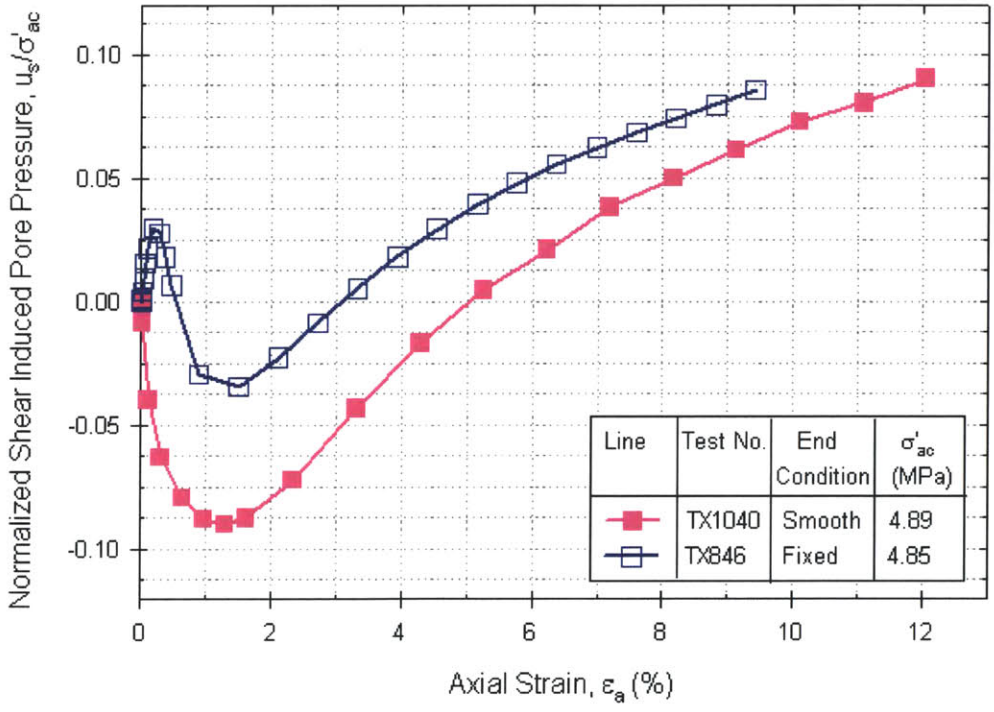

Figure 5-14: Normalized shear induced pore pressures measured during undrained shearing for tests performed with smooth and fixed ends at OCR = 2

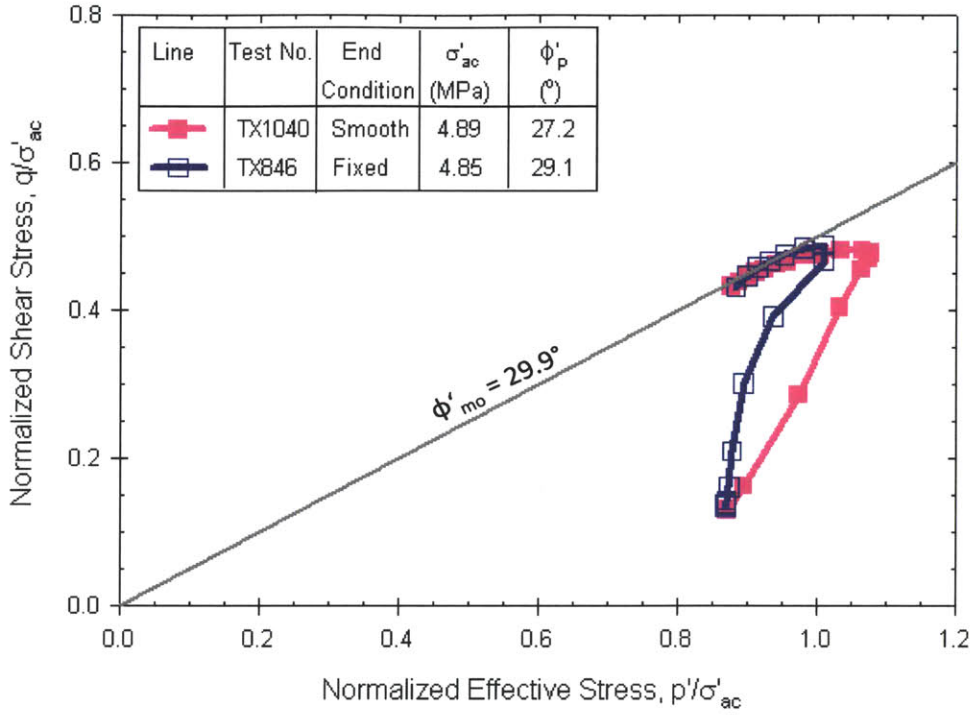

Figure 5-15: Normalized effective stress paths measured during undrained shearing for tests performed with smooth and fixed ends at OCR = 2

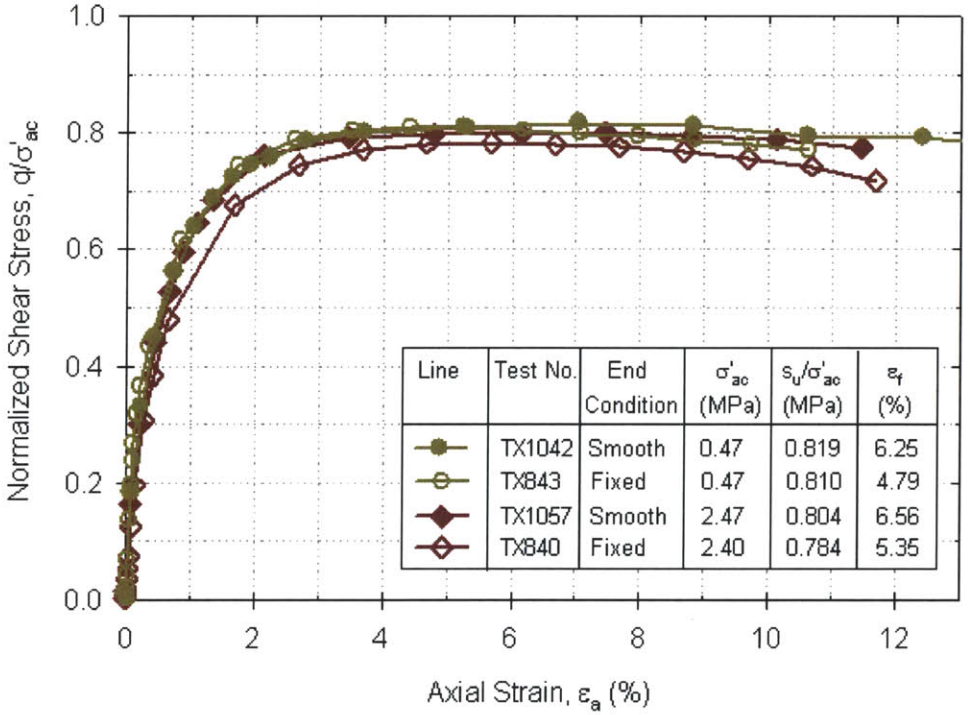

Figure 5-16: Normalized stress-strain responses measured during undrained shearing for tests performed with smooth and fixed ends at OCR = 4

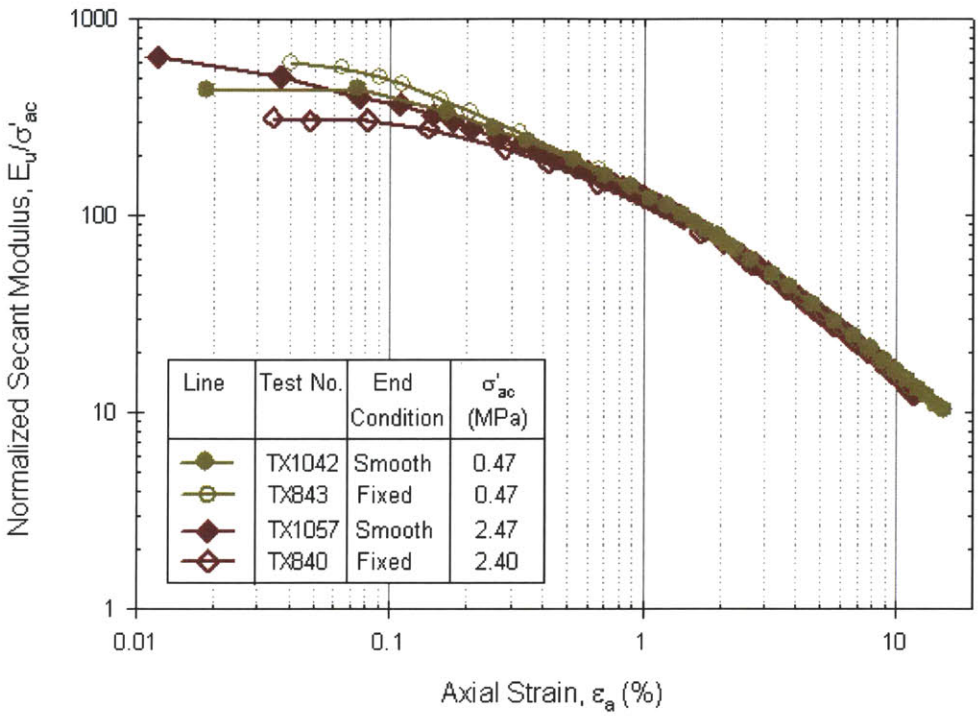

Figure 5-17: The variation in normalized secant Young's modulus with axial strain measured during undrained shearing for tests performed with smooth and fixed ends at OCR = 4

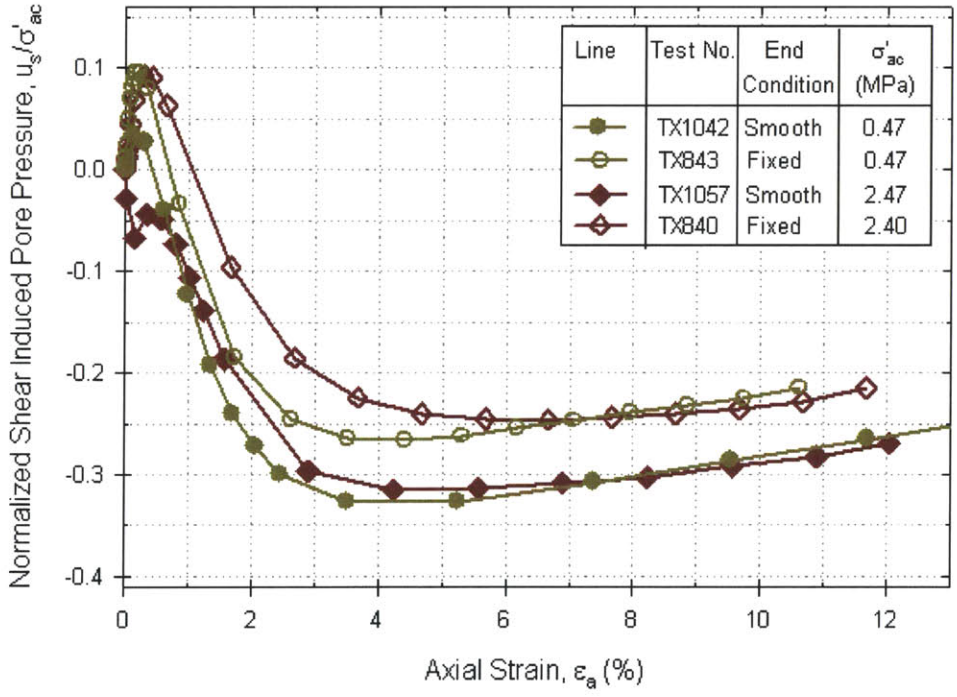

Figure 5-18: Normalized shear induced pore pressures measured during undrained shearing for tests performed with smooth and fixed ends at OCR = 4

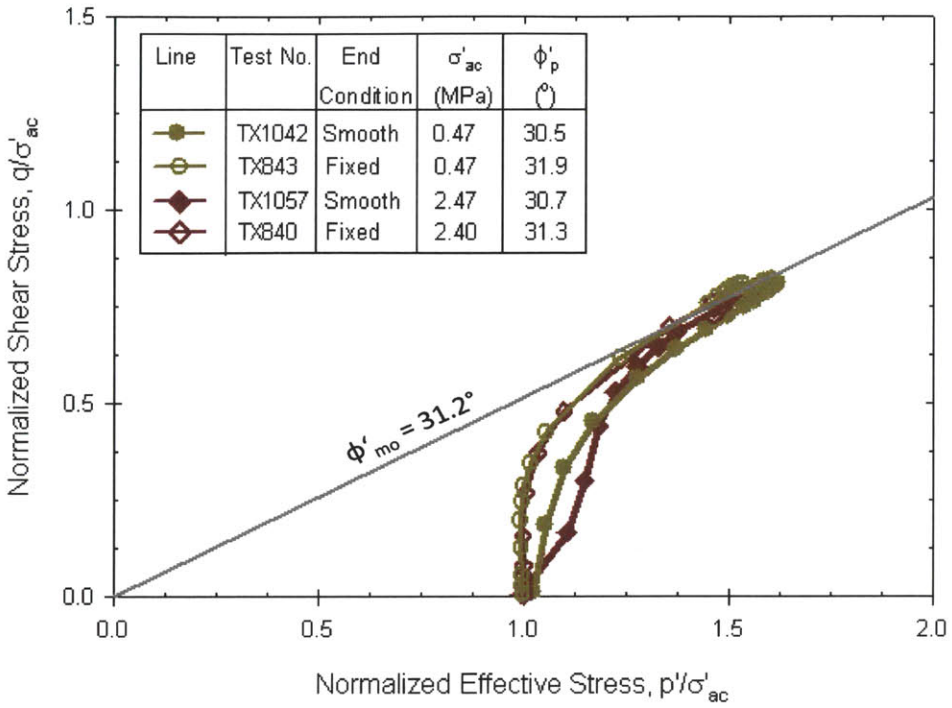

Figure 5-19: Normalized effective stress paths measured during undrained shearing for tests performed with smooth and fixed ends at OCR = 4

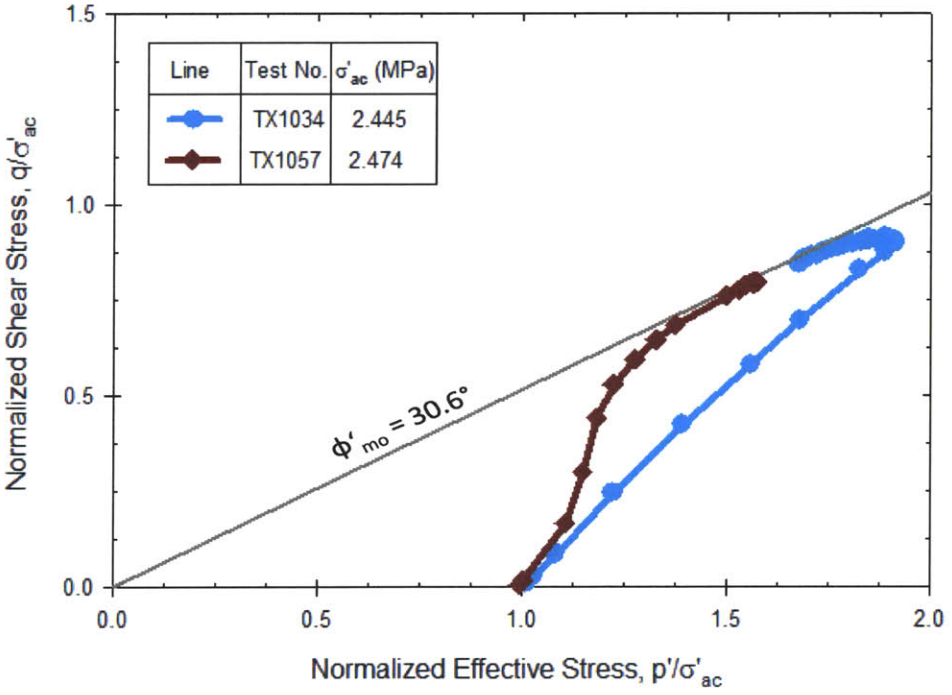

Figure 5-20: Comparison of normalized effective stress paths measured during undrained shearing for tests TX1034 and TX1057 at OCR = 4

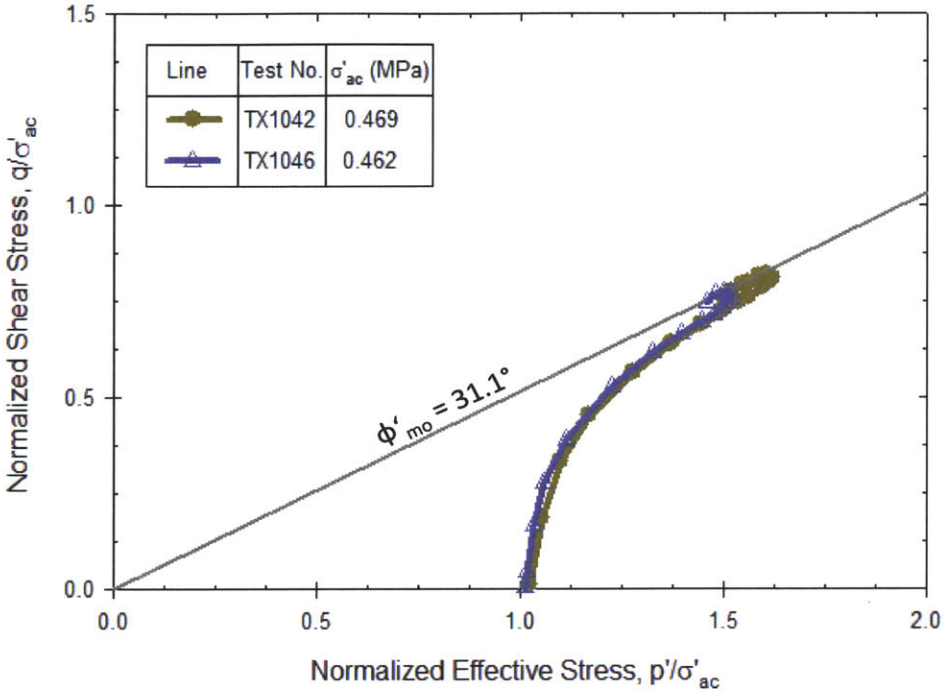

Figure 5-21: Comparison of normalized effective stress paths measured during undrained shearing for tests TX1042 and TX1046 at OCR = 4

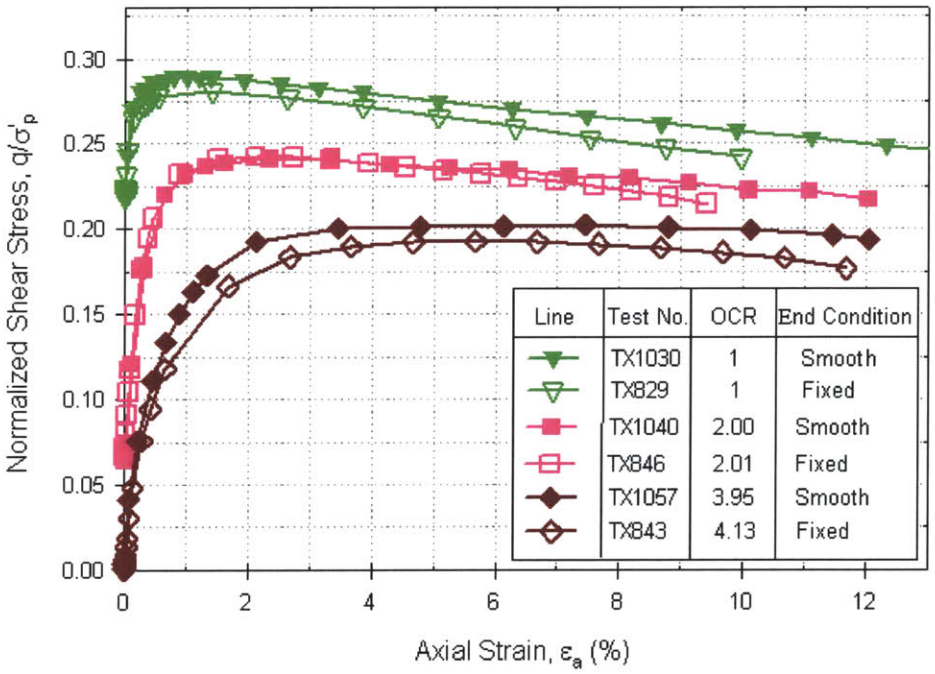

Figure 5-22: Normalized stress-strain responses measured during undrained shearing for tests performed with smooth and fixed ends at OCRs 1, 2 and 4

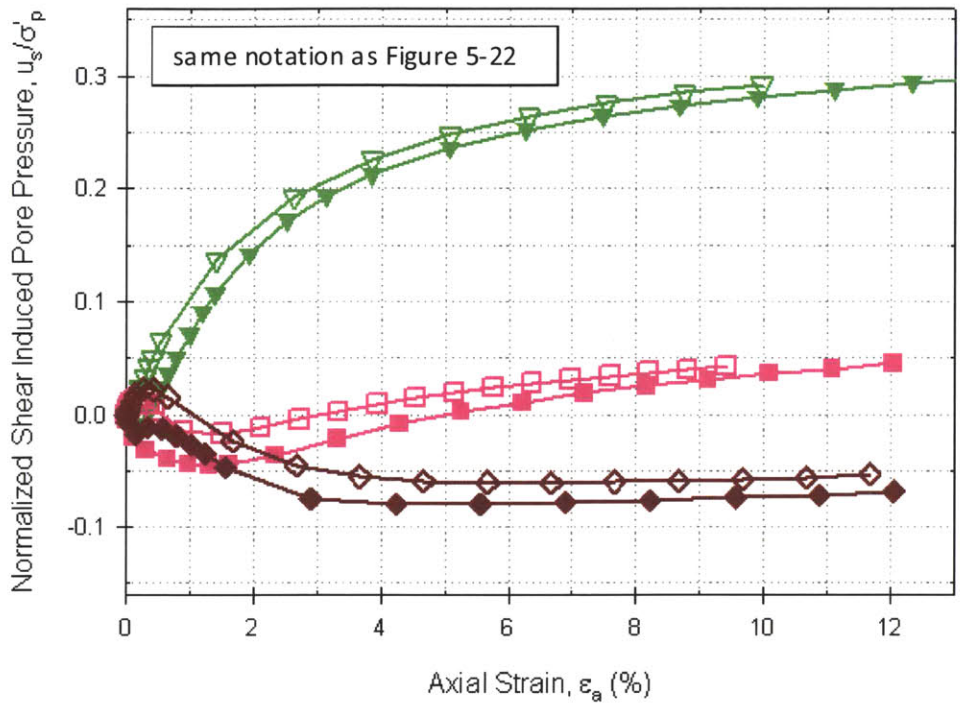

Figure 5-23: Normalized shear induced pore pressures measured during undrained shearing for tests performed with smooth and fixed ends at OCRs 1, 2 and 4

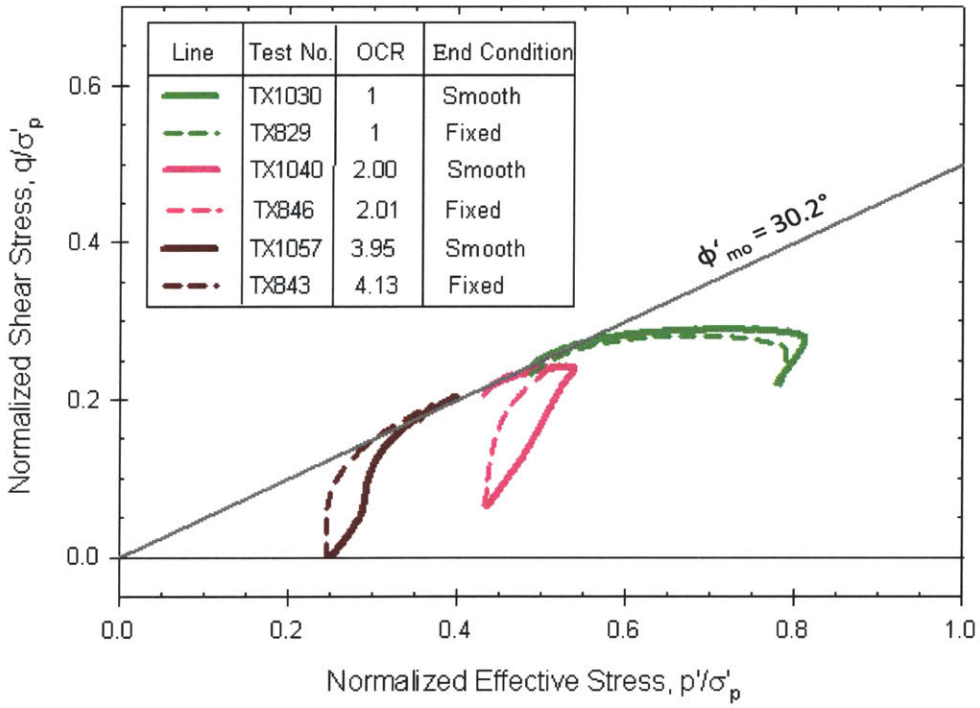

Figure 5-24: Normalized effective stress paths measured during undrained shearing for tests performed with smooth and fixed ends at OCRs 1,2 and 4

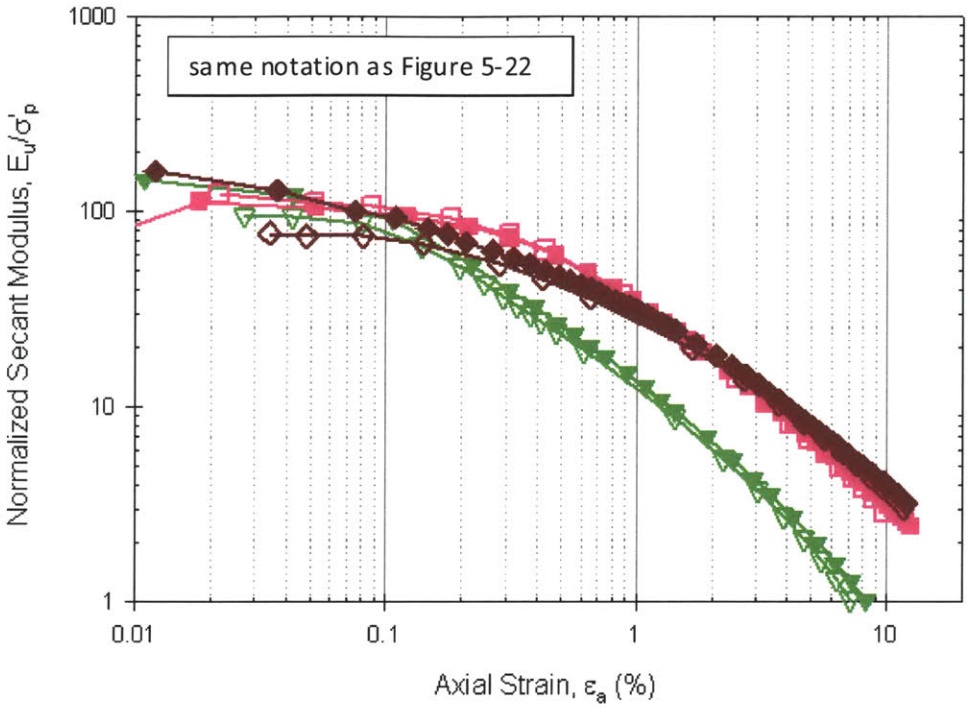

Figure 5-25: The variation in normalized secant Young's modulus with axial strain measured during undrained shearing for tests performed with smooth and fixed ends at OCRs 1, 2 and 4

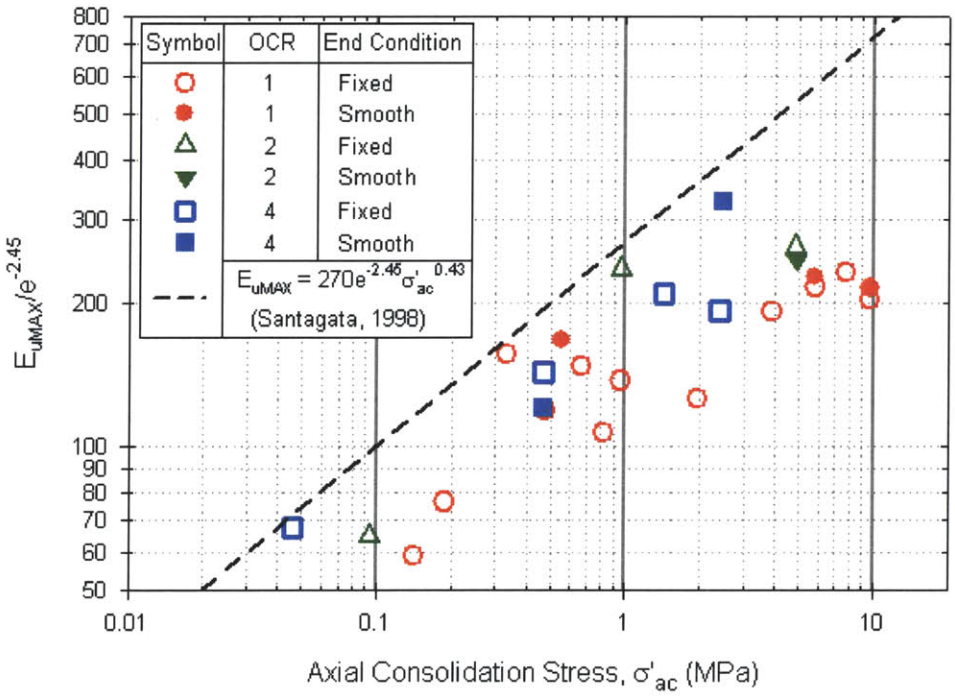

Figure 5-26: Initial undrained secant Young's modulus normalized with respect to void ratio versus stress level

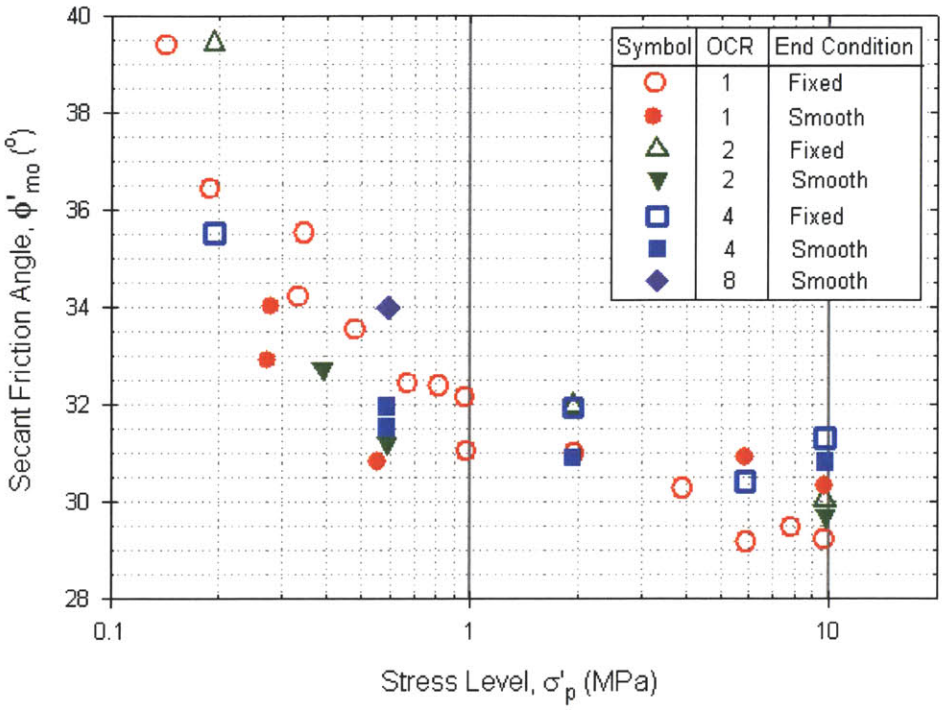

Figure 5-27: The variation in secant friction angle with stress level as obtained from tests performed with smooth and fixed ends at OCRs 1, 2 and 4

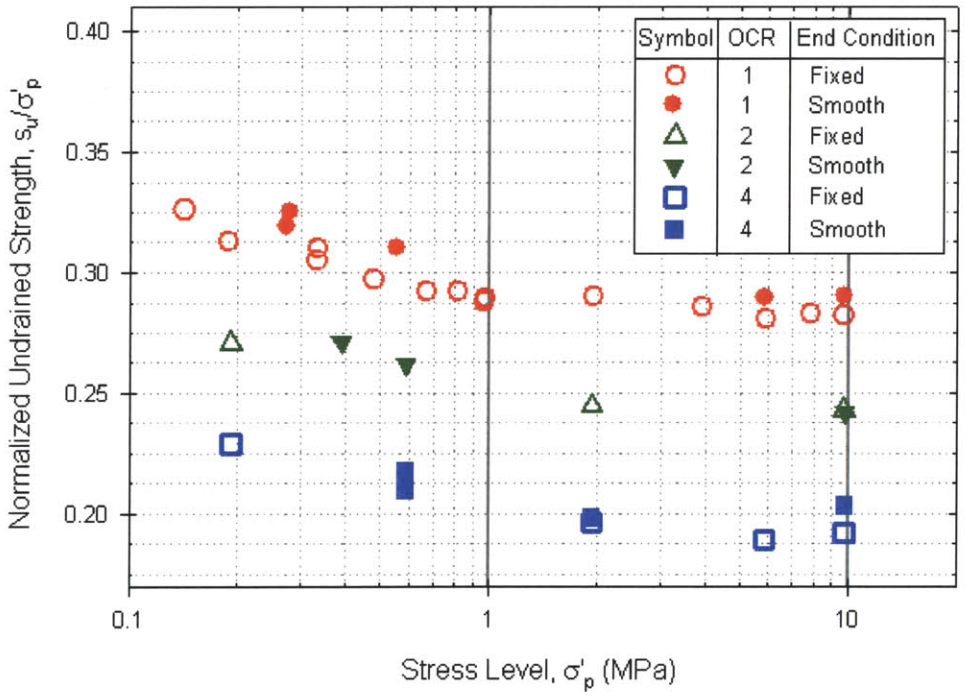

Figure 5-28: The variation in normalized undrained strength with stress level as obtained from tests performed with smooth and fixed ends at OCRs 1, 2 and 4

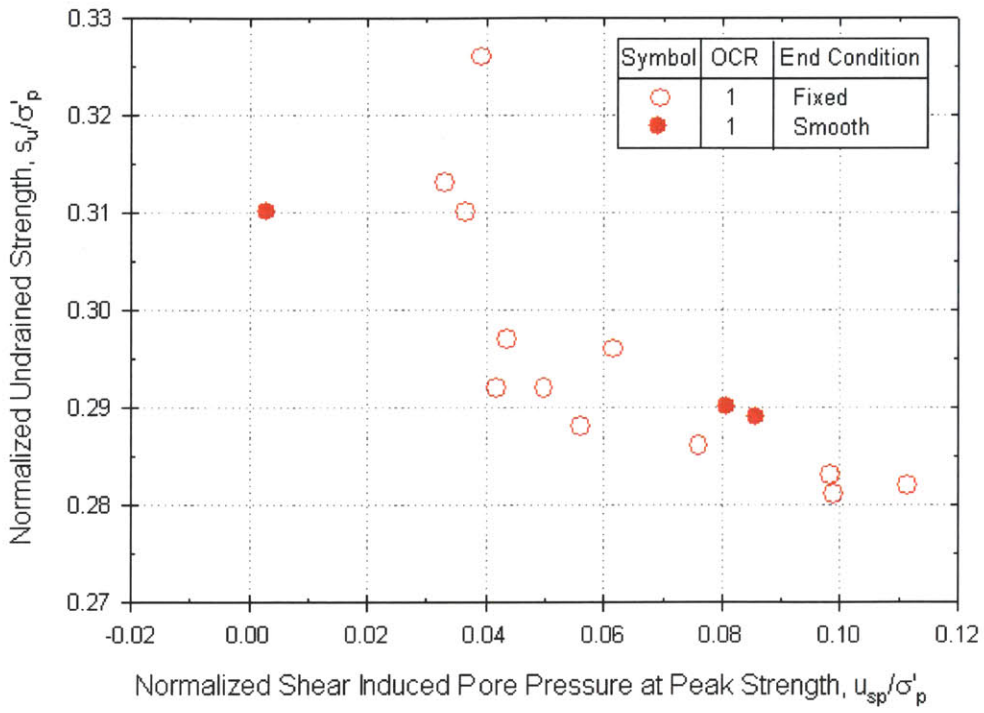

Figure 5-29: Normalized peak undrained strength versus normalized shear induced pore pressures at peak strength for OCR = 1

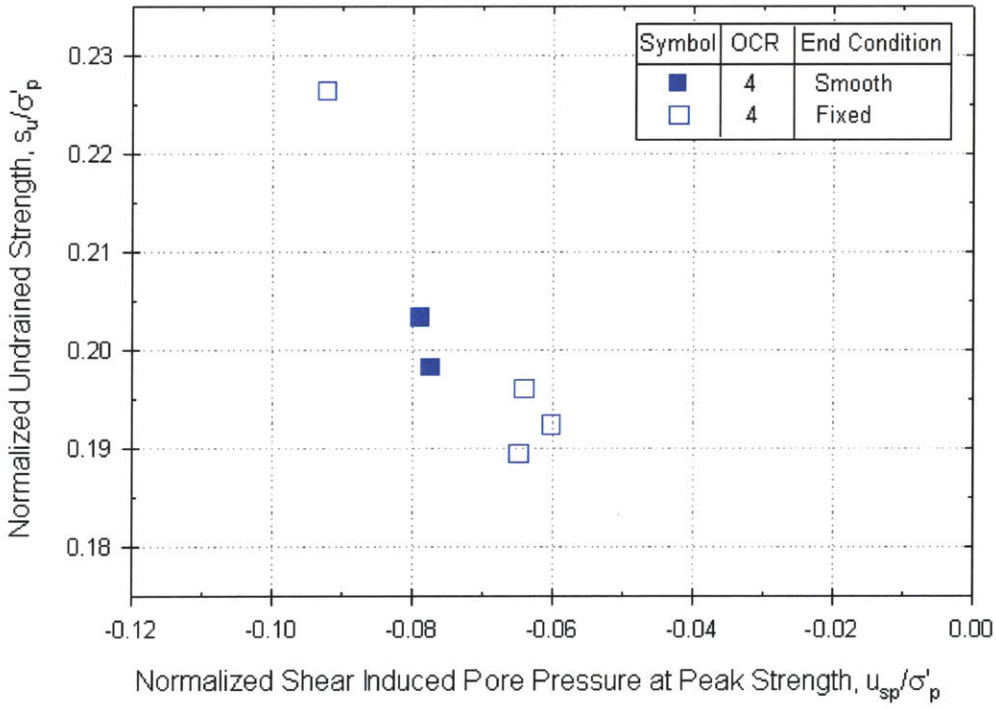

Figure 5-30: Normalized peak undrained strength versus normalized shear induced pore pressures at peak strength for OCR = 4

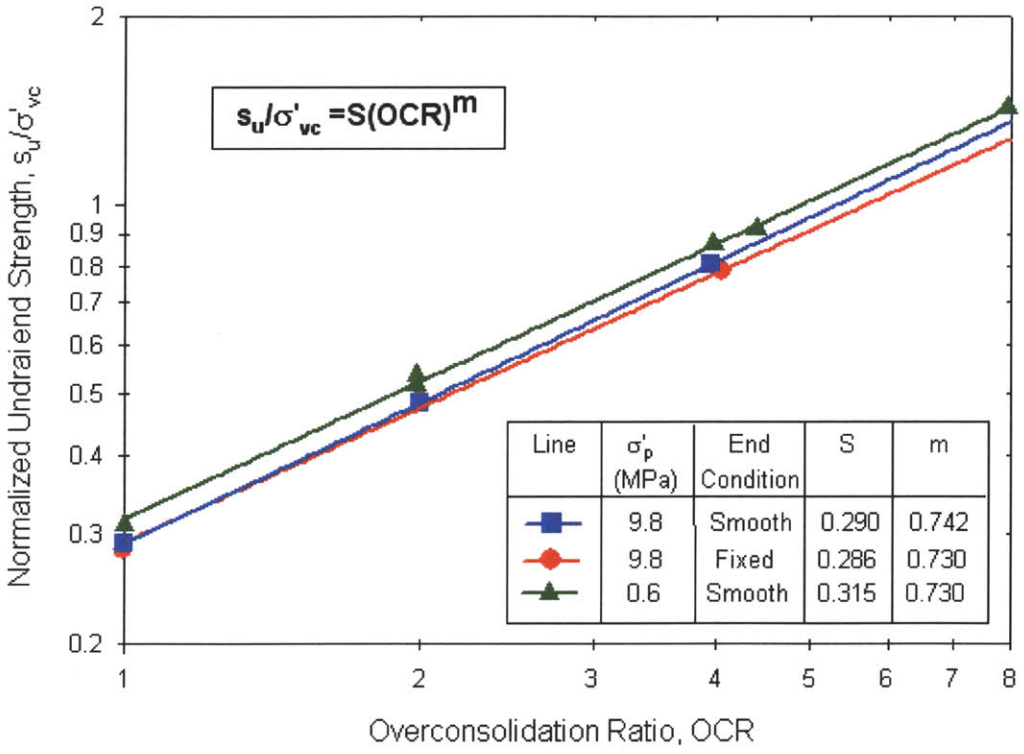

Figure 5-31: The influence of stress level and specimen end condition on the SHANSEP parameters

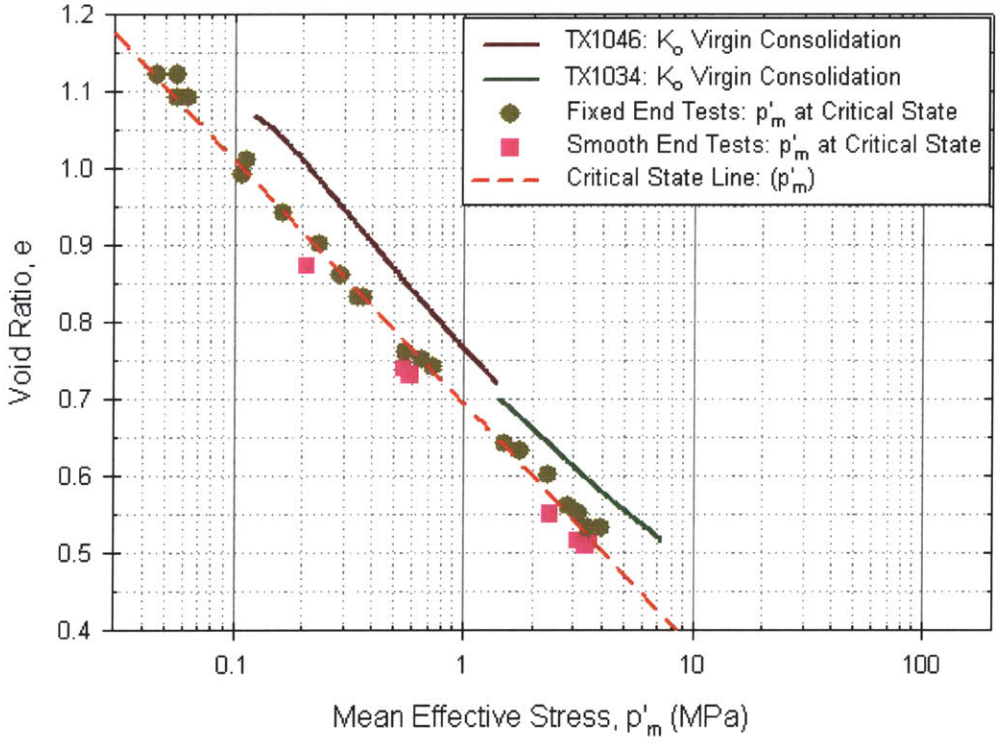

Figure 5-32: Effective stresses at critical state for RBBC as obtained from tests with smooth and fixed ends compared to the K_O virgin consolidation line

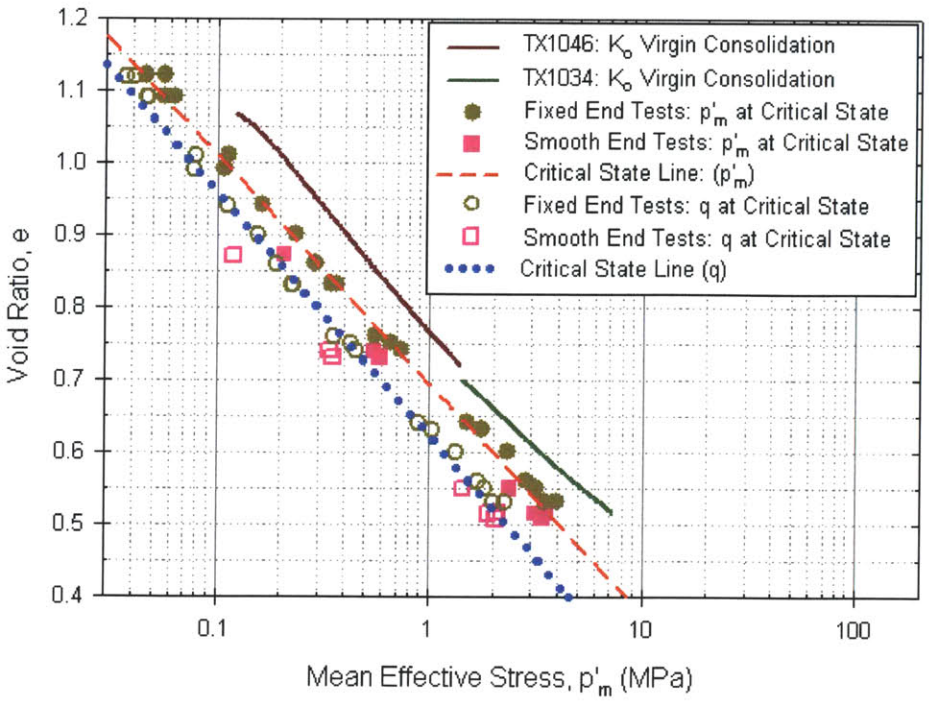

Figure 5-33: Effective stresses and shear stresses at critical state for RBBC as obtained from tests with smooth and fixed ends compared to the K_O virgin consolidation line

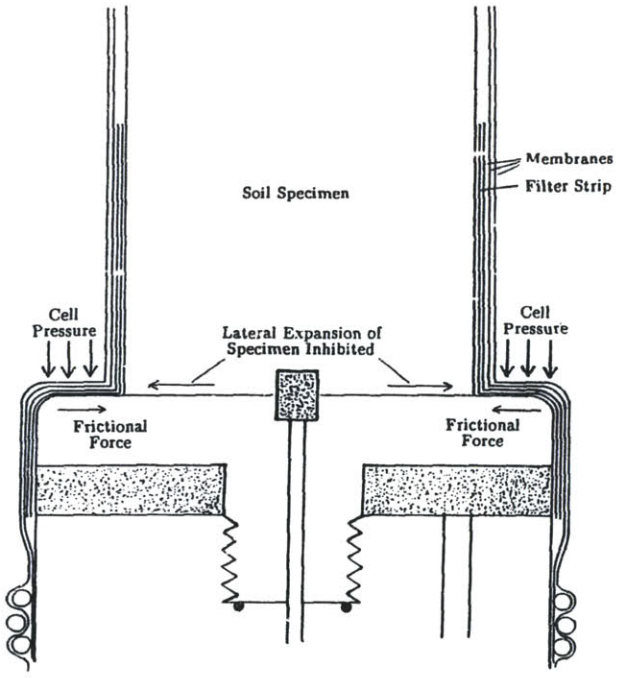

Figure 5-34: Possible cause for insufficient radial spreading of the ends of specimens when using smooth ends (Sheahan, 1991)

6 CONCLUSIONS AND RECOMMENDATIONS

6.1 INTRODUCTION

This chapter presents a summary of the main results and conclusions which can be drawn from the research along with recommendations for future work. One of the goals of the research has been to gain an improved understanding of the mechanical behaviour of cohesive soil at high consolidation stresses, particularly as a function of stress history and stress level. This has been done by examining work carried out by previous researchers in this area and by analyzing the results of a series of triaxial compression tests carried out by the author. The second and primary goal of the research has been to investigate the significance of specimen end restraint in the triaxial testing of cohesive soil at high stresses. This has been achieved by comparing the results of the author's triaxial tests performed using smooth end platens with corresponding results obtained using conventional fixed ends. This comparison has allowed the relative importance of the issue of specimen end restraint to be established.

The triaxial tests carried out in the course of the research were performed on Resedimented Boston Blue Clay. RBBC is a soil resedimented in the laboratory from natural Boston Blue Clay, a low plasticity illitic clay. The resedimentation process allows reproducible behaviour to be achieved in laboratory testing of the soil. In addition, because the soil has been tested at MIT for the past 50 years, a large database exists on its properties against which new test results have been compared and contrasted.

Section 6.2 summarizes the results obtained from the consolidation phase of triaxial tests. In Section 6.3 the main results and conclusions drawn from the undrained shear portion of tests are presented. Finally, in Section 6.4 recommendations are made for further research.

6.2 CONSOLIDATION BEHAVIOUR

The compression behaviour measured during the K_O consolidation phase of triaxial tests compares very well with that reported by Abdulhadi (2009). This is encouraging given that very different specimen drainage conditions were adopted in each experimental program, as the author's tests involved only radial drainage through filter paper strips while Abdulhadi used standard end drainage through porous stones. It can be concluded that the axial strain rate of 0.15 %/hr used during virgin consolidation is sufficiently slow to prevent the development of non-negligible excess

pore pressures within a specimen. When specimens need to be swelled into the OC range, a rate of 0.10 %/hr is sufficiently slow when standard end drainage is used, though a rate 0.05 %/hr is necessary for radial drainage.

It was found that the yield stresses of the compression curves are considerably lower than the preconsolidation pressures supposedly applied during the resedimentation process. The yield points are also quite poorly defined. This is believed to be caused by friction acting between the soil sample and the sides of the consolidometer during resedimentation. However, following the SHANSEP reconsolidation technique any impact which this would have on undrained shear behaviour is eliminated following K_O consolidation in the triaxial device to stresses much higher than the batch preconsolidation pressure.

Values of K_O measured during consolidation in the triaxial device show relatively poor repeatability between tests. However, the overall trend for the change in K_O during consolidation is the same as that reported by Abdulhadi (2009), though is somewhat different to that found by previous researchers for RBBC.

6.3 UNDRAINED SHEAR BEHAVIOUR

The reduction in normalized undrained shear strength with increasing consolidation stress reported by Abdulhadi (2009) has been confirmed by the author's triaxial tests. For both experimental programs normalized undrained strength is found to decrease by approximately the same degree at each OCR as stress level increases. This is indicated by SHANSEP S and m parameters which decrease, and remain fairly constant, respectively with increasing consolidation stress. This decrease in normalized undrained strength is closely linked to an increase in shear induced pore pressures at the point of peak strength, which cause failure to occur at lower normalized effective stresses as stress level is increased. In addition, for NC RBBC normalized undrained strength is found to be negatively correlated with the pre-shear K_{ONC}, a result which is consistent with the findings of Santagata (1994) and Abdulhadi (2009).

The author's triaxial test results also fit the trend of a decrease in the large strain secant friction angle with increasing consolidation stress as reported by Abdulhadi (2009). This is illustrated in Figure. The figure also shows that the friction angle is unaffected by OCR, a finding which is consistent with the notion that the failure envelope of a resedimented soil is unique and does not depend on the pre-shear degree of mechanical overconsolidation.

In the test program carried out using fixed ends by Abdulhadi an axial strain rate of 0.5 %/hr was used for undrained shearing. For RBBC this rate is sufficiently slow to ensure that the increase in pore pressure generated at the ends of a specimen due to the use of fixed end platens is equilibrated throughout the specimen. As a result, the pore pressure measured at the base of a specimen should be representative of the pore pressure throughout the specimen. According to standard end restraint theory such tests would therefore be regarded as slow. Figure 2-27 by Germaine and Ladd (1988) summarizes conceptually the main differences in the results obtained from slow and fast tests with fixed ends. Since representative pore pressures are measured in slow tests, the interpreted friction angle should correspond to the true friction angle of the soil. The experimental results confirm this prediction. As shown in Figure 5-27, the measured friction angle does not appear to be affected by the use of fixed versus smooth ends.

For slow tests pore pressure equilibration requires pore water to redistribute within the specimen and, since stress-strain characteristics are predominantly controlled by the material in the middle portion of a specimen, the increase in water content in this region can lead to a lower (and incorrect) undrained shear strength being measured. Again the experimental results are consistent with this prediction. With reference to Figure 5-28, it can be seen that in general the undrained strength measured in tests with fixed ends is lower than that measured using smooth ends at a given stress level. For NC clay failure is typically reached at strains less than 1 %, so significant pore water migration is unlikely to be able to occur prior to the undrained strength being attained. The consistently lower undrained strengths measured in tests with fixed ends at OCR = 1 are instead caused by the higher shear induced pore pressures generated at peak strength in these tests. Since φ'_p is unaffected by stress level or specimen end condition at OCR = 1, these higher pore pressures result in both lower effective stresses and shear stresses at failure. End restraint theory would predict that the error in the measured undrained strength associated with the use of fixed ends should become more pronounced with increasing overconsolidation. However this trend is not demonstrated in Figure 5-28. It is believed that this is due to the fact that the highest OCR reached in the tests of 4 could still be regarded as relatively low, and that a more dramatic error in undrained strength may in fact occur at higher OCRs.

With reference to Figure 2-27 by Germaine and Ladd (1988), the figure shows that for slow tests with fixed ends the measured effective stress path follows the true effective stress path of the soil. However, the comparison between the slow tests of Abdulhadi with fixed ends against those of the author with smooth ends shows that this in fact is not the case. Assuming that a test performed with smooth ends predicts more closely the true effective stress path of the soil, Figure 5-24 shows that even for slow tests the stress path measured in a fixed end test may not be representative of the true stress path. The reason for this is that in slow tests the higher pore pressures generated at the

ends when fixed ends are used equilibrate throughout the specimen. Therefore, while the measured pore pressures are representative of those throughout the specimen, they are still higher than those which would exist in a specimen without end restraint. Figure 5-23 illustrates this. These misleadingly high pore pressures in turn push the measured effective stress path to the left, this being particularly pronounced for OC soil as the pore pressures generated by end restraint become greater. Accounting for this observation, Figure 6-1 shows more realistically the effect of specimen end restraint on the form of the effective stress path than Figure 2-27 by Germaine and Ladd (1988) for the case of slow tests. Note that Figure 6-1 is conceptual and not based on data from any specific tests. It should also be kept in mind that at large strains the stress path measured in a slow test with fixed ends will converge with the true stress path, thereby still allowing for a correct interpretation of the failure envelope.

At large strains effective stresses and shear stresses measured in tests with smooth ends are lower than those measured in tests with fixed ends at the same void ratio. This may be due to a more uniform stress state being achieved in specimens sheared using smooth ends, thereby allowing for a more accurate interpretation of the critical state.

It does have to be pointed out that the smooth end platens adopted in the author's research were not entirely successful in allowing a triaxial specimen to deform in a completely uniform fashion, i.e. as a right cylinder. This is indicated by area uniformity ratios which generally lie between those corresponding to parabolic and right cylinder deformation. The same finding was reported by Sheahan (1991) who used a very similar end platen design for his tests. A possible explanation for this observation is that cell pressure acting on the membranes and filter strips between the edge of the end platen and the specimen creates a frictional force which may hinder the specimen from expanding at the ends. The development of truly effective smooth ends which allow for ideal right cylinder deformation at high consolidation stresses is likely to be extremely challenging. Despite this, the smooth ends adopted in the research are believed to have resulted in a sufficient reduction in end restraint. In all of the triaxial tests performed, slip surfaces were found not to develop during undrained shear. In contrast, Abdulhadi (2009) has shown that slip surfaces do occur if fixed ends are used. It is concluded that the occurrence of a slip surface in resedimented clay is only a function of the boundary conditions of the test. Furthermore, it can be concluded that the reduction in both normalized undrained strength and friction angle with increasing stress level is not merely a consequence of increased strain localization due to the use of fixed ends, since the same trends are also observed when smooth end platens are used.

6.4 RECOMMENDATIONS FOR FUTURE RESEARCH

The following are areas in which it is believed future experimental studies would be most beneficial:

- Triaxial testing should be extended to higher stress levels. The use of resedimented soil as an analogue test material allows for a fundamental mechanical behaviour to be established, though there is still a severe lack of reliable experimental data on resedimented soil for consolidation stresses greater than 10 MPa.
- The issue of specimen end restraint should be investigated at higher OCRs. End restraint theory predicts that end effects become more significant with increasing overconsolidation. The maximum OCR of 4 achieved in the author's experimental program could be regarded as still being relatively low and tests performed at higher OCRs would demonstrate the more pronounced effects of end restraint for highly overconsolidated specimens.
- The vast majority of research investigating high pressure mechanical behaviour of soils, including the research presented in this thesis, has only focused on triaxial compression mode of shear. Laboratory testing programs should be carried out which employ other modes of shear, such as triaxial extension, plane strain compression and extension and direct simple shear, for example. Soil can exhibit highly anisotropic mechanical properties, and such testing programs may enable a better understanding of the evolution of anisotropy as a function of stress level and stress history. This would in turn allow more realistic analyses of field situations to be conducted.
- At high in situ stresses the mechanical behaviour of soils can become more influenced by diagenetic processes such as cementation. Unlike mechanical overconsolidation, such processes cannot be mimicked in laboratory testing of resedimented soil. Despite the problems of high cost and sampling disturbance associated with obtaining deep samples, it would be of great benefit to carry out more high quality testing of these intact materials and to examine the extinct to which their measured behaviour can be predicted by testing of the corresponding resedimented material.
- The effects of in situ salt concentration and temperature on shear behaviour should be given more consideration. Cohesive materials which exist at high in situ pressures are often subjected to salt concentrations and temperatures significantly higher than those typically encountered in shallower deposits. Although it is generally well recognized that salt concentration can play a significant role in the mechanical behaviour of cohesive soils, efforts to quantify this effect as a function of mineralogy are lacking. Even less appears to be known regarding the effects of temperature. The use of resedimented soil may be ideal for carrying out a systematic laboratory investigation to quantify the effects of salt concentration and temperature on shear behaviour.

- The smooth end platens adopted in the research were not entirely effective in allowing a triaxial specimen to deform in a completely uniform fashion. Although achieving ideal right cylinder deformation of a specimen at high consolidation stresses is likely to be extremely difficult, different end platen designs or materials should be tested to determine if they can provide more uniform deformation of a specimen compared to the smooth brass end platens used in the author's research.

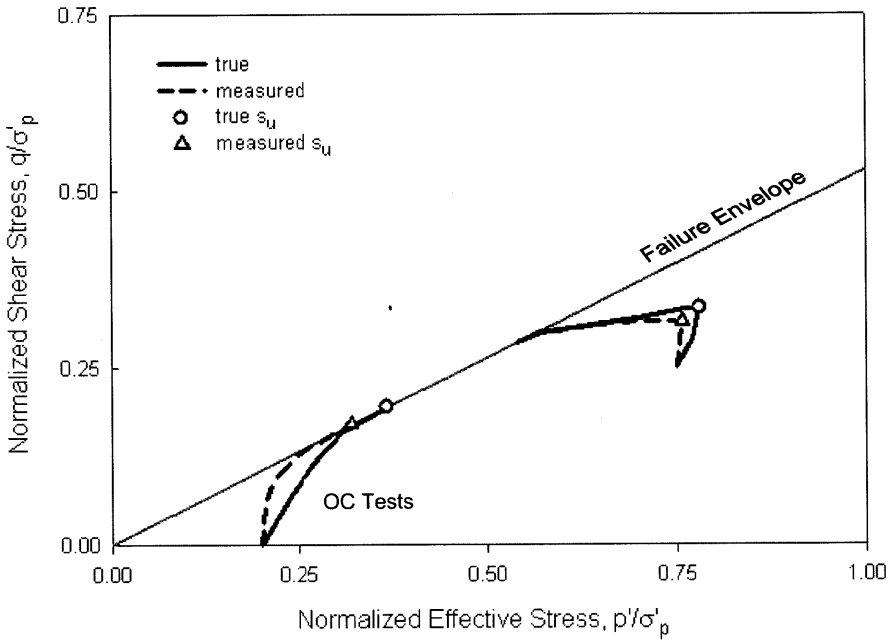

Figure 6-1: Impact of specimen end restraint caused by the use of fixed ends on the form of the effective stress path in slow tests

References

Abdulhadi, N.O. (2009). "An Experimental Investigation into the Stress-Dependent Mechanical Behavior of Cohesive Soil with Application to Wellbore Instability", Ph.D. Thesis, Massachusetts Institute of Technology

Ahmed, I. (1990). "Investigation of Normalized Behaviour of Resedimented Boston Blue Clay using Geonor Direct Simple Shear", S.M. Thesis, Massachusetts Institute of Technology

Amorosi, A. & Rampello, S. (2007). "An Experimental Investigation into the Mechanical Behavior of a Structured Stiff Clay", *Géotechnique* 57 (2), pp. 153-166

Bailey, W.A. (1961). "Effects of Salt on the Shear Strength of Boston Blue Clay", SB Thesis, Massachusetts Institute of Technology

Barden, L. & McDermott, R.J.W. (1965). "Use of Free Ends in Triaxial Testing of Clays", *Journal of Soil Mechanics and Foundations Division, ASCE* 91 (S.M.6), pp. 1 – 23

Becker, D.E., Crooks, J.H.A., Been, K., & Jefferies, M.G. (1987) "Work as a Criterion for Determining In-Situ and Yield Stresses in Clays", *Canadian Geotechnical Journal*, 24 (1), pp. 549 - 564.

Bellwald, P. (1990). "A Contribution to the Design of Tunnels in Argillaceous Rock", Ph.D. Thesis, Massachusetts Institute of Technology

Belviso, R., Federico, A. & Popescu, M. (2001). "K_o-Undrained Shear Strength Ratio of Normally Consolidated Clays from CIUC tests", *Soft Soil Engineering*, Zwets & Zeitlinger, pp. 575-579

Berman, D.R. (1993). "Characterization of the Engineering Properties of Boston Blue Clay at the MIT Campus", S.M. Thesis, Massachusetts Institute of Technology

Berre, T. (1985). "Suggested International Code of Soil Engineering Practice for Triaxial Compression Tests", Report No. 56103-30. Norwegian Geotechnical Institute

Berre, T. (1992). "Geotechnical Properties of Clay-Shales", Report No. 541082-3. Norwegian Geotechnical Institute

Biot, M.A. (1941). "General Theory of Three-Dimensional Consolidation", *Journal of Applied Physics* 12 (2), pp. 155-164

Bishop, A.W. & Eldin, A.K.G. (1950). "Undrained Triaxial Tests on Saturated Sands and Their Significance in the General Theory of Shear Strength", *Géotechnique* 2 (1), pp. 13-32

Bishop, A.W. & Henkel, D.J. (1962). The Measurement of Soil Properties in the Triaxial Test, Edward Arnold Ltd., London

Bishop, A.W., Webb, D.L. & Lewin, P.I. (1965). "Undisturbed Samples of London Clay from the Ashford Common Shaft: Strength-Effective Stress Relationships", *Géotechnique* 15 (1), pp. 1 - 31

Bishop, A.W. (1973). "The Influence of an Undrained Change in Stress on the Pore Pressure in Porous Media of Low Compressibility" (Technical Note), *Géotechnique* 23 (3), pp. 435-442

Bishop, A.W. (1976). "The Influence of System Compressibility on the Observed Pore-Pressure Response to an Undrained Change in Stress in Saturated Rock" (Technical Note), *Géotechnique* 26, (2), pp. 435-442

Bishop, A.W., Kumapley, N.K. & El-Ruwayih, A. (1975). "The Influence of Pore-Water Tension on the Strength of Clay", *Philosophical Transactions of the Royal Society of London*, 278, pp. 511-554

Bishop, A.W. & Skinner, A.E. (1977). "The Influence of High Pore-Water Pressure on the Strength of Cohesionless Soils", *Philosophical Transactions of the Royal Society of London*, 284, pp. 91-130

Bjerrum, L. (1973). "Problems of Soil Mechanics and Construction on Soft Clays", State-of-the-Art Report to Session IV, 8th International Conference on Soil Mechanics and Foundation Engineering, Moscow, 1973

Burland, J.B. (1990). "On the Compressibility and Shear Strength of Natural Soils", *Géotechnique* 40 (3), pp. 329-378

Cauble, D.F. (1993). "The Behavior of Resedimented Boston Blue Clay at OCR4 in Cyclic and Post-Cyclic Undrained Direct Simple Shear", S.M. Thesis, Massachusetts Institute of Technology

Cauble, D.F. (1996). "An Experimental Investigation of the Behavior of a Model Suction Caisson in a Cohesive Soil", Ph.D. Thesis, Massachusetts Institute of Technology

Cotecchia, F. & Chandler, R.J. (2000). "A General Framework for the Mechanical Behaviour of Clays", *Géotechnique* 50 (4), pp. 431 – 447

Da Re, G. (2000). "Constitutive Modeling of Frozen Sand", Ph.D. Thesis, Massachusetts Institute of Technology

de La Beaumelle, A.C.L.A., (1991). "Evaluation of SHANSEP Strength-Deformation Properties of Undisturbed Boston Blue Clay from Automated Triaxial Testing", S.M. Thesis, Massachusetts Institute of Technology

Duncan, J.M. & Dunlop, P. (1968). "The Significance of Cap and Base Restraint", *Journal of Soil Mechanics and Foundations Division, ASCE* 94 (S.M.1), pp. 271 – 290

Estabrook, A.H. (1991). "Comparison of Recompression and SHANSEP Strength-Deformation Properties of Undisturbed Boston Blue Clay from Automated Triaxial Testing", S.M. Thesis, Massachusetts Institute of Technology

Force, E.A. (1998). "Factors Controlling Pore-Pressure Generation during K_o-Consolidation of Laboratory Tests", S.M. Thesis, Massachusetts Institute of Technology

Germaine, J.T. (1982). "Development of the Directional Shear Cell for Measuring Cross-Anisotropic Clay Properties", Sc.D. Thesis, Massachusetts Institute of Technology

Germaine, J.T. & Germaine, A.V. (2009). Geotechnical Laboratory Measurements for Engineers, John Wiley and Sons

Germaine, J.T. & Ladd, C.C. (1988). "Triaxial Testing of Saturated Cohesive Soils: State of the Art Paper", *Advanced Triaxial Testing of Soil and Rock*, ASTM STP 977, pp. 421 – 459

Green, (1956). "Effects of Pore Water Salt Concentration of Homoionic Clays", S.M. Thesis, Massachusetts Institute of Technology

Grennan, J.T. (2010). "Characterization of a Low Plasticity Silt", S.M. Thesis, Massachusetts Institute of Technology

Gutierrez, M., Nygard, R., Hoeg, K. & Berre, T. (2008). "Normalized Undrained Shear Strength of Clay Shales", *Engineering Geology* 99, pp. 31-39

Horseman, S.T., Winter, M.G., & Entwistle, D.C. (1993). "Triaxial Experiments on Boom Clay", *The Engineering Geology of Weak Rock*, Balkema, Rotterdam

Jones, C.A. (2010). "Engineering Properties of Resedimented Ugnu Clay from the Alaskan North Slope", S.M. Thesis, Massachusetts Institute of Technology

Kavvadas, M. (1982). "Non-linear Consolidation around Driven Piles in Clays", Sc.D. Thesis, Massachusetts Institute of Technology

Kenney, T.C. (1964). "Sea-Level Movements and the Geologic Histories of the Postglacial Marine Soils at Boston, Nicolet, Ottawa and Oslo", *Géotechnique* 14 (3), pp. 203-230

Koutsoftas, D.C. & Ladd, C.C. (1985). "Design Strengths for an Offshore Clay", ASCE, *Journal of Geotechnical Engineering Division* 111(3), pp. 337-355

Ladd, C.C. (1985). "Overview of Clay Behaviour", MIT Special Summer Course 1.605

Ladd, C.C. (1991). "Stability Evaluation during Staged Construction", 22nd Karl Terzahgi Lecture, *Journal of Geotechnical Engineering* 117 (4), pp. 540-615

Ladd, C.C. & Varallyay, J. (1965). "The Influence of Stress System on the Behavior of Saturated Clays during Undrained Shear", Research Report R65-11, Soil Publication No. 177, Department of Civil Engineering, Massachusetts Institute of Technology

Ladd, C.C. & Foott, R. (1974). "New Design Procedure for Stability of Soft Clay", *Journal of the Geotechnical Engineering Division*, ASCE, 100 (7), pp. 763-786

Ladd, C.C., Young, G.A., Kraemer, S.R. & Burke D.M. (1999). "Engineering properties of Boston Blue Clay from special testing program", Special Geotechnical Testing: Central Artery/Tunnel Project in Boston, Massachusetts. ASCE GSP 91, pp. 1-24

Lade, P.V. & de Boer, R. (1997). "The Concept of Effective Stress for Soil, Concrete and Rock", *Géotechnique* 47 (1), pp. 61-78

Lambe, T.W. & Whitman R.V. (1969). Soil Mechanics, John Wiley and Sons

Marsden, J.R., Holt, R.M., Nakken, S.J. & Raaen, A.M. (1992). "Mechanical and Petrophysical Characterization of Highly Stress Mudstones", *Proceedings of Eurock 92 Conference*, Balkema, Rotterdam, pp. 51-56

Mesri, G. & Castro, A. (1987). "C_α/C_c Concept and K_0 during Secondary Compression", *Journal of the Geotechnical Engineering Division*, ASCE, 113 (3), pp. 230-247

Moniz, S.R. (2009). "The Influence of Effective Consolidation Stress on the Normalized Extension Strength Properties of Resedimented Boston Blue Clay", M.Eng Thesis, Massachusetts Institute of Technology

Olsen, R.E. & Campbell L.M. (1964). Discussion of "Importance of Free Ends in Triaxial Testing" by P.W. Rowe and L. Barden, *Journal of Soil Mechanics and Foundations Division, ASCE* 90 (S.M.6), pp. 167 – 173

O'Neill, D. (1985). "Undrained Strength Anisotropy of an Overconsolidated Thixotropic Clay", S.M. Thesis, Massachusetts Institute of Technology

Paterson, M.S. & Wong, T.F. (2005). Experimental Rock Deformation – The Brittle Field, Springer-Verlag, Berlin Heidelberg

Pestana, J.M. (1994). "A Unified Constitutive Model for Clays and Sands", Sc.D. Thesis, Massachusetts Institute of Technology

Petley, D.N. (1999). "Failure Envelopes of Mudrocks at High Confining Pressures", Geological Society of London, Special Publications, 158, pp. 61-71

Petley, D.N., Jones, M.E., Stafford, C., Leddra, M.J. & Kageson-Loe, N.L. (1993). "Deformation and fabric changes in weak fine-grained rocks during high pressure consolidation and shear", *Geotechnical Engineering of Hard Soils-Soft Rocks*, Balkema, Rotterdam, pp. 737-743

Poulus, H.G. & Davis, E.H. (1974). Elastic Solutions for Soil and Rock Mechanics, John Wiley and Sons

Raju, J.S., Sadaswan, S.K. and Venkataraman, M. (1972). "Soil and Foundations", Japanese Society of Soil Mechanics and Foundation Engineering 12 (4), pp. 25 - 43

Richardson, A.M. & Whitman, R.V. (1963). "Effect of Strain-Rate Upon Undrained Shear Resistance of a Saturated Remolded Fat Clay", *Géotechnique* 13 (3), pp. 310 – 324

Roscoe, K.H. & Burland, J.B. (1968). "On the Generalized Stress-Strain Behaviour of 'Wet' Clay", in *Engineering Plasticity*, Cambridge University Press, pp. 535 - 609

Rowe, P.W. & Barden, L. (1964). "Importance of Free Ends in Triaxial Testing", *Journal of Soil Mechanics and Foundations Division, ASCE* 90 (S.M.1), pp. 1 – 27

Saada, A.S. & Townsend, F.C. (1981). "State of the Art: Laboratory Strength Testing of Soils", *Laboratory Shear Strength of Soil.* ASTM STP 740, pp. 7 - 77

Santagata, M.C. (1994). "Investigation of Sample Disturbance in Soft Clays Using Triaxial Element Tests", S.M. Thesis, Massachusetts Institute of Technology

Santagata, M.C. (1998). "Factors Affecting the Initial Stiffness and Stiffness Degradation of Cohesive Soils", Ph.D. Thesis, Massachusetts Institute of Technology

Schofield, A.N. & Wroth, C.P. (1968). Critical State Soil Mechanics, McGraw-Hill

Seah, T.H. (1990). "Anisotropy of Resedimented Boston Blue Clay", Sc.D. Thesis, Massachusetts Institute of Technology

Sheahan, T.C. (1991). "An Experimental Study of the Time-Dependent Undrained Shear Behaviour of Resedimented Clay Using Automated Stress-Path Triaxial Equipment", Ph.D. Thesis, Massachusetts Institute of Technology

Skempton, A.W. (1954). "The Pore Pressure Coefficients A and B", *Géotechnique* 4 (4), pp. 143-147

Skempton, A.W. (1960). "Effective Stress in Soils, Concrete and Rocks", Conference on Pore Pressure and Suction in Soils, Butterworths, pp. 4-16

Skinner, A.E. (1969). "A Note on the Influence of Interparticle Friction on the Shearing Strength of a Random Assembly of Spherical Particles", *Géotechnique* 19 (1), pp. 150-157

Stokes, W.L. & Varnes, D.J. (1955). Glossary of Selected Geologic Terms, Colorado Scientific Society Proceedings 16, Denver, Colorado

Suklje, L. (1969). Rheological Aspects of Soil Mechanics, Wiley Interscience, New York, 123

Taylor, R.N. & Coop, M.R. (1993). "Stress Path Testing of Boom Clay from Mol, Belgium", *The Engineering Geology of Weak Rock*, Balkema, Rotterdam, pp. 77-82

Terzaghi, K. & Peck R.B. (1967). Soil Mechanics in Engineering Practice, Second Edition, John Wiley and Sons

Whittle, A.J. & Kavvadas, M. (1994). "Formulation of the MIT-E3 Constitutive Model for Overconsolidated Clays", *Journal of the Geotechnical Engineering Division*, ASCE, 120 (1), pp. 173-198

William, E. (2007). "Engineering Performance of Bringelly Shale", Ph.D. Thesis, University of Sydney

Wissa, A.E.Z. (1961). "A Study of the Effects of Environmental Changes on the Stress-Strain Properties of Kaolinite", S.M. Thesis, Massachusetts Institute of Technology

Wissa, A.E.Z. (1969). "Pore Pressure Measurement in Saturated Stiff Soils" *Journal of Soil Mechanics and Foundations Division, ASCE* 95 (S.M.4), pp. 1063-1073

Yassir, N. A. (1989). "Mud Volcanoes and the Behavior of Overpressured Clays and Silts", Ph.D. Thesis, University College London, University College London